Science and Technology
of the
Mechanical/Thermal Dewatering

Habilitationsschrift
im Fachgebiet Energieverfahrenstechnik
vorgelegt dem
Fachbereich Bio- und Chemieingenieurwesen
der Universität Dortmund

Dr.-Ing. Christian Bergins

aus
Recklinghausen

Dortmund 2005

Gutachter:
Prof. Dr.-Ing. Karl Strauß, Universität Dortmund
Prof. Dr.-Ing. Klaus R. G. Hein, Universität Stuttgart

Summary

In the work at hand basic experimental results are presented for the mechanical/thermal dewatering (MTE, German abbreviation for 'Mechanisch/Thermische Entwässerung', also used for 'mechanical/thermal expression' in English), during which lignites or other moisture containing materials are dewatered by the combined application of heat and mechanical forces. Models are developed for the description of the kinetics during the dewatering of the different materials based on soil-mechanical fundamentals, rheology and rate-process-theory.

Using mercury intrusion porosimetry (MIP), helium pycnometry, CO_2 adsorption and other techniques, it is investigated, how MTE process conditions, such as temperature and pressure, affect the physical properties pore size distribution and pore diameters, specific surface area, skeletal and 'true' density, hardening, compressibility and shrinkage behaviour of low rank coals from Australia, Greece and Germany.

The results provide a detailed insight in process kinetics and mechanism, in coal structure and structural changes during the dewatering process. Additionally re-hydration and combustibility of MTE products as well as the removal of minerals from lignites during the MTE process is investigated. Results from the mechanical/thermal dewatering and water leaching tests are compared, which prove, that the MTE process is a powerful technique for the removal of both water and alkali components from lignite and younger biomass fuels like straw. Reductions of the concentration of sodium in lignite and potassium in straw between 70 and 85 % are obtained. The results thus demonstrate, that the MTE process is also suitable for the upgrading of lignites and biomass fuels to prevent corrosion and slagging in power plants.

The development of the plant and process engineering for the dewatering of lignite and for the combined leaching and dewatering of biomass fuels is presented and technological modifications required for the dewatering of waste materials and suspensions like galvanising sludge are described. The technical implementation is demonstrated based on the laboratory and technical scale dewatering units at the University of Dortmund and the pilot and demonstration plants located in Frechen and at the power plant Niederaußem.

Efficiencies for different dry lignite fired power plant concepts with integrated mechanical/thermal lignite dewatering are calculated and compared to the results obtained for other drying and dewatering processes. Depending on the origin and water content of the lignite, power plant efficiencies can be increased by up to 20 percent and specific CO_2 emissions can be reduced by the same amount by the implementation of the MTE process in technical scale power plants. The results prove, that the MTE process is a remarkable advance compared to the existing methods.

Vorwort – Foreword

Christian Bergins   Datteln, im Mai 2005

Christian Bergins   Datteln, 2007

Contents

1 Introduction

The future energy supply of mankind is characterised by the increasing energy demand of the growing population, the limitation of fossil fuels and the impacts of the energy utilisation on the environment, in particular the question of greenhouse gas emissions. Therefore the utilisation of fossil fuels for power generation is likely to depend upon the development of advanced technologies with minimal environmental impact and high efficiencies.

Lignite is one of the most favorable and largest energy sources worldwide and there is still a large potential for an efficiency increase during electric power generation with low rank coals. The water content of lignites typically ranges from 50 to over 60 % by weight and if high-moisture coal is burnt in conventional power plants, a substantial amount of the energy content is required to evaporate the water. With a view to secure and strengthen the position of brown coal as a highly available energy source in a rising global energy market, many attempts have been made to develop new technologies for energy-efficient drying or dewatering processes in recent years.

Despite an almost one-hundred-year development of the drying processes and power plant technology the potential for the energy efficient use of brown coal resources is not fully exploited yet. Optimised power plants indeed allow efficiencies – based on the lower heating value – of up to 43 percent today [Pfl99, HK99], however, economic limits are already reached or exceeded by the implementation of expensive heat transfer systems. Nevertheless still a large amount of the chemical energy of the coal is wasted burning raw coal using conventional technology since the whole water contained in the coal is evaporated during the mill-drying process. Depending on the origin and water content of the coal the power plant efficiencies could be increased by up to 20 percent and specific CO_2 emissions could be reduced by the same amount [BSS04, HB97] by the implementation of drying or dewatering processes in technical scale power plants.

The mechanical/thermal dewatering (German abbreviation: MTE, 'Mechanisch/Thermische Entwässerung', also used for 'mechanical/thermal expression' in English) is a new energy efficient process for the non-evaporative reduction of the water content of lignite prior to combustion by means of mechanical forces at elevated temperatures. The process was developed at the University of Dortmund by Prof. KARL STRAUSS [Str94, Str96a, SBB$^+$96] and is a remarkable advance on existing methods like the well known thermal [Fle26, FLWT87, DA92] and mechanical [BB84, BB89] dewatering processes, which are restricted in the technical application due to very high temperatures (>235°C) respectively pressures (> 16MPa). During the MTE process the coal water is removed in liquid state without evaporation by means of mechanical pressure (4 to 6 MPa) and moderate heating (between 180 and 200°C) with a comparatively low energy demand.

Detailed research has been done on the process fundamentals at the University of Dortmund since 1995 and a 25 t/h MTE demonstration plant has been constructed at the Niederaußem power station of RWE in Germany and came into operation in 2001 [SBB01].

In this work the results of basic experiments are presented for the dewatering of lignite from different origins. The influence of the process parameters temperature, pressure and time is investigated in a wide range and models for the description of process kinetics and dewatering are developed based on soil mechanics and rheological principles.

As a consequence of the MTE process design, both structural changes and the temperature dependency of thermodynamic properties of the wet coal have to be taken into account in experimental investigations. During the heating the coal releases parts of the water as a result of the collapse of the colloidal lignite structure. The subsequent mechanical dewatering is improved and accelerated by the decrease in fluid viscosity and density at elevated temperatures, leading to a highly consolidated coal. This way both physical changes in the porous structure occur, which are investigated by means of different characterisation techniques. Considering storage, transport and firing of MTE
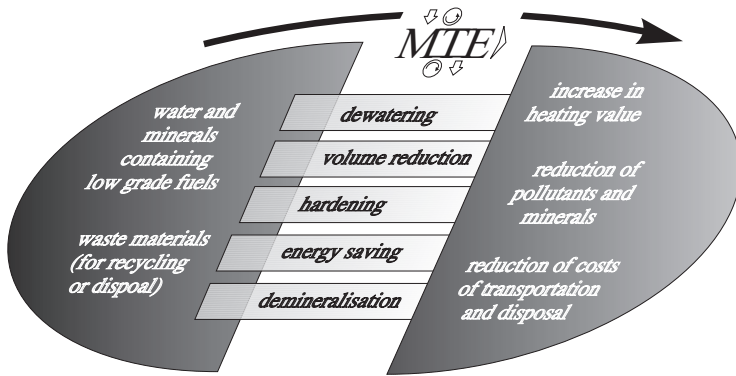
Figure 1.1:
Beneficial effects from mechanical/thermal treatment of water containing fuels and waste material.

products properties like pore volume, specific surface area, apparent density, compressibility as well as shrinkage behaviour upon drying, water re-adsorption and ignition behaviour play an important role and will therefore be investigated.

Apart from the energy efficient dewatering of solid materials the MTE process also provides a simple technology for the dewatering and volume reduction of suspensions of ultra fine particles and semisolid materials and sludges [SB99], which offers a great potential for cost reduction in the disposal of waste materials (Figure 1.1).

Both in the solid dewatering and in the water removal from waste materials the direct contact of the heating fluid (water or steam) with the materials treated and the removal of the water in its liquid state leads to a leaching of inorganic (demineralization) and organic compounds which has an beneficial effect on the properties of the dewatered products. Especially for low grade lignites and biomass fuels the dewatering as well as the demineralisation are effects which are of interest as advanced technologies.

Therefore an overview on different areas of application for the MTE process is given as well as a review on the different MTE technologies and scales of technical implementation of the MTE process (Figure 1.2). Calculations are presented which prove, that the procedure is an economical alternative to existing concepts for the dewatering of moist solid fuels such as peat or brown coal just by increasing the net calorific value and simplifying power plant technology. The implementation of the mechanical/thermal dewatering in a dry lignite fired power plant will be demonstrated for a $500\,\mathrm{MW_{el}}$ power station concept.
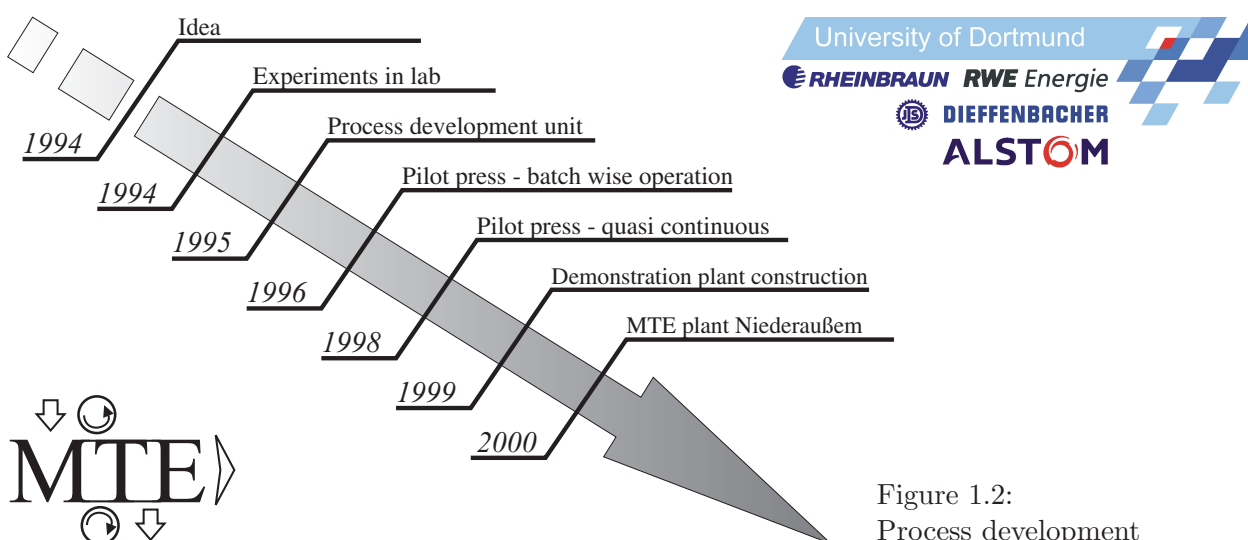
Figure 1.2:
Process development

2 Motivation

Low-rank coals[1] constitute almost half of the reserves of the coal existing worldwide. Typically deposits occur in thick seams with relatively thin cover and mining operations are generally inexpensive. Despite their excellent combustion characteristics and other attractive properties, utilization of lignite and subbituminous coal has been largely confined to the generating of electrical power at or nearby the mining site [SS99] up to the present. The widespread utilization of low rank coals in traditional and/or distant black coal markets is constrained by

- the high inherent moisture content and high energy specific cost of transportation,
- the fouling and slagging problems in power plants caused by high alkali metal contents,
- the high risk of spontaneous combustion and the
- weathering and resultant dust emissions.

Although high moisture contents lower the heating values and thus increase the costs of transportation and handling, positive features, such as low cost per MJ and excellent combustion characteristics have been ignored except for few countries like Australia and Germany where lignite dust or briquette firing also is used in district energy systems and industrial firings [Dur91, SS99]. Nevertheless, no commercial drying process is currently available that can economically produce a conventional, dried bulk coal product, that will conform to the demands of storage, handling, and transportation.

In the following a brief overview on coal structure and technologies and technological limits of lignite utilisation is given. Special attention is drawn to new opportunities resulting from the development of the mechanical/thermal dewatering and its application in lignite preparation.

2.1 Coal structure

Lignites are a relatively young product from the coalification process from plants to black coal and anthracite. The solid structure consists of a complex system of condensed aromatics with many different, particulary oxygen containing functional groups. Due to the complexity of the main components, lignin and humic acids, and the number of possible variations, only statistical models for the chemical structure of coal have been developed so far. From analytical investigations on elemental composition and functional groups HÜTTINGER and MICHENFELDER [HM87] constructed the model for the chemical structure of German lignite (Rhineland) shown in Figure 2.1b. From X-ray scattering experiments of HIRSCH et al. [Hir54, BH55, CH60] a more dimensional model for the development of coal fine structure during coalification was developed (Figure 2.1a).

For the explanation of colloidal properties of lignites like high water holding capacity, shrinkage, swelling and ion-exchange properties also micellar models (Figure 2.2) where introduced by AGDE et al. [ASJ42a] and CARMIER and SIEMON [CS78a]. The colloidal properties can be summarised as follows: Lignite consists of finely dispersed solid particles ($<1\,\mu$m) [ASJ42b, CS78a, CS78b] with a comparatively high ($280\,\text{m}^2$/g dry basis) specific surface [BS52, SAE74, ASM95]. So in raw coal solid and water form a gel structure [Eva73b]. Effects of an electrical double layer at the coal/water interface can be detected which play an important role on physical structure and ion exchange [RQ88, QR87]. During adsorption and desorption of water a hysteresis can be observed and the coal structure undergoes swelling and shrinkage [AE71b, Eva73a].

---

[1]Lignite and brown coal (German: Braunkohle) are used synonymous with low rank coal in this work. Nevertheless it has to be considered, that there are different classification systems in Germany and the United States of Amerika [FLW87, TT02] with additional sub-divisions.

(a)

(b)
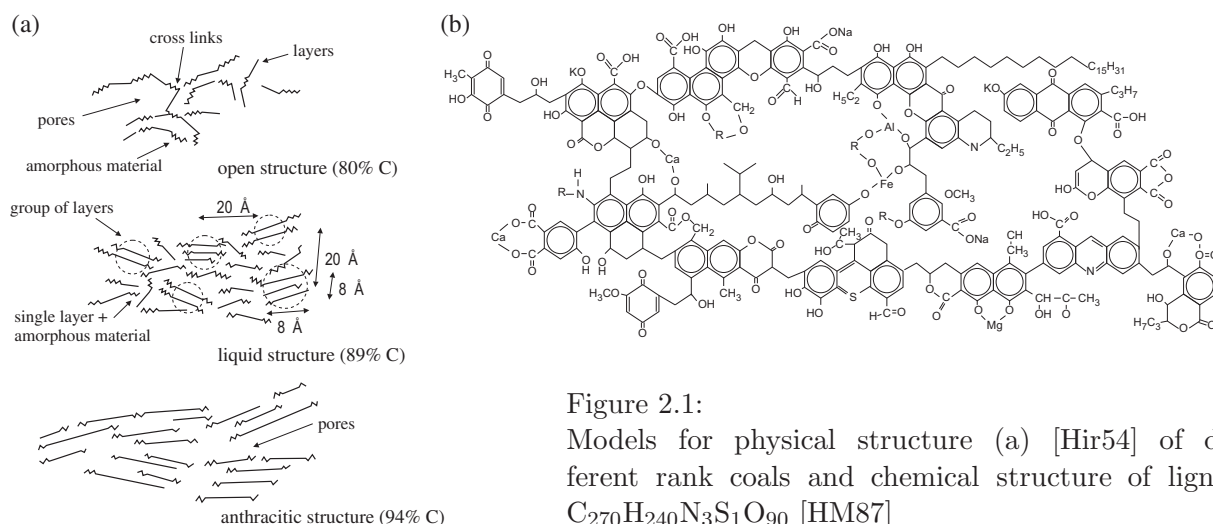
Figure 2.1:
Models for physical structure (a) [Hir54] of different rank coals and chemical structure of lignite $C_{270}H_{240}N_3S_1O_{90}$ [HM87]
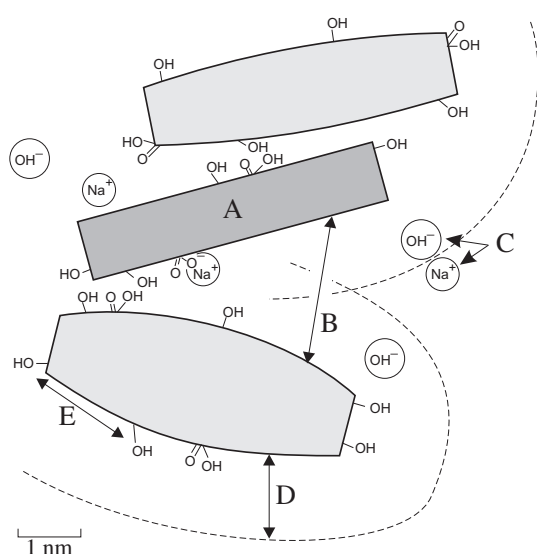
A. Theoretical micelle $(1\,\text{nm} \times 5\,\text{nm})$ [ASJ42a].

B. Capillary diameter corresponding to sorbed water on coal [Eva73a].

C. Solvated ionic radii of hydroxyl ion $\approx 0.246\,\text{nm}$, of sodium ion $\approx 0.217\,\text{nm}$.

D. Maximum distance for hydrogen bonding $(4\,H_2O\ \text{molecules} \approx 1.6\,\text{nm}$ [AE71b]).

E. Spacing of carboxyl groups $\approx 6.2\,\text{nm}$ and phenolic groups $\approx 2.9\,\text{nm}$. Calculated from the specific surface [SAE74] and analysis of functional groups.

Figure 2.2:
Conceptual structure of rod shaped
brown coal micelles [CS78a]

For Australian brown coal (water content $W \approx 1.5\,\text{g/g}$ db.) detailed investigations of ALLARDICE, EVANS and STEWART [SE67, AE71a, AE71b, Eva73a] lead to a characterisation of the different portions of water as follows:

- More than $60\,\text{g/g}$ of water is contained in pores larger than $100\,\text{nm}$ as capillary water,
- about $7\text{-}12\,\text{g/g}$ water is adsorbed in multi layers,
- about $7\text{-}8\,\text{g/g}$ water is adsorbed in mono layers and
- about $1.5\,\text{g/g}$ water is chemisorbed to the coals surface.

According to results from differential scanning calorimetry (DSC) and ^1H NMR measurements [LW79b, LW82, NKH$^+$97, FCMJ04] the different proportions of water in lignite can also be classified as 'bulk' or 'free' water (freezing at $0°C$), 'bound' water (freezing between -40 and $-30°C$: 20 to $30\,\text{g/g}$ of dry coal) and 'non freezing' water (by difference: 40 to $55\,\text{g/g}$ of dry coal).

2.2   Drying and dewatering

When lignite is heated at ambient pressure to temperatures above $100°C$, most of the water can be removed by evaporative drying. For water contents below $15\,\text{wt.}\%$ higher temperatures are required and the heat of evaporation increases due to higher binding forces [AE71b, FLW87, WF90]. However, traditional thermal drying methods (Table 2.1) are not effective on the production of

bulk products from lignite, because of the resulting disintegration of the structure during drying as a consequence of shrinkage. Therefore bulk fuels from coal have been produced for centuries by crushing, grinding and subsequent briquetting, which is an expensive and energy consuming method.

When lignite is heated under pressure to temperatures above 180°C, increasing amounts of the coal water are released from the coal by the different chemical and physical mechanisms, which are commonly described as thermal dewatering (TD) [Fle26, Ros29, ES70, ME72]. Above 150°C decomposition of organic functional groups (mainly -COOH) takes place and the released CO_2 displaces and expels coal water. Further heating to higher temperatures changes the surface properties of the lignite due to the increasing loss of functional groups. The coal becomes more and more hydrophobic and a hardening of the lignite can be observed which leads to a rigid coal structure. In addition to this, at higher temperatures the viscosity, density and surface tension of the water decrease, which promotes the release of the water from this heat-mobilised system. Usually thermal dewatering processes are designed for temperatures above 230°C for optimum operation and low water contents (<30 wt.%). Due to the increased rigidity, the dried products can be utilised also as bulk fuels for industrial or private heating [Fle26, Ros29, HF90].

A purely mechanical dewatering is not practicable for the technical application, since the required pressures and dewatering times are too high (>16 MPa, >1 hr) [Dul54, BB89]. This would lead to enormous costs for large plants. But in combination with higher temperatures (180°C), where the intermolecular forces between water and solid matrix are reduced, increased amounts of water can be removed (water contents below 25 wt.%) by applying comparatively low pressures (6 MPa) [Ber03, Ber04]. In this temperature range the melting of waxy and bituminous components further eases the compression of the solid coal structure by weakening the mechanical rigidity of the entire coal/water system.

There are also concepts for microwave drying of lignite, solar drying, drying with low temperature flue gas [ZL95], solvent extraction [MMA+02], but the respective processes have either not been proven in technical scale or are regionally limited (solar drying) or are even more energy consuming than the known processes (microwave drying). Reviews on the stage of development of alternative methods are given by ALLARDICE [All91] and FOHL et al. [FLW87].

Technologies Since a process for the dewatering of lignite in large power stations must be suitable for handling mass flow rates as high as some hundred metric tons per hour (tph) and it must have

Table 2.1: Processes for the drying and dewatering of lignite

Process	Thermal drying	Thermal dewatering	Mechanical dewatering
Energy type	Thermal energy	Thermal energy	Mechanical energy
Physical principle	Evaporation of the water after heating to approx. 100°C at atmospheric pressure	Removing water in liquid form by heating to >235°C at the corresponding saturated steam pressure of >3 MPa	Removing water in liquid form by compression to >16 MPa at ambient temperature
Commercial operations	Mill-drying plants Rotary tube dryer SFBD-process WTA-process	Fleißner process (steam heating) Viag process (hot water) Voest-Alpine process (steam) HTD / HWD process (hot water)	Not in commercial use for lignite

		Mechanical/thermal dewatering
MTE⟩	*Physical principle*	• removing the coal's water in liquid form by –heating the coal to 180-200°C and –compressing to 4 - 6 MPa
	Features compared to other processes	• low energy demand • consolidation pressure and saturated steam temperature at low level • short process times
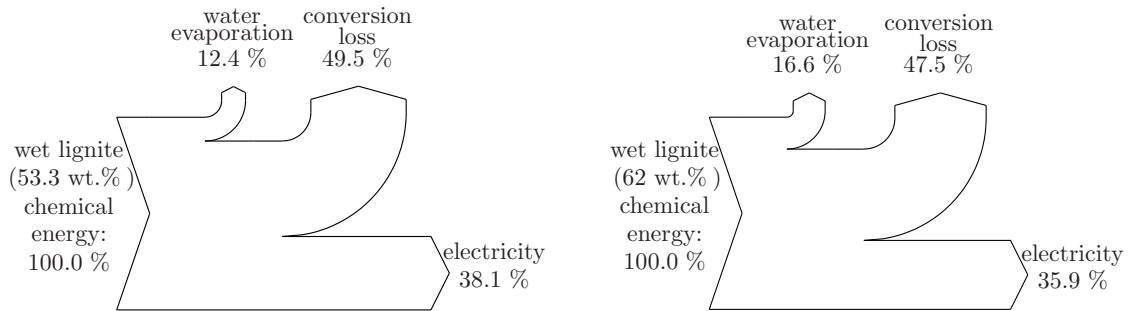
Figure 2.3: Energy loss due to coal water evaporation in conventional lignite fired power plants for German (53.3 wt.%, left) and Australian (62 wt.%, right) lignite

a low energy consumption, the development of plant technology for various drying and dewatering processes was intensified in the last decade. The technologies described in the respective literature can be classified roughly according to the type of water removal into the categories of drying (evaporative removal of the water) or dewatering (removal of the water in its liquid state) as shown in Table 2.1.

In conventional power plants lignite is dried with hot flue gas (1000°C) and air in so called beater wheel mills during a combined grinding and drying step. Due to the high temperatures of the flue gas this drying method is exergetically disadvantageous. The maintenance costs for the mills are high and the latent heat of the water vapour is released from the power plant without being used for the energy conversion process. The heat losses for a German (53.3 wt.%, Rhineland) and Australian lignite (62 wt.%, Latrobe Valley) are shown in Figure 2.3.

In view of reducing the energy consumption (or the loss by the release of vapour), the development of advanced drying processes was particularly concentrated on lowering the temperature and pressure level of the heating medium and also on recovering the energy contained in the vapour. Particularly to be mentioned here are the steam-fluidised bed drying process (SFBD, German abbreviation: DWT, Dampf-Wirbelschichttrocknung) which was originally developed at the Monash University, Melbourne [Pot81] and as a further development the WTA process (fluidised bed drying with internal waste heat recovery, German: Wirbelschichttrocknung mit interner Abwärmenutzung) of Rheinbraun [Klu88]. In the latter case, the vapour leaving the dryer is cleaned and compressed according to the heat pump principle to such an extent that its latent heat can be used to heat the dryer. Both the SFBD process and the WTA process exist as technical scale demonstration units with about 50 tph capacity (SFBD: Loy Yang power station, Australia [ST96], WTA: Rheinbraun AG, briquetting factory Frechen [KKL94] and power station Niederaußem).

Previous implementations of thermal dewatering processes were of comparable size (up to 100 tph dry coal [HF90]) but according to its own information, the only European manufacturer (Voest-Alpine) has abandoned work on this field. Nevertheless both in the USA and in Australia research work is done on hydrothermal dewatering (HTD) and hot water drying (HWD) which utilised hot water instead of steam as heating medium. In all variations of the process the coal is heated with steam (Fleissner process) or water (VIAG process [Wir52]) to temperatures above 235°C assuring pressures high enough to prevent the evaporation of water. In this temperature range the coal water is released from the coal structure in liquid state and can be used for the preheating of raw coal.

Based on the synergetic effect of heat and mechanical pressure the development of the mechanical/thermal dewatering process – which combines the advantages of thermal and mechanical dewatering and avoids their disadvantages – began in 1994 as an idea of Prof. STRAUSS at the University of Dortmund, Germany [Str96a, BBS98]. Meanwhile the process is proven in pilot scale and a 25 tph technical scale demonstration unit has been commissioned successfully in 2002 at the power station Niederaußem [BSS04, BBS+99]. Additionally other technologies for this process have been proposed [MH03].

2.3 Minerals in fuels, slagging and fouling

Based on different mechanisms involved in the development of ash deposits on heating surface, two general types of ash deposition have been defined as slagging and fouling. Slagging is the formation of molten or partially fused deposits on furnace walls or convection surfaces exposed to radiant heat. Fouling is defined as the formation of deposit on convection heat surfaces such as superheater and reheaters [Smo93].

Typical initial deformation temperatures (or so called 'ash fusion' temperatures) are $1100 - 1200°C$. At furnace gas temperatures in excess of $1350°C$ semi-molten ash exists, that may stick to the cooler walls and tube surfaces. If the furnace is too small and the exit gas temperature therefore is too high or if the melting point of the ash is relatively low, molten ash may not have enough time to cool down and resolidify before hitting the heating surface. This ash then easy sticks to the surface and causes the accumulation of deposits leading to slagging. Depending on the strength and physical characteristic of the deposit, steam or air soot blower may be able to remove most of them. However, the base deposit generally remains attached to the tube and allows subsequent deposits to accumulate much more rapidly.

Fouling is generally caused by the vaporisation of volatile inorganic elements in the coal during combustion. When heat is absorbed and temperatures decrease in the convection area of the boiler, compounds formed by these elements condense on ash particles and heating surface, forming a glue which initiates deposition.

Inorganic species, such as alkaline and alkaline earth metals (AAEM) play an important role in low temperature fouling and slagging since they both evaporate at low temperatures and also form low melting eutectic solutions with other components of the ash. Inorganic species in coals are typically present in three main forms. The first form includes species that exist as discrete mineral inclusions in the coal matrix (e.g. Fe in the form of pyrite). The second form includes species that are dissolved in the interstitial pore water (e.g. NaCl), while the third form includes species that are ion exchanged onto carboxylic and phenolic functional groups (e.g. Na^+, Ca^{2+}), see Figure 2.4 [Smo93].

The binding strength to oxygen containing functional groups largely varies depending on the inorganic species and functional group type. Additionally, it has to be distinguished between acid soluble and inert discrete minerals. Therefore usually four different types of minerals in lignites are distinguished:

- A water-soluble fraction,
- an organically bound fraction, ion exchangeable at pH 7,
- a fraction soluble in acidic solutions and
- an inert fraction.

The first three types can be quantified directly by chemical fractioning [LG52]. The inert fraction can be calculated by the mass differences determined by acid leaching and ash analysis.
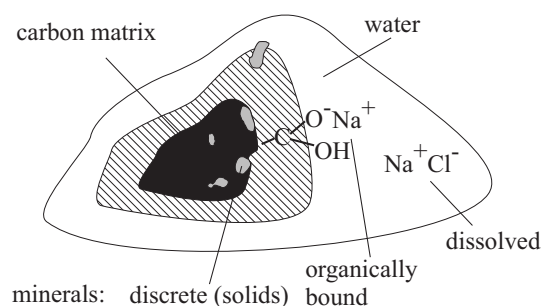
Figure 2.4: Types of minerals in coal

Water-soluble minerals   The water-soluble fraction mostly consists of salts, that dissolve easily in water. These are mainly salts of alkaline and alkaline earth metals like e.g. sodium chloride. By adding an excess of water to a moist coal sample, it is to be expected that the solubility of the salts is not exceeded in the solution and all water-soluble minerals dissolve. The organically bound minerals are hardly soluble in water so that they are not expected to dissociate in this step. Nevertheless they can partially dissociate in very diluted coal/water suspensions. Therefore the influence of the coal concentration usually has to be taken into account.

Organically bound minerals   The organically bound fraction is formed by metal cations, which are bound to functional groups in the coal matrix, like carboxyl or, in a certain amount, also weaker acidic hydroxyl groups [QR87]. These bonds are often chelates and can be compared to the bonds in technical cation exchangers like resins or zeolites. A cation exchanger is able to exchange the bound cations against protons, or the other way round, as shown in Eq. 2.1.

$$2\,H^+R^- + Ca^{2+} + H_2O \xrightarrow{\;\;\longleftarrow\;\;} Ca^{2+}R_2^- + H_3O^+ \tag{2.1}$$
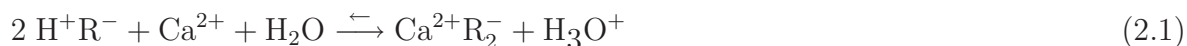
Concerning lignite, an equilibrium on the left hand side (lhs) of the reaction is preferred during the removal of bound cations in leaching processes. This can be achieved by adding hydronium ions using acidic solutions. But in this case, also acid soluble minerals are removed. Therefore the samples are prepared with an ammonium acetate solution for the quantification of the organic fraction. Organically bound univalent and divalent cations then can be exchanged forming hardly dissolving ammonium humates and alkali metal acetates [LG52]. As ammonium acetate has pH buffering properties, the pH value of the solution remains in a neutral range. Furthermore, no other cations are added to the solution, which could influence the results.

Acid soluble minerals   The acid soluble fraction is made up of discrete salts, which have a low solubility in water, but dissolve easily in acids. Examples are the carbonates or sulphates of alkaline earth metals. These minerals are dissolved during the treatment of lignite with hydrochloric acid and can be detected in the solution afterwards.

Inert minerals   The inert fraction of the minerals is formed by even in acidic solutions hardly dissolving minerals, like feldspar or other silicates. These minerals can only be dissolved in hydrofluoric or nitrohydrochloric acid. They are also thermally stable, so that they can be quantified by the ash analysis in addition to the chemical fractioning. The ash analysis then shows the total amount of a metal in the coal, where the other three fractions (determined by the chemical fractioning) can be subtracted from.

Solubility   In addition to the differences in solubility in water and acid, also the solids concentration in the solution and temperature show an influence on the mineral release during leaching experiments. As shown by BÖHLMANN [Böh02] the organically bound minerals can be dissolved partly in very diluted suspensions, depending on the coal/water concentration. Furthermore the solution equilibrium of the acid soluble fraction can be shifted towards the lhs of Eq. 2.1 by increasing the temperature. This effect is due to the increased mobility of the ions, which provides the energy to overcome weaker electrostatic bonds, and to the dissolution and the partial thermal decomposition of functional groups (at temperatures >150°C).

Depending on the absolute solubility for some species also a limit of solubility is reached at higher solid concentrations. This requires that the maximum solubility is already reached or exceeded in the coal water itself. Therefore also in water leaching experiments at different concentrations three cases of solubility can be distinguished as follows. Minerals contained in the coal

- are soluble in water infinitely,
- they are organically bound and partly dissociating or
- their solubility is limited by the solubility product, which is exceeded in the raw coal.
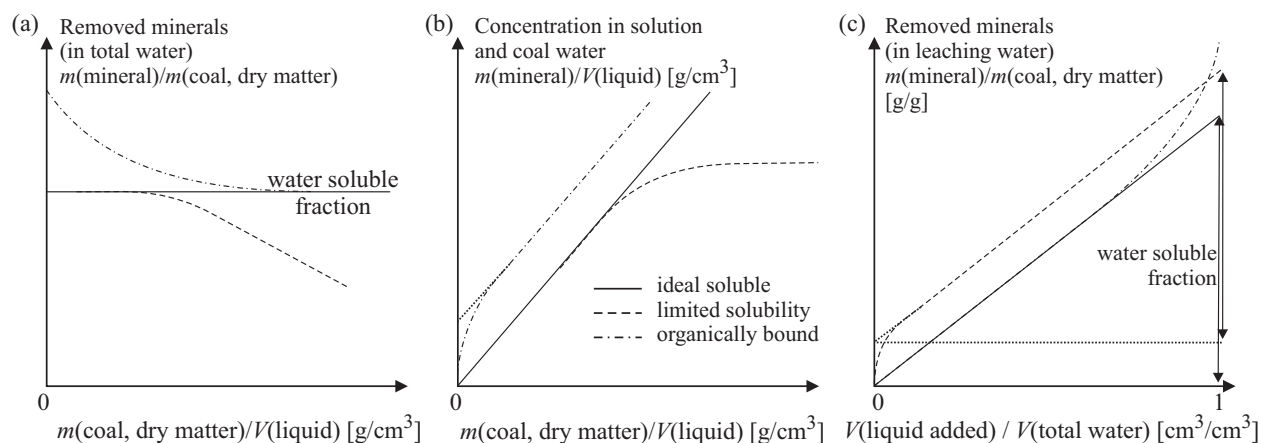
Figure 2.5: Different types of mineral release during leaching

The mineral release for the three cases is shown in Figure 2.5 as a function of wet coal to water concentration and scaled water volume. The graphical representations in (a) and (b) are often used for the description of equilibrium leaching experiments [GM79, Böh02]. For the calculation it is assumed that the complete water (coal water + leaching water) is removed to reach the given concentration and mineral removal.

Nevertheless during the mechanical/thermal dewatering the water is not removed completely during the combined heating and demineralization stage and even after the expression stage parts of the coal water remain in the product. Therefore the graphical representation in Figure 2.5(c) is chosen in Chapter 3.4.3 for the comparison of equilibrium leaching and MTE experiments since both the removal during heating and leaching – from the knowledge of the specific water volume added to the coal – and the maximum removal of water soluble salts for infinite dilution – from the extrapolation to the right axis of the diagram (c) – can be estimated this way.

2.4 Physical and chemical properties of dry products

Chapter 3.3 of this work focuses on the effects of MTE on the physical properties of low rank coals. Of particular interest are the effects of MTE temperature and pressure on pore structure, specific surface area determined by mercury intrusion porosimetry (MIP) and CO_2 adsorption, apparent density, compressibility as well as shrinkage behaviour upon drying and water re-adsorption. This will provide valuable information for the utilisation of MTE products in current and new generation power plants and gives an indication to their suitability for the export market.

Currently, there is no clear understanding of the basic parameters which are influencing the above described physical properties during the coalification process, despite some properties appearing to correlate to coal rank and carbon content [SDK54, GNWJ72, TT72, NFK84, Mah84]. As studies by HULSTON et al. [HBCS04, HBCS, HBCS05] and CHAFFEE et al. [CFJ00] have shown the chemical composition of MTE treated coals to remain relatively unchanged during the MTE process, MTE treated coals provide an excellent system for disentangling the effects of physical and chemical factors. In the early stages of coalification [ONLC96, Hua96, CB97, BCOB00] it is thought that conditions can to some extent be mimicked by those found during the MTE process, so that the effects of processing conditions on physical properties will also shed light on changes occurring during natural coalification [TT02].

The physical structure of dried porous materials, including coal, can be characterised by a number of techniques, including CO_2 adsorption experiments and mercury intrusion porosimetry. While CO_2 gas adsorption provides information on the specific surface area, pore volume and pore size distribution of pores in the micopore size region, MIP provides similar information in the macro- and mesopore size region. Numerous MIP studies on coal have been undertaken

since the first experiments of ZWIETERING and VAN KREVELEN [ZK54], including detailed analyses of compressibility [SDY95, NFK84], reintrusion and retention of mercury [Klo94], as well as pore volume and mercury surface area determinations for coals of different rank and location [NFK84, GNWJ72, TT72, FM88]. Since the combined application of CO_2 gas adsorption and MIP covers the whole range of dimensions describing the micro, meso and macro structure of porous solids, both techniques are applied in characterisation of MTE products.

Combined physical and chemical effects play an important role in water reabsorption into the porous coal structure and ignition and combustion of coal. Knowledge about changes in both processes resulting from the MTE treatment is of interest especially considering storage and handling of the dry products and firing of the coal in power plants and will therefore also be investigated.

2.5 Biomass fuels

With their huge potential, the widespread application of renewable energy systems can contribute significantly to the longterm world energy supply. One of the various renewable energy options is the utilisation of biomass. Today, biomass already contributes to about 14 % of the world's energy supply and is considered as one of the key renewable energy resources of the future. Biomass refers to all forms of plant-based material, that can be converted into usable energy, such as wood and residues from wood processing, straw, sugarcane and forestry residues. The energy supply from biomass is considered nearly CO_2-neutral and the utilisation of biomass as substitution of fossil fuels therefore contributes to the reduction of CO_2 emissions.

Biomass offers considerable flexibility of fuel supply due to the range and the diversity of fuels which can be produced at small or large scales, in a centralised or dispersed manner. It can be burnt directly, converted to liquid fuels (for transportation), anaerobically digested to produce biogas, or gasified by means of pyrolysis.

At present, solid biomass is usually burnt directly and then used to produce energy for room heating or for other heat-demanding applications like cooking or certain industrial applications, such as co-generation of electricity and process steam at sugar factories, paper mills and wood processing factories.

However, due to the high potassium and chlorine concentrations (straw) and the high humidity (bark) there are still many problems in the utilization of renewable energy sources [BP97, SHL+00, Val00]. Although systems have been developed for the straw leaching and drying to reduce the corrosion rate at the heating surfaces and slagging and fouling in power plants, these systems result in considerable energy losses caused by leaching, dewatering and thermal drying which are in the range of approx. 8 % of the calorific value of the raw material [NLN+98]. Additionally, low fuel densities cause increasing costs of storage and transport, when utilising biomass in centralised plants. This cost is partly offset by the prolonged life of the boilers, because corrosion problems are avoided. Leaching of straw is also expected to give advantages in respect of the subsequent application of the fly ash, since straw ash, that does not contain alkaline salts and other impurities, can be used as a filler in building materials [JBW96, NLN+98].

As for lignite, a combination of leaching, dewatering and compaction by MTE processing is thought to offer a simplified and energy efficient possibility for a economical preparation of such biomass fuels, which is investigated in Chapter 4.1.

2.6 Treatment of other materials

Apart from the energy efficient dewatering and demineralisation of carbonaceous solids the MTE process also provides a simple technology for the dewatering and volume reduction of suspensions of ultra fine particles and semisolid materials which offers a great potential for cost reduction in the disposal of waste materials [SB99, BCBS99]. Different sludges and semi solids are investigated in Chapter 4.2 and the materials for which the MTE process is applicable are classified according to their behaviour during dewatering.

3 Lignites

One mayor issue during the development of the mechanical thermal dewatering was the investigation of the influence of the parameters temperature, pressure and time on the dewatering of lignites from different locations. Additionally models were developed to describe the dewatering kinetics depending on the process parameters and dried products were characterised physically and chemically [Ber03, Ber04, BHSC, HBCS05]. During the chemical characterisation also leaching experiments have been performed in laboratory scale to gain further information about the amount of minerals that can be removed from lignites with the MTE process. In this chapter the results from the dewatering and demineralization of lignites and from the characterisation of raw and dewatered samples are presented.

Basically three lignites from Australia, Greece and Germany (Table 3.1) are investigated in detail. While the Australian coal has a high moisture, but low ash content, the Greek coal has high levels of both moisture and ash. The German coal has a slightly lower moisture content, with an ash level between those of the other two coals.

Table 3.1: Properties of the raw coals investigated

Provenance	Germany Rhineland	Greece Ptolemais	Australia Latrobe Valley
Open cut	Hambach		Loy Yang
water [wt.% wb.]	53.1	60.4	60.8
ash [wt.% db.]	6.3-8.1	14.1-17.4	1-1.2
heating value [MJ/kg db.]	24.9		26.4

wb.: wet basis, db.: dry basis

3.1 Experimental methods

During the development of the MTE process different experimental rigs and technical scale units have been constructed at the Chair of Energy Process Engineering and Fluid Dynamics, University of Dortmund, which have been used for the investigation of dewatering and heating kinetics, equilibrium and kinetics of the removal of water soluble salts from fuels and for the testing of the process scale up. In the following a brief description of the laboratory unit, which was used for all basic investigations, and details on the physical and chemical methods for analyzing removed water and dry solids are given.

3.1.1 Laboratory dewatering unit

The experimental apparatus used in this study is a double wall cylindric compression cell ($\varnothing$ 70 mm) made of stainless steel, see Figure 3.1. It is designed for pressures up to 13 MPa and can be heated and cooled by oil. A combination of a fine steel mesh (40 μm) and a coarse steel filter cloth is used as filter medium for the dewatering as well as the retention of the solid material both at the piston and at the bottom of the cylinder.

Temperatures and pressures at the bottom filter medium and the piston can be measured by means of thermocouples (T) and two inductive pressure sensors (p), respectively. The compression of the solid is carried out via a piston sealed with two O-rings against the cylinder. The piston is driven by a tension/compression device (model 1195) made by INSTRON. The entire force (max. 50 kN) applied by the machine is measured with a load cell attached to the top of the compression device. The water released from the coal structure during axial consolidation leaves the cylinder through a cooler and a pressure relief valve – set to at least 3 MPa – and is collected in a vessel. Its weight is measured continuously by a balance. The position of the piston and therefore the height of the bulk
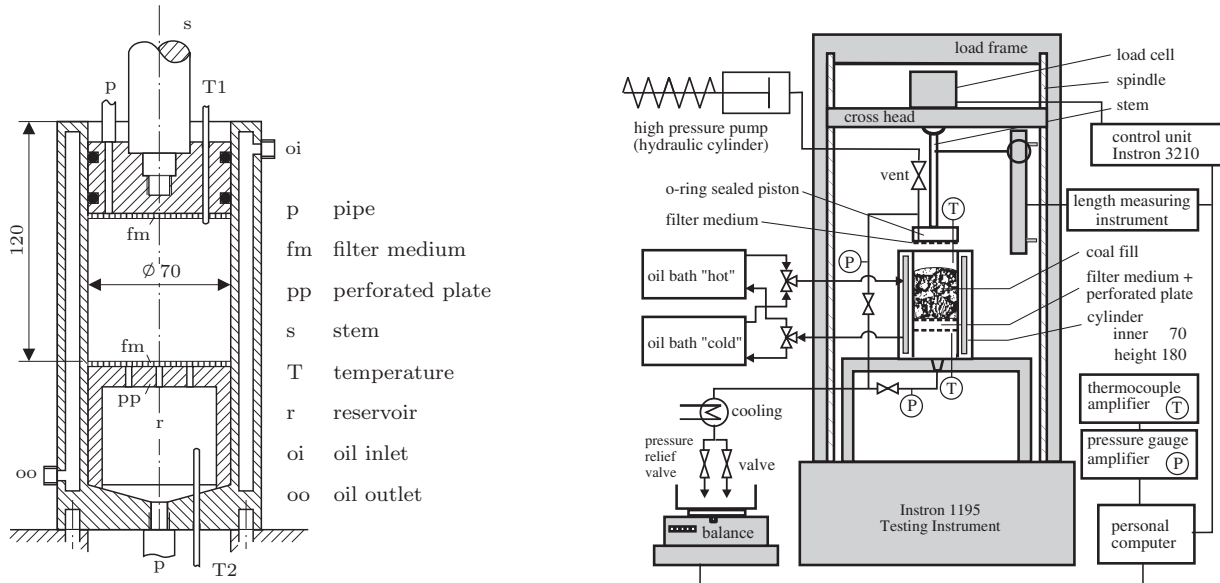
Figure 3.1: Compression cell and experimental rig

is determined by a length measurement device attached to the frame of the INSTRON machine[1]. All experimental data are recorded by a computer.

The setting of the pressure relief valve avoids the evaporation of the coal water during heating. The water pressure inside the vessel is always kept higher than the saturated steam pressure corresponding to the temperature of the experiments. The effective compression pressure p_s^∞ of the solid is therefore calculated from the difference of applied pressure and water pressure.

Mechanical/thermal dewatering   The experiments are carried out at temperatures between 25 and 235°C and pressures from 1 to 10 MPa with crushed lignite (100 g, 0-10 mm) in 4 steps:

- Filling the lignite into the cylinder with additional deionised water. The use of this slurry ensures a completely filled pore space between the particles.

- Heating the coal up to a chosen temperature (2400 s for the highest temperatures investigated) and waiting for 1200 s afterwards for an equilibrium of thermal dewatering. A total leaching time of at least 1 h also was ensured for experiments at ambient temperature to enable the comparability of dewatering and leaching experiments.

- Fast lowering of the piston (50 mm/min) until the desired pressure is reached and then compression with constant pressure for 10 000 s or 100 000 s.

- Cooling of the coal still under pressure to prevent flash evaporation and removing the coal for further analysis.

For the product coal the final water content, the weight loss due to thermal decomposition and the density of the solid matter are determined. The latter one is calculated from the water content and volume of the compressed coal. Additionally samples are characterised physically and chemically as described later.

Experiments with smaller and larger coal fillings (50 g, 200 g) have been done to check the influence of ω_0 [$\mathrm{m_{solid}^3/m^2}$] on the required time for the completion of the primary consolidation process. For the determination of the amount of salts removable at different coal/water concentrations experiments are performed also with a second laboratory rig described in [WQCS02, WBS04].

---

[1]The time dependent water content of the coal can be back-calculated either from the final water content of the coal and the water mass measured by the balance or from the final water content and the time dependent position of the piston, which also gives a displaced fluid volume. The latter calculation scheme always is used at higher temperatures, when thermal decomposition of parts of the coal structure leads to gas formation and the expelling of additional amounts of water from the apparatus.

Thermal dewatering   Additionally experiments are performed in the same apparatus to investigate the thermal dewatering of German lignite. In these experiments coarse lignite particles are heated under steam pressure for 1200 s and then slowly cooled down under pressure again. The coal is kept in a bag made of a stainless steel mesh hanging below the piston in steam atmosphere with the 'reservoir' only half filled with water during the whole process. Therefore the water, which was released from the coal and has dripped from the mesh during shrinkage and thermal dewatering, can not be reabsorbed during thermal treatment and cooling. In a second set of experiments the coal bag is kept under water only during the thermal treatment and lifted to the steam atmosphere for the cooling phase (hydrothermal dewatering).

Dry coal compression   To quantify the influence of temperature on the consolidation and shrinkage of the coal, some constant rate consolidation experiments are also carried out with dried lignite in nitrogen atmosphere at temperatures up to 235°C.

Permeability measurement   Furthermore the pressure drop at constant flow rate is measured for this lignite during steady state flows applied by a high pressure pump (up to 16 MPa). According to DARCYS-law [Dar56, Sch74] the permeability

$$K = \frac{\mu_\ell}{\Delta p_\ell} H u_{\mathrm{D}} = \frac{\mu_\ell}{\Delta p_\ell} H u \varepsilon \tag{3.1}$$

is calculated from the pressure difference Δp_ℓ and the DARCY velocity u_{D} (velocity of the fluid before entering the porous medium) or the pore velocity u. H is the filling height, μ_ℓ the dynamic viscosity of the liquid and ε the porosity.

3.1.2 Moisture content

The moisture content was determined based on a method similar to the DIN 51718 standard [DIN02]. Since the shrinkage behaviour of samples was investigated, the whole pellets were dried in an air atmosphere at 105°C for 48 hours to ensure complete moisture removal. The oven dried MTE products were subsequently used for helium density and mercury intrusion porosimetry experiments.

3.1.3 Helium density

The helium density of the coal ϱ_{He}, is determined by helium pycnometry using an AccuPyc 1330 (Micromeritics, Norcorss, GA, USA) Pycnometer. The unit is calibrated on a daily basis and measurements were carried out on oven dried 1.5 to 2.5 g subsamples. Prior to taking measurements, samples are purged with helium 99 times to ensure complete removal of adsorbed gases. The helium density is determined from an average of ten measurements.

3.1.4 Mercury intrusion porosimetry

Pore size measurements are obtained by mercury porosimetry, using an AUTOPORE II 9220 mercury porosimeter (Micromeritics). The instrument is capable of applying pressures p between 3.4 kPa and 414 MPa, which, according to the Washburn equation [WO97]

$$p = -\frac{2\sigma \cos \Theta}{r} = -\frac{4\sigma \cos \Theta}{d} \tag{3.2}$$

equates to a pore size range of 0.0036 to 437 μm diameter d at a surface tension σ of 0.485 Nm^{-1} and a contact angle Θ of 140°. r is the pore radius. Experiments are carried out in calibrated powder and solid penetrometers with a volume of 3 cm^3 using about 0.5 g oven dried MTE product with a particle diameter of 2 to 10 mm. All experimental data are corrected for mercury compressibility and penetrometer deformation by subtracting the intruded volume of blank runs with empty penetrometers.

All results are expressed on the basis of volumes per gram of dry coal (db.) or on a dry and ash free basis (daf.). During the course of an experiment, both the intruded and extruded mercury volumes (V_i [cm^3], v_i [cm^3/g]) are determined. This allows to determine the compressibility κ of the coal matrix from the slopes of either a cumulative intrusion volume versus intrusion (compression) pressure graph, or from a cumulative extrusion volume versus extrusion (decompression) pressure graph.

$$\kappa = -\frac{1}{V}\frac{\partial V}{\partial p}\Big|_T = \varrho_{\text{He}}\frac{\partial V_{\text{mercury}}/m_{\text{sample}}}{\partial p}\Big|_T = \varrho_{\text{He}}\frac{\partial v_{\text{mercury}}}{\partial p}\Big|_T \ . \tag{3.3}$$

For reasons described in more detail in Section 3.3.2, the compressibility correction for the coal matrix is based on the slope of the extrusion, rather than intrusion data.

$$v_i^{\text{corrected}} = v_i - \frac{\kappa}{\varrho_{\text{He}}}p_i \ . \tag{3.4}$$

The extrusion is measured down to at least 0.21 MPa (corresponding to a pore diameter of 7 µm), up to which point the extrusion curve is parallel to the intrusion curve. The percentage of retained mercury upon extrusion R [%] can therefore be calculated via the following relationship:

$$R = \frac{V_{7\mu\text{m}}^{\text{extrusion}} - V_{7\mu\text{m}}^{\text{intrusion}}}{V_{0.0036\mu\text{m}}^{\text{intrusion}} - V_{7\mu\text{m}}^{\text{intrusion}}} \ . \tag{3.5}$$

The inter/intra particle boundary is taken as 50 µm. The macro and mesopore volumes (V_{macro}, V_{meso} [cm^3] or v_{macro}, v_{meso} [cm^3/g]) are taken as the total volumes with diameters ranging between 0.05 and 50 µm and 0.0036 and 0.05 µm respectively. The micropore volume (v_{micro}) is calculated from skeletal density (calculated from maximum mercury intrusion after compressibility correction) and He density (Figure 3.29, page 41).

$$v_{\text{micro}} = \frac{1}{\varrho_{\text{skeletal}}} - \frac{1}{\varrho_{\text{He}}} \ . \tag{3.6}$$

Intrusion volumes expressed on a dry and ash free basis are calculated based on the mean values of the ash content and helium densities (Table 3.2). The density of the mineral matter is taken as 2.7 g/cm^3 [GNWJ72].

Table 3.2: Ash content and He density of MTE samples

Provenance	Germany	Greece	Australia	
	Rhineland	Ptolemais	Latrobe Valley	
Open cut	Hambach		Loy Yang	
ash [wt.% db.]	6.3	14.1	1	
He denstity [g/cm^3] db.	1.444	1.517	1.407	db.: dry basis

Pore size distributions are calculated from the compressibility corrected intrusion data as logarithmic differential intrusions

$$LDI = \frac{v_{i+1} - v_i}{\log d_i - \log d_{i+1}} \tag{3.7}$$

after interpolating the 240 experimental data points to 80 diameters which are equally spaced in the logarithmic scale. From the corrected MIP data also specific surface area A (from the work of wetting)

$$A = -\frac{\sum_{d_i=50\mu\text{m}}^{d_i=0.0036\mu\text{m}} p_i\,\Delta V_i}{\sigma\cos\Theta}\frac{1}{m_{\text{sample}}} \tag{3.8}$$

and the mean pore diameter $d_{\text{mean}}^{\text{volume}}$ (by volume)

$$d_{\text{mean}}^{\text{volume}} = d(V = \frac{1}{2} \sum_{d_i=50\,\mu\text{m}}^{d_i=0.0036\,\mu\text{m}} V_i) \tag{3.9}$$

are calculated. To avoid errors introduced by inter-particle void space filling at the beginning of an MIP experiment, the surface area and mean pore diameter calculations according to Eqs. (3.8) and (3.9) are based on intrusion data collected in the macro- and mesopore size regions.

3.1.5   Pore volume and shrinkage

During MTE experiments the pore volume of both wet and oven dried MTE filter cakes is determined. This allows the characterisation of the effect of MTE and oven drying on pellet shrinkage. The pore volume of wet MTE filter cakes $V_{\text{pore}}^{\text{wet pellet}}$ is calculated from the difference between the total pellet volume (determined from calliper measurements) and the volume occupied by the coal, such that

$$V_{\text{pore}}^{\text{wet pellet}} = \frac{\pi}{4} D_{\text{wet}}^2 H_{\text{wet}} - \frac{m_{\text{coal}}}{\varrho_{\text{He}}} = V_{\text{water}} + V_{\text{gas}} , \tag{3.10}$$

where D_{wet} and H_{wet} represent the diameter and height of the wet pellet, and m_{coal} and ϱ_{He} the mass and helium density of the dry coal respectively. It should be pointed out, that while the pores are predominantly filled with water, V_{water}, they contain a small amount of gas, V_{gas}, which is produced during thermal dewatering. In addition, a small amount of gas (i.e. air) is introduced when the pellet expands upon release of the applied pressure after the MTE process [HBCS04].

The pore volume of oven dried MTE products, $V_{\text{pore}}^{\text{dry pellet}}$, is determined from the mercury intrusion experiment as sum of macro, meso and micropore volume. Additionally the dry pore volume is determined from the difference between the total dry pellet volume (determined from calliper measurements) and the volume occupied by coal, such that

$$V_{\text{pore}}^{\text{dry pellet}} = \frac{\pi}{4} D_{\text{dry}}^2 H_{\text{dry}} - \frac{m_{\text{coal}}}{\varrho_{\text{He}}} , \tag{3.11}$$

where D_{dry} and H_{dry} represent the diameter and height of the dry pellet. The pellet shrinkage is thus determined from the difference between the wet and dry pore volumes.

3.1.6   Water uptake measurements and equilibrium moisture content

To mimic the water uptake of MTE pellets under ambient conditions, samples are exposed to a constant relative humidity of 52 %. As the samples have previously been oven dried for the exact determination of shrinkage, water content and mass loss, the MTE pellets are initially re-hydrated in an atmosphere of 100 % relative humidity. This is achieved by placing samples inside a partially water filled and evacuated desiccator for 73 days. Samples are then exposed to a relative humidity of 52 %, which is created inside an evacuated desiccator using a saturated $Mg(NO_3)_2 \cdot 6H_2O$ solution kept at 30°C. A constant solution temperature is maintained by storing the desiccators in a constant temperature incubator. After completion of the experiment (14 days), the samples are removed and their equilibrium moisture content (EMC) is determined.

3.1.7   Surface area and micropore volume

Surface area and micropore volume measurements are determined by CO_2 adsorption at 0°C using a Coulter Omnisorp 360 CX analyser. Experiments are carried out on oven-dried 0.3 g sub-samples, which are further dried under vacuum at 105°C for 12 hours to ensure complete drying and removal

of adsorbed gases. CO_2 surface areas and micropore volumes (pores $< 2\,\mathrm{nm}$ diameter) are calculated using the DUBININ-RADUSHKEVITCH [Dub66, DIN01] equation

$$W_\mathrm{a} = W_0 \exp\left[-\left(\frac{R\,T}{\beta\,E_0}\right)^2 \left(\frac{p_0}{p}\right)^2\right]\,, \tag{3.12}$$

where W_a [cm^3 S.T.P] is the CO_2 adsorbed in the micropore structure at a relative pressure p/p_0, W_0 the limiting micropore volume. E_0 is a characteristic energy of adsorption for the reference vapour and β is the affinity coefficient, which has a value of unity when the adsorptive is the reference vapour, R the universal gas constant and T the absolute temperature.

3.1.8 Differential Thermal Analysis

Differential Thermal Analysis (DTA) is carried out with simultaneous Thermogravimetric Analysis (TGA) on a Setaram TAG24 Thermobalance. Tests were carried out on $8\,\mathrm{mg}$ samples with a heating rate of $5°\mathrm{C/min}$ and an air flow rate of $50\,\mathrm{cm}^3/\mathrm{min}$. Measurements with a particle size of less than $63\,\mu\mathrm{m}$ were carried out on air dried samples. During the tests samples were heated to $650°\mathrm{C}$ before being cooled down again. An Al_2O_3 crucible was used as a reference. Results are corrected by blank tests with empty crucibles.

3.1.9 Chemical Analysis

Chemical fractioning $5\,\mathrm{g}$ of each coal in raw condition is mixed with $50\,\mathrm{ml}$ of fully desalted water (determination of water soluble fractions), $50\,\mathrm{ml}$ of a 1.5-molar solution of ammonium acetate (organic fraction) or $50\,\mathrm{ml}$ of a 1-molar hydrochloric acid (acid-soluble fraction) and is shaken at least 24 hours at ambient temperature. Afterwards the liquid is separated from the coal by vacuum filtration, the solids are discarded and the residual liquid is diluted for concentration measuring by atom absorption spectrophotometry (AAS).

Equilibrium leaching experiments Different concentrations of lignite in water are prepared and stored for 24 hours in stainless steel pressure vessels at $25°\mathrm{C}$, $115°\mathrm{C}$ and $200°\mathrm{C}$ respectively. After this time the vessels are cooled down to ambient temperature, the solids are separated from the liquid by vacuum filtration and the liquid fraction is analysed for cations by AAS.

Acid exctractable metals in dry MTE samples Acid extractable metals Al, Fe, Ca, Mg and Na in dried MTE products were determined by HRL Technology Pty. Ltd. (Melbourne) by a method based on Australian Standard AS 2434.9 [AS200]: An oven dried coal sample ($105°\mathrm{C/N_2}$) is wetted with ethanol and a solution of $0.003\,\mathrm{M}$ H_2SO_4 is added to the mixture which is then brought to boil, allowed to simmer uncovered for $15\,\mathrm{min}$ and covered (with a watch glass) for a further $45\,\mathrm{min}$. The mixture is then filtered and the filter cake is washed with more hot $0.003\,\mathrm{M}$ H_2SO_4. The Al, Fe, Mg, Ca and Na contents of the filtrate are determined by AAS.

Ultimate and proximate analysis of MTE samples The analysis of dry MTE samples and the corresponding raw coals was done by HRL Technology Pty. Ltd. (Melbourne). Carbon, hydrogen and nitrogen levels were determined on a Leco CHN600 analyser, while ash yields were measured on a Leco MAC400 analyser. Total sulphur and chlorine levels were determined using an inductively-coupled plasma-optical emission spectrometer (ICP-OES). Total Al, Fe, Ca, Mg, Na and Si concentrations present in the ash were determined by a borate fusion/ICP-OES method. Acid extractable species including Al, Fe, Ca, Mg and Na were measured by AAS.

Additional ash analysis was done by Rheinbraun and EON Engineering. The ash for these tests was produced in a muffle furnace at $575°\mathrm{C}$.

3.2 Dewatering

Mechanical dewatering of porous materials is a time dependent volume reducing process. Generally three phases occur (Figure 3.2). During the initial consolidation the gas filled pore volume is instantly reduced by the external pressure. This stage can be neglected in the present case, since the pore volume of brown coal is completely filled with water [GA71].
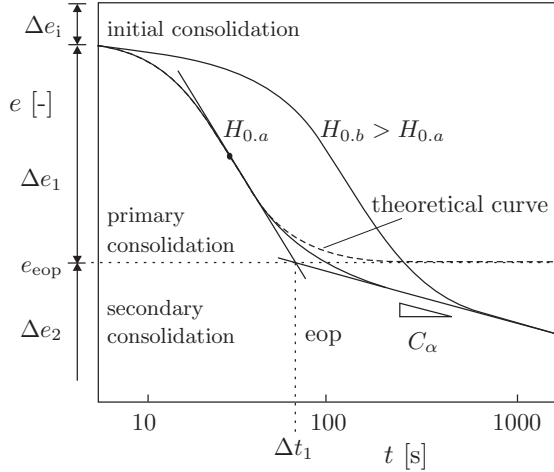
Figure 3.2: Decrease in void ratio e during consolidation [LW79a]
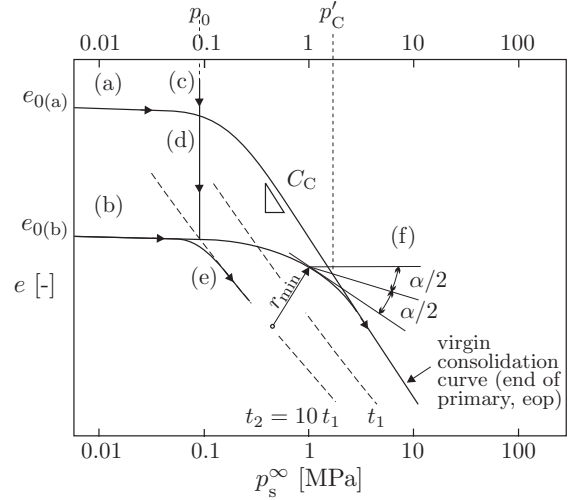
Figure 3.3: Decrease in void ratio due to primary consolidation (a,b,e) and creep (c,d) [LW79a]. Determination of the preconsolidation pressure (f) according to [Cas36].

During the primary consolidation, which is traditionally described by the TERZAGHI theory [LW79a, Ter25] (theoretical curve in Figure 3.2), the excess pore pressure p_ℓ (pressure of the water flowing out) decreases while the effective pressure p_s^∞ carried by the solid skeleton increases (Figure 3.4). This stage is completed when the excess pore pressure has vanished everywhere in the porous structure.

During the consolidation of soft soils like clay and lignite the secondary consolidation can be observed as a third phase. BUISMAN [Bui36] was the first who investigated this 'creep' phase. Generally a linear relationship between the void ratio[2] e and the logarithm of time t is found during the consolidation of soft soils. For consolidation pressures lower than the apparent preconsolidation pressure p_C' of the respective materials 'creep' is the dominating parameter in consolidation kinetics.

p_C' results from the geological history (time, temperature, overburden (geological) pressure p_g, chemical and biological environment) and can only be determined experimentally as shown in Figure 3.3. The diagram shows the relationship of void ratio e and effective pressure p_s^∞ at the end

---

[2]$e = \varepsilon/(1-\varepsilon)$, ε is the porosity
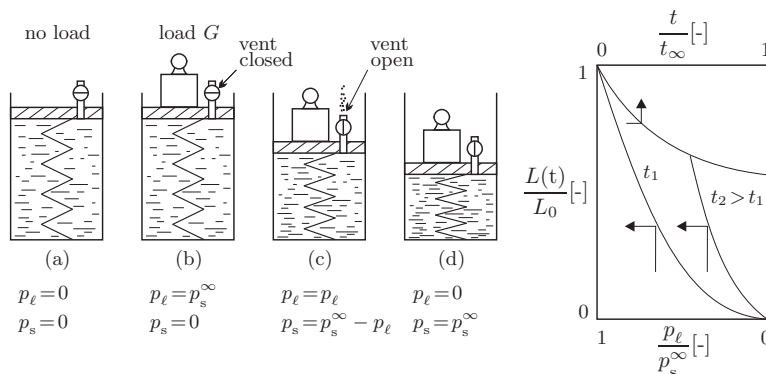
Figure 3.4: TERZAGHI model of the primary consolidation and pressure distribution inside the solid [TP61, SMI86].

of the primary consolidation for low (a) and high (b) preconsolidated materials which are subjected to rising pressure (a,b,e) or creep under constant geological pressure (c,d). The determination of the preconsolidation pressure (f) according to CASAGRANDE [Cas36], which is suitable for lignite too [Ana82], is also shown in the figure.

For pressures higher than p'_{C} the consolidation velocity $\dot{e}$ is limited by the pressure drop of the water flowing inside the coal's macro structure during the primary consolidation.

In the following the creep and consolidation phases will be investigated in detail for the three coals from Australia, Greece and Germany and a model will be developed for the description of both consolidation stages including the effects of initial layer height, temperature and consolidation pressure on the time dependent void-ratio e [Ber03, Ber04]. It will be shown, that for lignites with low preconsolidation pressures, high water contents and low permeabilities especially the influence of the coal layer height on the kinetics of the dewatering process has an important impact on the process parameters, which have to be chosen for the technical implementation of the process while the influence of the coal layer height can be neglected for highly preconsolidated coals. The creep phase will be investigated first since then its influence on the primary consolidation can be accounted for in the development of a model for both phases (Chapter 3.2.3).

3.2.1   Creep of lignite

In Figure 3.5 the water content wet basis (w) and dry basis (W) during mechanical/thermal dewatering at different temperatures is plotted versus time in a semi logarithmic scale for a consolidation pressure p_{s}^{∞} of 5 MPa. According to soil mechanics a straight line (as for all experiments with German lignite) is characteristic for long term creep or 'secondary consolidation'. Deviations from this straight line can only be observed for the lignites from Greece and Australia for the first 500 s of mechanical expression at lower temperatures. During this time of 'primary consolidation' the expression rate is limited by the pressure loss Δp_{ℓ} of the water flowing out. In this stage Δp_{ℓ} decreases continuously, while the pressure load on the solid matrix increases with time. The 'primary consolidation' only takes place for consolidation pressures, that are significantly higher than the apparent preconsolidation pressure p'_{C} of the coal. This condition is only true for the coals from Greece and Australia but not for the German lignite which is from a very deep open cut (340 m).

Nevertheless, even if a primary consolidation period is found in the experiments it is very short compared to observations of other researchers [Ros63] who measured values between 1 000 s and 10 000 s. This is due to the fact, that they used solid samples with a lower porosity and permeability than the crushed coal used in the experiments presented here. Once the coal is crushed, additional larger channels and fractures between the individual particles are present for the water removal during compression.
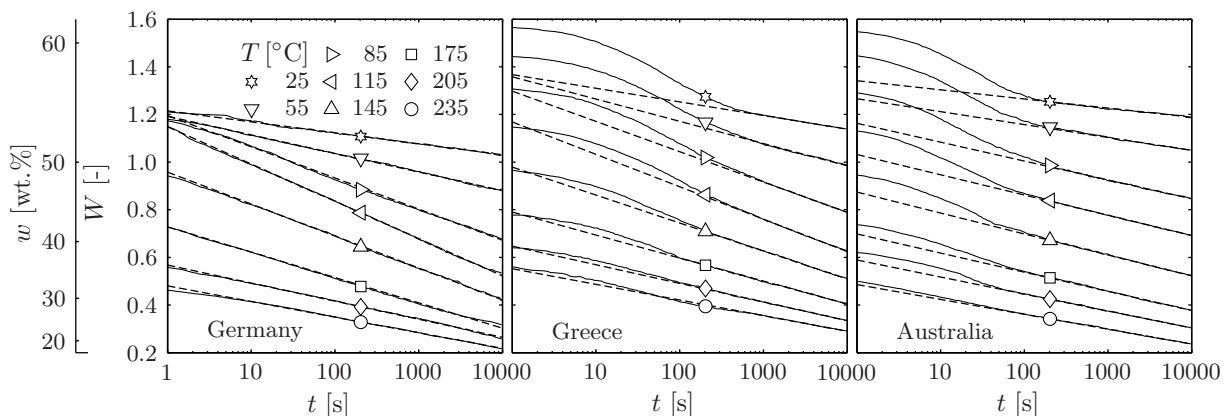
Figure 3.5: Time dependent water content during mechanical/thermal dewatering of the three coal samples at 5MPa pressure. ($-$) experimental ($-$ $-$) regression for creep.
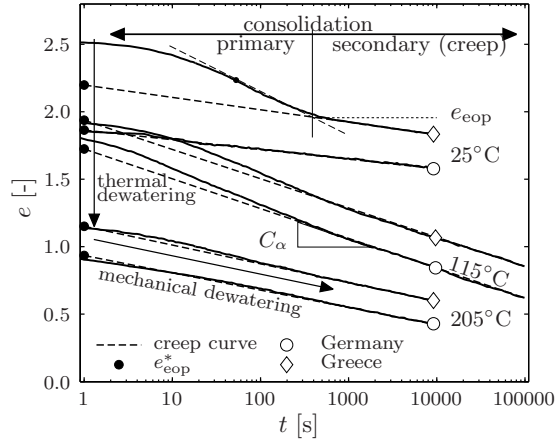
Figure 3.6: Determination of creep curve and constants. p_{s}^{∞}=5MPa for all experiments
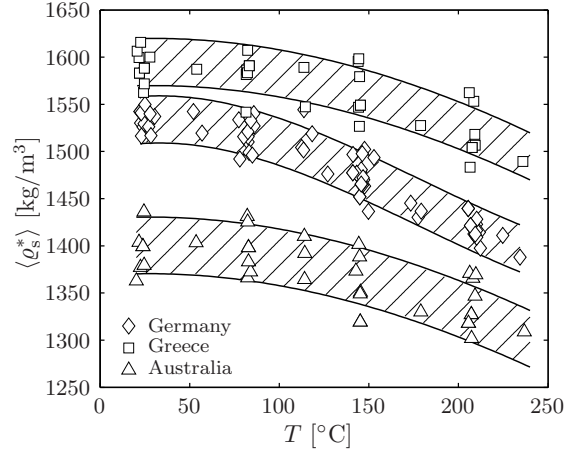
Figure 3.7: Densities calculated from experiments

The 'void ratio' $e = W\varrho_{\mathrm{s}}/\varrho_{\mathrm{w}}$ (ratio of pore volume and solid volume, ϱ_{s} and ϱ_{w} are the densities of the solid phase and water) is a more common variable for the description of consolidation processes. In Figure 3.6 the void ratio e is shown for two coals and three temperatures as a function of time in a semi logarithmic scale. The mean solid densities $\langle\varrho_{\mathrm{s}}^{*}\rangle$ for each coal sample were determined from water content and volume balance of the compressed coal at the end of the experiment (see Figure 3.7). Of course the pore space contains some gases from the thermal decomposition at higher temperatures [Ber01, HBCS04] and it also has to be mentioned that the values are higher than the He and MIP densities of dried products given later (Figure 3.29, page 41). Due to several uncertainties in the determination of densities from dried lignite samples (discussed in Chapter 3.3) the values given in Figure 3.7 are thought to be more reliable for the description of the mixed coal and ash density of wet MTE pellets and therefore these values are used for the calculation of the water filled pore space which is the main variable during the investigation of the dewatering and consolidation process.

From the results shown in Figure 3.6 the void ratio e_{eop} at the end of the primary consolidation can be determined with two tangents on the primary and secondary consolidation branches. Due to variations in permeability and height of the initial coal filling, the times for primary consolidation and therefore also the value of e_{eop} vary depending on the experimental conditions. For this reason the value e_{eop}^{*} which can easily be determined by regression with

$$e(t, T, p_{\mathrm{s}}) = e_{\mathrm{eop}}^{*}(T, p_{\mathrm{s}}) - C_{\alpha}(T, p_{\mathrm{s}}) \log(t/[\mathrm{s}]) \tag{3.13}$$

is used instead. Since e_{eop}^{*} is linearly extrapolated to t=1s it is a characteristic value for all experiments and independent of the height dependent course of primary consolidation. In Eq. (3.13) C_{α} represents the slope in the semi logarithmic plot. This parameter is a measure for the velocity of consolidation and is called 'coefficient of secondary consolidation' or 'creep coefficient'.

Below 145°C Figure 3.5 and 3.6 show a nearly constant e_{eop}^{*} while C_{α} increases (see also Figure 3.8, I), especially in case of the German lignite. From the increase in creep velocity an energy of activation for the creep can be determined (dashed line from Eq. (3.19), discussed on page 23).

At higher temperatures e_{eop}^{*} decreases as a result of the 'thermal dewatering' during heating and also C_{α} decreases (Figure 3.8, II). In this stage the colloidal structure of the coal is partially destroyed and the water is released from the coal structure without additional forces [ME72]. Figure 3.8 also includes the results for the other two coals (b) and the variation of C_{α} with pressure (c)-(e). In all cases C_{α} first increases with rising temperature (I) or pressure (III) due to the higher mobility or force applied to the process and stagnates or decreases at high temperatures (II) and high pressures (IV) due to the simultaneous decrease of the void ratio.
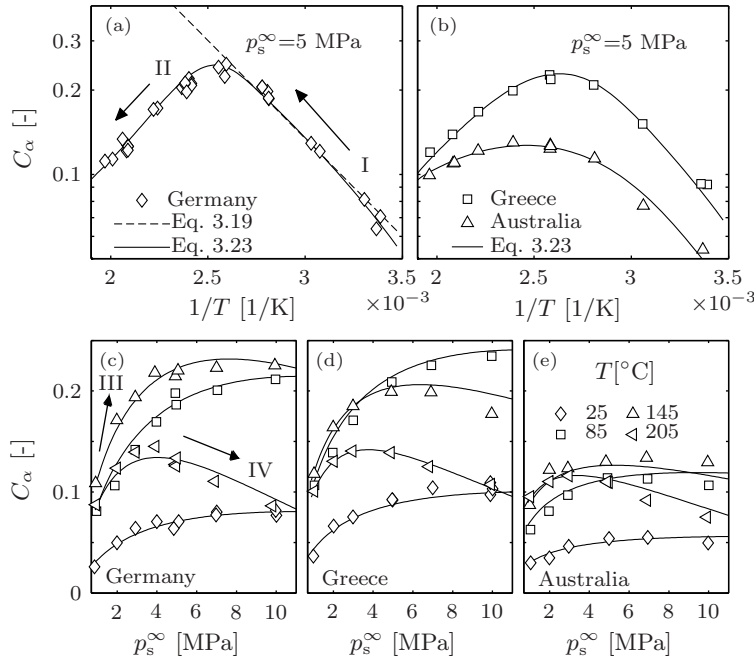
Figure 3.8:
Variation of the creep coefficient
with temperature and pressure

Consolidation at ambient temperature   The pressure dependence of the void ratio e^*_{eop} and water content W^*_{eop} can be compared to literature data [NJ56, Ros63] only for the measurements at ambient temperature, since to the author's knowledge no similar experiments on the creep of lignite at elevated temperature have been done before. The work of GUO [Guo00, GTU03] only provides short compression times which can not ensure, that the secondary consolidation phase has already been reached. This may explain his conclusion that the creep constant (defined by the TERZAGHI-VOIGT model [SMI86], Figure 3.14, page 27) is 'virtually constant', independent of p^∞_{s} and T.

The comparison with data from NEUMANN and JACOB [NJ56] for German coal (a) and ROSENGREN [Ros63] for Australian coal from the Latrobe valley (b) is shown in Figure 3.9. Since these authors obtained their results from long term consolidation tests (Neumann: 24 h, Rosengren: 7 days) the values measured here have to be compared with a corrected 'virgin consolidation curve'. The correction

$$\Delta W = C_\alpha \frac{\varrho_{\mathrm{w}}}{\varrho_{\mathrm{s}}} \log \frac{t_{\max}/[\mathrm{s}]}{1\,\mathrm{s}/[\mathrm{s}]}. \tag{3.14}$$
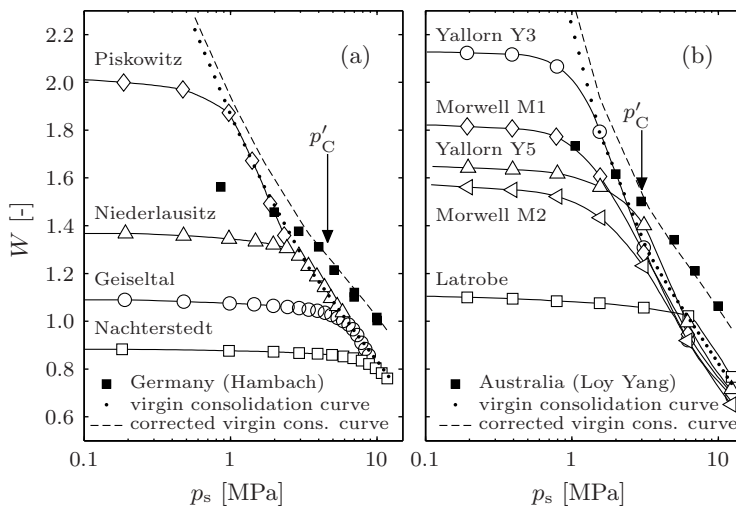
Figure 3.9:
Comparison of experimental re-
sults (25°C, W^*_{eop}) with data
from literature [NJ56, Ros63]
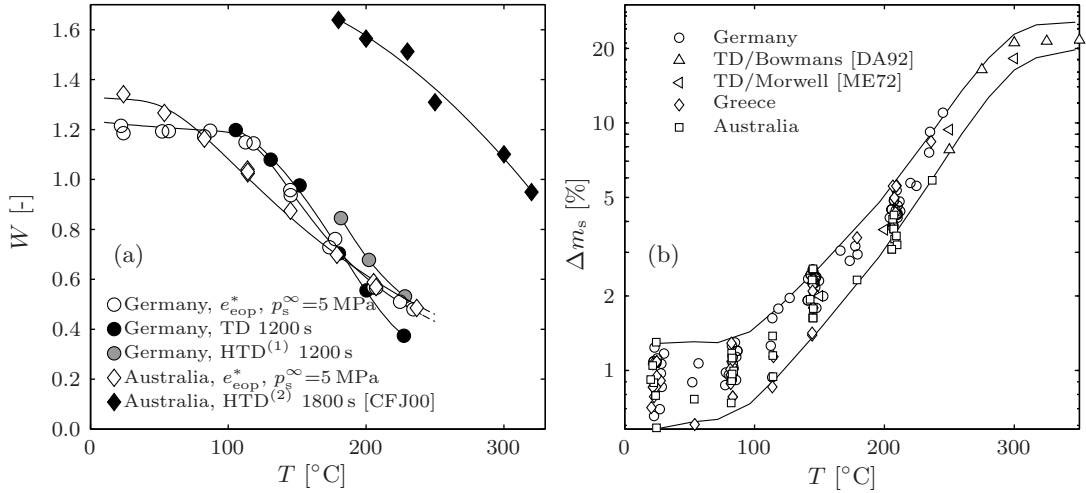
Figure 3.10: (a) Comparison of thermal TD, hydro-thermal HTD and mechanical/thermal (MTE) dewatering at elevated temperature, (b) mass loss of dry solid Δm_s due to thermal decomposition.

can be calculated from the literature data using the secondary consolidation coefficient shown in Figure 3.8 assuming that the creep coefficient is of the same order of magnitude.

The measured values for lignites from Hambach and Loy Yang start at higher values of the water content compared to the raw coal because crushed coal is used in this work instead of solid samples like in the experiments in literature. Nevertheless it can be observed, that at higher pressures the measured curves are identical with the corrected virgin consolidation curve. From the intersection of the corrected virgin consolidation curve and experimental data the apparent preconsolidation pressure p'_C of the coals can be estimated to 4.5 MPa for the Hambach coal and 3 MPa for Loy Yang coal. A comparison of the experiments for Greek coal with data from KAVVADAS et al. [KPK94] and ANAGNOSTOPOULOS [Ana82] also results in a value of 3 MPa.

Thermal dewatering   The decrease in water content due to thermal dewatering can also be obtained from separate experiments, if lignite is treated in steam or water atmosphere under pressure. The results of these experiments performed with German and Australian [CFJ00] lignite are shown in Figure 3.10a. For comparison, the water content W^*_{eop} from consolidation at 5 MPa pressure is additionally depicted in this figure. Since this pressure is only slightly above the apparent preconsolidation pressure p'_C of German lignite, in the beginning of consolidation no dewatering takes place. Only the pore space, which is additionally created during the grinding, is closed. Therefore a good agreement between mechanical/thermal and thermal dewatering can be observed up to 150°C. The deviation at higher temperatures results from the difference in both processes. The thermal dewatering is done in steam atmosphere – as in the original FLEISSNER process [Fle26] – where the gases resulting from decomposition can drive out additional water easily. In contrast to that the mechanical dewatering experiments are performed with water filled samples. Therefore the coal can reabsorb the water which was expelled during heating, when the decomposition is completed after the process temperature is reached [ME72]. This is also in good agreement with the mass loss of dry substance, which increases from 2 % at 150°C to 10 % at 250°C due to the rising thermal decomposition (Figure 3.10b).

During hydrothermal dewatering the coal is heated in water and cooled down either in steam atmosphere according to the experimental procedure described by MURRAY and EVANS [ME72] and BERGINS [Ber01] or also cooled in water. Cooling in steam atmosphere – as during the Viag process [Wir52] – results in slightly increased water contents (Figure 3.10a, German coal, HTD$^{(1)}$). Heating and cooling under water as during hydrothermal dewatering (Figure 3.10a, Australian coal, HTD$^{(2)}$) [AA95, CFJ00, FJM03] leads to an significant increase in residual water content since water can be reabsorbed during cooling and also additional water on the surface of small

coal particles and in larger cracks can not be separated sufficiently from the mixture after thermal treatment.

3.2.2 Creep kinetics

In order to describe the influence of time, temperature and pressure on the creep process a new semi-heuristic model was developed. This approach covers both the physics of flow-processes by the application of rate process theory for the secondary consolidation coefficient C_α and the complex behaviour of porous media by the heuristic description of the temperature and pressure dependency of the void ratio after primary consolidation e^*_{eop}.

According to rate process theory [GLE41, Eyr36] the activation energy for flow-processes can be calculated from

$$\Delta u = \frac{2\,k\,T\,\lambda}{h}\exp\left(-\frac{\Delta G}{RT}\right)\sinh\left(\frac{\frac{1}{2}\tau\lambda^3}{kT}\right). \tag{3.15}$$

In this equation Δu is the velocity of a volume λ^3 at a temperature T and a shear stress τ. k is Boltzmann's constant and h Planck's constant. ΔG is the free energy of activation for the flow process, see Figure 3.11. If the energy supplied by shear stress is small compared to the thermal energy $2kT \gg \tau\lambda^3$, which is true especially for small particles and dimensions ($\sim 10^{-10}$m) Eq. (3.15) can be simplified by approximating $\sinh\left(\frac{\tau\lambda^3}{2kT}\right) \approx \left(\frac{\tau\lambda^3}{2kT}\right)$:

$$\Delta u = \frac{\tau\,\lambda^4}{h}\exp\left(-\frac{\Delta G}{RT}\right). \tag{3.16}$$

For fluids the term λ^3 can be obtained from the quotient of molar volume V_M and Avogadro's constant N. Furthermore the relation between velocity Δu, which is proportional to the time derivative of void ratio $\dot{e}$ or height $\dot{L}$ of the material in consolidation, and the viscosity of the liquid phase μ_ℓ is given as

$$\Delta u = \frac{\tau\,\lambda}{\mu_\ell} \sim -\dot{e} \sim -\dot{L}\,. \tag{3.17}$$

Since strong hydrogen bonds exist in fluids like water, the free energy of activation is not temperature-independent. Especially at low temperatures the hydrogen bonds restrict the molec-
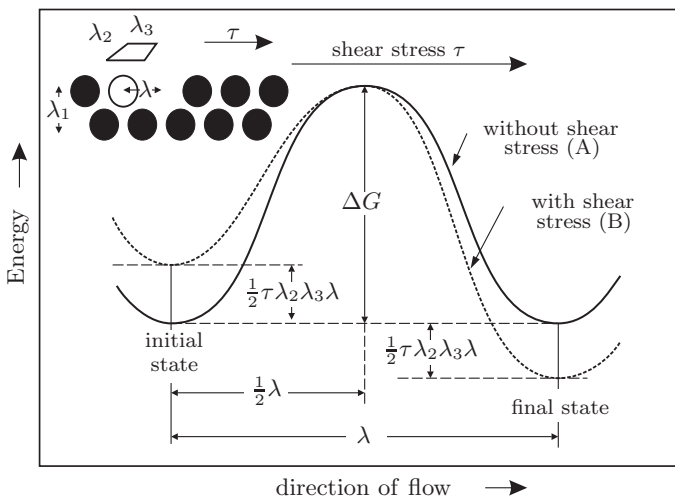
Figure 3.11:
Potential-energy barrier for viscous flow [GLE41, MCS68]

ular mobility which leads to higher activation energies. Inserting Eq. (3.17) in (3.16) and differentiating leads to

$$\Delta G_{\mathrm{w}} = +R \, \frac{1}{T_2 - T_1} \int_{T_1}^{T_2} \frac{\partial \ln(\mu_{\mathrm{w}} V_{\mathrm{M}})}{\partial(1/T)} \, \mathrm{d}T = 13.2 \, \mathrm{kJ/mol}. \tag{3.18}$$

for the *mean* activation energy for water between 25 and 120°C. Precise viscosities and densities according to the IAPWS-IF97 steam table [WCD$^+$00] were used for the calculation of ΔG_{w}.

Creep coefficient The determination of activation energies from the experiments requires the comparison of dewatering velocities at process times revealing 'similar' porous structures. For this reason only the experiments for German coal between 25 and 120°C were used since the starting point e_{eop}^* is identical for all experiments at 5 MPa pressure. Using

$$\left. \frac{\partial \ln(-\dot{e}/T)}{\partial(1/T)} \right|_{e=\mathrm{const}} = -\frac{\Delta G_{\mathrm{exp}}}{R} \tag{3.19}$$

and the time derivative of Eq. (3.13)

$$\dot{e} = -\frac{C_\alpha(T)}{t} \frac{1}{\ln 10} \tag{3.20}$$

with $t=1$ s an activation energy of 13.4 kJ/mol is found. Eq. (3.19) is drawn as a dashed line in Figure 3.8a and shows excellent agreement with the experiments. From this and the good agreement of the theoretical and experimental activation energies it can be concluded that the pressure drop of the water-outflow from smallest pores within the micro-porous structure of the lignite particles is the time dominating mechanism during creep. With respect to temperature the parameter C_α should therefore be inversely proportional to the viscosity of water.

$$C_\alpha(T) \sim 1/\mu_{\mathrm{w}}(T) \,. \tag{3.21}$$

Regarding pressure it is known from literature, that C_α first increases with rising p_{s}^∞ for highly precompressed materials [Ana82]. This is in accordance with rate process theory, see Eq. (3.17) and (3.20). Since the decrease in void ratio with increasing pressure also leads to smaller capillaries inside the porous structure, C_α decreases, if the compression force is higher than the preconsolidation pressure p_{C}'. This was also found in experiments from [Mes73, MSAC97, AM73]. In the current investigation both effects are covered by

$$C_\alpha(T, p_{\mathrm{s}}) \sim p_{\mathrm{s}}^{C_1} \, e_{\mathrm{eop}}^*(T, p_{\mathrm{s}})^{C_2} \,, \tag{3.22}$$

where e_{eop} is replaced by e_{eop}^*, which is independent of the initial coal filling level. As a consequence the increase of C_α with increasing temperature, pressure and void ratio can be described as

$$C_\alpha(T, p_{\mathrm{s}}) = \frac{\mu_{\mathrm{w}}(25°\mathrm{C})}{\mu_{\mathrm{w}}(T)} \left(\frac{p_{\mathrm{s}}/[\mathrm{MPa}]}{p_0} \right)^{C_1} e_{\mathrm{eop}}^*(T, p_{\mathrm{s}})^{C_2} \,, \tag{3.23}$$

with $\mu_{\mathrm{w}}(25°\mathrm{C})$ and p_0 as normalization constants.

Void ratio   To complete the description of the creep process with Eq. (3.13), also e^*_{eop} has to be expressed as a function of pressure and temperature (Eq. (3.24)). In Figure 3.9 the semilogarithmic plot shows a straight line, at least for pressures above the apparent preconsolidation pressure p'_{C}. Therefore the expression $C_4 \log(p_{\mathrm{s}}/[\mathrm{MPa}] + C_{\Delta\mathrm{p}})$ describes the consolidiation in the whole pressure range. The additional constant $C_{\Delta\mathrm{p}}$ takes the precompression into account. Due to the shrinkage and thermal dewatering the variation of e^*_{eop} with temperature is more complicated. The thermal dewatering starts at different temperatures (see Figure 3.13) depending on the geological history of the coals and also includes the effect of thermal decomposition at higher temperatures. For this reason, based on the experimental results the heuristic formulation

$$e^*_{\mathrm{eop}}(T, p_{\mathrm{s}}) = C_3 - C_4 \log\left(\frac{p_{\mathrm{s}}}{[\mathrm{MPa}]} + C_{\Delta\mathrm{p}}\right) + C_5 \exp\left(\frac{-C_6}{(T/[^\circ\mathrm{C}] - C_7)^{C_8}}\right) \tag{3.24}$$

is used. The constants of Eqs. (3.23) and (3.24) have been determined from the experimental data by multidimensional regression and are listed in Table 3.3. The table also includes the constants of the regression function

$$\langle \varrho^*_{\mathrm{s}} \rangle = C_a\, T^3 + C_b\, T^2 + C_c\, T + C_d \tag{3.25}$$

for the description of the mean solid density $\langle \varrho^*_{\mathrm{s}} \rangle$ $[\mathrm{kg/m^3}]$ from Figure 3.7 as a function of temperature T $[^\circ\mathrm{C}]$, which is used for the conversion between water content W (db.) and void ratio e with $e = W \varrho_{\mathrm{s}}/\varrho_{\mathrm{w}}$.

For all three coals the different constants are of the same order of magnitude. Of course they cannot be identical due to the complex process of consolidation, the differences in ash content and geological history. Nevertheless the model gives the opportunity for quantitative investigations of consolidation and consolidation kinetics.

Equilibrium of dewatering   Even if in the experiments an equilibrium is not reached[3], the linear decrease of the water content as a function of time in the semi logarithmic scale and the increase of C_α with temperature indicate, that a rise in temperature not only leads to an increase of the creep velocity at the beginning of consolidation but also increases the amount of water that can be removed at all. There are at least two reasons that support this assumption:

---

[3]Investigating lignite DULHUNTY [Dul60] measured a time of about 750h for 98% of the equilibrium response to the given force. ROSENGREN found the linear course of e in the logarithmic timescale even after 7 days of compression [Ros63].

Table 3.3: Model constants determined by the regression analysis shown in Figure 3.13

Provenance	Germany	Greece	Australia
C_1	0.7757	0.7639	0.5848
C_2	1.9489	2.3174	1.6020
p_0	739.73	1336.3	4489.5
C_3	3.3620	3.4598	2.9508
C_4	1.6617	1.4929	1.3368
$C_{\Delta\mathrm{p}}$	2.8397	1.9196	1.5332
C_5 for $T>C_7$	-1.5271	-2.0184	-2.2147
otherwise C_5	0	-	-
C_6	22543	9392.4	454.37
C_7	51.017	0	0
C_8	2.1198	1.7923	1.1774
C_a	1.4522e-5	-2.2811e-6	6.5457e-7
C_b	-7.7932e-3	-1.0610e-3	-1.8666e-3
C_c	4.8242e-1	-8.8068e-2	-3.5050e-2
C_d	1.5247e+3	1.6072e+3	1.4061e+3
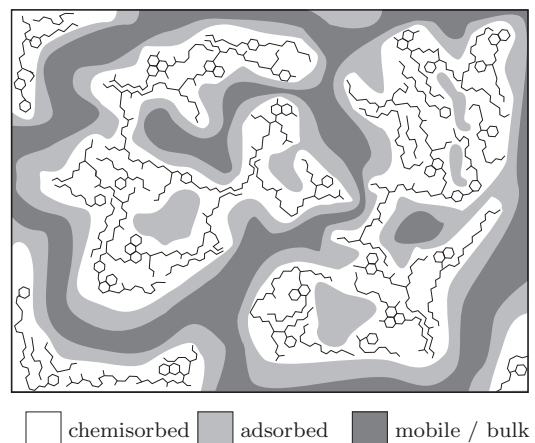
Figure 3.12: Classification of water in lignite (micro- and mesoporous system)

1. From the observation of the two experiments at 115°C in Figure 3.6 it is obvious, that void ratios and water contents are reached within one day compression at comparatively low pressures, that are much lower than the water contents originating from millions of years natural compression. For German lignite a minimum value of $W=0.4$ (0.6 for Greek lignite) was determined.

2. The rise in consolidation velocity ($\partial \dot{e}/\partial T$) according to Eq. (3.20) for two experiments (1,2) with different temperatures is only constant – which is a physical necessity – if it is calculated at an arbitrary but constant time t. As a consequence the change in equilibrium water content $\Delta e = e^*_{\text{eop}} - e(t)$ (or so called mobile water) from (Eq. 3.13) is given as

$$\frac{\Delta e(T_1)}{\Delta e(T_2)} = \frac{C_\alpha(T_1)}{C_\alpha(T_2)}. \tag{3.26}$$

On the other hand the comparison at constant values of $e = e_1(T_1) = e_2(T_2)$ below e^*_{eop} giving $\Delta e(T_1) = \Delta e(T_2)$ would lead to a permanent increase in acceleration with time according to

$$\frac{\dot{e}(T_2)}{\dot{e}(T_1)} = \frac{C_\alpha(T_2)}{C_\alpha(T_1)} \cdot t(T_2)^{\frac{C_\alpha(T_2)}{C_\alpha(T_1)} - 1} \tag{3.27}$$

with $\frac{C_\alpha(T_2)}{C_\alpha(T_1)} - 1$ always > 0 for $T_2 > T_1$. This additional acceleration with increasing time and simultaneously decreasing void ratio can only be explained by a better mobility of the water and therefore by an increasing amount of removable water at higher temperatures.

For this reason, the current experiments can also give an additional evidence, that apart from the water directly chemisorbed by polar groups of the solid matrix [AE71a], large amounts of the water in lignite are strongly adsorbed within the porous structure, see Figure 3.12. Parts of this can be mobilised easily by increasing the molecular kinetic energy at higher temperatures.

Comparison of experiments and model Figure 3.13 shows a normalised comparison between experiments and the model for C_α as a function of e^*_{eop} (a) and for e^*_{eop} dependent on temperature (b) and pressure (c). For normalization the following expressions are used:

$$f_1(e^*_{\text{eop}}) = \frac{C_\alpha^{(\text{exp.})}}{\frac{\mu_\ell(25°\text{C})}{\mu_\ell(T)} \left(\frac{p_{\text{s}}/[\text{MPa}]}{p_0}\right)^{C_1}} , \tag{3.28}$$

$$f_2(T) = e^{*(\text{exp.})}_{\text{eop}} - C_3 + C_4 \log\left(p_{\text{s}}/[\text{MPa}] + C_{\Delta\text{p}}\right) , \tag{3.29}$$
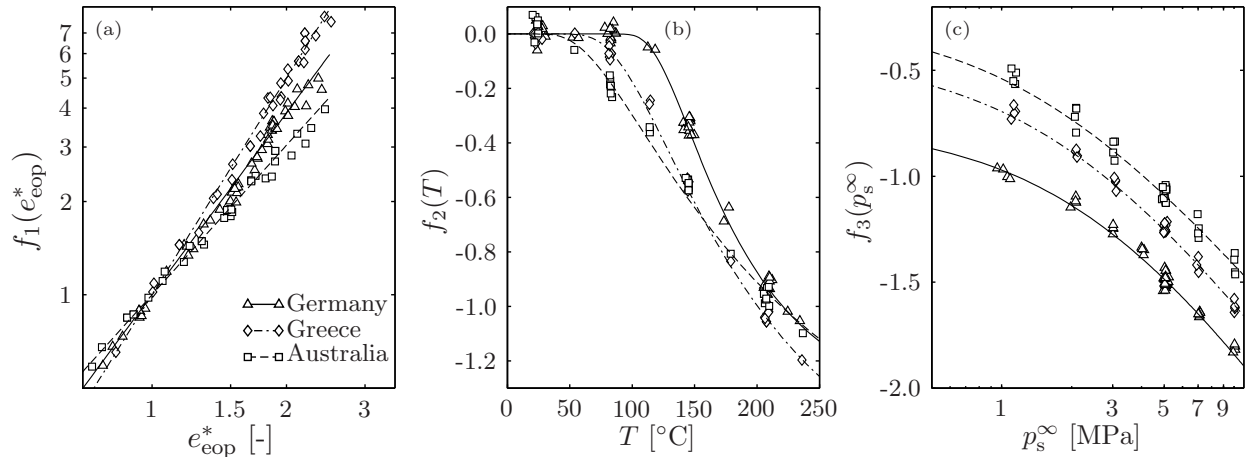
Figure 3.13: Comparison of experimental data and model

$$f_3(p_{\rm s}) = e_{\rm eop}^{*(\rm exp.)} - C_3 - C_5 \exp\left(\frac{-C_6}{(T/[^\circ {\rm C}] - C_7)^{C_8}}\right). \tag{3.30}$$

Since the effects of pressure and temperature on C_α are eliminated in the normalised form, the slope of the straight line in Figure 3.13a gives C_2 in Eq. (3.23). The good agreement between the lines and the experimental data points confirms the validity of the applied functions and the constants determined from the experiments. For a direct comparison between experiments and calculations the values obtained from Eq. (3.23) are also plotted in Figure 3.8a to 3.8e as lines.

In the same manner there is a good agreement of experimental and theoretical values for $e_{\rm eop}^*$ in Figure 3.13, if the influence of pressure (b) or temperature (c) is eliminated. This also gives evidence for the underlying assumption, that the influence of temperature and pressure on $e_{\rm eop}^*$ can be considered separately.

3.2.3   Primary consolidation of lignite

The change of void-ratio e during primary consolidation can be described by the differential equation

$$\frac{\partial e}{\partial t} = \frac{\partial}{\partial w}\left(C_{\rm e}\frac{\partial e}{\partial w}\right) = \frac{\partial}{\partial w}\left(\frac{-K\frac{\partial p_{\rm s}}{\partial e}}{\mu_\ell\,(1+e)}\frac{\partial e}{\partial w}\right), \tag{3.31}$$

which results from a material balance of solid material and water and also includes Darcys-law [Dar56] for the description of the pressure loss $\partial p_\ell/\partial x$ in the liquid. In Eq. (3.31) K represents the permeability of the macro-porous coal structure during the primary consolidation, μ_ℓ is the liquid viscosity and $p_{\rm s}$ the pressure carried by the solid matrix. Since both particles and fluid move towards the filter medium during compression, the length scale x is already substituted in Eq. (3.31) by solid particle distribution w (solid volume per unit sectional area) and porosity ε is replaced by void space e:

$$\frac{\partial x}{\partial w} = \frac{1}{1-\varepsilon} = 1 + e. \tag{3.32}$$

The analytical solution of Eq. (3.31) according to Terzaghi [Ter25] or Shirato et al. [SMI86] is

$$\Delta e = a\,\Delta p\left[1 - \frac{8}{\pi^2}\sum_{n=1}^{\infty}\frac{1}{(2n-1)^2}\exp\left(-\frac{(2n-1)^2\pi^2}{4}\Theta\right)\right]. \tag{3.33}$$

In this equation a is the coefficient of compressibility ($a = \Delta e^\infty/\Delta p$) and Θ is the time factor

$$\Theta = \frac{c_v\,i^2\,t}{H^2} = \frac{C_{\rm e}\,i^2\,t}{\omega_0^2} \tag{3.34}$$

with Terzaghis coefficient of consolidation c_v, the initial height of the coal filling H, the number of drainage surfaces i (1 or 2, always 2 for the experiments presented in this section), Shiratos modified consolidation coefficient $C_{\rm e}$ and the total solid volume per unit sectional area ω_0.

Equation (3.33) – which is the physical description of the Kelvin-body in Figure 3.14a – provides a good representation of the hydrodynamic (dashpot, water) and compression (spring, solid) effects during primary consolidation, but can not describe the creep behaviour during secondary consolidation of soft soils and lignite, which undergo a delayed compression (creep) without reaching an ultimate void ratio change Δe^∞ in technical time scale (Footnote 3, page 24) as shown in the

previous section. Nevertheless Eq. (3.33) is often used for the determination of permeability data from lignite consolidation experiments [Ros63, Ana82], neglecting the deviations due to creep.

For a better description of the whole process the secondary consolidation, which also takes place partially during the primary consolidation, has to be taken into account. SHIRATO et al. [SMIN86, SMI86] developed an extension of the TERZAGHI model by adding a secondary KELVIN-body to the solid model (Figure 3.14a). The analytical solution [SMIN86] derived for this model – containing two time constants – is also used for the description of mechanical dewatering by MURASE et al. [MIB$^+$89] or of mechanical/thermal dewatering by GUO et al. [Guo00, GTU99, GTU03]. Both authors found a 'virtually constant' time constant for creep of $0.0004\mathrm{s}^{-1}$, independent of consolidation pressure p_s^∞ and temperature T, since a simple exponential function can not describe the course of the dewatering during creep. A rheological model, which seems to be more applicable for this purpose, was developed by WAHLS [Wah62] and is briefly described and modified for physical necessities neglected in the original development in the following.

Rheological model   The model shown in Figure 3.14c represents an infinite series of KELVIN-bodies (a) (for the description of the primary consolidation) in series with an additional secondary dashpot (for the description of the secondary consolidation) and can be regarded as a superposition of primary and secondary consolidation

$$\Delta e(t) = \Delta e_1(t) + \Delta e_2(t) , \tag{3.35}$$

which in particular takes into account, that the secondary consolidation already starts before primary consolidation is completed.

For the nth KELVIN-body in the series the deformation equation of the spring and the dashpot in terms of void-ratio reduction are $\Delta e^{(n)} = A^{(n)}\,(p_\mathrm{s} - p_0)$ and $\partial e^{(n)}/\partial t = B^{(n)}\,p_\ell$. p_0 is the preconsolidation pressure from a preceding consolidation step ($p_0{=}0$ for all experiments in this paper), p_s the pressure carried by the solid matrix, p_ℓ the pressure loss of water outflow and Δp the actual

(a) Kelvin body

(b) Kelvin body and secondary dashpot

(c) model for consolidation process

(d) Shirato model
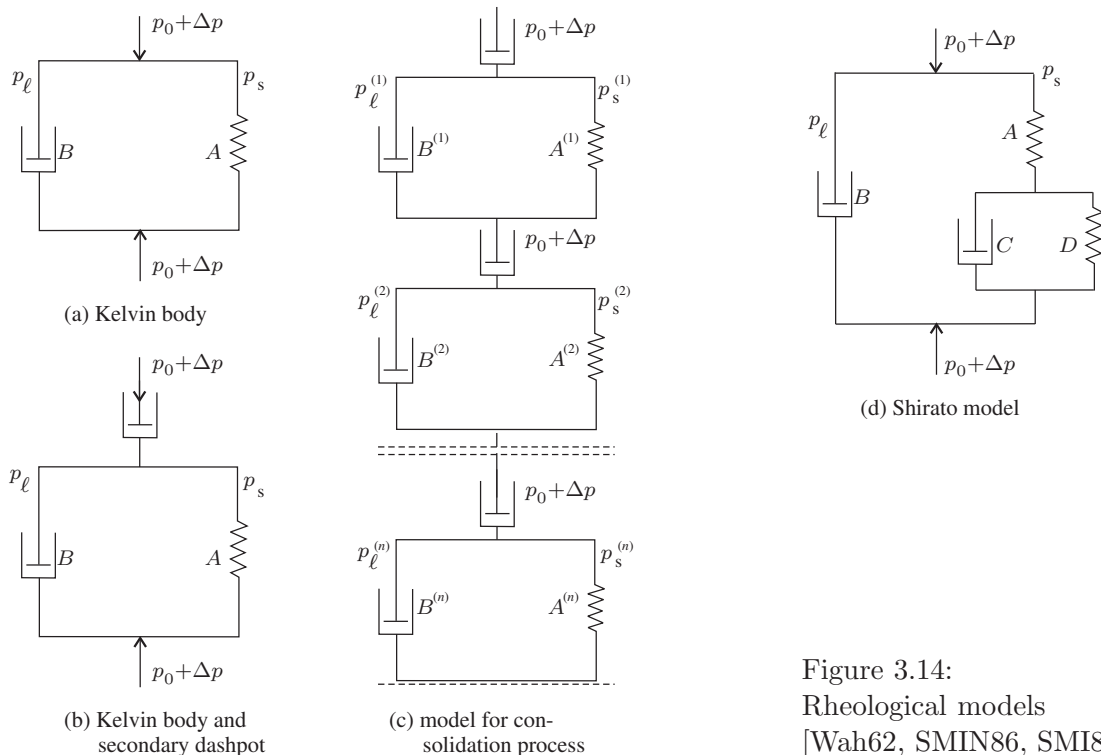
Figure 3.14:
Rheological models
[Wah62, SMIN86, SMI86]

pressure increment. Then the void-ratio reduction is

$$\Delta e_1 = \Delta p \sum_{n=1}^{\infty} A^{(n)} \left[1 - \exp\left(-\frac{B^{(n)}}{A^{(n)}} t \right) \right] = \Delta p \, A_p \left[1 - \frac{1}{A_p} \sum_{n=1}^{\infty} A^{(n)} \exp\left(-\frac{B^{(n)}}{A^{(n)}} t \right) \right]. \quad (3.36)$$

The constants are expressed in terms of the TERZAGHI solution (Eq. 3.33), since this equation is a good representation of the kinetic of primary consolidation:

$$A^{(n)} = A_p \frac{8}{\pi^2} \frac{1}{(2n-1)^2}, \quad B^{(n)} = 2 \, A_p \frac{\Theta}{t} \quad \text{and} \quad \Theta = \frac{C_e \, i^2 \, t}{\omega_0^2}. \quad (3.37)$$

$$\Delta e_1 = A_p \, \Delta p \left[1 - \frac{8}{\pi^2} \sum_{n=1}^{\infty} \frac{1}{(2n-1)^2} \exp\left(-\frac{(2n-1)^2 \pi^2}{4} \Theta \right) \right]. \quad (3.38)$$

In the development of the model WAHLS [Wah62] assumed 'viscous yielding' of the grain structure as the main reason for the secondary consolidation. In his opinion 'viscous reorientation of the grains gradually reduces the capacity of the intergranular pressure to be transferred to the pore water' and 'it is assumed, that the particle reorientation occurs so slowly, that the pore pressure developed by the process is negligible'. For the dewatering of lignite it was shown before (Chapter 3.2.1, [Ber03]) from the process activation energies, that the outflow of water from the microstructure is the time determining step in the dewatering during the secondary consolidation comparing probes with similar void-space. An influence of the solid matrix on the process kinetics can only be found with decreasing void-ratio. From both results it can be deduced, that the 'void-ratio effect' is based on a rapid decrease of the microstructure permeability with decreasing void-ratio.

SCHIFFMAN et al. [SLC66] have shown, that 'an infinite number of parameters (continuous distribution)' in a series of KELVIN elements 'would provide a secondary curve which is linear in the logarithm of time'. Such a model can also be interpreted as a description of a solid matrix with a wide distribution of micropores, which are connected to a network of macropores for the water removal[4]. A similar conclusion was drawn from BERRY and POSKITT [BP72] during the investigation of peat consolidation.

A system showing such a behaviour should consequentially be regarded as non-linear. This is also confirmed by investigations of peat and clay consolidation by BARDEN [Bar68]. For this reason the simple extension of the TERZAGHI model by an additional (linear) KELVIN-body [SMIN86] can not describe the real behaviour of the creep phase, even if these models are often used for simplicity in the mechanical dewatering of lignite [MIB+89, Guo00].

There are many suggestions for the extension of rheological models by non-linear elements [Bar68]. In most cases the complexity of the single systems leads to a large number of unknown parameters, which can not be determined exclusively by independent experiments. Therefore these models can only provide a mathematical description of the consolidation process. In contrast to this the model proposed by WAHLS with a single secondary dashpot

$$\frac{\partial e^{(n)}}{\partial t} = \frac{C^{(n)}}{1 + \frac{B^{(n)}}{A^{(n)}} t} (p_0 + \Delta p) \quad (3.39)$$

has many advantages.

---

[4]Investigations on the capillary microstructure of lignite, which also confirm such a structure for lignites have been performed by EVANS et al. [AE71a, Eva73b]

- The 'dashpot constant' $C^{(n)}$ for the nth dashpot is the only unknown parameter in the system. In the following it will be expressed in terms of the coefficient of secondary consolidation C_α, which is well investigated as a function of temperature, pressure and void-ratio (Chapter 3.2.1) and also describes the time dependent behaviour of Eq. (3.39), since the rate of compression during secondary consolidation is inversely proportional to time, if $(B^{(n)}/A^{(n)})\,t$ is much greater than 1.

- $A^{(n)}/B^{(n)}$ is the time-constant in Eq. (3.36) and determines the time required to complete the primary consolidation. Now this time is also related to that which is necessary for the secondary consolidation to develop the linear relationship in the logarithmic scale. The relation is a physical necessity, since the velocity of the secondary compression depends on the pressure transferred to the solid matrix $p_{\text{s}} = p_0 + \Delta p - p_\ell$, which increases with time. On the other hand the driving force p_ℓ for the primary consolidation and therefore the proportion of Eq. (3.36) on the whole process decreases with time.

- The factor '1' in the expression $1 + (B^{(n)}/A^{(n)})\,t = 1 + (2n-1)^2\,(\pi^2/4)\,\Theta$ is not chosen arbitrarily but provides for a smooth transition of the two consolidation phases for $\Theta \approx 1$ (see Fig. 3.15).

The void-ratio reduction for an infinite series of secondary dashpots then is

$$\Delta e_2 = \sum_{n=1}^{\infty} e^{(n)} = C_{\text{creep}} \sum_{n=1}^{\infty} A^{(n)} \log\left[1 + \frac{B^{(n)}}{A^{(n)}}\,t\right] , \qquad (3.40)$$

with

$$C_{\text{creep}} = (p_0 + \Delta p)\,\ln(10) \sum_{n=1}^{\infty} \frac{C^{(n)}}{B^{(n)}} \stackrel{!}{=} C_\alpha. \qquad (3.41)$$

Substituting the values of $A^{(n)}$ and $B^{(n)}$ leads to

$$\Delta e_2 = C_\alpha \frac{8}{\pi^2} \sum_{n=1}^{\infty} \frac{1}{(2n-1)^2} \log\left[1 + \frac{(2n-1)^2 \pi^2}{4}\Theta\right]. \qquad (3.42)$$
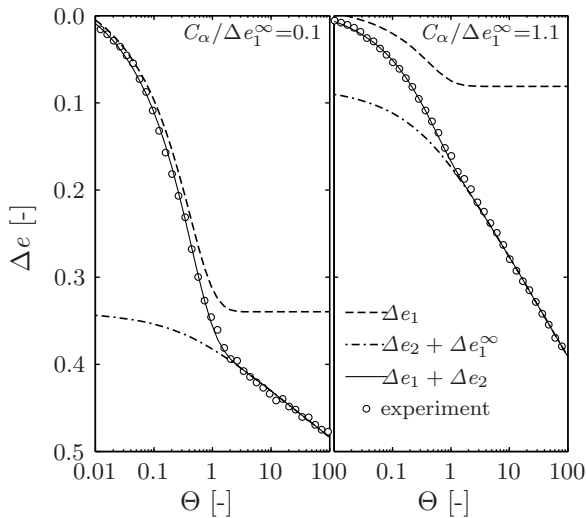
Figure 3.15: $\Delta e(\Theta)$ for two ratios of consolidation due to secondary (creep) and primary effects.
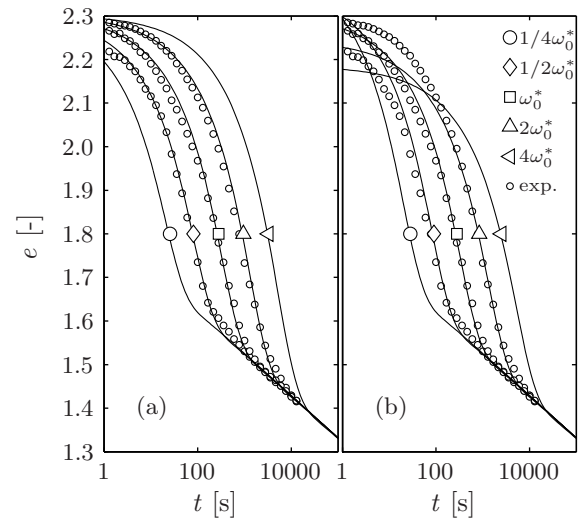
Figure 3.16: $e(t)$ for different values of ω_0 with (a) and without (b) the correction in Eq. (3.44).

Then the whole consolidation process is described by

$$
\begin{aligned}
e(T, p_{\mathrm{s}}^{\infty}, \omega_0, t) = \ & \Delta e_1^{\infty}(T, p_{\mathrm{s}}^{\infty}, \omega_0) \frac{8}{\pi^2} \sum_{n=1}^{\infty} \frac{1}{(2n-1)^2} \exp\left(-\frac{(2n-1)^2 \pi^2}{4} \Theta(T, p_{\mathrm{s}}^{\infty}, \omega_0, t)\right) \\
& -C_{\alpha}(T, p_{\mathrm{s}}^{\infty}) \frac{8}{\pi^2} \sum_{n=1}^{\infty} \frac{1}{(2n-1)^2} \log\left[1 + \frac{(2n-1)^2 \pi^2}{4} \Theta(T, p_{\mathrm{s}}^{\infty}, \omega_0, t)\right] \\
& +C_{\alpha}(T, p_{\mathrm{s}}^{\infty}) \frac{8}{\pi^2} \sum_{n=1}^{\infty} \frac{1}{(2n-1)^2} \log\left[\frac{(2n-1)^2 \pi^2}{4} \Theta(T, p_{\mathrm{s}}^{\infty}, \omega_0, 1\mathrm{s})\right] \\
& +e_{\mathrm{eop}}^{*}(T, p_{\mathrm{s}}^{\infty})
\end{aligned}
\tag{3.43}
$$

with

$$
\Delta e_1^{\infty}(T, p_{\mathrm{s}}^{\infty}, \omega_0) = \Delta e_1^{*}(T, p_{\mathrm{s}}^{\infty}) + C_{\alpha}(T, p_{\mathrm{s}}^{\infty}) \log\left(\frac{\omega_0}{\omega_0^{*}}\right)^2
\tag{3.44}
$$

and

$$
\Theta(T, p_{\mathrm{s}}^{\infty}, \omega_0, t) = \frac{C_{\mathrm{e}}(T, p_{\mathrm{s}}^{\infty})\, i^2}{\omega_0^2} t = \frac{i^2}{\omega_0^2} \frac{\langle K(T, p_{\mathrm{s}}^{\infty})\rangle}{\mu_{\ell}(T)\, \langle \frac{\partial e}{\partial p_{\mathrm{s}}}(1+e)\rangle} t.
\tag{3.45}
$$

In Eq. (3.45) $\langle K \rangle$ represents the mean permeability of the macro-porous structure. Compared to the formulation of WAHLS, Eq. (3.43) has been modified for two physical necessities: The curves for constant pressures $p_{\mathrm{s}}^{\infty} = p_0 + \Delta p$ and temperature T should start at the same e-value at $t{=}0$ *and* merge into identical creep-curves for large times independent of the total volume of solid per unit sectional area ω_0 [LW79a, Ler96]. As a result Δe_1^{∞} increases with increasing ω_0. Eq. (3.44) follows from the increase in time necessary for the completion of the primary consolidation, which is quadratical with ω_0, cf. Eq. (3.45). The dependency of $e(t)$ on ω_0 according to Eq. (3.43) with and without the correction of Eq. (3.44) is shown in Figure 3.16.

As an advantage of Eq. (3.43) the two constants e_{eop}^{*} and C_{α} can be determined easily and precisely by linear regression of the consolidation data for long term creep (Chapter 3.2.1, [Ber03]) according to

$$
e(t, T, p_{\mathrm{s}}^{\infty}) = e_{\mathrm{eop}}^{*}(T, p_{\mathrm{s}}^{\infty}) - C_{\alpha}(T, p_{\mathrm{s}}^{\infty}) \log(t/[\mathrm{s}]) ,
\tag{3.46}
$$

while only $C_{\mathrm{e}}(T, p_{\mathrm{s}}^{\infty})$ and $\Delta e_1^{*}(T, p_{\mathrm{s}}^{\infty})$ have to be determined by a curve-fitting procedure. Therefore the error in the determination of all parameters is reduced and the fitted curve is especially forced to fit the course of the experimental data during the creep phase.

While the modified coefficient of consolidation C_{e} can be assumed to be constant during one pressure step in consolidation [SMI86], it is known, that both the permeability K and the value of $\partial e/\partial p_{\mathrm{s}}\,(1+e)$ decrease with time during the primary consolidation.

Nevertheless the mean permeability $\langle K \rangle$ can be calculated by use of the proper mean value of $\langle \partial e/\partial p_{\mathrm{s}}\,(1+e)\rangle$, which is approximated as

$$
\left\langle \frac{\partial e}{\partial p_{\mathrm{s}}}(1+e) \right\rangle = \left.\frac{\partial e}{\partial p_{\mathrm{s}}}\right|_{T, p_{\mathrm{s}}^{\infty}/2,\, t=\tau/2} \cdot \overline{(1+e)}.
\tag{3.47}
$$

The compressibility of the solid matrix $\partial e/\partial p_{\mathrm{s}}$ can easily be calculated by differentiation of Eq. (3.46) with all dependencies as described in Chapter 3.2.1. In each experiment $\overline{(1+e)}$ is calculated from the mean value of e during primary consolidation. τ is the time constant calculated from the fitted value of $C_{\mathrm{e}} = \omega_0^2/(i^2\,\tau)$.
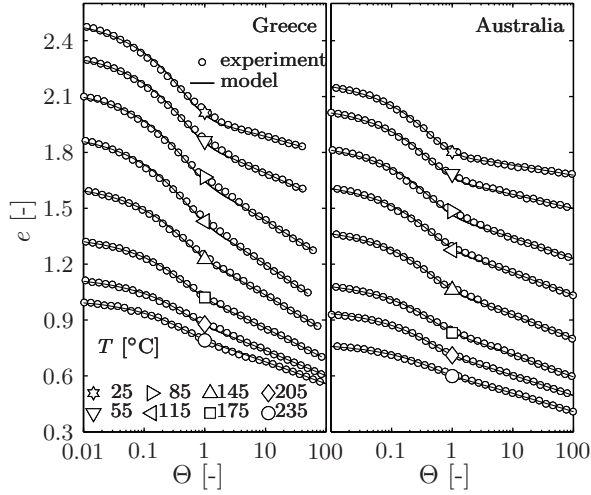
Figure 3.17: Comparison of experiments (○) and calculations (–) for the pore volume as a function of the time factor for different temperatures, (p_s^∞=5MPa, Greek and Australian lignite)
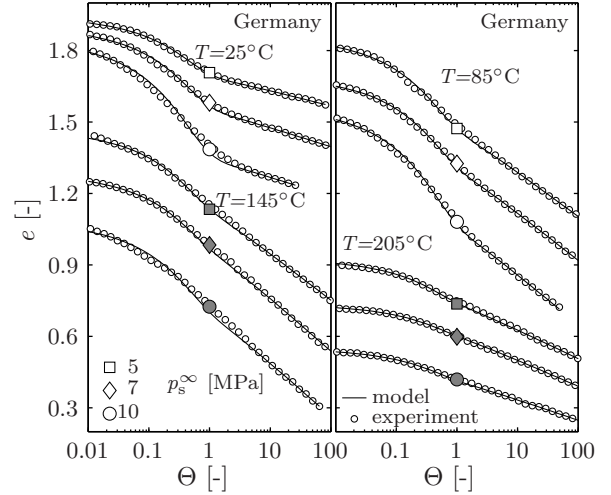
Figure 3.18: Comparison of experiments (○) and calculations (–) for the pore volume as a function of the time factor for different temperatures and pressures (German lignite)

Comparison of model calculations and experiments   In Figures 3.17 and 3.19 a comparison of the void ratio from experiments and model calculations is shown for the lignites from Greece and Australia. There is an excellent agreement for all experiments, while only in the range of $\Theta \approx 1$ slight deviations can be recognised. This is due to the fact that the primary consolidation is nearly finished in this stage while the secondary consolidation is still developing according to Eq. (3.42). The slope of Eq. (3.42) is only $0.771\,C_\alpha$ at $\Theta = 1$ and reaches $0.97\,C_\alpha$ at $\Theta = 10$. The deviation only appears for experiments with both high creep rates and high void-ratio changes during primary
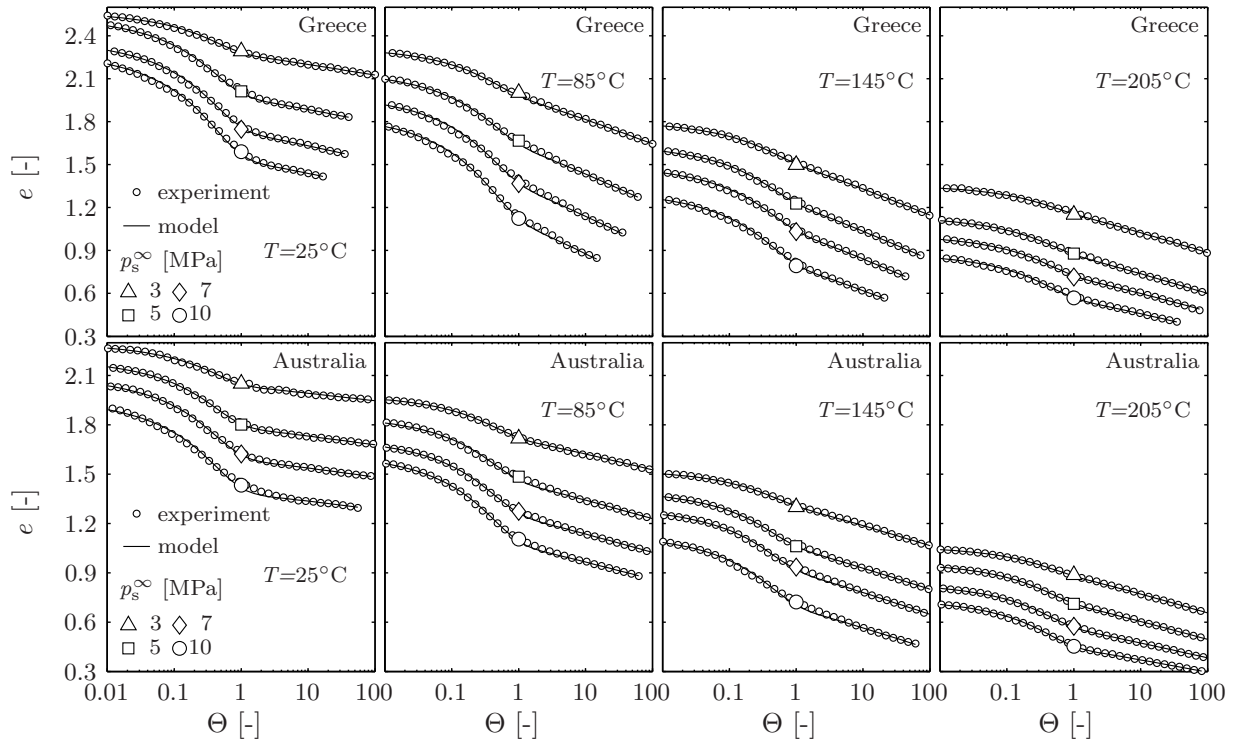
Figure 3.19: Comparison of experiments (○) and calculations (–) for the pore volume as a function of the time factor for different temperatures and pressures (Greek and Australian lignite)

consolidation (between 50 and 150°C and at pressures above 5 MPa) and disappears completely, if either the creep rate or void-ratio change is sufficiently small.

The results for the German lignite are shown in Figure 3.18. The agreement between model calculations and experimental data is also very good except for the time range $0.5 < \Theta < 5$ at higher pressures. For the German lignite the void ratio change in the primary consolidation phase is very small as a result of the high preconsolidation pressure of the coal. At the beginning of the consolidation only parts of the additional void space created by grinding are closed at pressures below the preconsolidation pressure. This happens very fast since the permeability of the coal is very high at low pressures.

Model parameters From the good agreement for all three lignites and in a wide range of temperatures and pressures it can be concluded that the model provides a good description of the consolidation process. Therefore the model parameters are used for further investigations of the process physics. The parameters from the regression analysis are shown in Figure 3.20 (a-d). Both $1/C_e$ (a measure of primary consolidation time) in Figure 3.20a and Δe_1^* (Figure 3.20b) decrease with temperature since the permeability of the coal is increased with rising temperature while the viscosity of the water is decreased. Additionally the amount of water which is removable only by high forces decreases with temperature because the coal structure shrinks as a result of the thermal dewatering. The water, which is released by thermal dewatering during heating, is no longer part of the coal structure itself and can be easily removed from the lignite without additional time and force requirement.

On the other hand the amount of water removed from the coal during primary consolidation increases with pressure (Figure 3.20d), especially above the preconsolidation pressure. Since the so called 'virgin consolidation curve' is linear with pressure in a semi logarithmic scale for pressures above the preconsolidation pressure, a similar behaviour is found for Δe_1^*. For a better comparison of the parameters all values $\Delta e_1^*(p_s^\infty, T)$ are normalised with the values of $\Delta e_1^*(10\,\mathrm{MPa}, T)$.

While the permeability of the coal decreases with higher pressure and decreasing void ratio the amount of removed water increases. Therefore also the duration of the primary consolidation and $1/C_e$ (Figure 3.20c, also normalised with the values at p_s^∞=10MPa) increases. This is of course a contradiction to the assumption $C_e \neq f(p_s)$ used for the analytical solution of Eq. (3.31). Nevertheless the good agreement of calculations and experimental data proves, that C_e can be
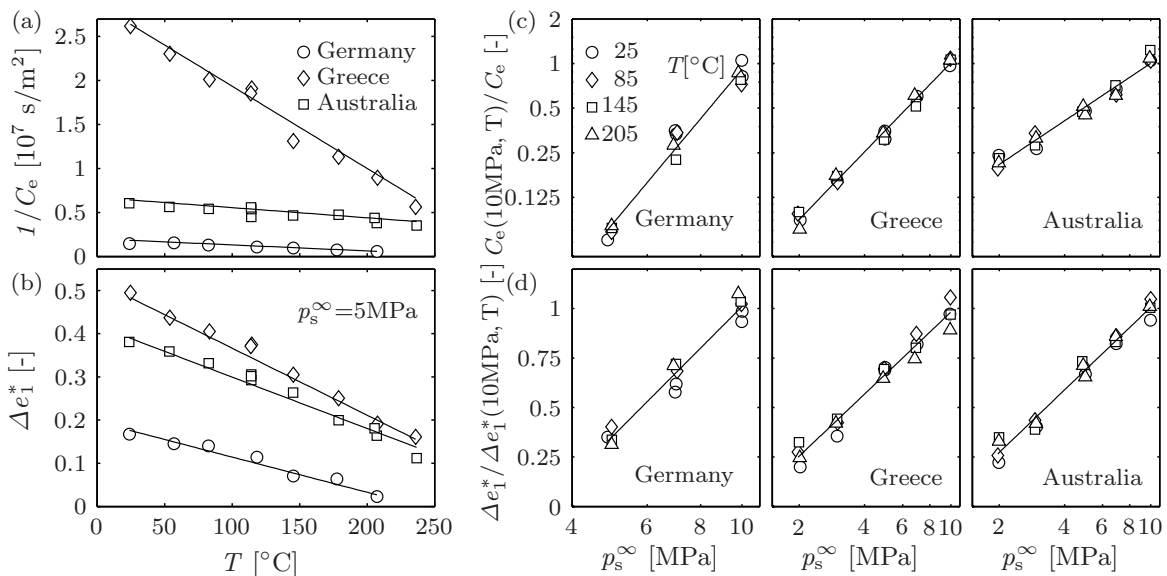
Figure 3.20: Modified consolidation coefficient (a,c) and change in void ratio (b,d) during primary consolidation as a function of temperature and pressure

Table 3.4: Model constants determined by regression analysis (consolidation)

Provenance	Germany	Greece	Australia
C_1	1.7881e+0	2.4249e+0	2.2358e+0
C_2	5.2038e+2	7.4429e+2	1.2933e+3
C_3	1.1406e+1	3.4412e+3	1.0790e+3
C_4	3.6157e+0	1.5015e+0	9.7560e–1
C_5	3.7029e–3	5.5695e–3	2.2807e–3
C_6	8.8913e–1	1.8723e+0	8.0108e–1
C_7	1.2531e+0	4.4874e–1	8.0305e–1
C_8	6.5544e–1	3.4997e–2	3.8400e–2
ω_0^* [m]	0.08	0.08	0.08

assumed to be constant for the small void ratio range Δe_1. At this point it has to be emphasised that not the consolidation pressure p_s^∞ but the void ratio and the void ratio change $\partial e/\partial p_s\,(1+e)$ are the primary variables in the dependency of C_e. On the other hand the use of T and p_s^∞ simplifies the description of the consolidation process since they are the primary process parameters. Therefore T and p_s^∞ are used in a second regression analysis for the description of C_e and Δe_1^* according to Equations (3.48) and (3.49).

$$C_e(T, p_s^\infty) = \frac{C_3\,(p_s^\infty/[\mathrm{MPa}])^{-C_4}}{-C_1\,T/[°\mathrm{C}] + C_2}\,,\tag{3.48}$$

$$\Delta e_1^*(T, p_s^\infty) = \left[C_7\,\log\left(\frac{p_s^\infty}{[\mathrm{MPa}]}\right) - C_8\right]\left[-C_5\,\frac{T}{[°\mathrm{C}]} + C_6\right]\,.\tag{3.49}$$

The results for all constants are listed in Table 3.4 and can be used (together with the description of the creep process in Chapter 3.2.1 for the calculation of void space/water contents as a function of temperature T, pressure p_s^∞ and initial solid volume charging w_0.

3.2.4 Model verification

Permeability In Figure 3.21 the mean lignite permeability $\langle K \rangle$ calculated with Eq. (3.45) from the experimental data and the permeabilities from steady state flows is drawn for the three lignites as a function of the mean void ratio $\langle e \rangle$ during primary consolidation. From the diagram it can be seen that the permeability decreases sharply with decreasing void ratio/increasing pressure as a result of the reduced hydraulic diameter. For the German lignite both the calculated values from the consolidation experiments and the direct measurements agree well and therefore also prove the theoretical model of consolidation. Slight deviations result from possible variations in the bulk properties of the coal due to the different experimental procedures.
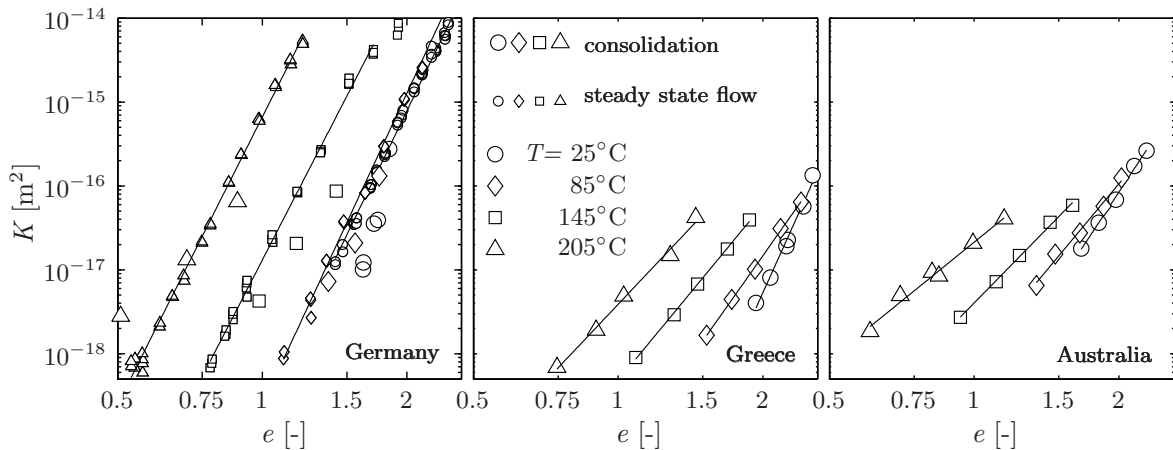
Figure 3.21:
Permeability measured in steady state flows and calculated from the consolidation experiment
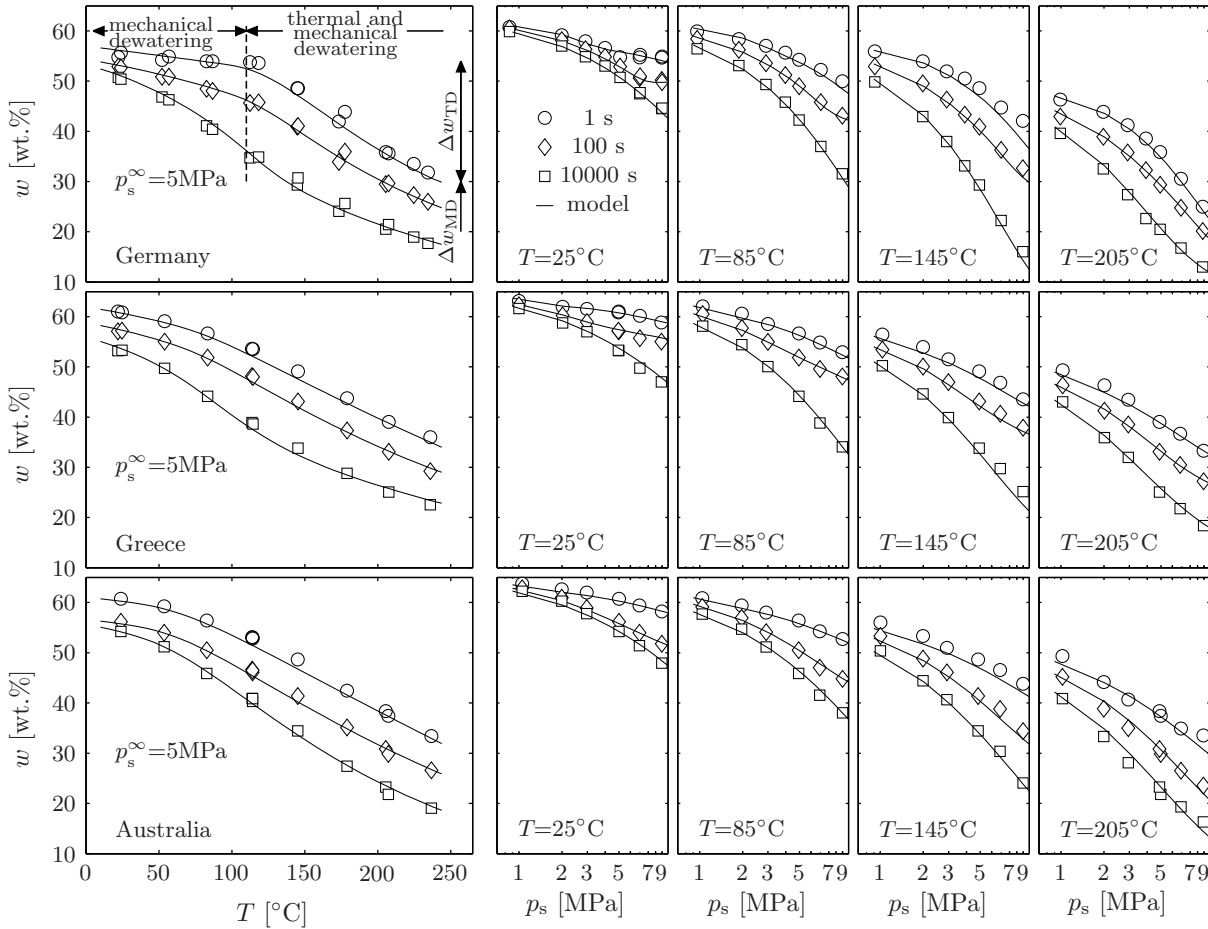
Figure 3.22: Comparison of the experimental results with model calculations for the water content at three times, depending on MTE temperature and pressure.

For the German coal much higher permeabilities than for the other lignites are found. This difference can be explained by the higher preconsolidation pressure p'_C. The porous structure formed of hard grains supports more channels for the water removal during primary consolidation than the softer particles of the Greek and Australian lignites. Those particles are distorted at relative low pressures whereby the porosity is reduced.

The permeability (compared at constant void ratios) increases with temperature which is simply a result of the thermal dewatering and shrinkage of the coal at temperatures above 100°C . Similar results are reported by BANKS and BURTON [BB89] who found an increase in permeability of lignite after thermal pre-treatment.

Water content   In Figure 3.22 the water content w (wet basis) of the three lignites is shown at three times of consolidation as a function of temperature and pressure. For all coals there is a very good agreement in the whole range of process parameters and times. Even at the beginning of consolidation or at low temperatures or high pressures, when primary consolidation plays an important role in the dewatering kinetics, only slight deviations occur. It was shown before (Chapter 3.2.1, [Ber03]) that the neglect of primary consolidation kinetics would lead to larger deviations in calculated process times.

The preconsolidation pressure p'_C of the Australian and Greek lignite was found to be much lower than p'_C of the German coal (Chapter 3.2.1, page 20) and therefore most of the bigger pores created by using crushed coal are closed at rather low pressures. Therefore with increasing pressure a delayed dewatering (higher water contents after 1 and 100 s compression) can be observed in comparison to the experiments with German coal.

3.3 Physical properties of dewatered coals

A detailed knowledge about physical properties of dried MTE coals besides the water content of the wet product is of importance for the use of MTE products in power plants, which always includes further drying and grinding or when considering the production of an economically transportable fuel by brown coal dewatering and densification. Therefore a detailed investigation of pore structure (related to the bulk density), mercury surface area and compressibility of dried coal samples [BHSC] as well as a quantitative analysis of the shrinkage behaviour during drying and the water uptake of dry products is presented in the following [HBCS04, HBCS05].

Temperature and pressure induced structural changes on the lignites during MTE processing are analysed which can explain also the variation of physical data for raw coals, which seem to be chemically identical but were maybe exposed to different physical environments for different durations during natural coalification. During MTE processing only minor changes in the chemical composition of the products occur [CFJ00, HBCS] (Chapter 3.4) due to the relatively mild process temperatures, so all results are related to the changes in pore volume, water content and microstructure and some 'artificial coalificiation', which is found to start at process parameters as low as during MTE processing [CB97], while also lower temperatures than during the MTE process (over longer periods of time) are thought to be the only factor explaining large scale incolation changes in coal basins during natural coalification [TT02].

To investigate the porous nature of MTE treated coals, MTE products from the dewatering experiments described in Chapters 3.2.1 and 3.2.3 were characterised by mercury intrusion porosimetry (MIP). The advantage of the MIP technique is, that it allows pore size distributions to be easily determined over a broad pore size range, spanning several orders of magnitude.

The technique is however limited, in that samples need to be completely dry, thus allowing porosity and pore size distribution data only to be obtained for oven dried MTE products, which are known to have undergone shrinkage [Ber01, HFC]. However, as the pore volume of the wet MTE product is known, the pore volume measured by MIP can be used to determine the degree of shrinkage during oven drying, an important parameter in itself and a useful index of physico-chemical changes occurring during the MTE process. This will be further analysed in Chapter 3.3.4.

Furthermore, care needs to be taken when interpreting the lower mesopore diameter range, as the high intrusion pressures required to measure pore sizes in this region may lead to sample compression or degradation [NFK84, SDY95]. There have been several attempts in the literature to calculate the compressibility of various coals by MIP and to correct the pore size distribution accordingly [TT72, Spi81, SDY95, ZK54]. As the literature data have shown coal compressibility to vary widely with coal rank and location [TT72, Spi81], all MTE products are characterised for their compressive behaviour and pore size distributions were corrected accordingly.

The fine structure of the coals (true density, surface area and microporosity) is investigated first, since it is an important factor influencing the ignition and combustion (Chapter 3.5) behaviour and since a 'true density' also is required for micropore volume calculation from MIP data.

3.3.1 True density, Helium density and CO_2 surface area

Even if the definition of a 'true density' for micro porous materials like coal is difficult, usually the He-densities are used for the calculation of volumetric changes in drying and dewatering processes. The uncertainties in the determination of the densities are the definition of an equilibrium criterion for the gas pressure measurement in He-pycnometry since even He-diffusion is slow in small micropores and also the structural changes during the drying and shrinkage of brown coal, which lead to smaller and partially closed pores. Nevertheless drying is essential in the application of He-pycnometry.

Similar problems occur on the determination of specific surface areas in micro porous materials.
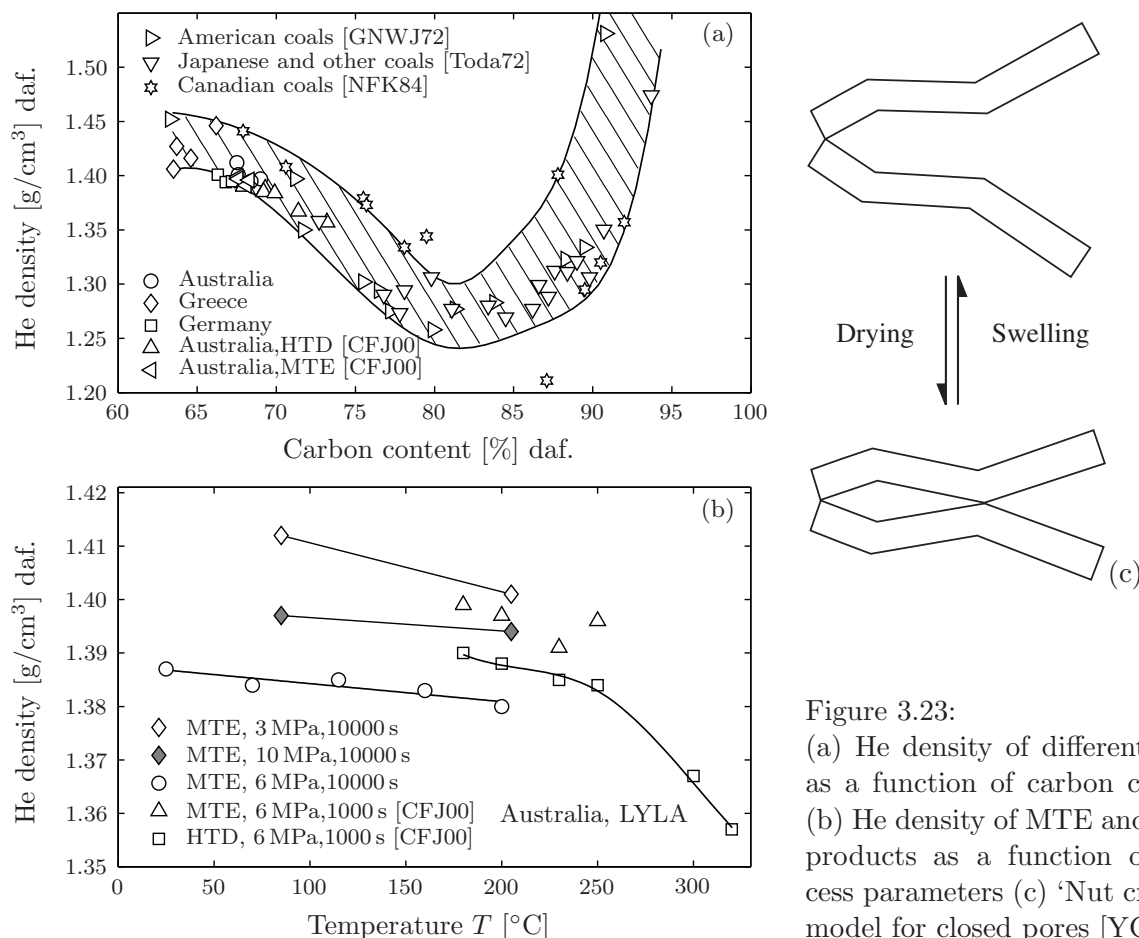
Figure 3.23:
(a) He density of different coals as a function of carbon content (b) He density of MTE and HTD products as a function of process parameters (c) 'Nut cracker' model for closed pores [YC90]

Nitrogen, which is usually used for the determination of specific surface areas in coal, does not possess enough kinetic energy to penetrate into the coal micropores at 77 K. Additionally at 77 K capillary condensation takes place before the apparent monolayer capacity is reached such that BET N_2 areas are unrealistic high. Therefore surface measurements using CO_2 at 0°C or 25°C [MS65, THT$^+$72] is thought to yield more realistic results, even if this method is also criticised [Mah91].

Density Measuring the pore volume of coals of different rank with Helium and also different organic liquids FRANKLIN [Fra49] and NELSON et al. [NMW80] found differences for the calculated densities of up to 10 %. NELSON et al. argued, that 'micro pores formed by cage-like structures' exist in dried low rank coals, which are accessible to solvents only as the extent of solvent induced swelling increases. Based on this work and their own measurements with water and methanol YOST and CREASY [YC90] developed the 'nut cracker model' (Figure 3.23c) as a mechanical model for the description of sealed cavities in lignites.

FRANKLIN [Fra49], FUJII and TSUBOI [FT67], GAN et al. [GNWJ72], TODA [Toda72] and NG et al. [NFK84] measured the He density for coals of different rank and found a decreasing density with increasing carbon content with a minimum at about 82 %, see Figure 3.23a. The Figure also contains the results for the Australian, Greek and German coal investigated in this work (see Table 3.5, page 52) as well as the densities for further MTE and HTD samples (Australian coal, LYLA) from [CFJ00], which all are in a narrow region for both density and carbon content. Though the change of carbon content is low for the MTE and HTD samples, the densities for MTE and HTD show a significant trend towards lower values for increased temperature, and pressure or dewatering time (Figure 3.23b). The lower densities of the samples from MTE experiments performed at 6 MPa/10000 s may result from the fact that these experiments have been performed with a different sub-sample of the coal.
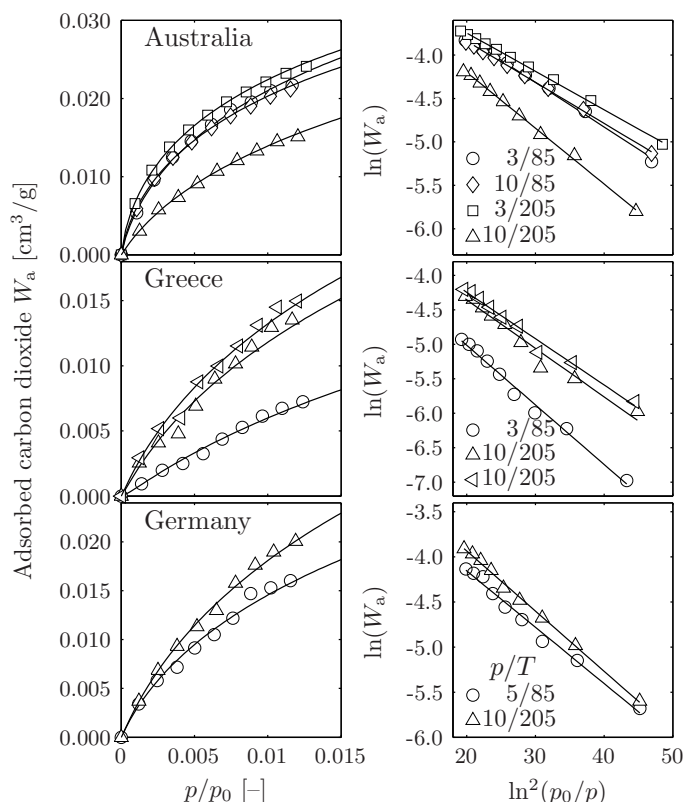
Australia

p/T	W_0	A
[MPa]/[°C]	[$10^{-3}\mathrm{cm}^3$/g]	[m²/g]
3/85	62.4	234
10/85	55.3	208
3/205	57.2	215
10/205	54.5	205

Greece

p/T	W_0	A
[MPa]/[°C]	[$10^{-3}\mathrm{cm}^3$/g]	[m²/g]
3/85	37.4	141
10/205	52.4	197
10/205	55.0	207

Germany

p/T	W_0	A
[MPa]/[°C]	[$10^{-3}\mathrm{cm}^3$/g]	[m²/g]
5/85	54.7	205
10/205	74.5	280

Figure 3.24:
Determination of surface area A and limiting micropore volume W_0 by CO_2 adsorption. Calculations are done using the DUBININ-RADUSHKEVICH equation (3.12)

CO_2 surface area The CO_2 surface areas shown in Figure 3.24 indicate a decrease of limiting micropore volume with increasing severity of MTE conditions and therefore also a decrease in specific surface area for the Australian coal. Similar results were found in the temperature region up to 400°C by TODA et al. [THT+72] during heat treatment of different Japanese coals. From their results they argued that in this temperature region very small micropores are closed during the treatment by tarry materials oozing out of the coal structure.

Similar CO_2 surface areas which show the same trends are reported by CHAFFEE et al. [CFJ00] for Australian coals treated hydrothermally while He densities (Figure 3.23b) also decreased with increasing temperature.

While the exact determination of daf. He densities was difficult for German and Greece coal due to the high ash content and large differences in the results for different coal samples, the measured CO_2 surface areas clearly show the trend of increasing surface areas with increasing processing temperature which is thought to result from structural changes further discussed in Chapter 3.3.3.

The results and literature data presented in this section for the Australian coal support – at least for this coal – the idea of an increase in closed pore volume with increasing severeness of dewatering conditions, whereas chemical changes of the coal structure are not required necessarily. This concept will be analysed further in the following sections.

3.3.2 Compressibility and density

Shown in Figure 3.25a are cumulative intrusion curves for the Australian coal. A sequential decrease in intrusion volume can be observed with increasing MTE temperature at a constant applied pressure of 5 MPa. The same results are shown in Figure 3.25b, where the applied pressure has been plotted on linear coordinates. For ease of interpretation, the intrusion volume for each set of curves has been offset by 0.015 cm³/g according to the maximum intrusion volume for each experiment. In addition, for each set of intrusion and extrusion data, a linear regression has been
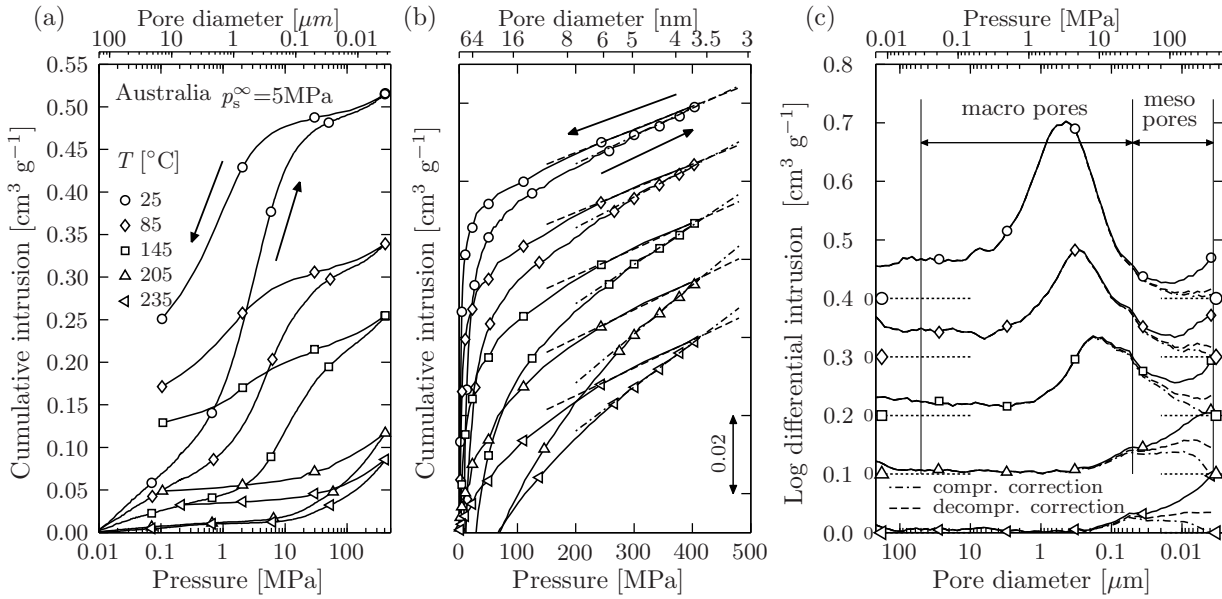
Figure 3.25: (a) Intrusion and extrusion of mercury, (b) determination of compressibility and (c) corrected LDI curves

done, which allows the compressibility of the sample to be determined according to Eq. (3.3). The corresponding pore size distributions, expressed as a logarithmic differential intrusion are shown in Figure 3.25c.

Extrusion data The linear regression line for the extrusion data, as illustrated by a dashed line in Figure 3.25b follows a linear part of the measured values over a broad pressure region, ranging between 200 and 400 MPa. Furthermore, the slope is fairly independent of temperature. This results in a constant compressibility value with temperature as shown in Figure 3.28b. The trends are also consistent for the two other coal types investigated (Figure 3.28b). Similar small changes in coal compressibility were seen by SCHUYER et al. [SDK54], who used sound velocity measurements to determine the compressibility of various coal ranks, with carbon content values varying between 82 and 90 %.

Intrusion data The corresponding mercury intrusion data in Figure 3.25b show a continuously changing slope, with the linear region (dash-dotted line) ranging over a much narrower pressure region of between 300 and 400 MPa. Such a change in slope is commonly associated with the simultaneous filling of pores and sample compression. It is interesting to note, that under the experimental conditions, no linear behaviour is observed for intrusion data in the 100 to 200 MPa region, as it has been reported for lignites and sub-bituminous coals by other researchers [TT72, FM88]. However, this effect may be due to the changes in slope becoming more pronounced due to the higher intrusion pressures (414 MPa) used in this investigation, compared to the previously reported studies, which used pressures up to 207 MPa.

Furthermore, from Figures 3.25b and 3.28a it can be seen that the slope determined from the intrusion data increases with increasing MTE temperature up to 205°C. Again, this could be due to changes occurring in pore filling, where an increase in temperature results in an increase in pore filling in the mesopore size region. Possible explanations are the transformation of macropores to mesopores by the MTE process and/or the suppression of mesopore shrinkage at higher MTE temperatures due to coal hardening which is discussed later. Other contributing factors could be increased sample compression, which would involve the compression of the coal skeleton, the deformation of the porous structure (with a closure of pores) or a combination of the two (Figure 3.26). Shown in Figure 3.28a, is the compressibility data obtained from the (uncorrected) mercury intrusion data as calculated according to Eq. (3.3). The values are significantly larger (up to 100 %)
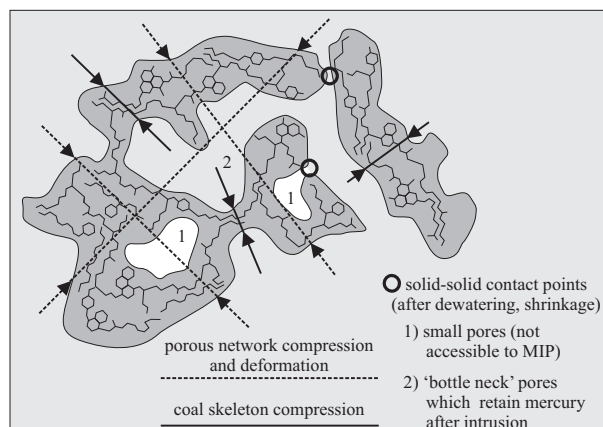
Figure 3.26:
Scales of compression and deformation
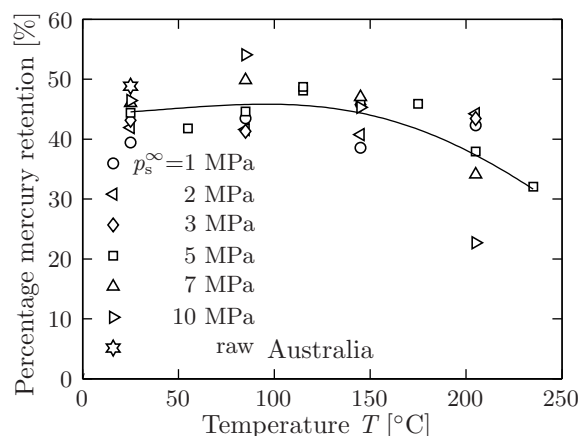
Figure 3.27:
Mercury retention at the end of MIP experiments for Australien coal

compared to compressibility data obtained from mercury extrusion data, and they increase with increasing temperature for all three coal types investigated.

If there is indeed a shift from larger to smaller sized pores with an overall reduction in total pore volume, one would expect a decrease in compressibility of the combined coal and pore matrix (Figure 3.26). This is due to the formation of an increasing number of particle-particle interactions, which increase the network strength and hence the resistance to further compaction.

Assuming the increase in mesopore volume with increasing MTE temperature to be true (as shown in Figure 3.34), the measured increase in intrusion compressibility should be due both to the coal skeleton and an increased number of empty meso- and micropores experiencing compressive forces (like also indicated by the detailed analysis of He densities in Chapter 3.3.1) and from the filling of mesopores with mercury. The observed increase in intrusion compressibility therefore just reflects structural changes of the porous network but not changes in the skeleton compressibility.

Intrusion versus Extrusion   From Figure 3.25a, it can be seen, that there is a hysteresis effect between the intrusion and extrusion curves. Such hysteresis is associated with mercury retention and has been ascribed to a number of factors. One such factor is the 'ink-bottle' effect, where the mercury is not being extruded due to a breakage of the mercury column in a narrow neck as a result of non-steady capillary pressure [Klo94, WO97] (Figure 3.26). Other possible reasons include contact angle hysteresis [Klo94, WO97], irreversible sample destruction, as well as the (reversible)
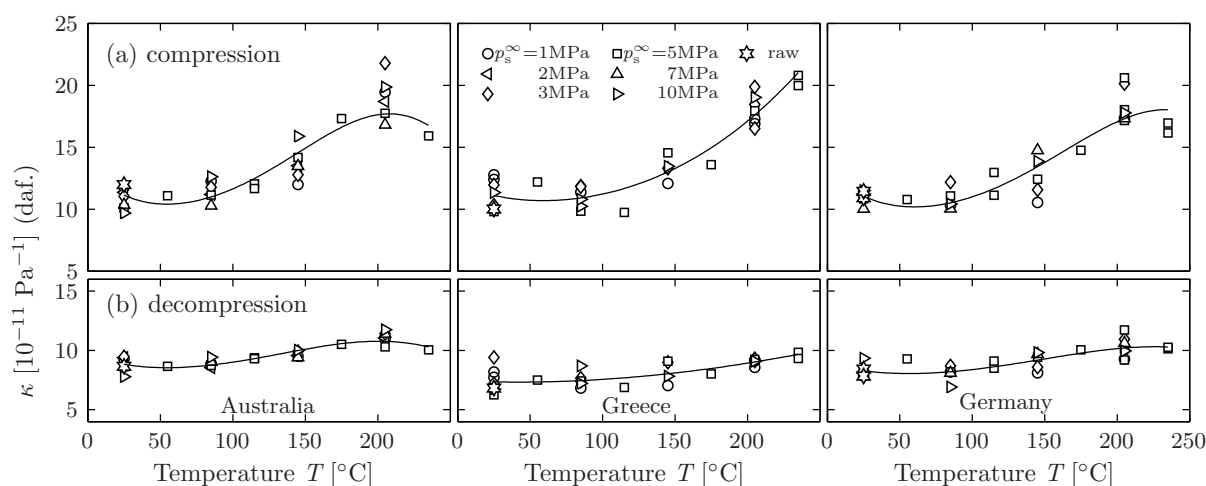
Figure 3.28: Compressibilities of the three coals

compression [SDY95] of meso- and micropores, which do not re-expand directly after lowering of the mercury pressure. Since the slope of the extrusion curves is similar for all experiments, while the slope of the intrusion curves increases with increasing MTE temperature this leads to an increase in the degree of hysteresis with increasing temperature.

It is interesting to note that for most experiments the percentage retention of mercury relative to the maximum intrusion volume remained relatively constant at around 45%, with a slight decrease to 35% for temperatures between 175 and 235°C as shown for the Australian coal in Figure 3.27. Consequently, while there is a larger difference between intrusion and extrusion volumes at higher MIP pressures with increasing MTE temperatures, this is equalised by higher extrusion volumes (i.e. higher gradients) at medium pressures. This behaviour is thought to result from a hindered/delayed, but fully reversible relaxation/reordering [SDY95], of the macro-molecular network structure in the coal samples treated at higher temperatures. This also shows, that an increase in irreversible destruction of pore structure during MIP experiments is out of question for these samples. For MIP pressures up to 100 MPa Spitzer [Spi81] did not found any destruction of coal samples at all.

From the mercury intrusion data shown in Figure 3.28a it is interesting to note, that no discernible trend in compressibility can be identified with increasing MTE pressure. This finding suggests that the increase in network compressibility is the result of an increase in MTE temperature. This effect could be due to thermal dewatering [Fle26, ME72]. From experiments on thermal and hydrothermal dewatering it is known that the colloidal structure (i.e. skeletal matrix) of coal shrinks during heating, resulting in the release of water and an increase in hardness after drying relative to conventionally dried lignites [Fle26]. Thermal dewatering starts at temperatures around 140°C [ME72], which is also the starting point of compressibility increase in Figure 3.28. Under the viewpoint of hydrogel physics the shrinkage and water release during thermal dewatering can be understood as an aggregation of the backbones/chains of the coal matrix which is thermodynamically more efficient due to the reduction of surface exposed to water [LHOB03]. This also leads to a more rigid structure. This increased rigidity of the wet coal then leads to a decrease in shrinkage (see Chapter 3.3.4), especially of the smaller pores, which consequently are believed to result in higher compressibilities.

When interpreting the above described results, great care must be taken as the effects of pore filling and compression are not easily separated, thus making corrections for sample compression difficult [FM88]. For this reason, the effects of coal skeleton and coal network compression can also not be separated based on compressibility data from MIP as tried by Xu et al. [XLXZ99].

From these considerations it can be recapitulated, that the change in curvature during intrusion as a function of increasing MTE temperature can be attributed to an increase in pore volume in the mesopore region (Figure 3.25c), the shift in pore size distribution to smaller diameter pores due to the transformation of larger to smaller sized pores (Figure 3.35) and suppressed shrinkage. From this, a coal structure results, which additionally contains more 'closed pores' (Chapter 3.3.1) and more pores which are too small for mercury intrusion and which has naturally a higher compressibility (including deformation of the network) than the coal skeleton itself (Figure 3.26).

Literature Data   Comparing the absolute values of compressibility $(0.6 \cdot 10^{-10} \, \mathrm{Pa}^{-1}$–$2.2 \cdot 10^{-10} \, \mathrm{Pa}^{-1})$ these values cover the whole range of values given in literature for coals with carbon contents between 65 and 95 % [ZK54, TT72, NFK84, SDY95]. Even if it is common to correlate the changes in compressibility to changes in carbon content – getting a curve with at least one minimum and one maximum at about 80 and 90 % carbon content [TT72, NFK84] – the results presented here only allow the conclusion, that the MIP determined compressibility is a function of porosity, pore structure and strength of (thermal) dewatering because the change in carbon content at the highest process temperature is as low as 2% [HBCS04]. This explains why the investigation of coals from different countries or open cuts results in different compressibility curves when plotted only as a function of carbon content, compare [TT72]. This result is also in accordance with the finding of Teichmüller that 'the water content of lignite stage is a far better
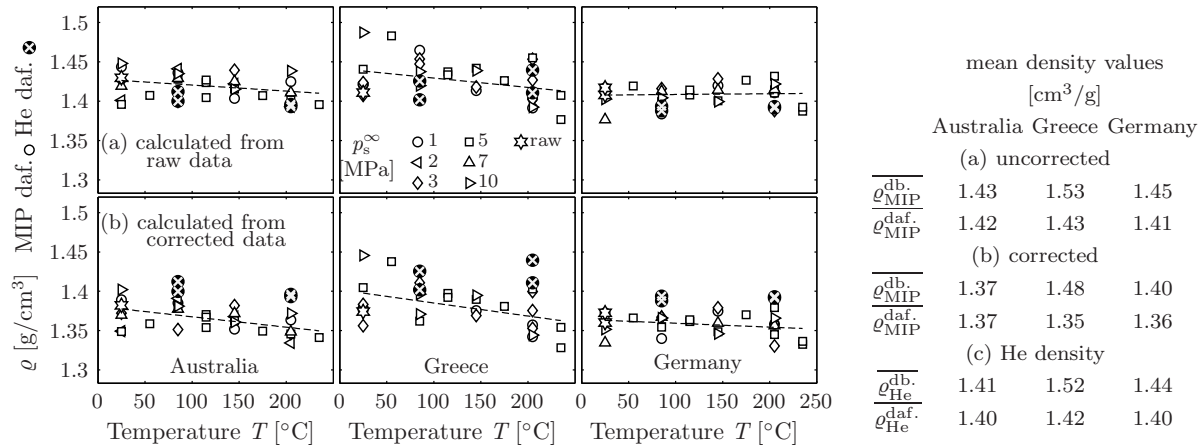
Figure 3.29: Skeletal densities calculated from mercury intrusion at maximum pressure (with and without correction for compressibility) and He densities

measure of the degree of incolation than the carbon content or content of volatiles' [TT02].

MIP data correction   Due to the potential compression of pores and coal matrix at higher intrusion pressures (i.e. mesopore diameter region), the intrusion volume needs to be corrected to prevent an overestimation of the micro- and mesopore volume. This can be seen clearly from the comparison of skeletal densities calculated from uncorrected MIP data with helium densities determined by helium pycnometry. As illustrated in Figure 3.29, for all three coal types investigated, the helium densities are found to be lower relative to the skeletal densities determined from MIP. This is unexpected as the MIP technique is only capable of measuring pore diameters down to $3.6\,\mathrm{nm}$, compared to $0.16\,\mathrm{nm}$ for a helium molecule. While a number of researchers base their intrusion volume corrections on compressibility values calculated from mercury intrusion data, it was decided to base the calculations on mercury extrusion data for the following reasons:

- Without the correction negative micropore volumes would result from Eq. (3.6) since MIP determined densities are higher than pycnometry densities.

- Using the extrusion compressibility at least takes into account all elastic deformations - neglecting relaxation effects which also take place in a longer time scale and at lower pressures but which are due to the 'reordering of the macromolecular network structure' [SDY95] and therefore mostly include reversible deformation of the coal network structure.

- Using the (higher) 'intrusion compressibility' for correction would lead to zero differential intrusion in the high pressure regime (Figure 3.25c, dash dotted lines) with an underestimation of the mesopore volume. Correction by the intrusion compressibility would also result in a positive intrusion during depressurisation, which can not be motivated physically.

The effect of compression correction calculated from both mercury intrusion and extrusion data is shown in Figure 3.25c. As illustrated, in both cases the correction results in a reduction in the overall mesopore volume. Furthermore, it should be noted, that the maximum difference in mesopore volume using both corrections is only about $0.02\,\mathrm{cm^3/g}$, which is reasonably low compared to the total pore volumes and could only lead to mayor errors calculating the micropore volumes from the differences of reciprocal helium and mercury densities. Nevertheless the calculation of micropore volumes from the corrected densities (Figure 3.34b) gives reasonable values for both corrections. These results are discussed in Chapter 3.3.3.

3.3.3   Pore size distribution, pore volume and surface area

In this section the logarithmic differential intrusion (LDI) curves (pore size distributions) and the other parameters derived from the intrusion data are discussed for the three coals for different MTE conditions.

Shown in Figure 3.30 is the effect of MTE temperature on the pore size distribution of all three coal types treated at a constant mechanical pressure of 5 MPa. The corresponding effects of MTE pressure for four different temperatures are shown in Figure 3.31 to Figure 3.33. All results have been expressed as logarithmic differential intrusion curves. The intrusion volumes have been corrected – as all other results – for compressibility effects. Furthermore, for each condition, the baseline has been offset by $0.05\,\mathrm{cm}^3/\mathrm{g}$, where the dashed lines (marked with corresponding symbols) represent the actual zero line for each experiment. For ease of interpretation, the pore size distributions have been divided into macro- and mesopore size regions, where the inter/intra particle boundary has been set at $50\,\mu\mathrm{m}$. To allow easy comparisons to be made between the different coal types and processing conditions, the individual macro- and mesopore volumes, as well as the calculated micropore and total pore volumes have been shown in Figure 3.34a to d. Additionally, from the distributions the mean pore diameter (Figure 3.35) and specific mercury surface areas (Figure 3.36) have been calculated. It should be noted that the surface areas calculated according to Eq. (3.8) are only valid for pores intruded by mercury, i.e. $3.6\,\mathrm{nm}$ to $50\,\mu\mathrm{m}$. No assumptions concerning the pore geometry are included in Eq. (3.9), since only the mechanical work of wetting the coal surface is calculated – even if the calculation of surface areas from the filling of cylindrical pores would lead to the same equation. Concerning the trends presented, also any error in compressibility correction seems neglectible, since similar curves with slightly higher or lower absolute values result from calculations, which have been performed without any correction or with a correction using the compressibility calculated from the intrusion curve.

As indicated by the water content values shown earlier (Figure 3.22, page 34) the total pore volume (including the presence of a small amount of gas) for all three coal types decreases significantly with increasing MTE processing severity. The results show the overall influence of MTE process *and* shrinkage during oven drying (resulting in further pore volume loss, see Chapter 3.3.4) on the pore size distributions and pore volumes. This has to be kept in mind during the data analysis.

Australian coal   As illustrated in Figure 3.30a and Figure 3.31, most of the pore volume for the Australian coal treated under mild MTE processing conditions is in the macropore size region,
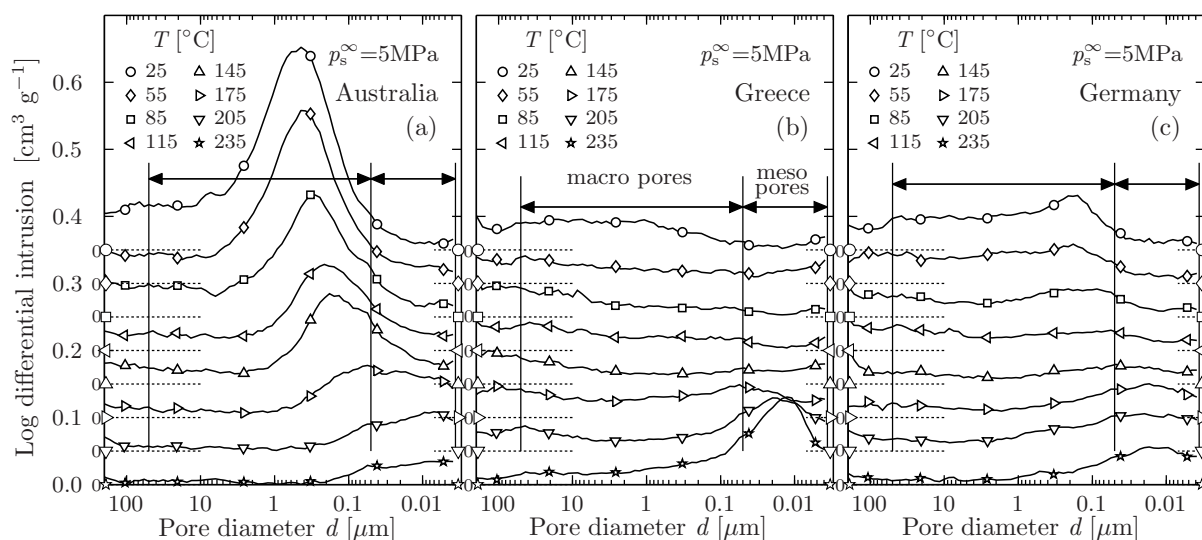
Figure 3.30: Logarithmic differential intrusion as a function of MTE process temperatures for the different coals
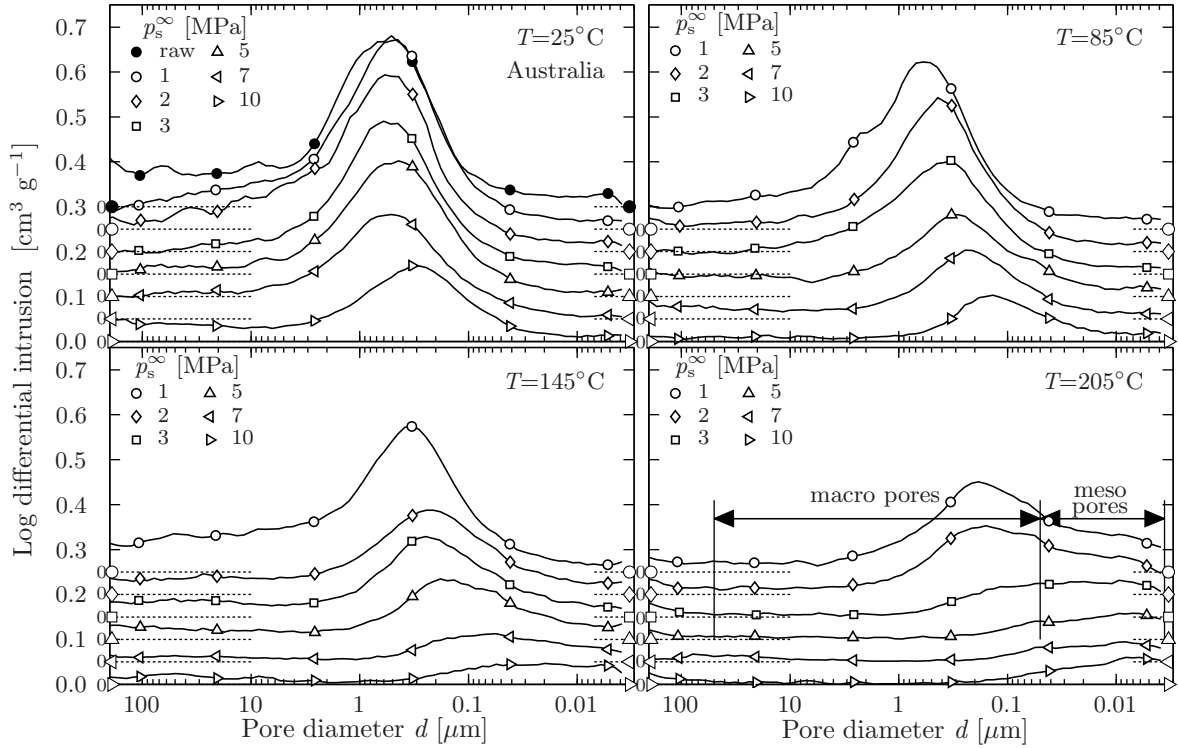
Figure 3.31: Logarithmic differential intrusion as a function of MTE process temperature and pressure for Australian coal
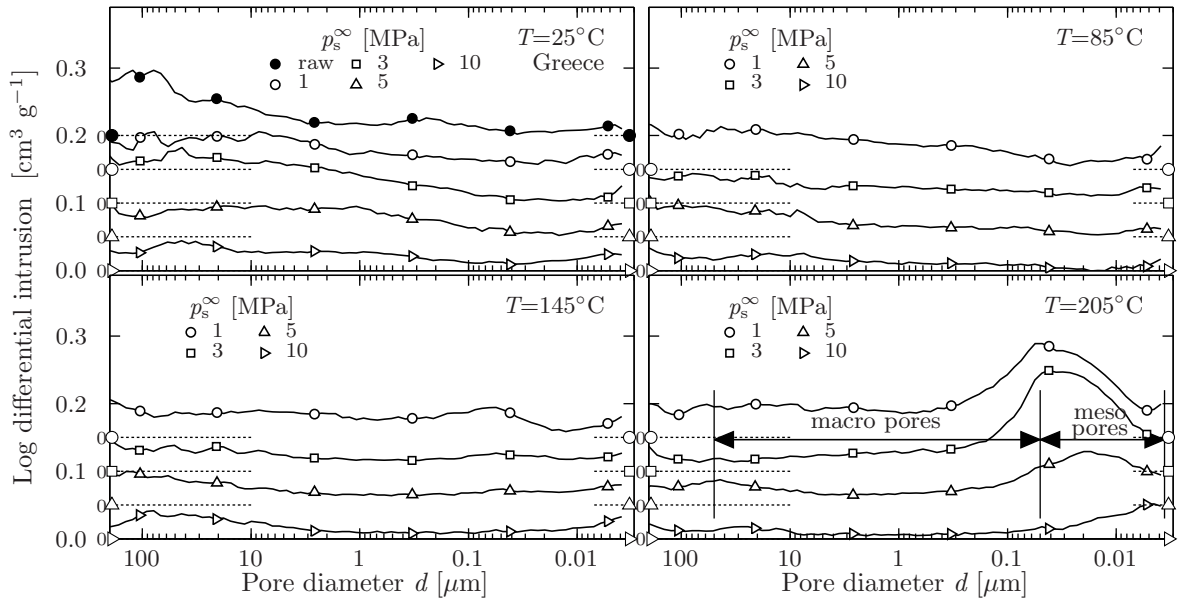
Figure 3.32: Logarithmic differential intrusion as a function of MTE process temperature and pressure for Greek coal

with a peak volume at a pore diameter of about $0.4\,\mu$m. Upon the application of increasing MTE temperature and pressure, the distribution is observed to flatten and shifted towards smaller diameter pores. The corresponding mean pore diameter results in Figure 3.35a show this shift to be more pronounced as a function of increasing temperature than pressure. Furthermore, Figure 3.34 shows, that while this shift is associated with a decrease in macopore volume and an increase in mesopore volume with increasing MTE temperature, both the macropore and mesopore volumes (at high temperatures) again decrease with increasing MTE pressure. The observed trends support the idea of the pores just being deformed during dewatering which then results in an increasing number of small pores just by the transformation of 'bigger pores' to 'smaller pores'.
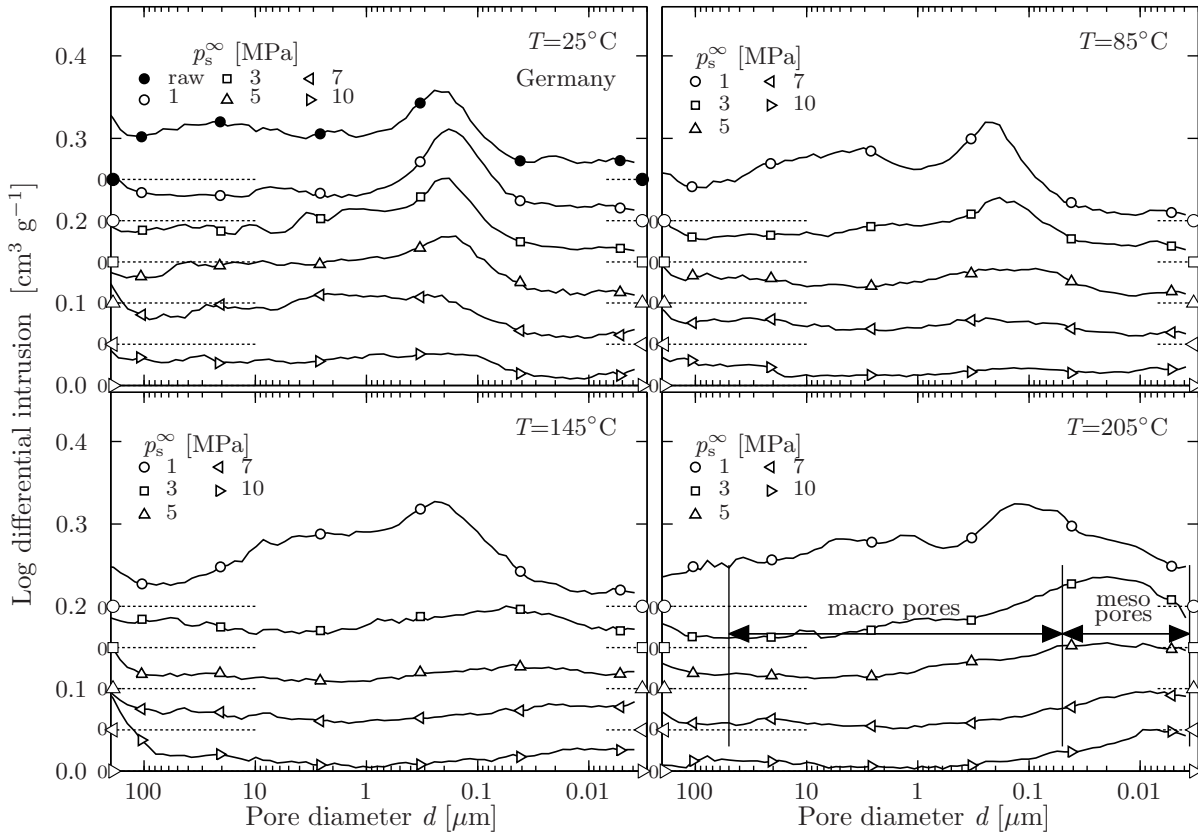
Figure 3.33: Logarithmic differential intrusion as a function of MTE process temperature and pressure for German coal

The MIP determined micropore volume shows a slight increases in MTE temperature (Figure 3.34c). Even if CO_2 adsorption experiments (Chapter 3.3.1) have shown different trends for Australian and Greek/German coals, the increase is consistent for all coal in this case. The observed difference in absolute numbers and trends is due to two different reasons. On the one hand the limiting micropore volume W_0 in the DUBININ-equation (3.12) just gives the extrapolated value of adsorbed CO_2 volume for $p_0/p \rightarrow 0$ and therefore maybe overestimates the micropore volume. On the other hand the He density used for the calculation of micropore volume according to Eq. (3.6) from MIP data is not the 'true density' and therefore underestimates the micropore volume. Since the shift towards smaller pores is evident for all MIP experiments performed the trends shown for the micropore volumes determined this way is thought to be more reliable.

Despite the observed decrease in macropore volume and increase in mesopore volume, the total pore volume decreases with increasing MTE temperature (Figure 3.34d), which is consistent with the decreased moisture content results. Similar decreases in total pore volume are also seen as a function of increasing MTE pressure.

As shown in Figure 3.36, the shift from macropores to mesopores with increasing MTE temperature is associated with an increase in surface area, as determined by mercury intrusion porosimetry experiments. The reverse trend was seen with increasing pressure, due to the continued decrease in mesopore volume. The surface area values obtained via this method are about 80 % smaller than the values obtained by CO_2 adsorption measurements with products from MTE experiments with Loy Yang Low Ash coal [HFC] and the three coals investigated in this work (Chapter 3.3.1). This is expected, as the MIP method is only valid for larger sized pores ranging between 3.6 nm and 50 μm in diameter. In comparison, the CO_2 adsorption method measures the area contribution of smaller sized (0.16 to 2 nm diameter) pores, which play a more significant role in controlling the surface area of a substance.
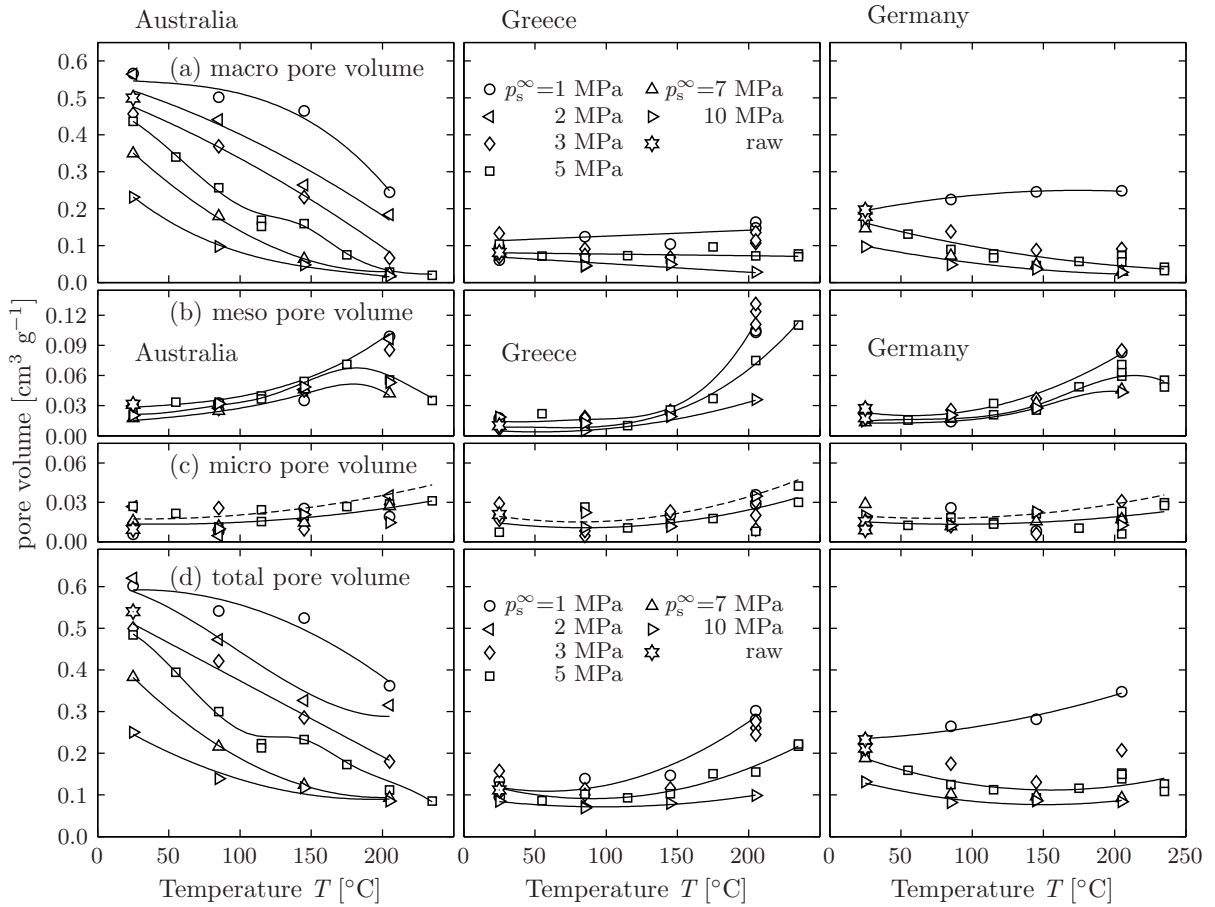
Figure 3.34: Macro, meso and micropore volume (dashed line for micropore volume gives maximum deviation for correction with intrusion compressibility)

Nevertheless the surface areas obtained from the MIP method are useful for a deeper understanding of trends in dewatering and combustion concerning the transport of water and gas, which mainly takes place in macro- and mesopores, rather than micropores.

In comparison to other researchers, surface areas calculated in this work are about three to ten times higher than values quoted in the literature [ZK54, Spi81]. This can be explained by the higher mercury intrusion pressures used in this work, which leads to the increased surface area contribution from smaller sized pores intruded at high pressures.

It is interesting to note that at very high temperatures ($>205°C$), the mesopore volume (Figure 3.34b) and surface area (Figure 3.36) decrease again. This is most likely due to the onset of severe thermal decomposition, leading to chemical changes [Ber03, HBCS04, HFC, HBCS] similar to those observed during natural coalification. In addition, there may be some melting of waxes, which can block parts of the pore system once the coal is highly compressed. The decrease can only be observed at intermediate and high consolidation pressures. There is also a slight decrease of mesopore volume and surface area with increasing pressure since parts of the porous network are possibly closed to mercury intrusion in highly compressed MTE products. Nevertheless this trend is not as pronounced as the increase with MTE temperature.

Greek and German coals Under mild MTE processing conditions, the total porosity of the Greek and German coals is significantly lower compared to the Australian coal (Figure 3.34d). This is due to the significantly lower macropore volume shown in Figure 3.34a, where the distinct macropore peak seen for the Australian coal (Figure 3.30a) is absent. Increasing the MTE temperature has only minor effect on the macropore volume, but significantly increases the mesopore volume.
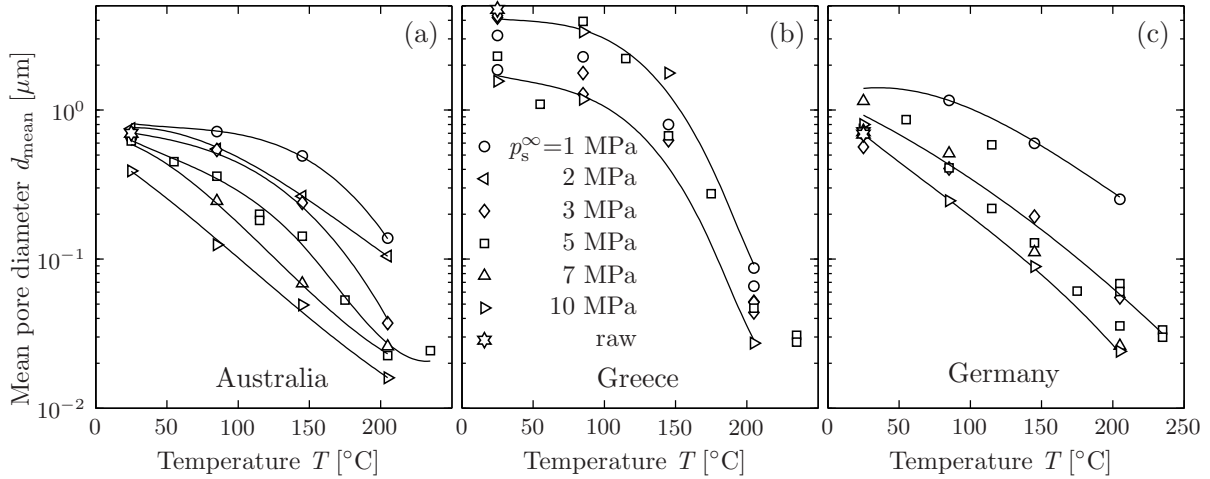
Figure 3.35: Mean pore diameter calculated from MIP data
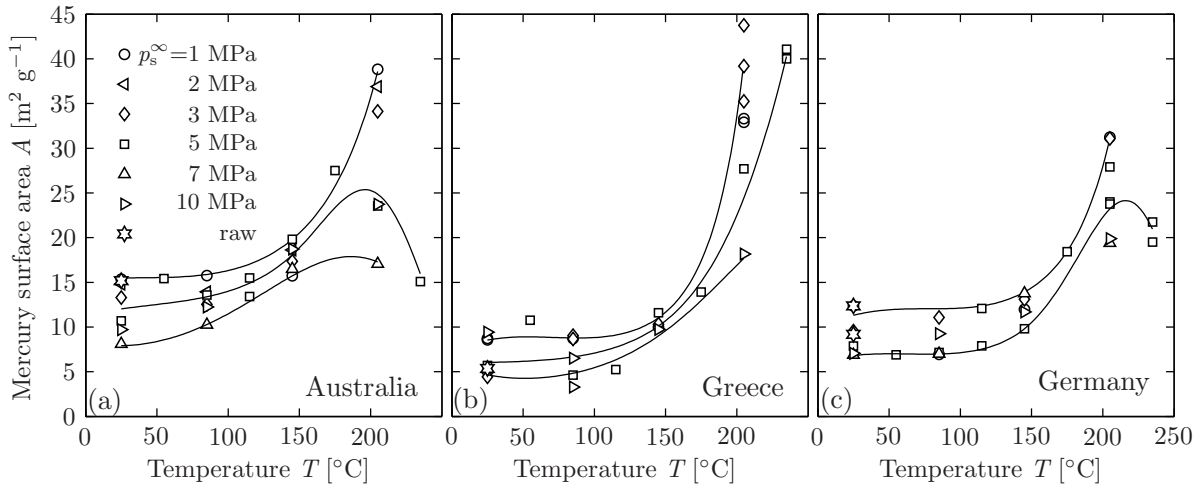
Figure 3.36: Specific surface area calculated from MIP data

This increase in mesopore volume is particularly pronounced for the Greek coal, where at temperatures and pressures above 175°C and 5 MPa the total pore volume exceeds the volume of the Greek coal treated under mild MTE processing conditions. The total pore volume increases continuously for all pressures with temperature (Figure 3.34d). Most of the increase in mesopore volume occurred in the 0.02 to 0.04 μm diameter region as shown in Figure 3.30b.

For both the Greek and German coals, this increase in mesopore volume was associated with a decrease in the mean pore diameter (Figure 3.35) and an increase in the MIP calculated surface area (Figure 3.36). As for the Australian coal, the micropore volume remains relatively unchanged (Figure 3.34c) and only increases slightly at the highest temperatures. An increase in pressure leads to a slight reduction in the macropore volume. Likewise, the mesopore volume decreases slightly, with the effect being most pronounced at higher temperatures, particularly for the Greek coal.

The observed increase in mesopore volume, particularly for the Greek coal, seen as a function of increasing MTE temperature could be due to a number of reasons, including the generation of pores during the MTE process. However, this mechanism is unlikely, considering, that thermal dewatering starts at about 140°C, leading to the collapse of the coal structure due to water release. Since the water contents of all coals are of the same order of magnitude for constant MTE process parameters, this suggests that the increase in mesopore volume is more likely due to a hardening of the coal structure and leading to changes in shrinkage behaviour as a function of increasing MTE temperature. This latter hypothesis is further supported by the fact, that for all three coal

types the increase in mesopore volume was not seen with increasing MTE pressure. To investigate this effect further, the shrinkage behaviour of all three coal types was monitored as a function of increasing MTE temperature and pressure.

3.3.4   Shrinkage

A comparison of the total pore volume of oven dried MTE products measured by the MIP method and the direct measurement of pellet dimensions using callipers (± 0.1 mm) is shown in Figure 3.37. As illustrated, the pore volumes from calliper measurements are significantly higher than those from the MIP measurements. This is believed to be due to the presence of cracks formed upon oven drying, which are not being captured by the MIP technique, even if the maximum pore volume is set to $420\,\mu m$ (grey symbols), which corresponds to the minimum pressure applied during MIP measurements. Since crack formation is dependent upon temperature, which affects the binding strength (e.g. during binderless briquetting), all shrinkage data are calculated using dry pore volumes determined from MIP measurements with an inter/intra particle cut off diameter of $50\,\mu m$.

Effect of temperature on shrinkage   Shown in Figure 3.38a is the effect of MTE temperature on the dry pore volume of all three coal types, plotted as a function of the total wet pore volume, determined from wet pellet dimensions. It should be noted, that since crack formation occurs in the later stages of drying, the error in the total wet pore volume can be neglected. The corresponding volume difference between wet and oven dried MTE products, as well as the percentage shrinkage (difference relative to the total wet pore volume) are shown in Figure 3.38b and c respectively.

For the Australian coal, at a constant applied MTE pressure of 5 MPa, the dry pore volume decreases continuously with increasing MTE temperature. In the case of the German coal, the dry pore volume remains relatively constant, while for the Greek coal, values are found to increase at the higher MTE temperatures investigated. The corresponding percentage shrinkage results shown in Figure 3.38c indicate, particularly for the Greek and German coals, a decrease in shrinkage at temperatures above about 85°C. Thus, indicating that a hardening of the coal structure is indeed occurring at elevated MTE temperatures. For the Australian coal similar behaviour is seen at various pressures, although the effect is not as pronounced.

Coal hardening and consequent porosity retention at elevated temperatures were also observed by BONGERS et al. [BJW00], who investigated the effects of steam drying on the pore structure of Loy Yang coal. BONGERS et al. observed that the use of steam drying at elevated temperatures (e.g. 182-225°C) with a low degree of superheat, resulted in little moisture loss, which lead to the retention of much of the bed moist porosity upon oven drying at 105°C. BONGERS et al. argued
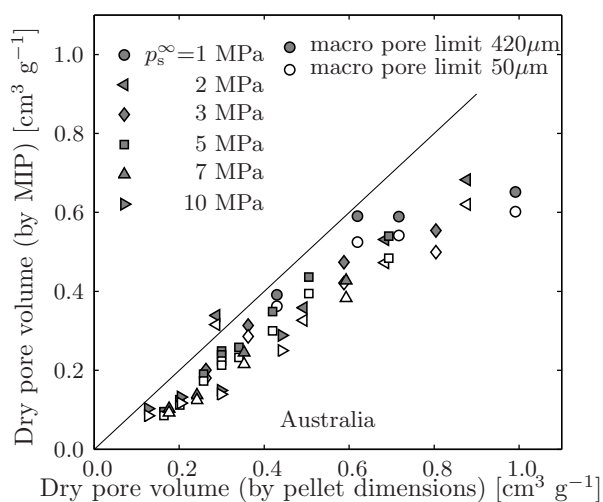
Figure 3.37:
Comparison of total pore volumes of dry MTE pellets measured by MIP and calculated from pellet dimensions
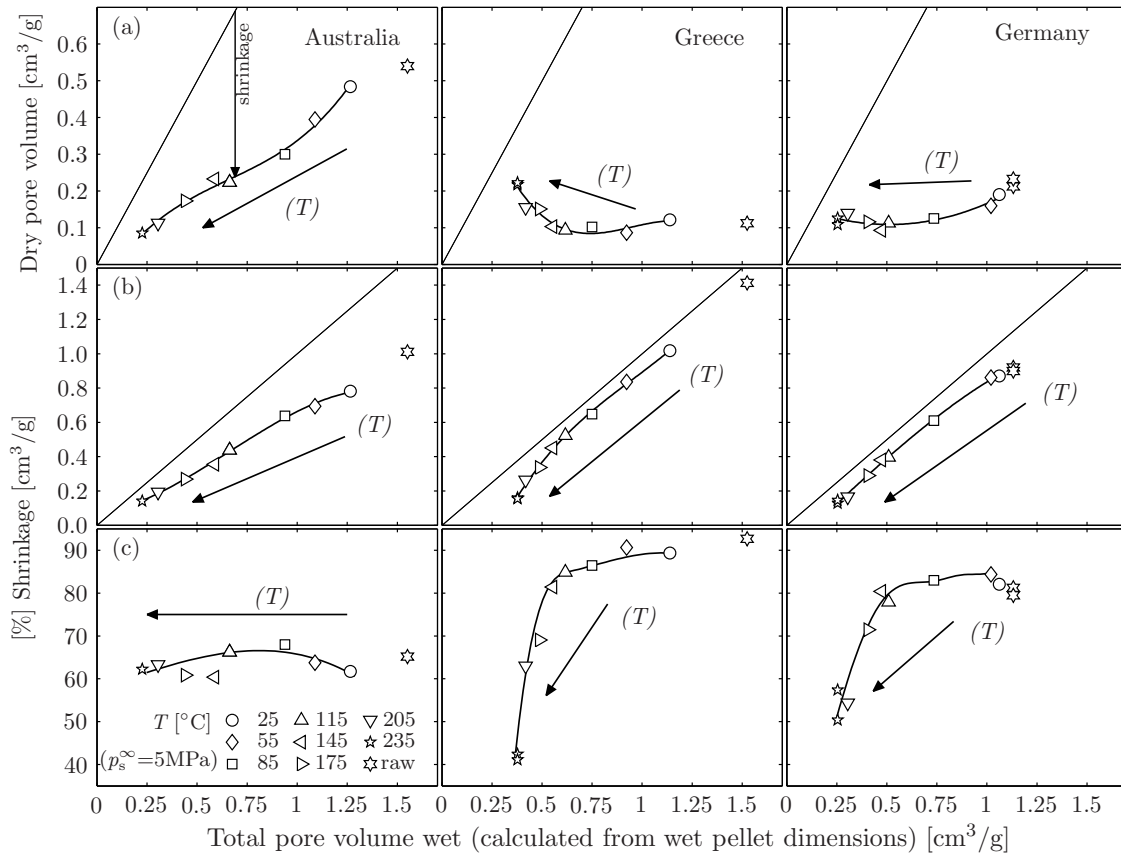
Figure 3.38: Total pore volume of wet and dry MTE pellets and shrinkage as a function of MTE temperature

that this effect is due to the occurrence of cross-linking reactions, where pore collapse is prevented by the presence of water inside the pores. The conditions experienced by the coal in the first stage of the MTE process (i.e. thermal dewatering), at very low applied pressures, are very similar to those of the low super heat steam drying experiments carried out by BONGERS et al. so that similar cross-linking reactions may be occurring during the MTE process. This again supports the conclusion that the non-evaporative water loss during thermal dewatering/treatment causes the observed effects of increased resistance to shrinkage.

Effect of pressure on shrinkage   The effects of MTE pressure on the dry pore volume, absolute volume reduction and percent shrinkage for all three MTE treated coal types are shown in Figure 3.39a to c. For the Australian coal, an increase in pressure leads to a reduction in the dry pore volume, which is associated with an increase in shrinkage. This trend is consistent for the various temperatures. The results therefore show, that MTE products treated at different temperatures and pressures may have similar moisture contents, but have very different shrinkage properties. For instance, while an Australian coal treated at $85°C/10\,MPa$ has a similar moisture content to a sample treated at $205°C/1\,MPa$, upon oven drying the sample treated at $205°C$ has twice the pore volume than a sample treated at $85°C$. Shrinkage studies undertaken by EVANS [Eva73a] on raw Yallourn coal showed, that shrinkage is mainly associated with the removal of capillary and multilayer water rather than bulk water due to the action of capillary forces. The observed increase in shrinkage of MTE products with increasing pressure could therefore be due to the shift from larger to smaller diameter pores as illustrated in Figure 3.35 and therefore increased capillary forces acting on the coal structure during drying. While a similar shift in pore size distribution is also seen as a function of temperature in Figure 3.35, the reverse trend in shrinkage i.e. a decreasing shrinkage with increasing MTE temperature in Figure 3.39c (T) is believed to be due to the dominating effects of hardening of the coal structure above $85°C$.
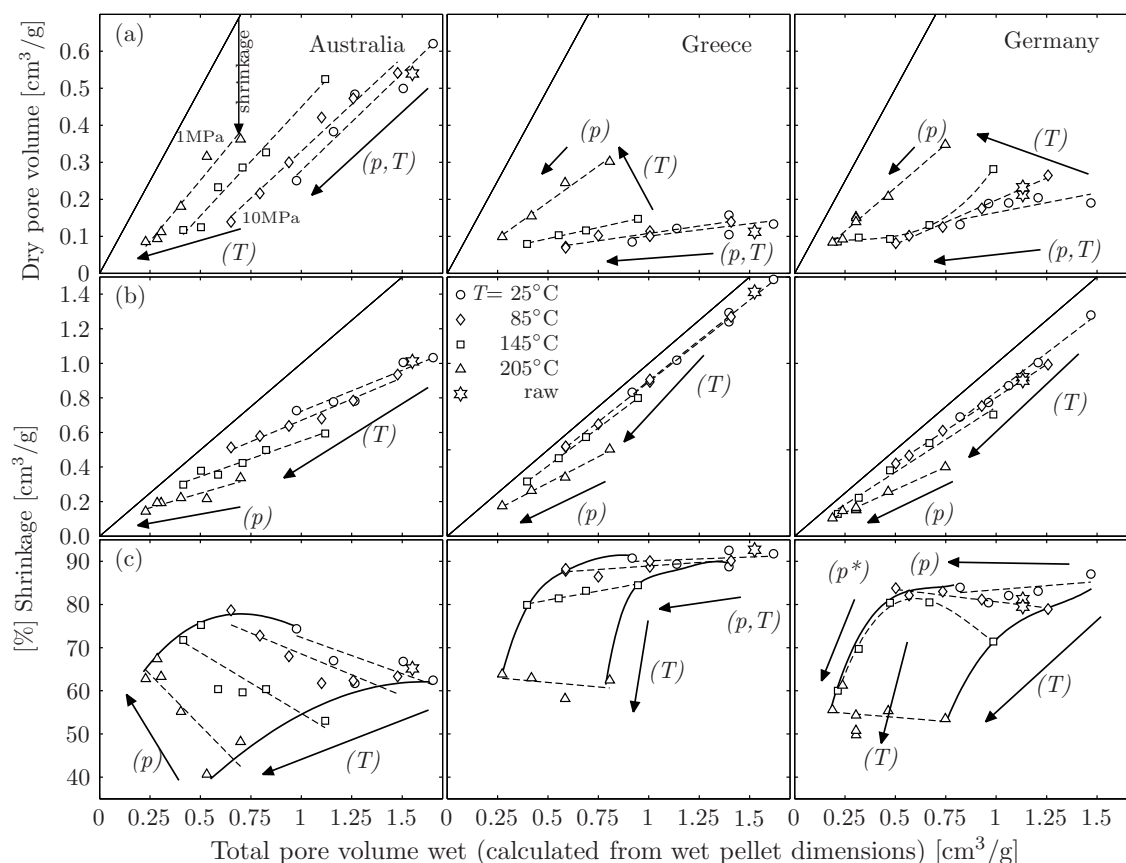
Figure 3.39: Total pore volume of wet and dry MTE pellets and shrinkage as a function of MTE pressure

For the German coal an increase in pressure at 85°C and 145°C results in an initial decrease in the dry pore volume (Figure 3.39a), which levels out at about $0.1\,\mathrm{cm^3/g}$ at the higher pressures tested. The corresponding percentage shrinkage results (Figure 3.39c) show an initial slight increase in shrinkage with increasing pressure (p) which, is believed to be due to a shift in porosity to smaller (e.g. capillary/multilayer) diameter pores as for the Australian coal.

At subsequently higher pressures, the degree of shrinkage for the 145°C case (squares) is found to decrease (p^*) again. This is believed to be due to the fact, that the minimum achievable pore volume (i.e. $0.1\,\mathrm{cm^3/g}$) is reached under these conditions. This minimum appears to be present for all three coals, and is consistent with the work of EVANS, who observed a zero differential shrinkage at a pore volume of about $0.1\,\mathrm{cm^3/g}$ [Eva73a]. At a temperature of 205°C, the shrinkage remains relatively constant with increasing pressure, which could be related to the hardening of the coal structure at elevated temperatures.

In terms of pressure dependent shrinkage behaviour, the Greek coal shows similar trends to the German coal, with the exception that the initial increase in shrinkage at 145°C is absent.

As shown above, temperature and consolidation pressure are the main factors in the dewatering, dominating the kinetics of the water removal during primary consolidation. For the evaluation of time effects on the pore structure six samples pressed for $10\,000$ and $100\,000\,\mathrm{s}$ (mainly creep phase/secondary consolidation) have been examined additionally. In Figure 3.40 also the total pore volumes and mean pore diameters determined by MIP and percentage shrinkage values are given. The results show a slight decrease for the total pore volume and for the mean pore diameter as well, which again supports the idea of transformation of bigger pores to smaller pores with increasing water removal. For the Australian coal percentage shrinkage increases while it slightly decreases for Greek and German coal. The shrinkage results therefore show the same trends as

	t	v_{pore}^{total}	d_{mean}	Shrinkage
	[s]	[cm³/g]	[µm]	[%]
○	10 000	0.223	0.201	66.3
□	100 000	0.168	0.110	71.7

	t	v_{pore}^{total}	d_{mean}	Shrinkage
	[s]	[cm³/g]	[µm]	[%]
○	10 000	0.093	2.217	84.9
□	100 000	0.088	0.643	83.2

	t	v_{pore}^{total}	d_{mean}	Shrinkage
	[s]	[cm³/g]	[µm]	[%]
○	10 000	0.113	0.585	77.9
□	100 000	0.112	0.219	75.0
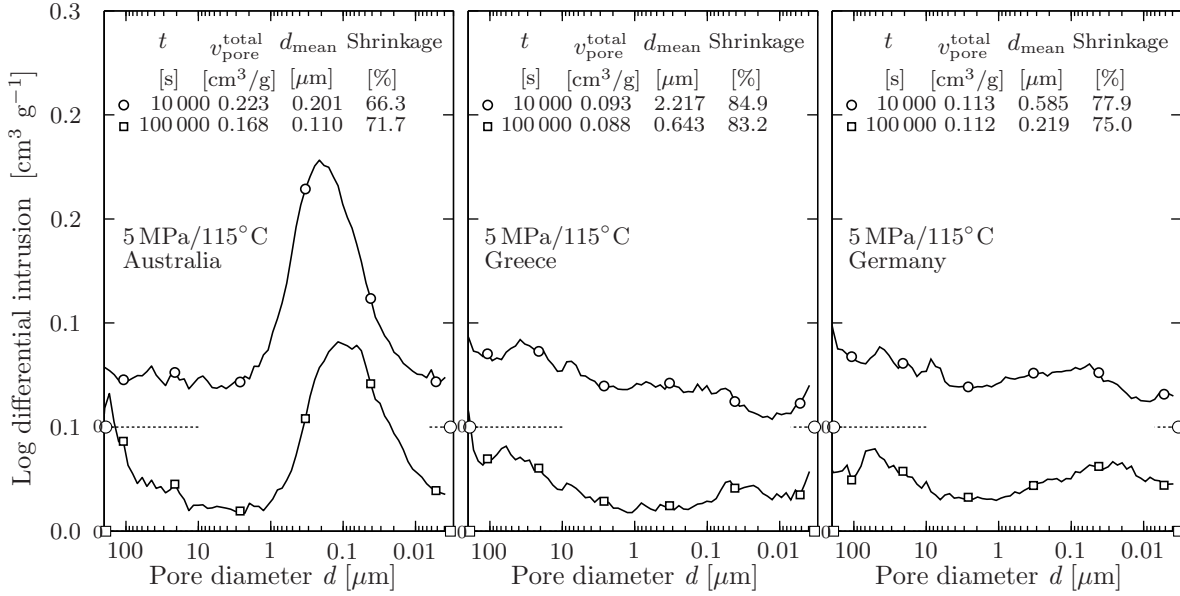
Figure 3.40: Influence of dewatering time on dry coal properties

can be seen for increasing consolidation pressure in Figure 3.39. Therefore it can be concluded that the hardening effect (and decrease in shrinkage) is only influenced by processing temperature, while pressure and consolidation time have similar effects (increase or decrease) depending on the absolute values of pore volume.

From the results obtained so far it is obvious, that the differences in pore size distribution between the three coal types mainly result from differences in shrinkage behaviour. The percentage shrinkage of the German and Greek coals is about twice as much as that of the Australian coal, even if the water contents of the MTE products are at the same order of magnitude for constant MTE process parameters. One explanation for this behaviour could be the higher ash content and elevated acid extractable Mg and Ca levels present in the Greek and German coals [HBCS04]. These elements and other clay components are known to undergo significant shrinkage and swelling [Vel95, Sch00]. On the other hand, there could also be differences in the origin of the plant material and cell wall structure contained in the amorphous phase of the coals.

3.3.5   Dry coal compression

To investigate the influence of temperature on the rigidity of the coal matrix itself, German dry coal samples (raw coal) were compressed at different temperatures in nitrogen atmosphere (Figure 3.41). All experiments were performed at constant consolidation rate and the relaxation of the pressure was measured at 4.5 and 6.5 MPa. The time dependent course of the pressure during the whole experiment is shown for three different temperatures in Figure 3.41a, relaxation of the pressure at 4.5 and 6.5 MPa is drawn normalised as a function of time in Figure 3.41b and c and as a function of temperature in Figure 3.41e. Pore volumes are calculated from the pellet height during the experiments. The coal mass was corrected for thermal decomposition (up to 5 % in these experiments) and density was corrected for thermal expansion [BF46, ZK54].

Compared to the total pore volumes measured during MIP experiments (Figure 3.34, page 45) all values given in Figure 3.41d are higher due to the additional inter-particle pore volume also included in the calculated values. Nevertheless, the relative changes also show significant trends which can be compared with the results measured by MIP.

Due to the softening of the coal structure above approx. 80°C the compressibility is increased and pore volumes are lower when compared at the same pressures (Figure 3.41d). With the onset of thermal decomposition hardening occurs i.e. the compressibility is decreased again and pore
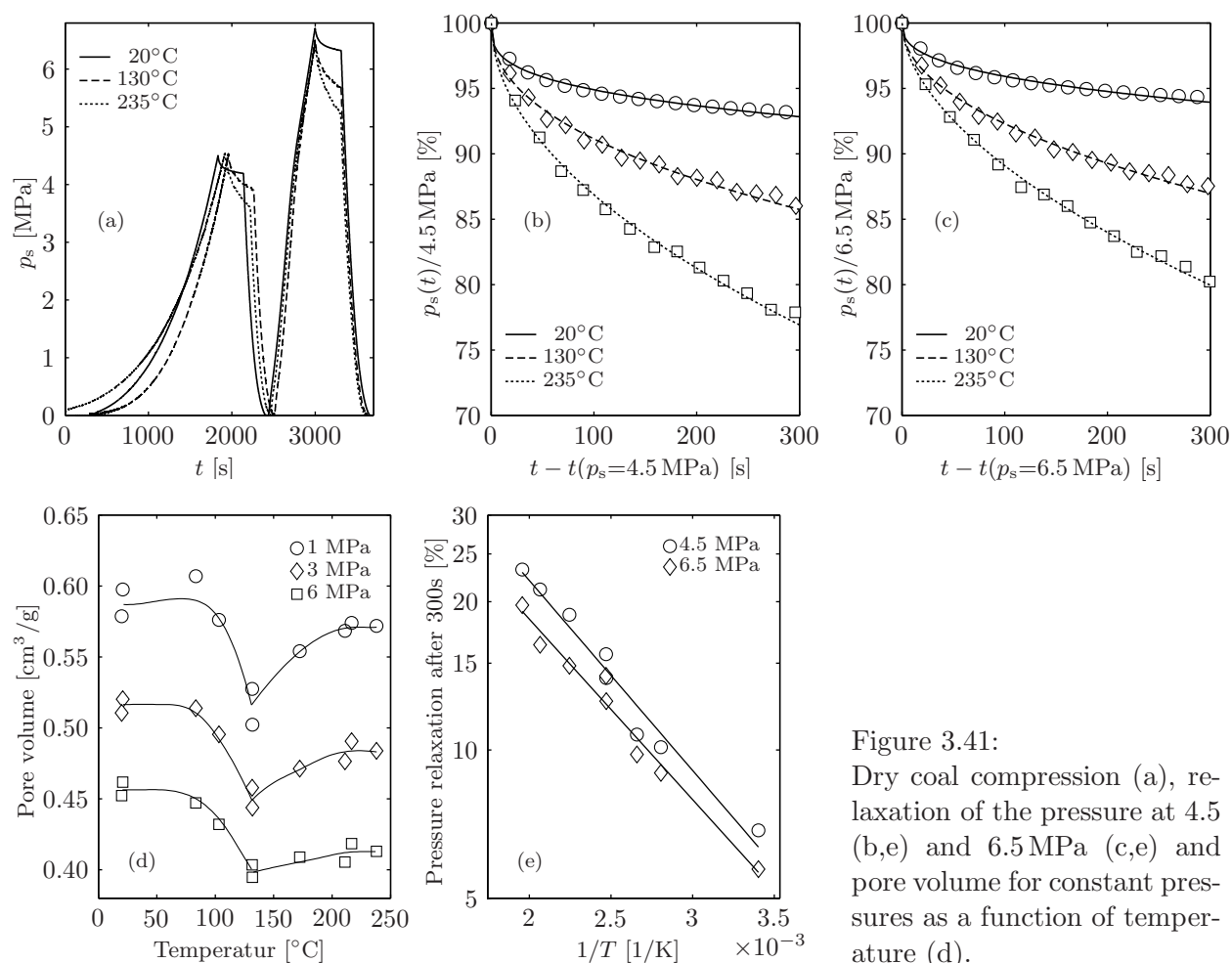
Figure 3.41:
Dry coal compression (a), relaxation of the pressure at 4.5 (b,e) and 6.5 MPa (c,e) and pore volume for constant pressures as a function of temperature (d).

volumes are increased. However, the rate of pressure relaxation continuously increases between 20 and 235°C due to the increasing thermal energy, since the relaxation is a dynamic process which can be described also by rate process theory (Chapter 3.2.1) as the linear course in the ARRHENIUS-plot in Figure 3.41e shows. Deviations from the regression line in this plot for 4.5 MPa and medium temperatures are thought to result from a slight influence of hardening on relaxation. At 6.5 MPa this influence disappears due to the high forces applied. Also the increase in pore volume at 6 MPa in Figure 3.41d is much smaller than at lower consolidation pressures.

These results give additional evidence for the increase in rigidity of the coal structure during the thermal treatment which consequently leads to a decreases shrinkage at higher temperatures. The difference in pore volume of approx. $0.1\,\text{cm}^3/\text{g}$ between 130 and 200°C in Figure 3.41d shows a good agreement with the difference in shrinkage and the increase in total pore volume for the German coal in Figure 3.34d.

3.4   Demineralisation

In order to determine the effect of MTE on the chemical composition of treated coals, samples of Australian, Greek and German coals were characterised in terms of their ultimate and proximate analyses and inorganic species concentration. Inorganic species, such as alkaline and alkaline earth metals (AAEM) play an important role in pyrolysis and combustion behaviour and lead to low temperature fouling and slagging [Smo93]. Thus, it is of importance, to establish, how the concentrations of these species are affected by the MTE process. In Chapter 3.4.3 the demineralization effect of the MTE process is therefore investigated and compared to leaching experiments, which allow the determination of the maximum fraction of inorganics removable from the coal.

3.4.1   Ultimate and Proximate Analysis

The MTE process has little effect on the ultimate analysis, which includes an analysis of the C, H, N and total S content, see Table 3.5. This suggests, that the MTE process, under the conditions tested, has little effect on the overall organic composition of the coals investigated. It should however be noted, that at present no investigation into the effects of MTE on changes in composition and nature of organic functional groups has been carried out.

Table 3.5:   Ultimate and proximate analysis of raw and MTE treated coals
(HRL Technology Pty. Ltd. analysis of dried samples)

Condition		Ash (%db) ±0.1	Volatile matter (%daf) ±0.7	Fixed carbon (%daf) ±0.7	C ±1.3%	H ±0.12%	wt.% daf N ±0.1%	S_{total} ±0.05%	O_{diff} ±0.14%
Australia (raw)		1.0	52.5	47.6	68.2	4.70	0.51	0.30	26.3
85°C	3 MPa	1.0	51.9	48.2	67.5	4.59	0.55	0.33	27.0
85°C	10 MPa	0.9	51.6	48.4	67.6	4.60	0.56	0.30	26.9
205°C	3 MPa	0.8	50.2	49.8	69.0	4.65	0.57	0.28	25.5
205°C	10 MPa	0.8	48.8	51.2	68.4	4.33	0.53	0.30	26.5
25°C	5 MPa	0.9	51.7	48.4	67.3	4.51	0.53	0.26	27.4
85°C	5 MPa	0.9	51.6	48.4	67.6	4.57	0.52	0.26	27.1
145°C	5 MPa	1.0	51.2	48.8	67.8	4.45	0.52	0.29	26.9
205°C	5 MPa	0.9	49.7	50.3	67.5	4.31	0.51	0.28	27.4
235°C	5 MPa	1.0	48.5	51.5	69.8	4.49	0.55	0.31	24.9
Greece (raw)		14.1	57.7	42.3	62.7	4.99	1.57	0.76	30.0
85°C	3 MPa	13.5	56.4	43.6	63.5	4.73	1.62	0.62	29.6
85°C	10 MPa	13.8	55.0	45.0	63.7	4.49	1.61	0.58	29.6
205°C	3 MPa	13.2	54.5	45.5	66.2	4.34	1.65	0.60	273
205°C	10 MPa	13.3	53.7	46.3	64.6	4.29	1.64	0.63	28.8
Germany (raw)		6.3	54.6	45.4	66.7	4.93	0.77	0.43	27.2
85°C	5 MPa	5.3	53.2	46.8	66.3	4.59	0.79	0.40	27.9
85°C	10 MPa	5.4	52.3	47.7	66.8	4.62	0.77	0.40	27.4
205°C	5 MPa	6.0	53.1	46.9	67.7	4.65	0.82	0.43	26.4
205°C	10 MPa	6.0	53.5	46.6	67.2	4.45	0.78	0.41	27.1

The effect of MTE on the ash yield is minimal, although any effect may be masked by sampling inhomogeneities (particularly for the German and Greek coals). The volatile content decreases for both the Australian and Greek coals, indicating the onset of thermal transformations (e.g. decarboxylation reactions, cross-linking etc). However, this effect is not as evident for the German coal, possibly because it has experienced greater compaction during its depositional history. The increase in fixed carbon content is a result of a decrease in volatile matter, which is not evident for the German coal.

3.4.2   Total elemental and acid extractable concentrations

To gain an understanding of how the MTE process affects the behaviour of these species, samples of all three coal types were characterised in terms of their total elemental as well as acid extractable concentrations (Table 3.6). The results of an additional ash analysis for the three coals and two other Hambach coals are given in Table 3.7.

Australian coal   With the exception of Na and Cl, the MTE process has little effect on the total elemental concentration of the Australian coal. Total Na levels are similar to the acid extractable values, indicating that the Na is present as a dissolved salt in the bulk water and/or is bound to surface functional groups such as carboxylates or phenolics. With increasing temperature increasing amounts of Na are removed, while increasing pressure only leads to slight changes in the Na content of the samples. These trends are discussed in detail in the next section.

After an initial loss of Cl for the Australian coal in Table 3.6 under mild MTE processing conditions (85°C/3 MPa), Cl levels remain relatively constant at elevated temperatures and pressures. A possible explanation is that some of the Cl is removed as NaCl, with the remainder consisting of organic Cl, which can not be removed by dewatering.

While the total elemental Al concentration remains unchanged by the MTE process, the acid extractable form of Al decreases in concentration with increasing MTE processing severity. This indicates that the Al species is changing to a less acid soluble form during MTE processing. Similar effects were observed by CHAFFEE et al. [CFJ00] and FAVAS [Fav00] for hydrothermally treated Loy Yang coal at significantly higher temperatures (>300°C). Nevertheless the total Al concentration of the Loy Yang coal is very low.

Table 3.6:   Acid extractable and total elemental concentrations
for raw and MTE treated coals (HRL Technology Pty. Ltd. analysis)

Condition		Acid Extractable Inorganics g/kg (db) (of untreated coal)*					Total Elements g/kg (db) (of untreated coal)*							
		Al	Fe	Ca	Mg	Na	Al	Fe	Ca	Mg	Na	Cl	Si	S
Australia (raw)		0.7	0.5	0.7	0.7	1.2	0.9	0.4	0.5	0.6	1.0	1.4	0.5	3.0
85°C	3 MPa	0.7	0.5	0.7	0.6	0.7						0.8		3.0
85°C	10 MPa	0.7	0.6	0.6	0.6	0.6						0.7		3.0
205°C	3 MPa	0.5	0.4	0.7	0.5	0.3						0.6		2.7
205°C	10 MPa	0.1	0.6	0.9	0.5	0.3	1.0	0.5	0.6	0.6	0.2	0.6	0.5	2.9
25°C	5 MPa	0.6	0.8	0.9	0.7	0.7						0.7		2.6
85°C	5 MPa	0.8	0.7	0.8	0.6	0.6						0.6		2.6
145°C	5 MPa	0.6	0.8	0.8	0.6	0.4						0.7		2.9
205°C	5 MPa	0.5	0.7	0.9	0.6	0.3						0.6		2.7
235°C	5 MPa	0.1	0.7	0.8	0.5	0.2						0.6		2.9
Greece (raw)		2.6	4.8	38.5	5.2	0.2	5.9	5.7	44	5.3	0.2	0.3	10.0	7.6
85°C	3 MPa	2.9	4.8	31.8	5.1	0.1						0.2		6.1
85°C	10 MPa	2.3	4.9	28.8	5.0	0.2						0.2		5.7
205°C	3 MPa	2.3	4.6	29.3	4.7	0.1						0.2		5.7
205°C	10 MPa	2.1	4.8	27.9	4.8	0.1	5.1	5.5	42	4.8	<0.1	0.2	7.7	6.0
Germany[+] (raw)		0.4	10.9	11.5	4.4	0.9	0.9	11.3	12.4	4.5	1.0	0.3	3.6	4.3
85°C	5 MPa	0.4	5.9	11.5	4.4	0.8						0.3		4.0
85°C	10 MPa	0.4	6.9	11.3	4.3	0.8						0.2		4.1
205°C	5 MPa	0.4	8.1	11.4	4.2	0.4						0.3		4.1
205°C	10 MPa	<0.1	2.0	9.6	3.4	0.3	0.9	6.1	12.1	4.0	0.3	0.2	5.6	3.9

*Error   ± 0.1 g/kg for concentrations of 0.1-1.0 g/kg
          ± 0.2 g/kg for concentrations ≥ 1 g/kg
[+]Hambach low ash, HLA I

Table 3.7:   Total elemental concentrations for raw coals
(Rheinbraun and EON Engineering ash analysis)

				g/kg (db)				
	Si	Al	Fe	Ti	Ca	Mg	Ba	Zn
Australia	0.24	1.42	0.26	0.02	0.38	0.98	<0.01	<0.01
Greece	12.12	7.83	6.90	0.44	63.20	7.27	0.05	0.04
Germany (HLA I)	1.43	0.69	5.40	0.06	12.66	4.59	0.12	
Germany (HLA II)	0.33	0.46	3.86	0.05	12.80	4.31	0.12	
Germany (HLA III)	2.08	0.35	2.81	0.12	12.61	5.43	0.15	<0.01
	Cu	Mn	Na	K	S	P	Cl	Cr
Australia	<0.01	<0.01	1.44	0.06	1.72	0.00	<0.01	<0.01
Greece	<0.04	0.07	0.23	0.79	11.41	0.29	0.13	0.08
Germany (HLA I)		0.09	1.15	0.28	2.66	0.12		
Germany (HLA II)		<0.04	2.27	0.28	2.78	0.10		
Germany (HLA III)	<0.01	<0.04	1.93	0.31	5.96	<0.01	0.23	<0.01

Greek coal   While the mineralogy of the Greek coal is not investigated, studies undertaken by FILIPPIDIS and GEORGAKOPOULOS have shown, that Greek coals obtained from the main and northern lignite fields in Ptolemais contain significant amounts of $CaCO_3$, SiO_2, feldspar and mica [FG92]. Consequently, as the coal sample studied in this investigation was sourced from Ptolemais, it is likely, that the sample contains similar mineral species. Under the processing conditions used, the MTE process has only little effect on the total elemental composition.

The sulphur content decreases slightly under mild MTE processing conditions, but remains constant at higher temperatures and pressures. This indicates that chemical changes are occurring at quite mild temperatures, making the sulphur less water-soluble. Thermal dewatering studies ($250°C$) carried out on South Australian coals by DUNNE and AGNEW [DA92] identified a decreasing amount of organic sulphur and an increasing amount of sulfate sulphur under the conditions tested.

The data for the extractable species and total elements show a significant reduction in Al and Mg concentration. The removed Al and Mg is thought to be mainly in the form of $AlCl_3$, $Al_2(SO_4)_3$, $MgCl_2$ or $MgSO_4$ since these salts are sufficiently soluble in water. The sulfates should contribute to the mayor part of the removal, because the Cl concentration both of raw and dewatered samples is low.

In terms of acid extractable species, a 25 % reduction in Ca levels is observed, which again indicates, that the chemical form of Ca is changing, since total Ca levels remain relatively unchanged. One explanation could be the formation of less soluble carbonates.

German coal   For the German coal, the MTE process results in significant reductions in total and acid extractable Na levels with increasing processing temperature. Similar to the Australian coal, the reductions in Na levels are smaller for increasing MTE pressures (and therefore just an increase in water removal). This implies, that most of the Na is present in forms other than dissolved salt in the German coal. Studies undertaken by WILD et al. [WQCS02, WBS04] and QI [Qi04] showed that significant amounts of Na are removed by MTE upon acidification, indicating that most of the Na is present in an organically bound or acid soluble mineral form.

In addition to lowering the Na level, the MTE process results in a reduction of more than 45 % in total and acid extractable Fe levels. For Mg and S under the most severe MTE condition tested ($205°C/10\,MPa$), a reduction of 10 % is found.

3.4.3 Sodium removal during dewatering and leaching

In the following the reduction of sodium content during the mechanical/thermal dewatering is examined in detail. The results from MTE experiments are compared to those obtained from 24 h (not stirred) leaching experiments. Sodium is chosen since high Na concentrations are known to be one crucial factor in fouling and slagging in boilers. Water and acid leaching of lignites is investigated for years to provide a clean fuel for burning in power plants. As examples, READETT and QUAST [Rea89] have shown for South Australian coals (Bowmanns) that more than 70 % of the sodium can be removed at lignite to water ratios of 1:5 and that a removal of up to 90 % is possible, if the coal additionally is dewatered mechanically at 16.8 MPa [RQFK87]. READETT and QUAST also showed, that the removal of the water soluble fraction of sodium is diffusion limited, i.e. only mild agitation is required to reach an equilibrium within 1 h for particles smaller than 8 mm [RQMK84, Rea89].

There where also several investigations, which showed an increase in removal kinetics and total amount of removed minerals by leaching at increased temperatures ([Rea89], South Australian coal; [NNK77], Illionois Coal) especially in combination with thermal or hydrothermal dewatering ([DA92], South Australian coals; [FJ03], Australian, Indonesian and American coals). Only few investigations are published concerning the removal of minerals during the mechanical/thermal dewatering [QL01, WQCS02, AC04, WBS04, HBCS04, HBCS05, HFC], which are all limited to the analysis of the change in concentration of selected elements depending on MTE process parameters
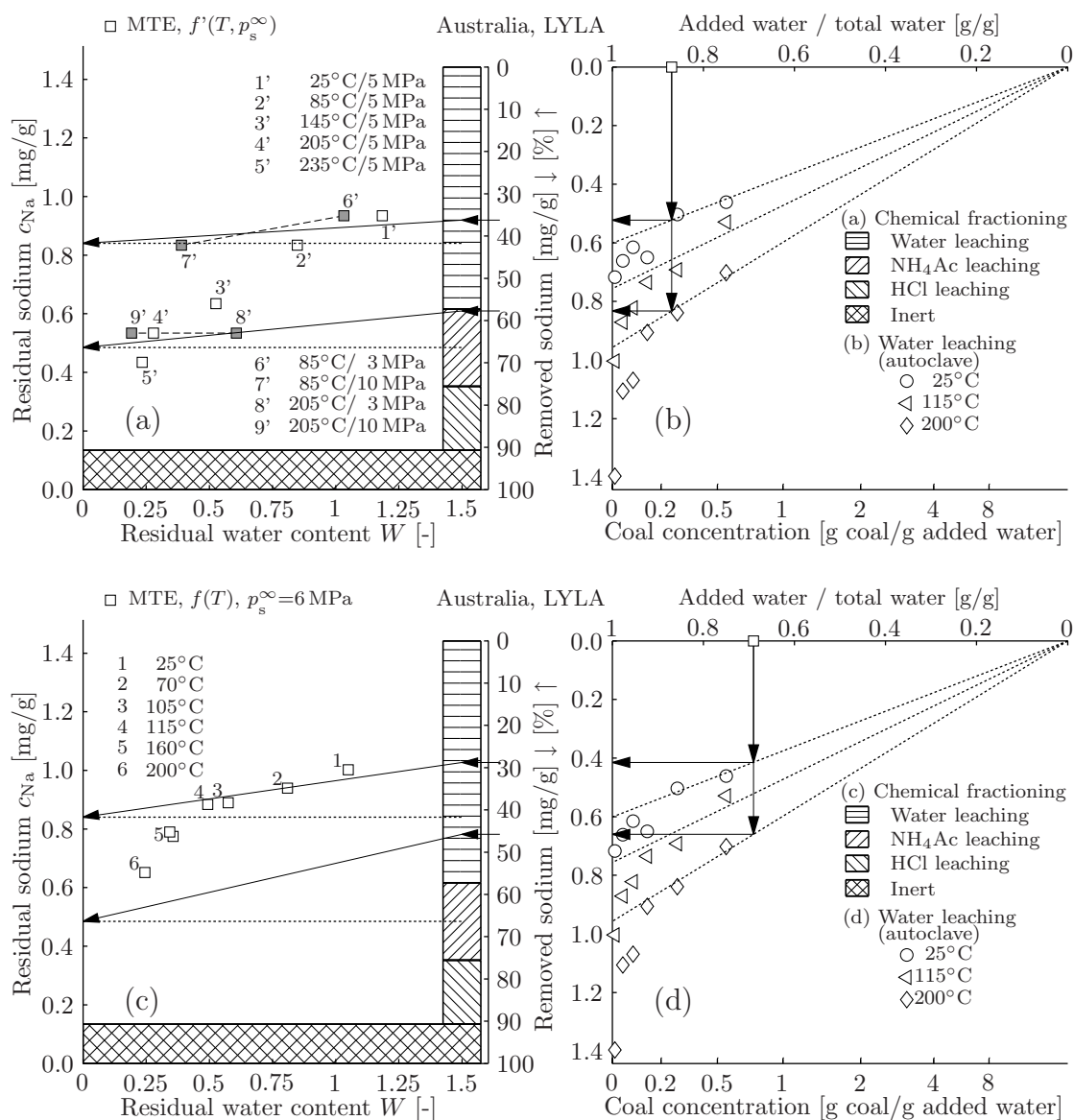
Figure 3.42: Dewatering and sodium removal during mechanical/thermal dewatering (a,c) and water leaching experiments (b,d) in comparison to the results of chemical fractioning (a,c), Loy Yang coal.

temperature and pressure. Therefore in the following the leaching process and its influence on the sodium removal is included in the investigation additionally. This will provide also a deeper understanding of the influence of the form of minerals (water or acid soluble, organically bound) on the removed fraction.

Australian coal The results for the dewatering and sodium removal during mechanical/thermal dewatering and water leaching experiments as well as the results of the chemical fractioning are shown for two sets of MTE experiments in Figure 3.42 as a function of residual water content after MTE (Figure 3.42a/c two different ratios of raw coal and water) and suspension concentration during leaching (Figure 3.42b).

The data in Figure 3.42a are taken from Table 3.6 and a value of 0.1 g/kg is added to correct for the differences in total elemental concentrations determined by HRL Technology Pty. Ltd. and EON Engineering and for the differences in acid extractable sodium determined by HRL Technology Pty. Ltd. and during chemical fractioning. This correction is essential for further comparisons and just compensates for systematic differences in German and Australian Standards and the procedure of

chemical fractioning. The results given in Figure 3.42b/d and c can be compared directly since they are calculated based on the AAS analysis of both water from leaching experiments and expressed water from MTE experiments.

The leaching results in Figure 3.42b/d show a deviation of the data points from the dotted line for concentrations lower than 0.1 g of raw coal per g of added water. In such diluted suspensions already sodium associated to functional coal groups is released to the leaching water. Therefore the water soluble fraction determined by chemical fractioning (measured at the same coal to water ratio of 0.1) is also too high in this case. With increasing temperature additional (organically bound) sodium is released to the leaching water, see also [Böh02, WBS04].

From the solids concentration in the MTE experiments – starting point of the arrows at the top of the plots in Figure 3.42b/d – and the extrapolation of the dotted leaching line to the dewatering diagrams (Figure 3.42a/c) the maximum and minimum concentrations to be expected during MTE processing can be estimated, which is graphically shown depending on the residual water content for 25°C and 200°C by the continuing arrows in Figure 3.42a/c. In both plots the results for MTE experiments at temperatures up to 115°C (1', 2', 6', 7' and 1-4) are in close agreement to the expected values. As the difference in the slope of the arrows in (a,c) shows, the residual sodium content after dewatering depends on the initial coal to water ratio, temperature and the residual water content.

From the investigations of other researchers [RQMK84, Rea89] and similar experiments with the coals investigated here [Wild] it is clear, that the results obtained from the laboratory MTE experiments (described in Chapter 3.1.1) only represent a conservative estimation on the total amount of minerals that can be removed during combined leaching and mechanical/thermal dewatering, since the heating is undertaken without further agitating of the suspension and only for one hour. This also explains the slightly higher residual sodium contents in comparison to the estimated values (Figure 3.42a/c).

While increased dewatering only leads to a small increase in sodium removal, a temperature increase can improve the sodium release dramatically by the additional release of organically bound fractions (3'-5', 8', 9' and 5, 6) as also found by BAILEY et al. during experimental diagenesis of peats [BCOB00].

In contrast to the results of chemical fractioning the leaching and dewatering results show that only about 40 % of the sodium in the Australian coal is present in the water as a dissolved salt, about 25 % are organically bound. During dewatering at low temperatures the water soluble fraction can be removed nearly complete by dilution and dewatering, see also [RQFK87]. Under the most severe conditions tested (e.g. 235°C/10 MPa) the MTE process is able to remove about 70 % of the initial sodium content of the raw coal, which includes – according to chemical fractioning – also a small fraction of acid soluble sodium. These findings are consistent with previous work undertaken by WILD et al. [WQCS02] and HULSTON et al. [HFC]. The reduction of mayor parts of the sodium may also be beneficial for the reduction of fouling problems in power station boilers [BSS04].

German coal Results for the dewatering and sodium removal during mechanical/thermal dewatering of the three Hambach coals (Table 3.7) and the corresponding water leaching experiments are plotted in Figure 3.43 as a function of residual water content after MTE (Figure 3.43a: Hambach coals I-III) and suspension concentration during leaching (Figure 3.43b: Hambach coals II & III). For the Hambach III coal absolute values for removed and residual sodium contents are given. For the two other coals the results are plotted as percentage values corresponding to the right axis of diagram Figure 3.43a. The acid extractable values for the Hambach I coal (Table 3.6) have been corrected for the differences of the two ash analyses and the inert fraction of sodium by adding 0.15 mg/g plus 0.1 mg/g.

During leaching at ambient temperature (circles in Figure 3.43b) the Hambach coals II & III show a similar behaviour with only about 10 to 15 % of water soluble sodium. There is an increasing
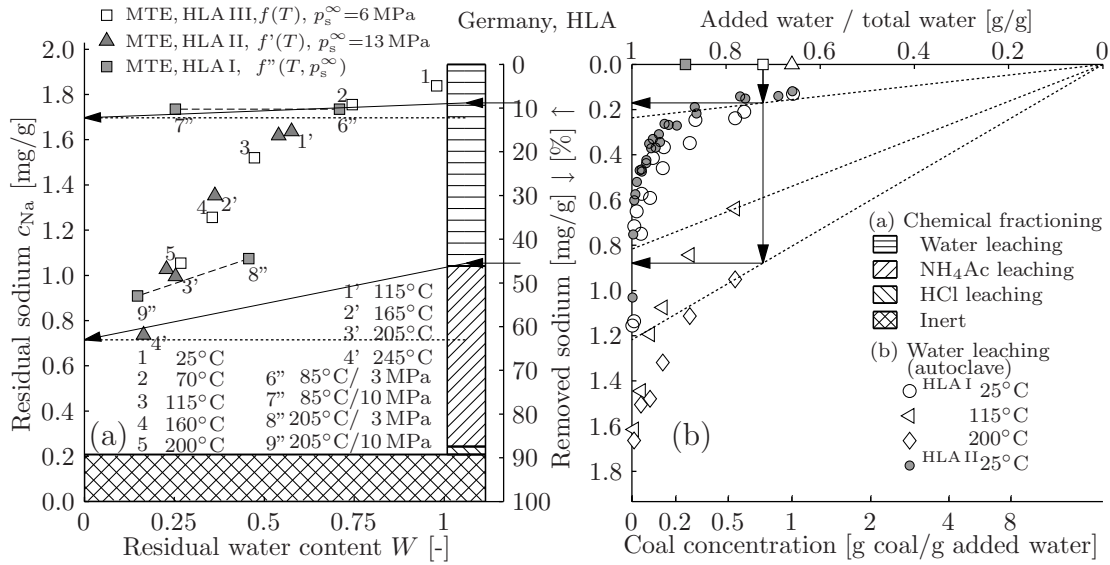
Figure 3.43: Dewatering and sodium removal during mechanical/thermal dewatering (a) and water leaching experiments (b) in comparison to the results of chemical fractioning (a), German coals (HLA III as absolute values, HLA I & II as percentage values).
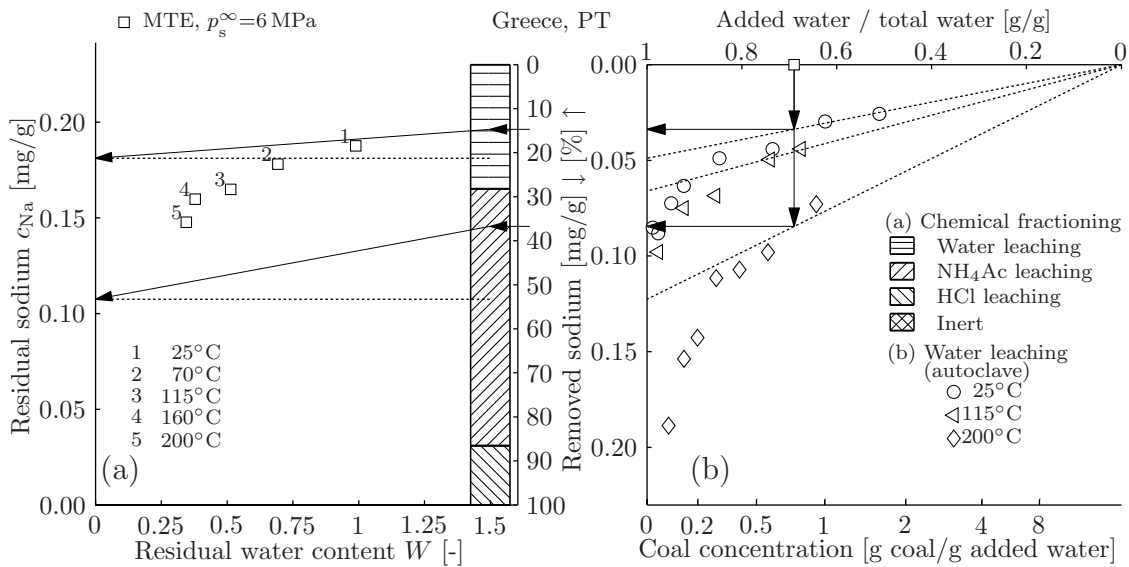

Figure 3.44: Dewatering and sodium removal during mechanical/thermal dewatering (a) and water leaching experiments (b) in comparison to the results of chemical fractioning (a), Greek coal.

deviation between the dotted line and the experimental values for solid concentrations below 0.5 g/g. Therefore it can be concluded, that the amount of organically bound sodium is much larger than for the Australian coal. Due to the larger deviation of the data points from the extrapolation, also the amount of water soluble sodium determined from chemical fractioning (45 %) is overestimated largely. Increasing the leaching temperature leads to a complete removal of the water soluble and organically bound sodium (Σ 88 %) at 200°C and the lowest solid concentration.

Using the leaching curves for the prediction of the percentage removal of sodium leads to a good agreement. A small overestimation of the removal is again due to the shorter leaching times and missing agitation in the MTE experiments.

There is also a good agreement in the course of percentage removal with the residual water content for all three coals. Slight differences in the water contents for similar temperatures can be explained with different consolidation pressures and solid loadings in the experiments (26 kg/m^2 for HLA I, 53 kg/m^2 for HLA II, and 39 kg/m^2 for HLA III) while the dewatering time was always 10 000 s.

Greek coal   The results for the dewatering and sodium removal during mechanical/thermal de-
watering of Greek coal and the corresponding water leaching experiments are shown in Figure
3.44. Even if the absolute Na levels are comparatively low for this lignite, the similar trends as
for the German coal can be observed. Only about 20 % of sodium are water soluble at ambient
temperature. Temperature and dilution of the coal/water mixture have to be increased severely
to remove additional amounts of Na during leaching (b) or dewatering (a, 5). Therefore it can
be assumed, that the stability of the sodium binding to the coal and the thermal stability of the
oxygen containing functional groups, which are thought to contribute for the mayor part of such
bindings, is much higher than for the German coal.

3.5   Physical/chemical properties of dewatered coals

Both physical and chemical properties play an important role in the further utilization of MTE
products. But besides the direct influence of physical and chemical properties like porosity, water
and minerals content on transportation, handling and grinding and slagging there are also indirect
effects. The long term stability of MTE products against re-wetting is of interest regarding the pro-
duction of an not only transportable but also exportable fuel from lignite in countries like Australia
[HBCS04]. Concerning the combustion of lignite in power plants it also has to be investigated, if
the compaction of the coal and the decrease in pore space has negative effects on ignition and
combustion behaviour.

3.5.1   Effect of MTE on water uptake behaviour

To gain a further understanding of how the MTE process affects the material properties of MTE
treated coals, samples are characterised for their water uptake properties. The effects of MTE on
the equilibrium moisture content (EMC) at ambient conditions are of particular interest. As the
samples have previously been oven dried (to establish shrinkage behaviour), the MTE treated prod-
ucts are re-hydrated at a relative humidity of 100 % for 73 days. To mimic ambient conditions, the
re-hydrated samples are then subsequently exposed to a relative humidity of 52 % at a temperature
of 30°C for 14 days.

The most significant water uptake occurred within the first three weeks, beyond which further
water uptake is relatively slow (Figure 3.45). Of the three coal types investigated, the Greek coal
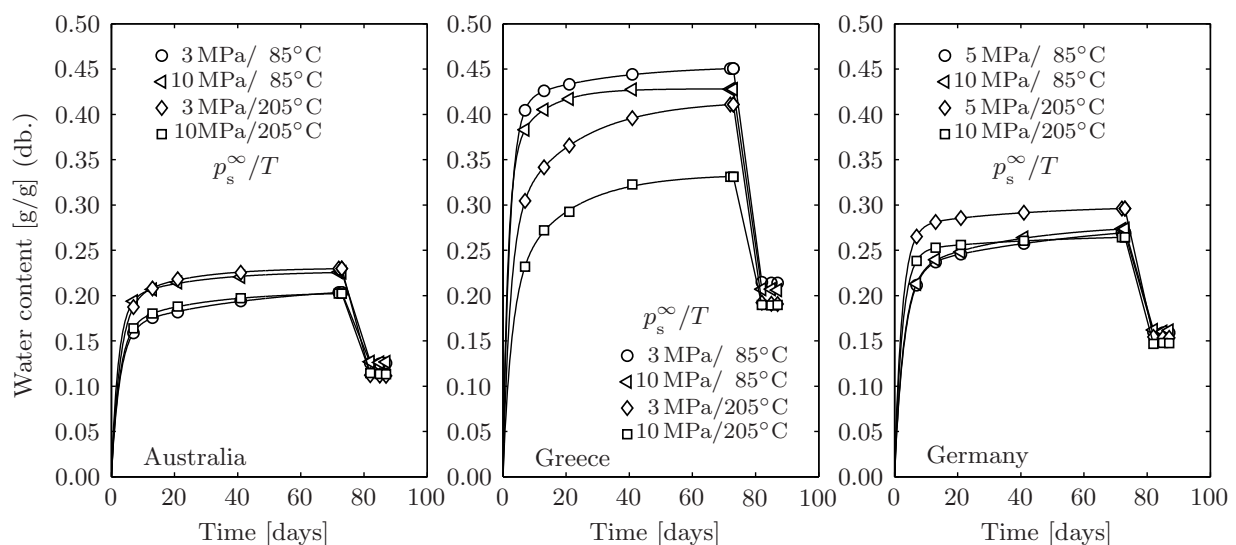
Figure 3.45: Rewetting of oven dried MTE products at 100 % relative humidity (day 1 to 73) and
determination of equilibrium moisture content at 52 % relative humidity (day 74 to 88)
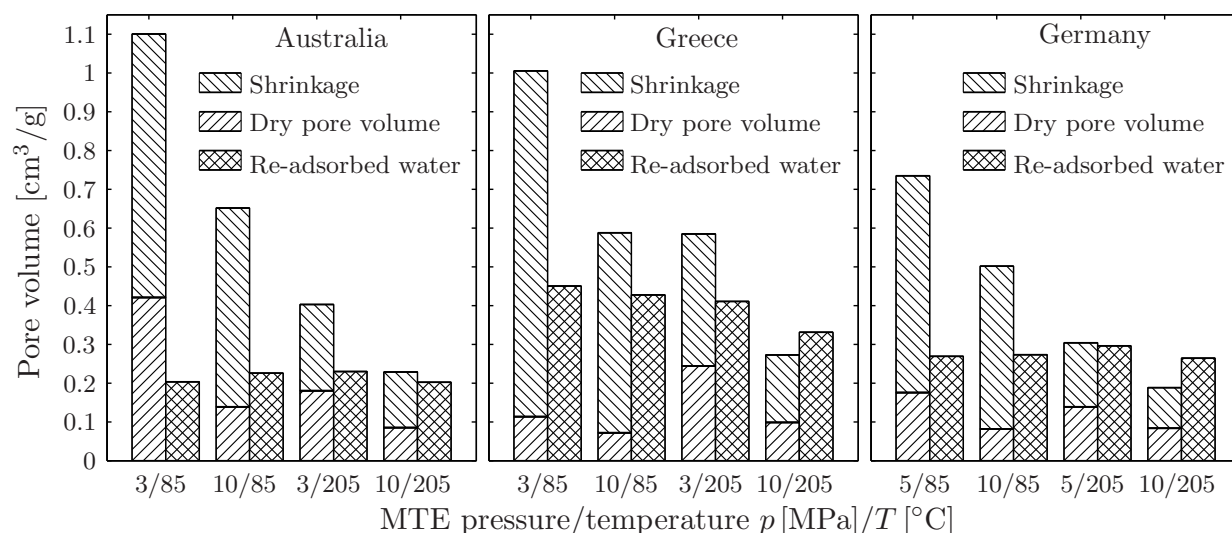
Figure 3.46: Comparison of the volume of re-adsorbed water (100% relative humidity) to the pore volume of wet and oven dried MTE products. The sum of 'shrinkage' and 'dry pore volume' gives the total pore volume of the wet MTE pellets.

has the highest overall moisture content after re-hydration, followed by the German coal, with the Australian coal having the lowest moisture content.

To determine if there is a relationship between water uptake and pore volume, the volume of re-adsorbed water is compared with the pore volume of wet and oven dried MTE products as shown in Figure 3.46. For all three coals investigated, the re-hydrated moisture content remains relatively constant for the various processing conditions investigated and no clear dependence on the pore volume of the wet and oven dried MTE products can be identified. Nevertheless, the results Greek coal indicate a decreasing re-hydrated moisture content with increasing severeness of MTE processing conditions.

In most cases, the volume of re-absorbed water exceeds the pore volume of the oven dried MTE products and in the case of the Greek and German coals even exceeds the total pore volume of the wet MTE filter cake under severe MTE processing conditions (e.g. $205°C/10\,MPa$). The results therefore indicate, that the forces associated with water diffusion into the dry coal structure can partly reverse the process of mechanical thermal dewatering and shrinkage. Studies undertaken by OZAKI et al. [ONG$^+$97] and GUY [Guy02] on the water absorption behaviour of Victorian brown coal model briquettes established, that the swelling behaviour of these coals is controlled by the concentration of metal carboxylates and the number of free carboxylic groups. Of the various cations present in Victorian brown coal, GUY [Guy02] identified the magnesium ion to be the most significant cation contributing to swelling behaviour in Yallourn and Morwell coals. OZAKI et al. [ONG$^+$97] also pointed out, that the degree of swelling is reduced by heat treatment at temperatures below $200°C$. The authors argued, that this effect is due to a hardening of the coal structure through the formation of hydrogen bonds, as well as the removal of water from the coal structure, which causes the collapse of micropores, thus preventing the re-absorption of water. As little correlation are observed between the re-hydrated moisture content and porosity, the observed trends are most likely controlled by the presence of inorganic species in the coals.

The chemical analysis of the inorganic content of the three coals showed elevated acid extractable Mg and Ca levels for the Greek and German coals (Chapter 3.4). This can explain the higher re-hydrated moisture content of these coals relative to the Australian coal. Another possible explanation could involve the re-hydration of clays, which are known to undergo significant swelling when in contact with water [Vel95, Sch00]. Furthermore, there may be differences in the surface

functionalities of the different coals, which could be contributing to the different water absorption capabilities.

Once the samples have been re-hydrated, the MTE products are exposed to a relative humidity of 52 % for 14 days. This causes the moisture content to drop significantly, and the equilibrium moisture content is reached after several days. As the results showed for the 100 % relative humidity experiment, the Greek coal has the highest equilibrium moisture content, followed by the German coal, with the Australian coal having the lowest moisture content. Very little difference in moisture content is observed for the various processing conditions investigated. Again, the results suggest, that the EMC may be controlled by other factors, such as the inorganic and mineral content, as well as the nature of surface functional groups.

3.5.2 Thermal analysis

Shown in Figure 3.47 are the DTA (Differential Thermal Analysis) curves for the three coals. For each coal four samples treated under mild and severe conditions were investigated. The integrated and normalised DTA curves as well as the mass loss from the Thermogravimetric Analysis (TGA) are shown in Figure 3.48.
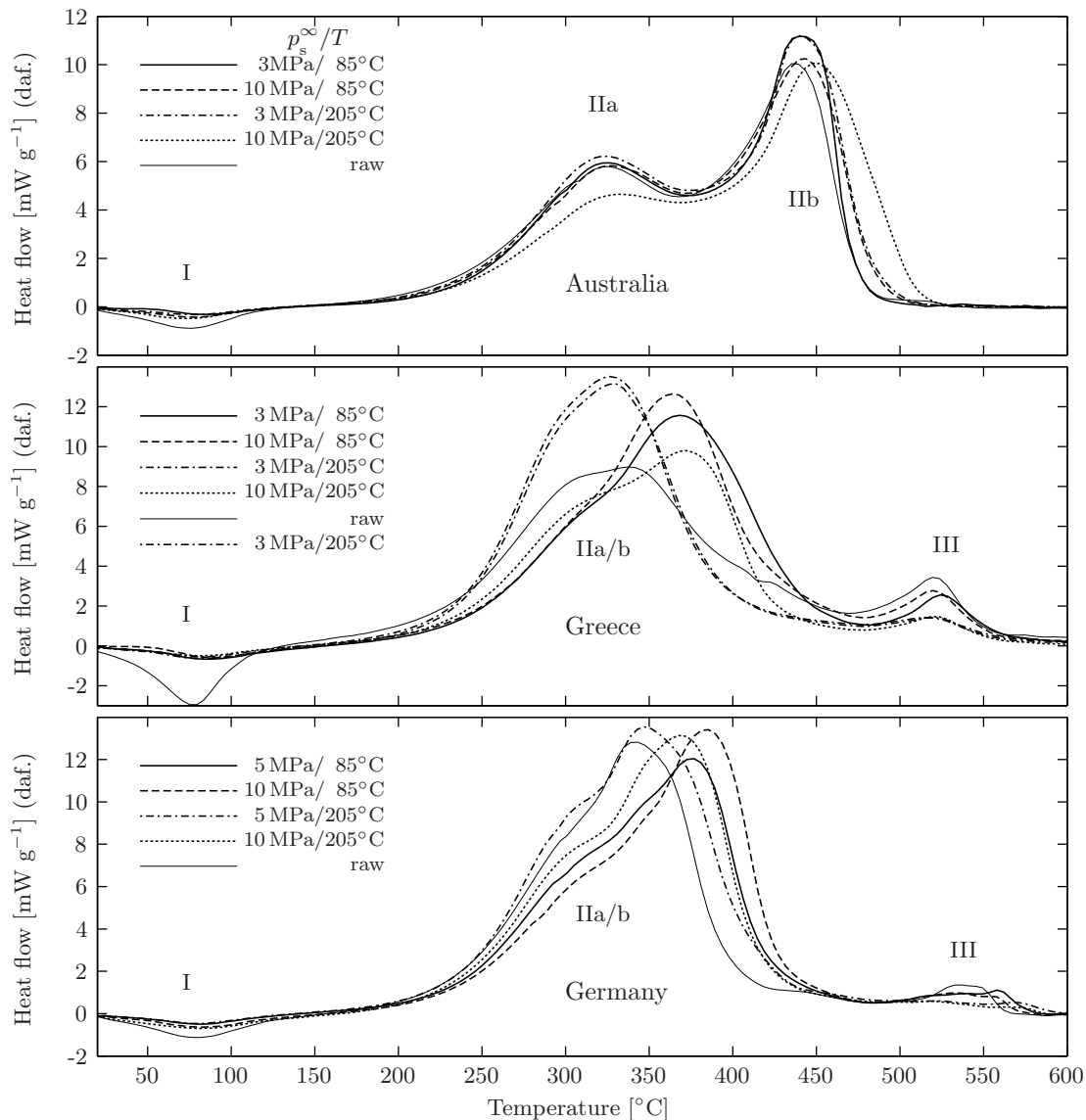
Figure 3.47: DTA curves for Australian, Greece and German coal

The zone labeled I (endothermic peak in Figure 3.47), around 100°C, is due to the loss of inherent moisture, which is re-adsorbed to the dry coal during the preparation of the sample. The combustion zone between 250 and 425°C can be subdivided in the release and combustion of volatile matter (IIa) and the combustion of residual char (IIb). From detailed analysis it is known that this separation results from (IIa) the destruction of aliphatic grouping, CH groups, carbohydrate components and to some extent of oxygen containing (alcoholic, phenolic) and amino groups and (IIb) the thermo-oxidation of aromatic, mono- or polycyclic rings [PTF93, KKP04].

For the Australian raw coal two well defined exothermic peaks for the two combustion zones are found. Similar results were obtained by CHEN et al. and ARENILLAS et al. for high volatile bituminous coals [CMP96, ARA+04]. The weight loss of the TG curve (Figure 3.48b) at the temperature determined by the tangents on the integrated DTA curve at the transition between IIa and IIB (Figure 3.48b) is almost equal to the volatile matter content of the Australian coal. The transition temperature of approx. 400°C is consistent with findings of CHEN et al. [CMP96] during the investigation of a similar Loy Yang coal.

However, the Greek and German coal show a totally different course of the DTA curves. The second combustion peak is shifted to lower temperatures such that one broader peak results for zone II. Therefore the whole combustion process is finished at lower temperatures which indicates a higher reactivity for these coals [ARA+04]. Similar results are reported by PAN et al. [Pan88] for a North Dakota lignite (33.9 % moisture, 32.9 % volatiles, 27.5 % fixed carbon, 5.7 % ash) and a further shifting of the combustion peaks to lower temperatures was reported due to treatment with calcium acetate. The calcium in form of its oxide is thought to promote the extent of decomposition via [McK83, Pan88]

$$CaO + \tfrac{1}{2}O_2 \; \rightarrow \; CaO_2 \,,$$
$$CaO_2 + C \; \rightarrow \; CaO + CO \,.$$
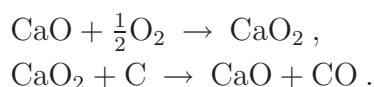
Since the Greek and German coal contain significant amounts of Ca and Mg the catalytic effect [McK83, RRP93] of these elements can explain the low ignition/combustion temperatures of these coals.

The additional exothermic peaks (III) for the Greek and German Coals at 540°C are probably due to the release of pyritic sulfur as suggested by SHAO et al. [SHH+94]. Both Fe and S are contained in larger quantities in the two coals.

From the comparison of the DTA-TGA curves for the different MTE conditions just on basis of the results in Figures 3.47 and 3.48 no clear trends for the variation of MTE pressure and temperature can be observed. But remembering the significant increase in mesopore volume (Chapter 3.3.3), there seems to be a shifting of both DTA and TGA curves to lower temperatures for samples treated at severe MTE temperaures/low consolidation pressures. This is true especially for the Greek samples treated at 3 MPa/205°C.

To investigate a possible correlation between mechanical/thermal treatment, pore volume and shape of the DTA curves as characteristic values, the temperatures for 50 % mass loss and 50 % heat release were determined from the curves in Figure 3.48a/b and plotted for the three coals as a function of the combined macro- and mesopore volume in Figure 3.49. From this, a clear trend towards lower temperatures for increasing pore volume becomes obvious.

This can be explained by the fact, that ignition at low temperature gradients also is a diffusion limited process which is promoted by larger pores and larger pore volumes and inhibited in low porosity fuels like high temperature and/or high pressure treated MTE products. Examples for the first case are the Greek coal samples treated at 3 MPa/205°C and the German coal samples treated at 5 MPa/205°C and for the latter one the Greek and German MTE samples treated at 10 MPa/205°C, 3 & 5 MPa/85°C and 10 MPa/85°C like the shift of the DTA curves in Figures 3.47 shows.
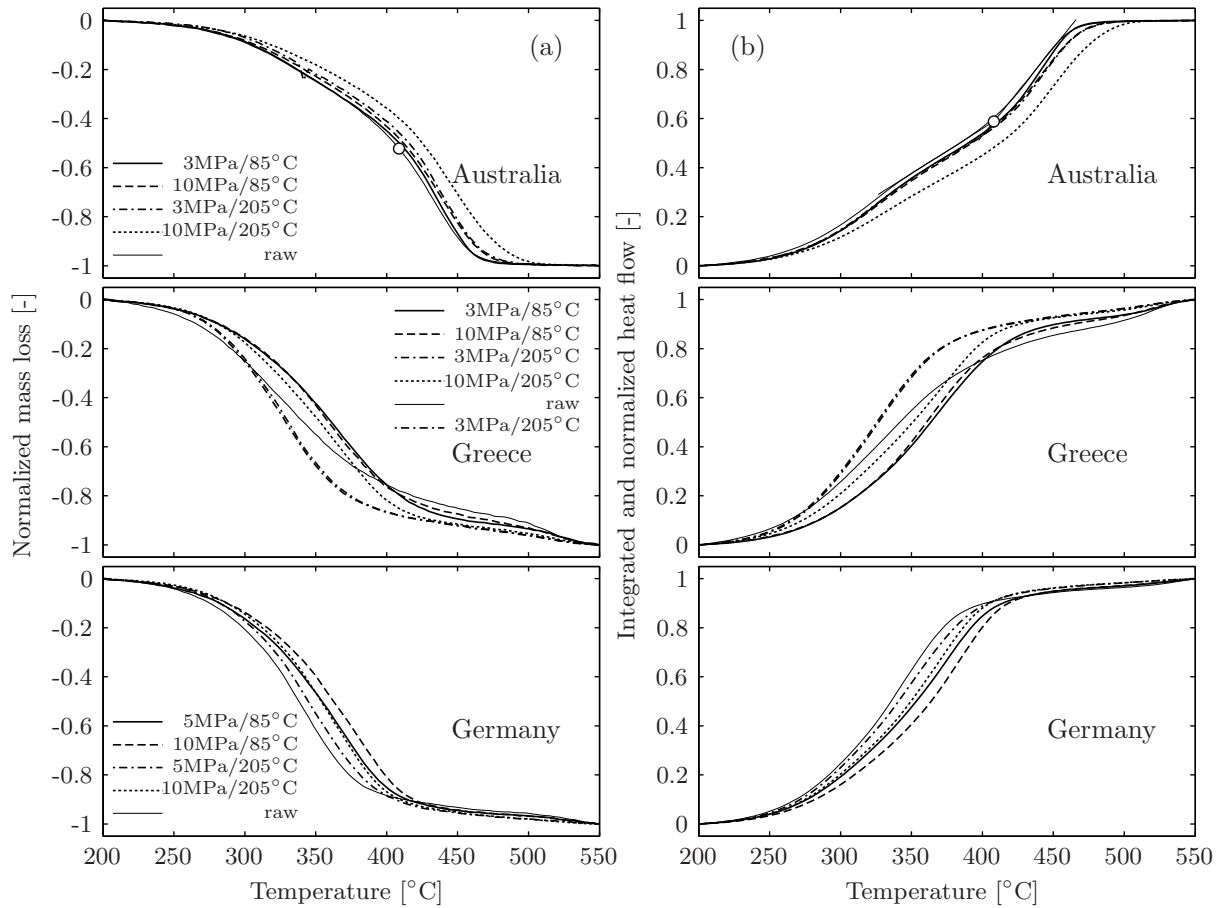
Figure 3.48: (top)
Normalised mass loss (a) and heat release
(b) during DTA-TGA experiments
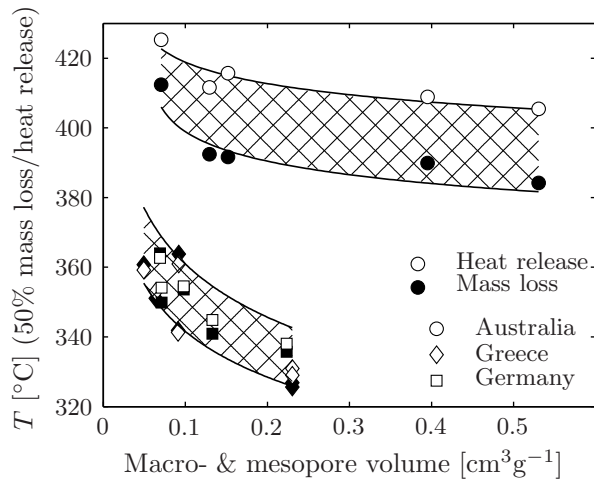
Figure 3.49: (left)
Temperatures at which half of the mass
and heat have been released

For the Australian coal this effect becomes significant only for most severe MTE processing at
10 MPa/205°C.

Similar results were obtained by Ogunsola and Mikula [OM92] who found a reduction in the
susceptibility to spontaneous combustion of western Canadian lignite and subbituminous coals after
thermal upgrading even at temperatures as low as 200°C. The authors argued that the thermal
treatment caused pore blockage which could reduce access of oxygen to the coal matrix.

4 Dewatering of biomass and sludges

4.1 Carbonaceous materials

During the last years a considerable interest in the utilisation of biomass for district energy systems has been developed. When readily available, wood or wood waste, sawdust and straw can be used as economical and ecological sustainable fuels for such systems. Virtually all biomass can be burned in energy conversion systems. This way also biomass waste can be converted to a valuable resource.

Nevertheless there are still many problems in the utilization of renewable energy sources like straw and bark due to the high potassium and chlorine concentrations (straw) and the humidity (bark). Therefore different systems have been investigated for the leaching and drying of biomass, especially straw or straw char, to reduce the corrosion rate at the heating surfaces of power plants [JBW96, KJSDJ98, JSDJ01, Dem03].

The MTE process provides a more energy efficient method for both leaching and dewatering of biomass due to its basic concept. While a leaching step already is included by the direct heating with water and steam, the energy consuming drying of the leached fuels is avoided by the mechanical dewatering at elevated temperatures. Additionally, the MTE pilot and demonstration plants already cover the range of capacity required for biomass fired power stations.

Therefore in the following also the results of the dewatering and leaching of different biomasses, which are younger than lignites, are presented.

4.1.1 Straw leaching and dewatering

For the water leaching of wheat straw JENKINS et al. [JBW96] found a decrease of the potassium content by 85 %. The chlorine content was decreased by 89 % and the total ash content by 49 %. For their experiments they submerged 100 g of straw in 7 liters of water for 24 hours, which leads to a rather low solids concentration compared to the MTE experiments undertaken in this work. For the leaching of rice straw they obtained similar results and a final water content after drainage of 85 wt.%.

THOMPSON et al. [TSL03] measured an increase in the removal rate at increased temperature but only investigated the region up to 50°C. Similar results for a variety of agriculture residues were reported by DEMIRBAŞ [Dem03].

During combined leaching and multi step mechanical dewatering of banana grass TURN et al. [TKI97] found a decrease in potassium (90 %), chlorine (98 %), sodium (68 %) and sulphur (55 %) with an estimated ash fusion temperature increase of more than 250°C (based on the phase diagram $SiO_2/CaO/K_2O$). For the combined leaching and mechanical dewatering KNUDSON et al. [KJSDJ98] determined a time of 10 minutes leaching at 60°C to be sufficient for the removal of 90 % of the potassium (8 to 24 g/kg in raw samples). Dewatering with a pressure of 3 MPa lead to a final water content of 54 wt.% at 50°C and an increased value of 58 wt.% at 80°C, possibly due to a degradation of the organic structure.

In Figure 4.1 the water content during the combined leaching (30 g straw per 300 g water, heated for 6 400 s) and mechanical/thermal dewatering (constant pressure expression for 10 000 s) of wheat straw is plotted as a function of time (Figure 4.1a) and temperature for two consolidation pressures (Figure 4.1b/c). As for lignite there is both an increase in consolidation rate and decrease in final water content with increasing temperature up to approx. 120°C. At this temperature the thermal decomposition already starts, which leads to an increase of water content in the high temperature range (Figure 4.1b/c).
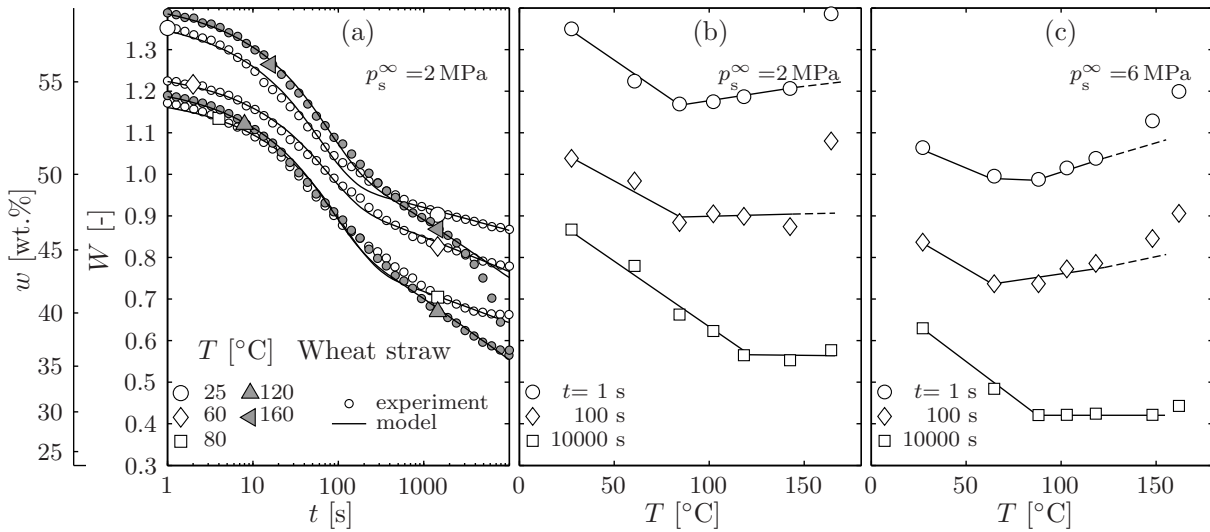
Figure 4.1:
(a) Time dependent water content during the mechanical/thermal dewatering of wheat straw, back-calculated from length measurement, and model calculations (–). (b, c) Final water content for different consolidation times (symbols) and corrected values for thermal decomposition at higher temperatures (- -)

The time dependent course is back-calculated (Chapter 3.1.1) based on the final water content, final mass of dry matter and time dependent change of the pellet height. For tests at higher temperatures and therefore higher rates of thermal decomposition these curves give exact values only for the end of the experiments. But especially at the highest temperatures a significant, increasing amount of the cellular material is released to the water and pressed out, which can be quantified easily by the loss of dry matter (Figure 4.2a). The thermal decomposition leads to a drift of the time dependent curve at 160°C only for longer dewatering/heating times, as it can be seen in Figure 4.1a. Therefore the effect can be neglected considering technical processes, since already a short time heating and dewatering (5 to 10 min) of the straw is sufficient for the removal of the water added for the leaching process. Neglecting the time range above 1 000 s for high temperatures, the model developed in section 3.2.3 also provides an excellent description for the time dependence of the water content.

As shown in Figure 4.2b/c, at higher temperatures also the removal of potassium and chloride is increased. While at 50°C only 78 % of the water soluble potassium is removed, the discharge is increased to up to 100 % at 160°C. In this temperature range the chloride removal is slightly increased by 0.5 g/kg. The amount of water soluble potassium $c_{K, 25°C}^{water\ soluble}$ [g/kg straw db.] was determined in a separate water leaching experiment with 1 g of straw in 50 g water.

Values of about 90 % removal of potassium are also reported in the literature for lower temperatures. Nevertheless in previous attempts always very low solid concentrations were investigated which are difficult to handle in technical implementations. The advantage of MTE processing is therefore that neither the high solids concentration nor salt concentrations of the leaching water influence the process negatively, since both dissolution/exchange of salts and water removal are affected favorably by increased temperatures.

It has to be mentioned, that the mass loss in Figure 4.2a not only reflects the release of organic material to the water but, also contains the decrease of ash content (from about 6.4 wt.% to 3.6 wt.% at an ashing temperature of 575°C), resulting from the dissolution of salts.

The values for the low temperature removal of inorganic and organic fractions of straw are in a good agreement with the cited data from literature. Furthermore the results show a great potential
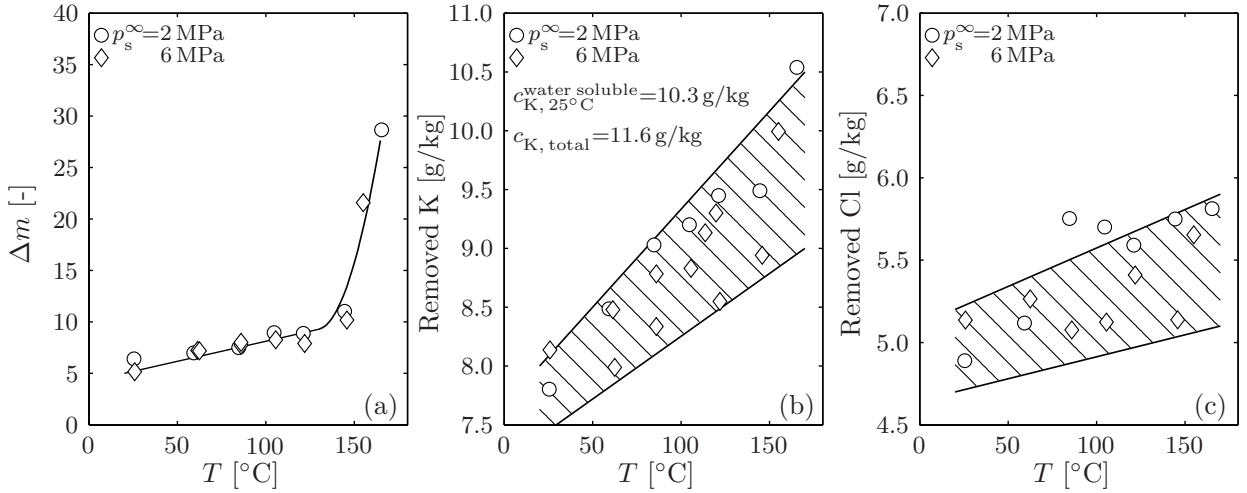
Figure 4.2: (a) Dry matter mass loss, (b) potassium removal and (c) chloride removal for straw leaching and MTE dewatering at two different consolidation pressures as a function of temperature

for the application of the MTE technique in biomass preparation since both demineralization and dewatering show an optimum at process parameters that are technically feasible with MTE technology ($100°C< T <140°C$; $2\,MPa< p <6\,MPa$). At process parameters which are in this range, a maximum dewatering ($w <40\,wt.\,\%$) and high K removal ($>80\,\%$) can be obtained at acceptable values of the mass loss ($< 10\,\%$) and expression times smaller than $10\,min$. The leachate itself can be further utilised as liquid fertiliser in agriculture. If the MTE process is performed at temperatures above $140°C$, the leachate then contains higher amounts of different sugars and can be used for the liquid bio-fuel production in fermentation processes [TTJ$^+$04], which further increases the overall efficiency of the straw utilization.

Higher temperatures do not only effect the absolute amount of potassium removed, but also increase the leaching rate. This is shown in Figure 4.3a/b for two temperatures and different particle sizes of the straw. The diffusion limited leaching process can be described by a two scale diffusion model (–) [JSDJ01] for the remaining potassium concentration

$$c_K^{remaining} = c_K^{raw} - \frac{\Delta c_K^\infty}{C_2}(1 - C_1)f(\tau_1, t) - \frac{\Delta c_K^\infty}{C_2} C_1\, f(\tau_2, t)\,,$$

$$f(\tau, t) = \sum_{n=1}^{\infty} \alpha \left[1 - \exp\left(-\frac{(\pi n)^2 t}{\tau} \right) \right]\,,$$

$$\alpha = \left[\frac{2}{\pi n} \right]^2 (\cos(\pi n) - 1)\cos(\pi n)\,, \quad D = \frac{L^2}{\tau} \tag{4.1}$$

with two time constants τ_1 and τ_2, which are inversely proportional to the effective diffusion coefficient D divided by the square of the length scale of diffusion L. Accordingly τ decreases with temperature, see ARRHENIUS-plot in Figure 4.3c. Leaching times of less than half an hour required for medium sized particles (Figure 4.3b) and also the other process parameters seem to be realistic for a technical implementation of combined straw leaching and mechanical/thermal dewatering.

4.1.2   Dewatering of other biomass fuels

In the following, the dewatering of paper sludge, bark and peat as alternative fuels treatable with MTE is investigated (Table 4.1). For the experiments with peat a commercial, pre-dried sample has been used which was also tested in its natural form with a water content of $87\,wt.\%$ after
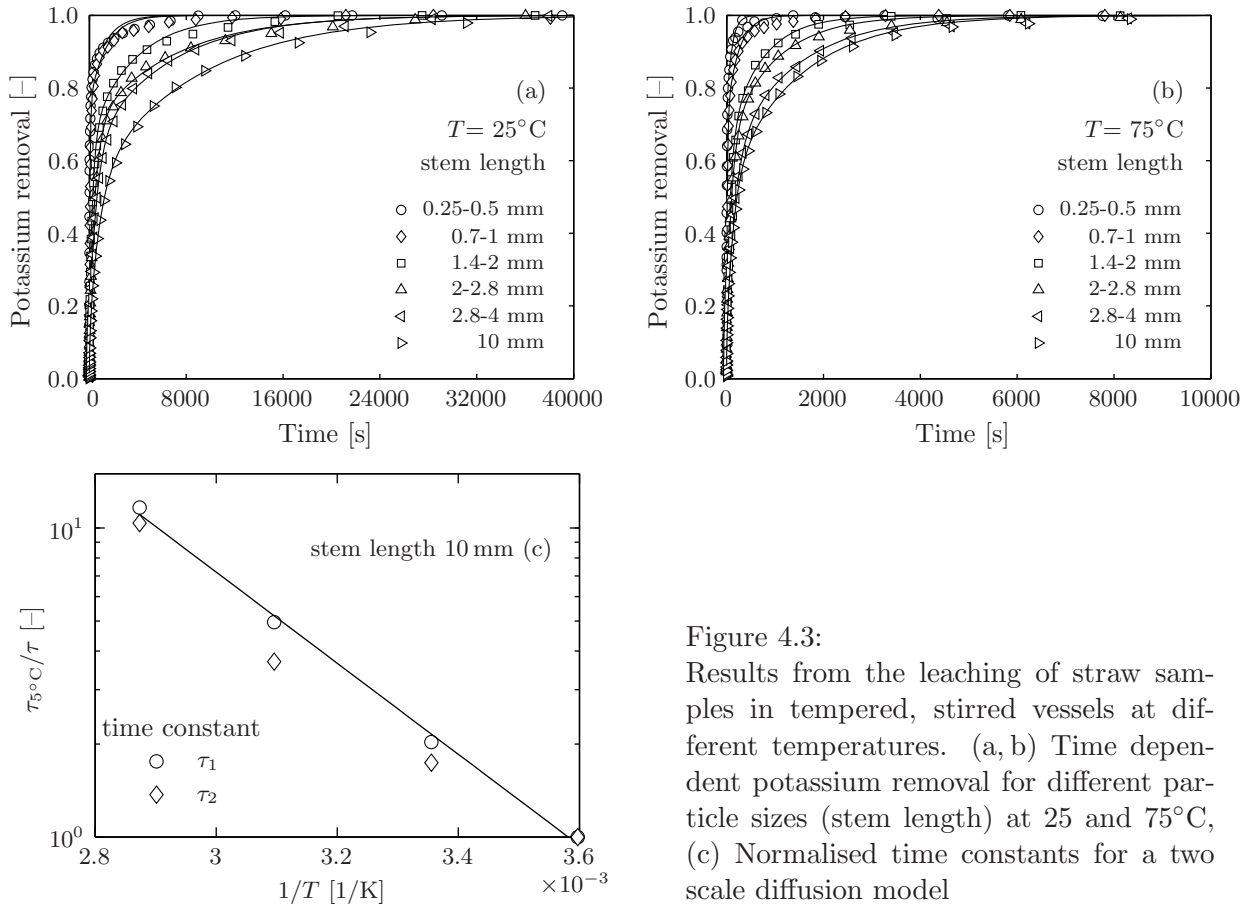
Figure 4.3:
Results from the leaching of straw samples in tempered, stirred vessels at different temperatures. (a, b) Time dependent potassium removal for different particle sizes (stem length) at 25 and 75°C, (c) Normalised time constants for a two scale diffusion model

being suspended in water for three days. The paper sludge used originated from a waste paper preparation plant and therefore also contains a high ash content.

The time dependent water contents for the dewatering of the different materials in Figure 4.4 show similar trends to the dewatering of lignite and straw, which were investigated in detail before. For low temperatures there is a significant influence of the primary consolidation on the process kinetics, which nearly disappears for high temperatures. At higher temperature lower water contents can be observed already at the beginning of the mechanical dewatering due to the thermal dewatering, which takes place during the heating process.

Even if the loading ℓ was low for the dewatering tests with paper sludge, especially for the low temperature experiments the primary consolidation was not finished within the first 2 000 s. This is likely due to the high mineral content resulting from kaolin coated paper residues in the sludge and leading to a low permeability of the filter cake, compare also Chapter 4.2.2. Nevertheless the time dependent course of dewatering is well described for all materials and temperatures by the model developed previously (−).

For all samples final water contents can be reached which are low enough to result in positive lower heating values without additional drying. This is an essential advantage for the treatment of residues from paper and wood processing, since these residues otherwise have to be burned using auxiliary fuels.

Table 4.1: Raw properties of MTE treatable fuels

	w [wt.%]	ash [wt.% db.]	loading ℓ [kg/m^2]
peat	63-87	3.0	23-64
pine bark	71	3.9	39
paper sludge	57	43.8	31
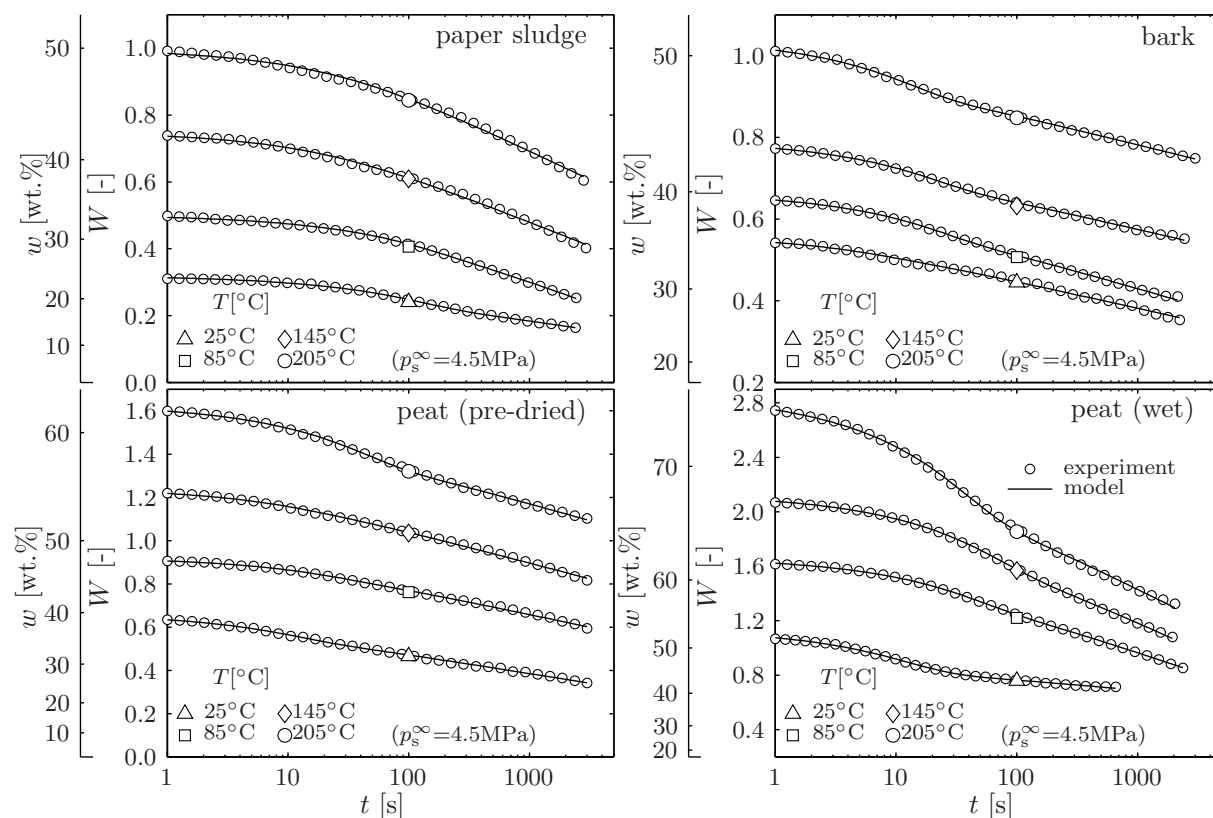
Figure 4.4: Time dependent water content during the mechanical/thermal dewatering of paper sludge, bark, and peat.

4.1.3   MTE products as economically transportable fuels

The FLEISSNER process [Fle26] was developed originally for the production of transportable fuel from lignite. The advantage was the mass reduction and increase of the lower heating value, the decrease of the (energetic) effort for the reduction of the water content and the production of a fuel with a rigid structure, which also could be utilised in house heating and industrial heating.

However, apart from raw lignite fired power plants the (binderless) briquetting is the second largest use for brown coal around the world. Even if the total production was reduced worldwide over the last two decades, still a substantial amount of industrial and commercial heat applications in countries like e.g. Germany, Australia and India relies on brown coal briquettes [AY01].

Due to the energy efficient water removal and significant volume reduction (see Figure 4.5), the MTE process thus also provides a new technology for the production of a transportable and exportable fuel, which is of interest for countries like Australia, where the coal mining in open cuts already starts few meters below the earth's surface. As the comparison in Figure 4.5 shows, MTE samples produced at 5 MPa/205°C and commercially available lignite briquettes (Loy Yang coal) have the same apparent density.

For the strengthening of the position of biomass fuels on the energy market, the cost of transportation and preparation have to be reduced. Thermal drying and pelletisation of wood chips, saw dust (see Figure 4.5) or straw actually already provides a method for the production of an economical transportable fuel. Nevertheless this process is very energy consuming – with a low overall efficiency – and the product prices are near to those of oil and gas with respect to the higher investment cost for the firing technology.

Straw and other biomass fuels are also considered to be utilised in large scale conventional power plants or liquefaction processes in Europe, but up to now none of the existing preparation processes
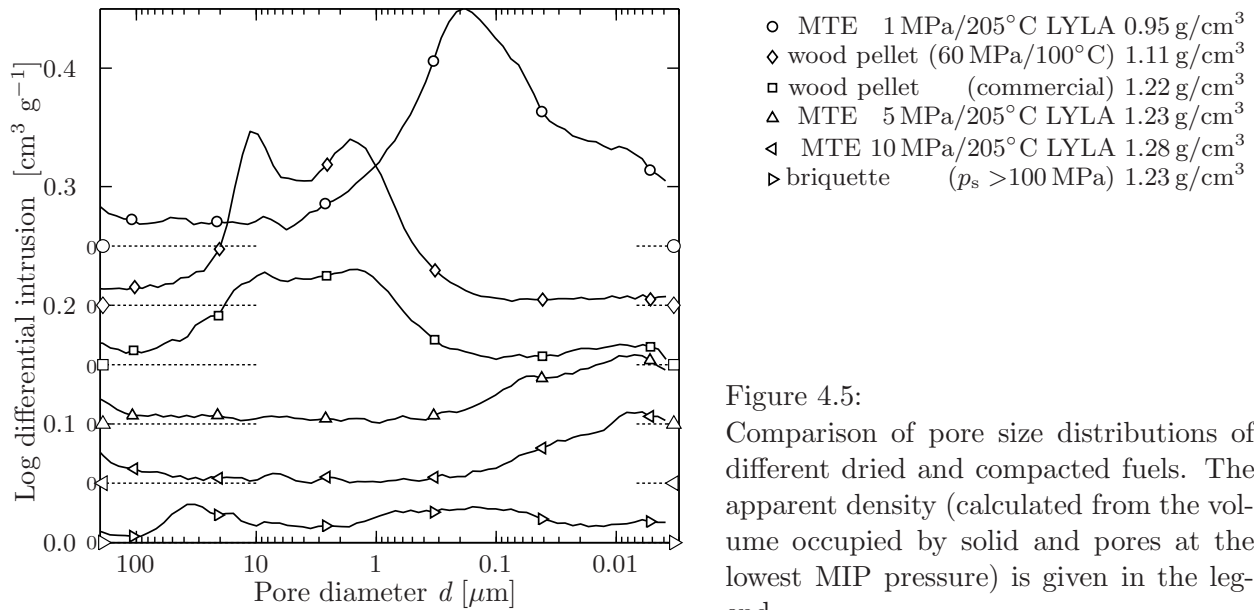
Figure 4.5:
Comparison of pore size distributions of different dried and compacted fuels. The apparent density (calculated from the volume occupied by solid and pores at the lowest MIP pressure) is given in the legend.

provides an economical method making such processes feasible. Due to the low densities of the raw materials transportation costs are high considering centralised conversion technologies.

By the combination of leaching and mechanical/thermal dewatering a high grade fuel both for conventional power plants and liquefaction process is produced. The energetic density of the MTE pellets can be adjusted by variation of process parameters, so that also transportation is an economical option, see Figure 4.6. Therefore the MTE processing of low density solids like straw or high water content residues from wood processing like bark leads to valuable biofuels.
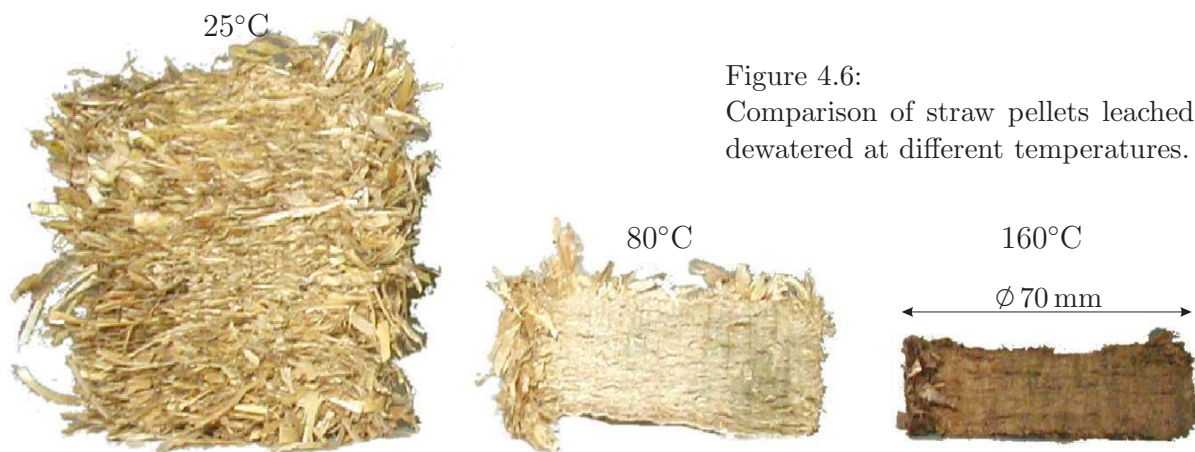
Figure 4.6:
Comparison of straw pellets leached and dewatered at different temperatures.

4.2   Suspensions and semi-solids

The application of the MTE process for the dewatering of suspensions and volume reduction of other wet, semisolid waste products was investigated in parallel to the technical development of the process for the integration in power plant process. In the following some results for the mechanical/thermal dewatering of different semi-solid sludges and suspensions are given.

4.2.1 Galvanizing sludge

For the experiments presented in this section a sludge from the water treatment (alkaline precipitation and flocculation) of a galvanizing plant is used. The composition (ICP measurements) is given in Table 4.2. The organic matter content was determined to 128 g/kg by acid flocculation with HCl, the mass loss on ashing at 550°C is 230 g/kg and the density of the dry matter is 2.82 g/cm^3. The particle size resulting from the alkaline precipitation was smaller than 1 μm, see Figure 4.14, page 75.

Table 4.2: Elemental concentrations of the galvanizing sludge

Element	Cu	Cr	Fe	Zn
Concentration [g/kg] db.	0.6	12.9	111	260

The sludge dewatering was tested on two samples containing 84.5 wt.% (semi-solid, predewatered at 2 MPa with a filter press) and 94 wt.% water (raw suspension). Additionally a series of thermally pretreated samples was dewatered at different temperatures. Between 120 and 240 g of suspension were dewatered through the lower filter medium in the laboratory MTE device at constant total pressure and temperature until the fluid pressure at (in these experiments impermeable) upper filter plate disappeared. In Figure 4.7 the typical course of fluid pressure (p_ℓ) and solid pressure (p_s) at the piston and the water content (db.) is shown as a function of time.

Due to the high water content and low rigidity of the solid matrix against compression, in all experiments also a constant-pressure filtration phase (II) after the initial constant-rate filtration (I) occurs in addition to the primary (III) and secondary (IV) filter cake consolidation. For the presentation of the results the two timescales $t - t_1$ (filtration analysis) and $t - t_2$ (consolidation analysis) are used.

In Figure 4.8 the time dependent water content for the experiments with the three samples is given both for the total filtration and consolidation (a) and the consolidation without filtration (b). Filtration and primary consolidation dominate the kinetics for all samples, since a larger amount of water has to be removed during these phases compared to the solids (lignite, biomass) investigated in the previous sections.

For the description of the filtration period a modified filtration equation is used. For filtration at cross sectional area A, with a filter cake of porosity ε_{fc} and permeability K the relationship between
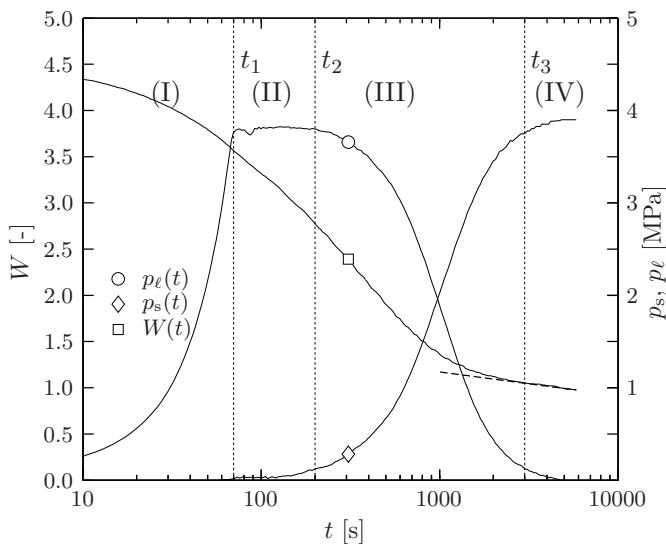
(I)   Constant-rate filtration
(II) Constant-pressure filtration
(III) Primary consolidation
(IV) Creep

Figure 4.7: Filtration, consolidation and creep during sludge dewatering
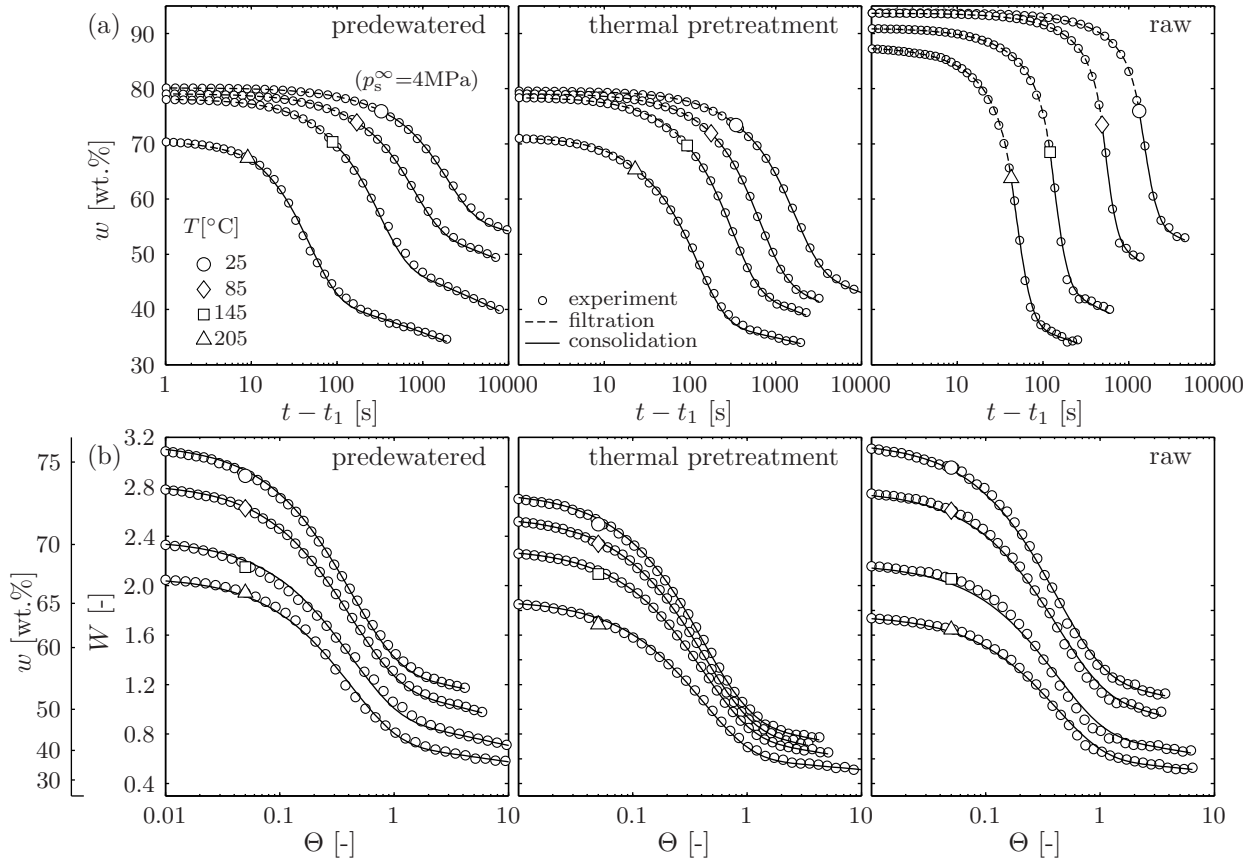
Figure 4.8: Mechanical/thermal dewatering of galvanizing sludge. a) Water content w during filtration and consolidation period. b) Water content W db. during consolidation period as a function of normalised time Θ (Eq. 4.7). The small circles are the experimental results, dashed and solid lines are values from the calculations with Eq. (4.3) and Eq. (4.5).

filtrate volume V or mean water content $W(t)$ db. and applied pressure Δp can be written as

$$\Delta p = \frac{\mu_\ell V}{K\,A^2}\frac{1-\varepsilon_{\mathrm{sp}}}{\varepsilon_{\mathrm{sp}}-\varepsilon_{\mathrm{fc}}}\frac{\partial V}{\partial t} = -\frac{\mu_\ell}{K\,A^2}\left[\frac{m_{\mathrm{s}}}{\varrho_\ell}\right]^2 (W_{\mathrm{sp}}-W(t))\frac{W_{\mathrm{fc}}+\varrho_\ell/\varrho_{\mathrm{s}}}{W_{\mathrm{sp}}-W_{\mathrm{fc}}}\frac{\partial W(t)}{\partial t}\;. \tag{4.2}$$

In this equation μ_{s} is the viscosity of the fluid, m_{s} the total dry mass of solid in suspension and filter cake. ϱ_{s} and ϱ_ℓ are the densities of solid and liquid phase, W_{fc} and W_{sp} are the water contents db. of filter cake and raw suspension.

The resistance of the filter medium can be omitted in the equation since the calculations are done only for the constant pressure filtration between t_1 and t_2. Due the the preceding constant rate filtration the pressure drop in the filter cake is already high enough to justify this simplification.

The time dependent mean water content, which is determined from the experiments, then can be calculated from

$$W(t) = W_{\mathrm{sp}} - \sqrt{(t-t_1)\frac{1}{C_{\mathrm{f}}} + (W_{\mathrm{sp}}-W_1)^2}\;, \tag{4.3}$$

with the water content W_1 after constant rate filtration time t_1.

$$C_{\mathrm{f}} = \frac{\mu_\ell}{2\,K\,A^2\,\Delta p}\left[\frac{m_{\mathrm{s}}}{\varrho_\ell}\right]^2\frac{W_{\mathrm{fc}}+\varrho_\ell/\varrho_{\mathrm{s}}}{W_{\mathrm{sp}}-W_{\mathrm{fc}}}\,. \tag{4.4}$$

The only unknown parameter in this equation is the permeability K of the filter cake, which is determined by regression. There is an excellent agreement between the model calculations according to Eq. (4.3) (dashed lines in Figure 4.8, symbols explained in the legend are drawn at the end of constant pressure filtration period) and the experimental values.

The consolidation process of the filter cake can be described by a slightly modified version of the model developed in Chapter 3.2.3 for the consolidation of lignite. The differential equation (3.31) (page 26) was solved assuming the fluid pressure to be zero at the beginning of the consolidation in the whole cake, which is true only for solid dewatering. In the case of sludge dewatering, a sinusoidal distribution can be assumed according to SHIRATO et al. [SMI86].

Therefore the equation which describes the water content during primary and secondary consolidation of the semi-solid sludge is

$$
\begin{aligned}
W(T, p_{\mathrm{s}}^{\infty}, \omega_0, t) =\ & \Delta W_1^{\infty}(T, p_{\mathrm{s}}^{\infty}, \omega_0)\ \exp\left(-\frac{\pi^2}{4}\Theta(T, p_{\mathrm{s}}^{\infty}, \omega_0, t - t_2)\right) \\
& -C_{\alpha}^{W}(T, p_{\mathrm{s}}^{\infty}) \log\left[1 + \frac{\pi^2}{4}\Theta(T, p_{\mathrm{s}}^{\infty}, \omega_0, t - t_2)\right] \\
& +C_{\alpha}^{W}(T, p_{\mathrm{s}}^{\infty}) \log\left[\frac{\pi^2}{4}\Theta(T, p_{\mathrm{s}}^{\infty}, \omega_0, t - t_2 = 1\mathrm{s})\right] \\
& +W_{\mathrm{eop}}^{*}(T, p_{\mathrm{s}}^{\infty})\,,
\end{aligned}
\tag{4.5}
$$

with

$$
\Delta W_1^{\infty}(T, p_{\mathrm{s}}^{\infty}, \omega_0) = \Delta W_1^{*}(T, p_{\mathrm{s}}^{\infty}) + C_{\alpha}^{W}(T, p_{\mathrm{s}}^{\infty}) \log\left(\frac{\omega_0}{\omega_0^{*}}\right)^2
\tag{4.6}
$$

and

$$
\Theta(T, p_{\mathrm{s}}^{\infty}, \omega_0, t - t_2) = \frac{C_{\mathrm{e}}(T, p_{\mathrm{s}}^{\infty})\, i^2}{\omega_0^2}\, (t - t_2) = \frac{i^2}{\omega_0^2}\frac{K(T, p_{\mathrm{s}}^{\infty}, e)}{\mu_{\ell}(T)\frac{\partial e}{\partial p_{\mathrm{s}}}(1 + e)}\, (t - t_2).
\tag{4.7}
$$

For simplicity the equation is written in terms of water content W instead of the void ratio e. C_{α}^{W} and W_{eop}^{*} are the slope and intercept at $t{=}1\,\mathrm{s}$ of the creep curve. C_{e} is the coefficient of primary consolidation and ω_0 is the total solid volume per unit sectional area. The number of drainage surfaces i is 1 for all experiments. p_{s}^{∞} is equal to the constant solid compression pressure Δp which is reached after primary consolidation in the whole filter cake.

As for lignite in the previous chapter, the parameters for creep (C_{α}^{W}, W_{eop}^{*}) and primary consolidation phase (C_{e}) are determined in two regression steps. The permeability K can be calculated afterwards according to Eq. (4.7) from the course of solid compression pressure p_{s} and water content (or void ratio e) with time.

The results from the detailed analysis of the dewatering process for the experiments shown in Figure 4.8 are given in Figure 4.9a-d. As for lignite the water contents (Figure 4.9a) at the start of the primary consolidation and the final water contents at the end of the experiments decrease with temperature (thermal dewatering) and pressure. There is also a small irreversible effect of the thermal pretreatment on the final water content.

The permeability (Figure 4.9b) determined during filtration does not change with temperature but there are two different levels for the dewatering at 2 MPa and the dewatering of the raw sludge on the one hand and the dewatering at 4 MPa on the other hand. The difference for the dewatering at 2 and 4 MPa results from the decrease of the permeability with pressure, which is usually found for highly compressible filter cakes. The difference for the dewatering of raw and predewatered sludge can be explained similarly by the higher precompression of the predewatered sludge.
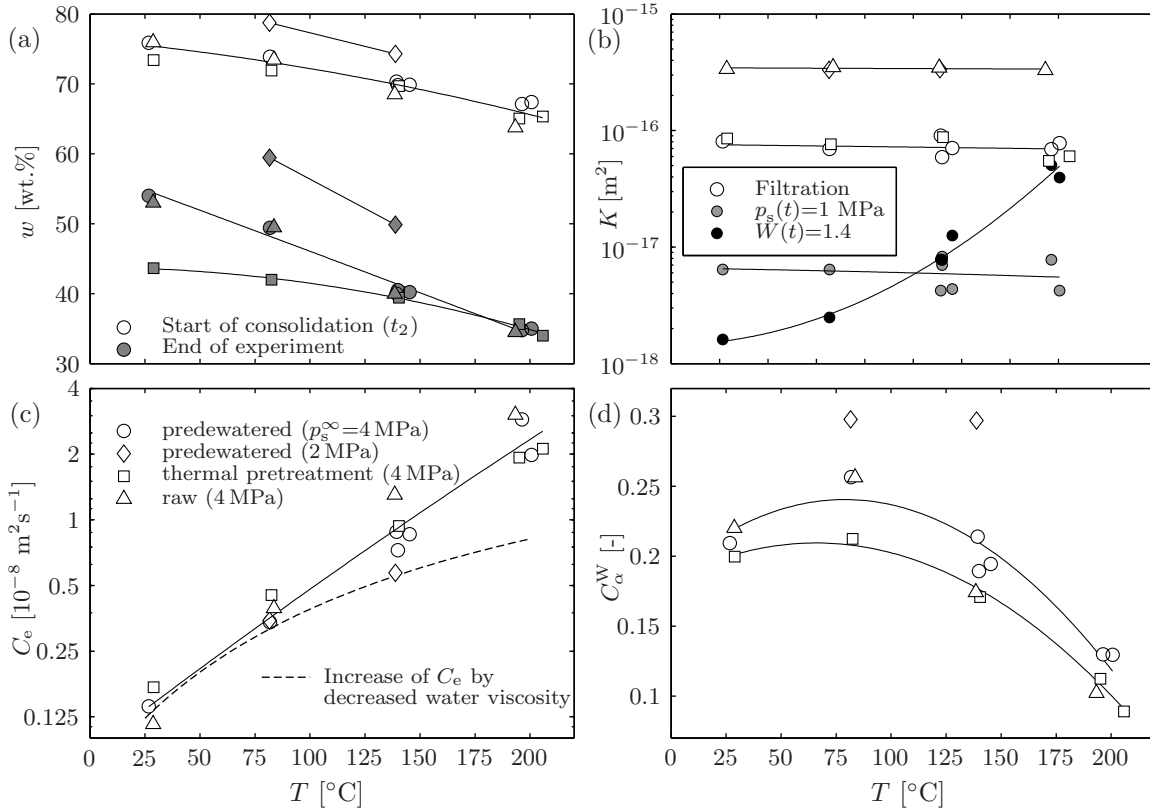
Figure 4.9: Model constants and further results of the dewatering of galvanizing sludge. a) Water content at start and end of consolidation b) Permeability during filtration and consolidation period c) Coefficient of consolidation d) Creep coefficient

As the permeability decreases continuously during consolidation, the values determined at constant solid compression pressure p_s or at constant water content W can be compared for the different temperatures. The results show again only a slight change in permeability, when comparing the values calculated from experimental data at constant pressures although porosity and water content decrease. Nevertheless the permeability is a physical constant, related to the pore size and pore structure and therefore values at constant water contents have to be compared to obtain expressive results. In this comparison, permeability (black circles) shows an increase with increasing temperatures, which only can be explained by changes in pore shape or size distribution and by temperature induced changes in the flow structure in the smallest pores. For the flow between very small particles, the breakdown of viscosity anomalies [Low61, DC81, TK94] near the particle surface is thought to give the largest contribution to this effect at elevated temperatures. Similar results are reported for lignites and clay [Ber04, TK94], compare Chapter 4.2.2.

The creep coefficient C_α^W in Figure 4.9d shows the same trends for the galvanizing sludge as for lignite, i.e. an increase with increasing temperature (in the low temperature region) and a decrease with decreasing water content at higher temperatures or pressures. This behaviour can be well described by the equations developed in Chapter 3.2.2, page 22.

4.2.2   Kaolin

The results for the filtration and consolidation of pasty kaolin sludge (particle size: 90 % $<2\,\mu$m, see Figure 4.14, page 75) are shown in Figure 4.10 and Figure 4.11. In contrast to the dewatering of the galvanizing sludge the increasing temperature does not influence the final water content and there is also only very little creep which therefore can be neglected in the determination of the model constants.
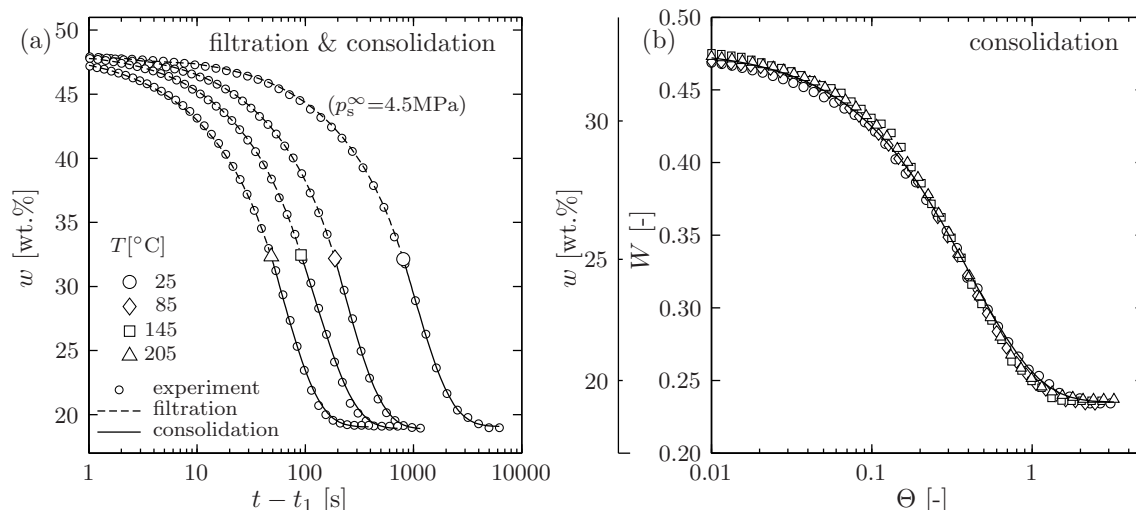
Figure 4.10: Mechanical/thermal dewatering of kaolin sludge. a) Water content during filtration and consolidation period. b) Water content (db.) during consolidation period as a function of normalised time Θ
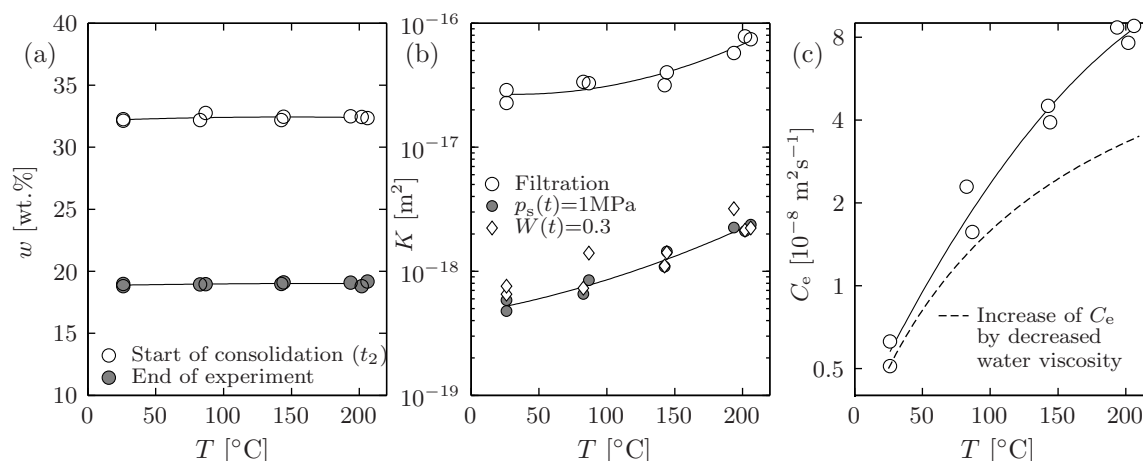
Figure 4.11: Model constants and further results of the dewatering of kaolin. a) Water content at start and end of consolidation b) Permeability during filtration and consolidation period c) Coefficient of consolidation

As for the galvanizing sludge there is a significant acceleration of the filtration phase – exceeding the decrease of fluid viscosity and indicated by a doubling of the permeability at an increase of temperature to 205°C, Figure 4.11b. This effect occurs both in filtration and primary consolidation phase and gives additional evidence for the breakdown of fluid-solid interactions at higher temperatures.

The excellent agreement of the course of water content with time during the consolidation period (Figure 4.10b) proves the reproducibility of the MTE experiments.

4.2.3 Coal suspension

In Figure 4.12 and Figure 4.13 the results for the filtration and consolidation of flotation coal residues (particle size: $90\% < 63\,\mu\text{m}$, see Figure 4.14, page 75) are shown.

As for kaolin there is no change in final water content with temperature. Due to the larger particle size, the increase in consolidation coefficient (Figure 4.13c) is limited to the decrease of viscosity with temperature. This behaviour is expected for larger particles and pore diameters due to the disappearing influence of viscosity anomalies [DC81].
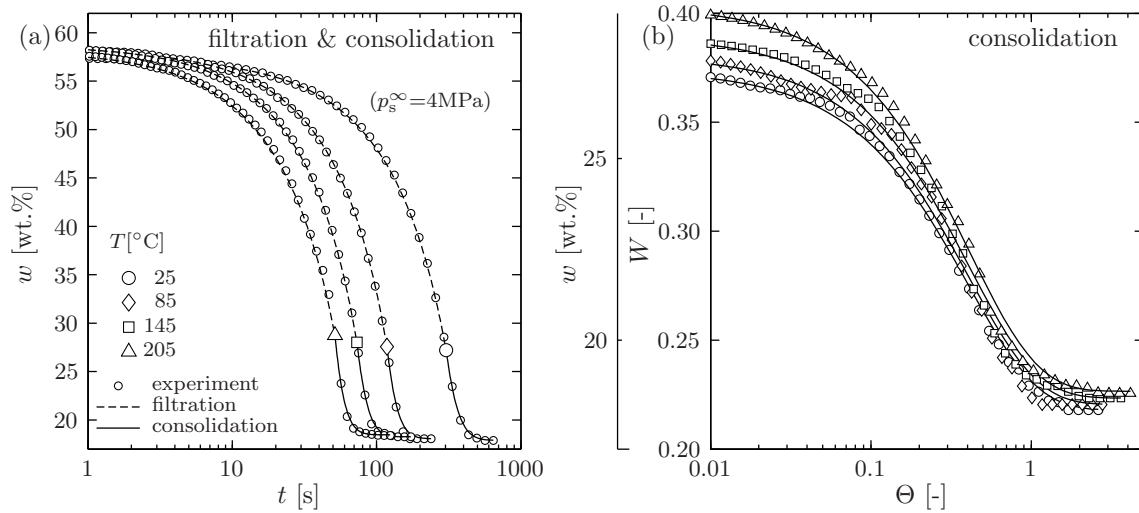
Figure 4.12: Mechanical/thermal dewatering of coal fines. a) Water content during filtration and consolidation period. b) Water content (db.) during consolidation period as a function of normalised time Θ
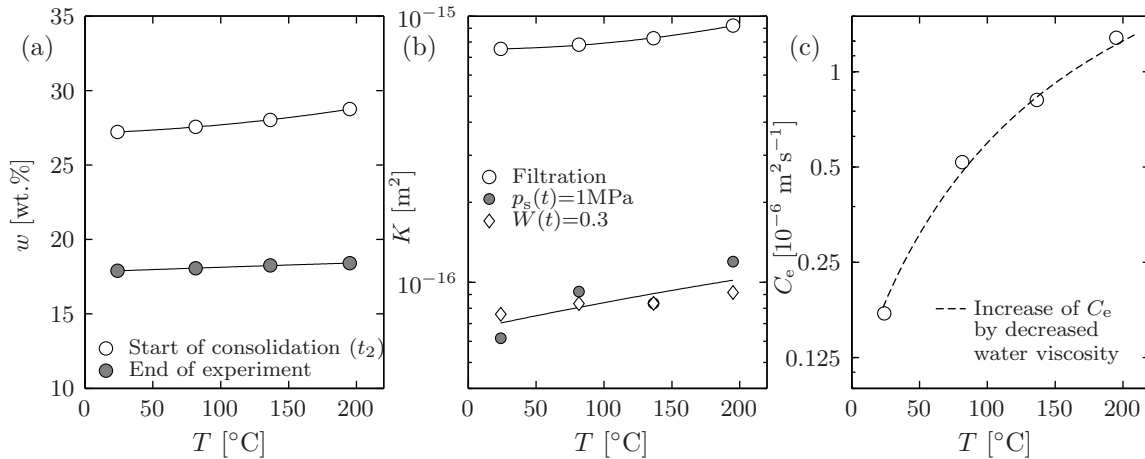
Figure 4.13: Model constants and further results of the dewatering of coal fines. a) Water content at start and end of consolidation b) Permeability during filtration and consolidation period c) Coefficient of consolidation

The permeability during filtration is nearly constant in the whole temperature range. A slight increase can be explained with sedimentation effects. Due to the larger particle size compared to kaolin and galvanizing sludge partial sedimentation can not be prevented during the heating of the sample. This may lead to a separation of particle fractions, an uneven distribution of porosity in the filter cake. As a consequence the total porosity of the filter cake and the permeability during filtration also slightly increase.

4.2.4   Classification of MTE-treatable materials

From the results presented in Chapters 3, 4.1 and 4.2 the different materials which can be treated with MTE can be classified according to the influence of temperature on the kinetics and water removal during the filtration and consolidation and the fraction of organic components contained.

In Figure 4.14 a summery of the results from the previous chapters is given. The final water content w_Θ (Figure 4.14a) is determined at the normalised time $\Theta = 1$. The reduction in dewatering time (Figure 4.14b) is the total filtration and primary consolidation time until $w = w(\Theta = 1)$ at a given temperature T normalised with the dewatering time at ambient temperature $T=25°C$. The time dependent water contents are given with a normalised time scale which removes the hydrodynamic

Figure 4.14: Treatment of solids, sludge and suspensions by mechanical/thermal dewatering

influence of solid mass and fluid properties on filtration and consolidation. Therefore all deviations of experiments for different temperatures are just the result of MTE specific mechanisms.

Category I All materials of category (I) are porous solids containing water in a capillary or colloidal structure. Examples are younger materials from the coal genesis like peat and brown coals but also residues from agriculture and forestry. Due to stronger bonds between water and solid matrix a purely mechanical dewatering requires the application of very high consolidation pressures (>15 MPa). The water can be mobilised (thermal dewatering) at higher temperatures during the MTE process, which enables a sufficient dewatering even at comparatively low pressures. The dewatering itself is not accelerated by a temperature increase since also the amount of water which is removed during primary consolidation is increased, see Figure 4.14.

The velocity of dewatering is high since bigger particles (>1 mm) provide channels sufficiently large for a low pressure loss in the water flowing out during primary consolidation. Nevertheless these particles also represent the rigid framework which is necessary to prevent the pores from being blocked during expression.

Once the primary consolidation is completed and all larger pores are closed, the kinetic is dominated by an ongoing creep of the solid matrix. This secondary consolidation proceeds for month or years [Dul60] with continuously decreasing rate. Therefore the creep is not off interest for technical processes but for the description of the whole kinetic, since it already starts during the primary consolidation.

Category II The materials of category (II) are suspensions with small particles (mean particle diameter <50 μm). Usually such suspensions are difficult to dewater by filtration, since the pressures required for sufficient short dewatering times are high due to small permeabilities of the filter cake. There is no influence of temperature on the physical properties of the solid material which leads to a constant final water content, which is reached quickly since there is nearly no creep.

Due to the decrease of viscosity with increasing temperature also the pressure loss of the water removed during filtration and the primary consolidation is smaller and the filtration rate is higher. For particles which are sufficiently large, this temperature induced filtration rate increase is the dominating kinetic effect. After normalization all time dependent curves are nearly identical (flotation coal in Figure 4.14).

For very small particles the high temperature breakdown of viscosity anomalies [DC81] near the particle surface leads to an additional increase in filtration velocity (Chapter 4.2.2, kaolin dewatering).

Category III Examples for materials of category (III) are industrial waste suspensions and pasty materials like galvanizing sludge and waterworks sludge. These are products of flocculation with mainly organic flocculants. The particle size of the solids is smaller than for category (II) even if the flocculation also leads to bigger aggregates.

The permeability of the filter cake is low due to the small particles and higher flocculant contents of these suspensions. Increasing dewatering temperatures therefore leads to an increase of both filtration and consolidation rate like for category (II). Additionally the compressibility and removable amount of water increases with temperature like for category (I) since the mechanical rigidity and stability of the flocculants is reduced.

The influence of secondary consolidation on the dewatering kinetics depends on the organic content of the filter cake and is lower than for category (I).

Due to both small particle sizes and organic content a combination of the mechanisms leading to a higher dewatering rate and lower water content is effective for these materials.

5 MTE process technology

In the following a short review is given on the different scales of technical development of the MTE process (Table 5.1). Following some in-depth research of the literature, the idea of combining the advantages offered by the thermal and mechanical dewatering processes – which are sufficiently known in the literature for reducing brown coal's water content – was developed by Prof. Strauss at the Chair Energy Process Engineering and Fluid Dynamics, University of Dortmund in spring 1994. In the summer of 1994, initial laboratory-scale tests on the mechanical/thermal dewatering were carried out at the University of Dortmund using a compression-tension testing machine (INSTRON), which proved the idea to reduce the water content by applying thermal energy and mechanical forces (project phase Ia). On the basis of the results obtained from the indirect heated laboratory unit, a process development unit was designed in summer 1995 to verify the water content reduction in a semi technical scale (larger area, greater fill height), when the coal is heated directly by saturated steam (project phase Ib).

Table 5.1:

Technical development		Laboratory plant		Process development unit	Pilot press	
Operating mode		discontinuous			quasi continuous	
Heating type		indirect		direct (steam)		
Preheating		without			with hot water	
Temperature	[°C]	180	180/250	190	210	210
Press area	[m^2]	0.008	0.004	0.06	1.2	1.3
Dimensions	[mm]	∅ 100	∅ 70	∅ 270	1500 x 780	1300 x 1000
Max. fill height	[mm]	200	200	650	450	460
Max. coal mass	[kg]	0.8	0.4	20	320	390
Max. pressure	[MPa]	3.2	6.5/13	6.0	7.0	6.1
Commissioned		June 94	Dez 94 March 95	Oct 95	March 96	Feb. 98
Project phase		Ia		Ib	II	III

A reduction of the amount of required heating steam was made possible by the development of a system for storing and recirculating the energy from the hot water pressed out from the coal. The process development unit was commissioned in Dortmund in October 1995. During project phase I the process parameters were optimised concerning the final water content, throughput per unit area and specific energy demand.

Following successful trials in mechanical/thermal dewatering using the laboratory-scale plant and the process development unit, the companies Maschinenfabrik J. Dieffenbacher GmbH & Co., Rheinbraun AG and RWE Energie, along with the University of Dortmund, Chair of Energy Process Engineering and Fluid Mechanics (Prof. Strauss) concluded a collaboration agreement for the further development of the MTE process. Within the scope of a joint project (project phase II) promoted by the Federal Education and Research Ministry (BMBF), a discontinuously working pilot press was developed for the implementation of the process, then set up at Rheinbraun AG's Sibylla research center, Frechen, and commissioned in the spring of 1996.

This pilot press proved the feasibility of scaling up the press area by a factor of 20 from the process development unit to pilot press, accounting for the given requirements for commercial implementation like high throughputs with even heating and dewatering of the coal layer as well as low specific energy requirements [SBB97].

In project phase III a newly developed dewatering unit has been built into the existing pilot press, and various plant-specific components have been tested [SBB99]. The new technology realised the quasi-continuous operation and permitted low-cost and reliable integration of the process into continuous power plant operations. From this development the process and technology for the dewatering of solid materials with a sufficiently rigid solid matrix resulted, which are described in the following.

5.1   Process design for the dewatering of solids

All basic investigations on mechanisms of dewatering and on the influence of process parameters on the dewatering results of coals off different origin were carried out in laboratory scale due to the excellent reproducibility of the results gained during MTE dewatering with indirect, even heating (see Chapter 3, [Ber01, Ber03, Ber04]). For the scale up of the process to technical scale, however, three other requirements must be met besides dewatering:

- Maximising throughput with a corresponding minimum plant set-up.
- Minimising energy consumption
- Reduction of effort for treating discharged water by optimising the process

At first, surface specific throughput can be increased by a reduction of process time. Instead of a time-intensive, indirect heating, a direct heating of the material is preferred. This can be achieved using saturated steam since the utilisation of condensation heat for direct heating provides the advantage of higher heat flows due to the high heat transfer coefficient.

Minimising the energy consumption can be achieved by optimising energy flows within the process. The hot waste process water expelled in the pressing phase can be used for the preheating of the next batch just by transferring latent heat to the raw coal. Therefore the hot water from a previous batch is lead through the raw coal.

Optimising the process is aimed to achieve a simplification of the required water treatment. Due to the filter effect and the adsorptive properties of the coal, the flow of preheating water through the bulk leads to a considerable reduction of waste water impurities and thus to a reduction of the equipment required for water treatment [Ber02].

The final process design developed from these considerations is shown in Figure 5.1. The MTE process involves, first of all, a slight precompression (0.2 - 0.5 MPa) to create a uniform permeability
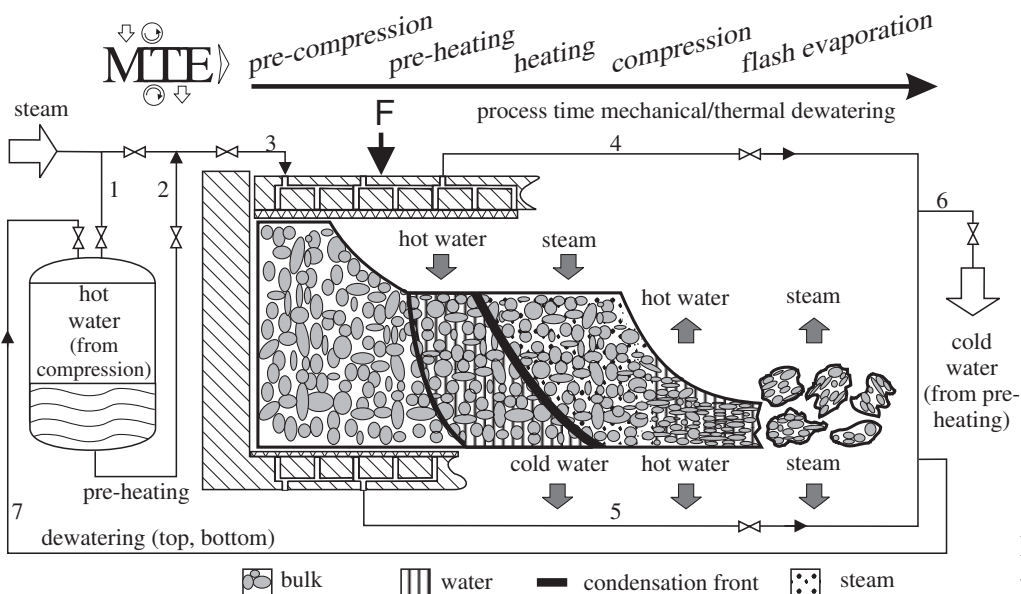
Figure 5.1: MTE process design

distribution throughout the coal filling. In the second step the coal is preheated by adding hot water from the previous batch (1, 2 in Figure 5.1). During flowing through the coal filling, driven by the steam pressure, its heat is directly transferred to the raw coal. Owing to the pronounced plug flow, the hot water and some of the steam condensate cool down to the coal temperature in the flow and can be removed from the process in a cold state (5, 6). Next, the steam condensing inside the coal fill heats the coal to process temperature [BBS98, CB02, BCS05]. In the following compression, the coal is dewatered mechanically and the removed hot water (4, 5) is stored (7) for the next process cycle. Once the mechanical pressure is removed, subsequent evaporation of the coal's residual water occurs, involving a pre-crushing of the coal cake and a further decrease in water content.

This process design was tested in numerous experiments at the process development unit and pilot plant. During these experiments the results of the laboratory test were verified concerning the dewatering kinetics. Additionally the influence of process parameters like loading, pre-compression pressure, steam pressure and particle size on heating times was determined [Ber01, Ber02, Cro03, CB02, BCS05].

Details of the process development unit are shown in Figure 5.2. The experimental rig consists of a steel cylinder ($\emptyset$ 270 mm) with an inner teflon insulation to prevent heat loss during consolidation phase. The pressure vessel is directly heated by hot water and steam. The heating medium is distributed across the surface of the piston by a system of channels and holes. A compression force up to 6 MPa can be applied by a hydraulic plunger. Temperatures and pressures inside the vessel can be measured at different locations inside the vessel to track the heating process. The stainless steel filter mesh, which is also used in the pilot and demonstration unit, is installed at the piston and the bottom of the vessel.

As an example, Figure 5.3 shows water content (a), temperatures (b), process pressure and compression height (c) of the bulk as function of process time and also surface-related throughput for a test run (d) at the process development unit.

if   inflow
of   outflow
fm   filter medium
st   stem
ti   teflon insulation
T   temp. measurement
P   pressure measurement

lf   load frame
hp   hydraulic plunger
st   stem
pm   pressure measurement
lm   length measurement
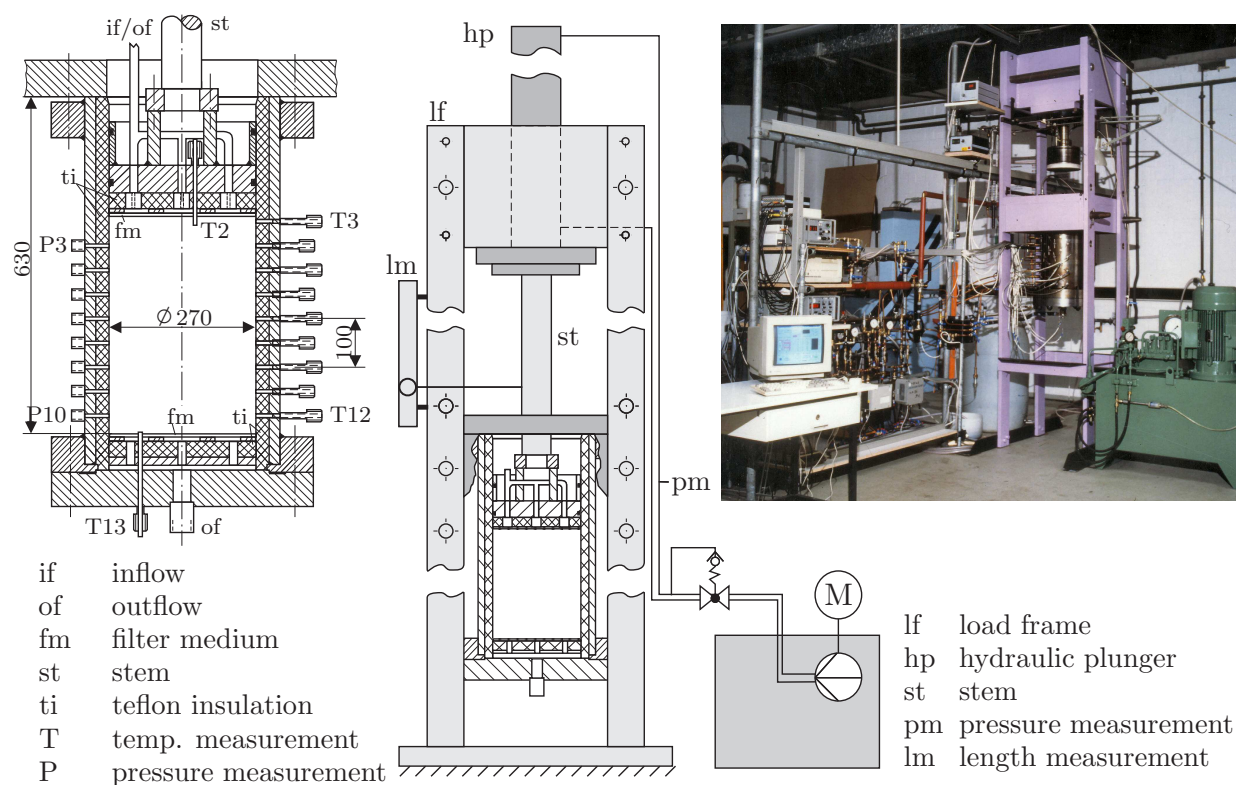
Figure 5.2: Process development unit
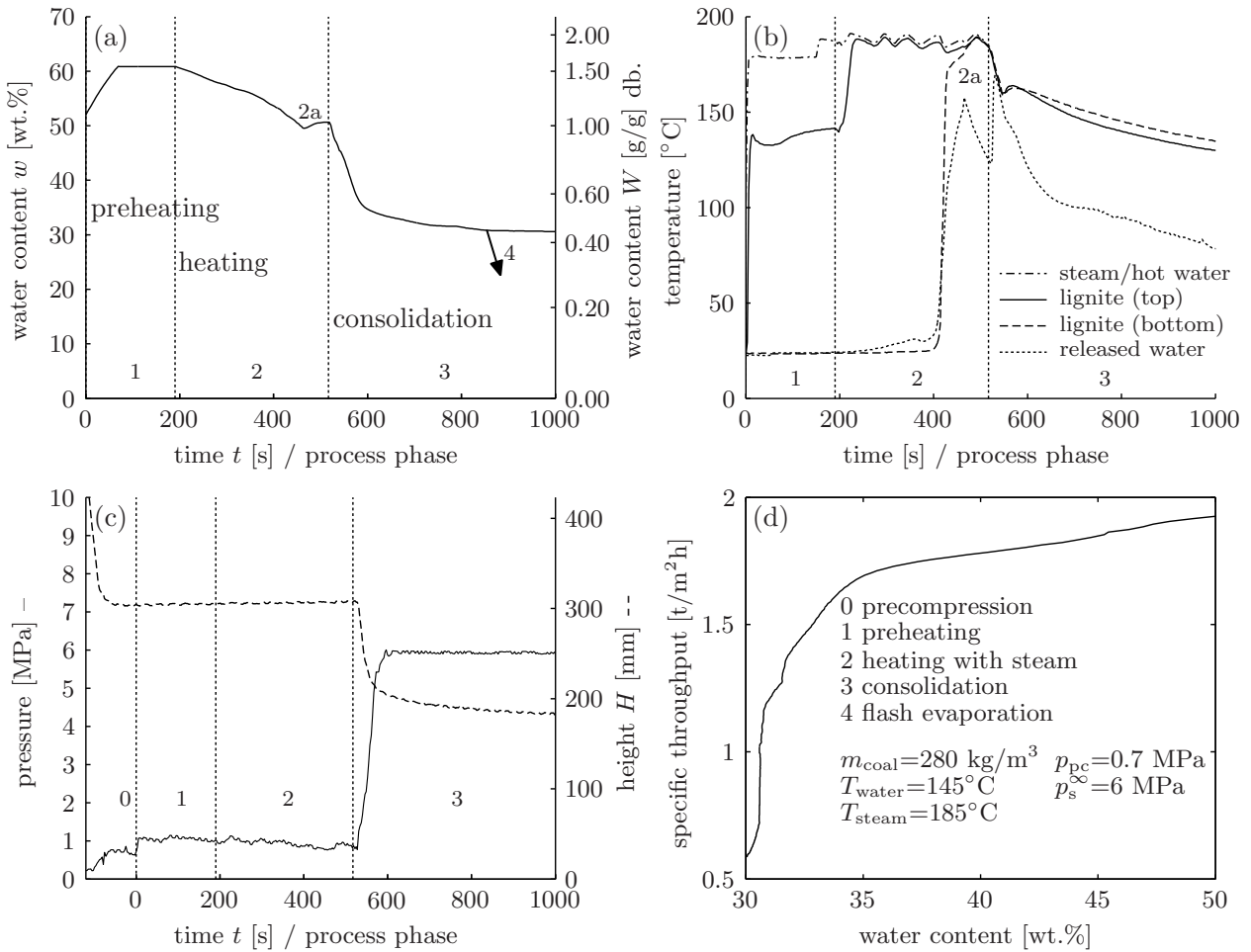
Figure 5.3: Course of process parameters during heating and dewatering

At the beginning of the process the coal filling is precompressed to p_{pc}=0.7 MPa (Figure 5.3c, phase 0), then the hot water is added to the coal. The water content (Figure 5.3a, w) is calculated from a mass balance for the test cylinder. It can be recognised that the input of preheating water (phase 1) causes a rapid increase in water content at the beginning of the process. During the flow of hot water through the bulk, the void volume in the bulk is filled completely, so that the water content remains constant in this phase.

In the subsequent course of the process, the steam displaces the preheating water from the bulk completely and the water content decreases again (phase 2). After an increase of temperature (Figure 5.3b, T bottom) of the outflowing steam condensate or when steam totally penetrates the bulk, the outlet of the press vessel to the atmosphere is closed and steaming is continued until the bottom of the bulk has also attained process temperature. The water content rises slightly during this additional steaming phase (phase 2a).

After attaining process temperature, the consolidation phase follows, in which the pressure is increased to 6 MPa by lowering the piston (Figure 5.3c, phase 3). The water content reveals an asymptotic curve with process time. While large quantities of water are discharged in a few seconds at the start of the pressing phase, small changes in water content require long times as the process progresses in the creep phase (Chapter 3.2.1). The flash evaporation (phase 4) leads to an additional decrease in water content to less than 25 wt.%.

The surface-related throughput illustrated in Figure 5.3d is calculated from the quantity of test material fed per surface unit [t/m^2] in relation to the process time t required to attain a certain

area $1.3\,\mathrm{m}^2$ throughput   2.6 tph raw lignite
pressure   6.1 MPa   1.6 tph dry lignite
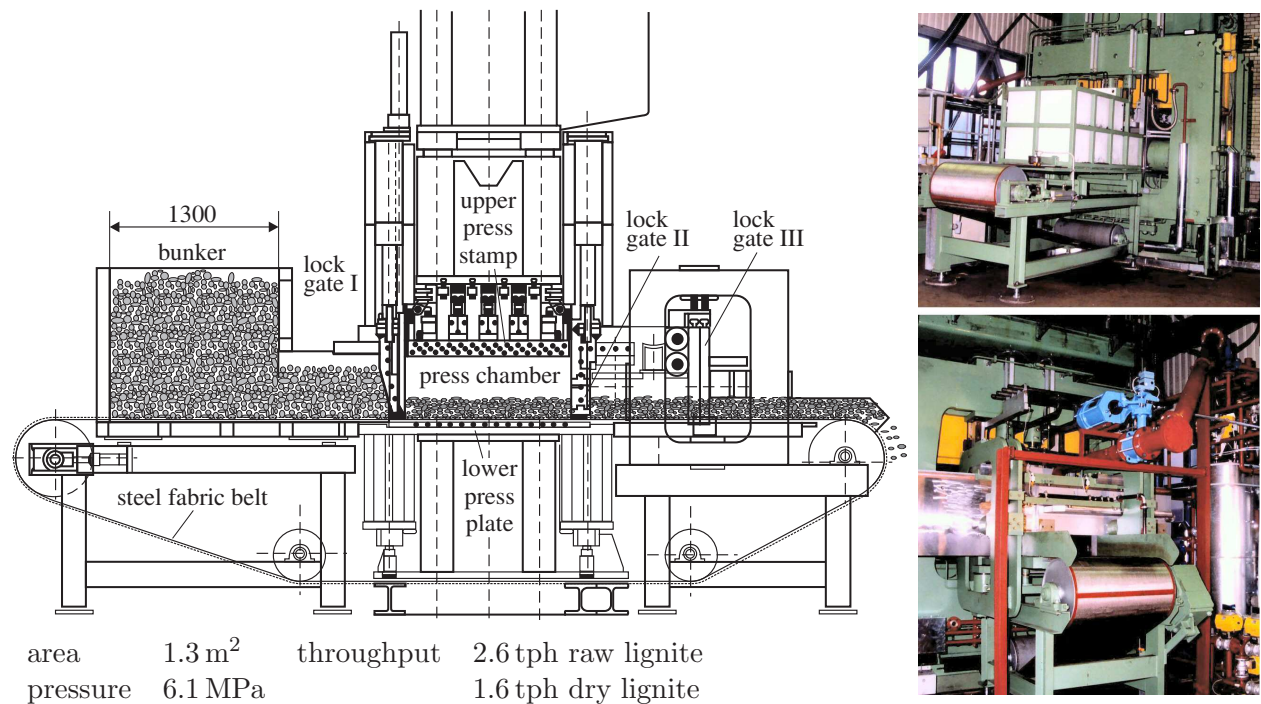
Figure 5.4: MTE pilot press Frechen

water content w. Here the process time is composed of heating phase and pressing phase, for which the representation of water content as a function of surface-related throughput first takes place at the start of the pressing phase since a reduction of water content first occurs here. As can be recognised, throughput decreases sharply as a result of the rapid decrease in the reduction of water content after primary consolidation is completed.

These results also were proven at the discontinuously working pilot press, which was constructed at Rheinbraun AG's Sibylla research center, Frechen, and commissioned in the spring of 1996. During operation of this MTE unit, also the feasibility of scaling up the press area by a factor of 20 from process development unit to pilot press has been demonstrated. Additionally, hot (preheating) and cold water was analysed and it could be shown, that the filtering effect of the coal during preheating leads to a significant reduction of the chemical and biological oxygen demand (COD, BOD_5). The COD value of the cold process water is reduced to 170-1100 g/m^3 (filtrated samples) and the BOD_5 to 50-350 g/m^3, respectively. Cooling the water to below 30°C during the MTE process permits direct discharge into a simple biological process water cleaning unit, which was also tested in Frechen. To clean the MTE 'cold water', a coke-based fixed-bed biology was installed on a laboratory scale, which provided evidence of a reduction of the COD value to below 50 g/m^3 [BBS⁺99]. However, there are also other methods for the MTE water cleaning and utilisation. NAKAGAWA et al. [NNBM04] have shown, that 90 % carbon conversion can be reached by catalytic hydrothermal gasification of the MTE waste water.

After intensive testing of different sealing systems, of the influence of coal preparation and coal type on the process results and optimisation of the control engineering, the press was modified completely in 1998 for testing a quasi-continuous MTE process with new plant components [SBB99]. Figure 5.4 shows the quasi-continuous pilot press. The press chamber consists of six components, movable relative to one another: the upper press stamp, the lower press plate, the two side walls (not shown in the drawing) and lock gates I (movable up and down) in the direction of flow at the feed-in side and lock gate II at the discharge side. The chamber formed by lock gates II and III has on the upper side a connection pipe on which a control valve is mounted, through which the flash vapour can be discharged into atmosphere. Lock gates I and II, side walls and press stamp have ducts permitting indirect heating of the plant with steam to compensate for heat losses.
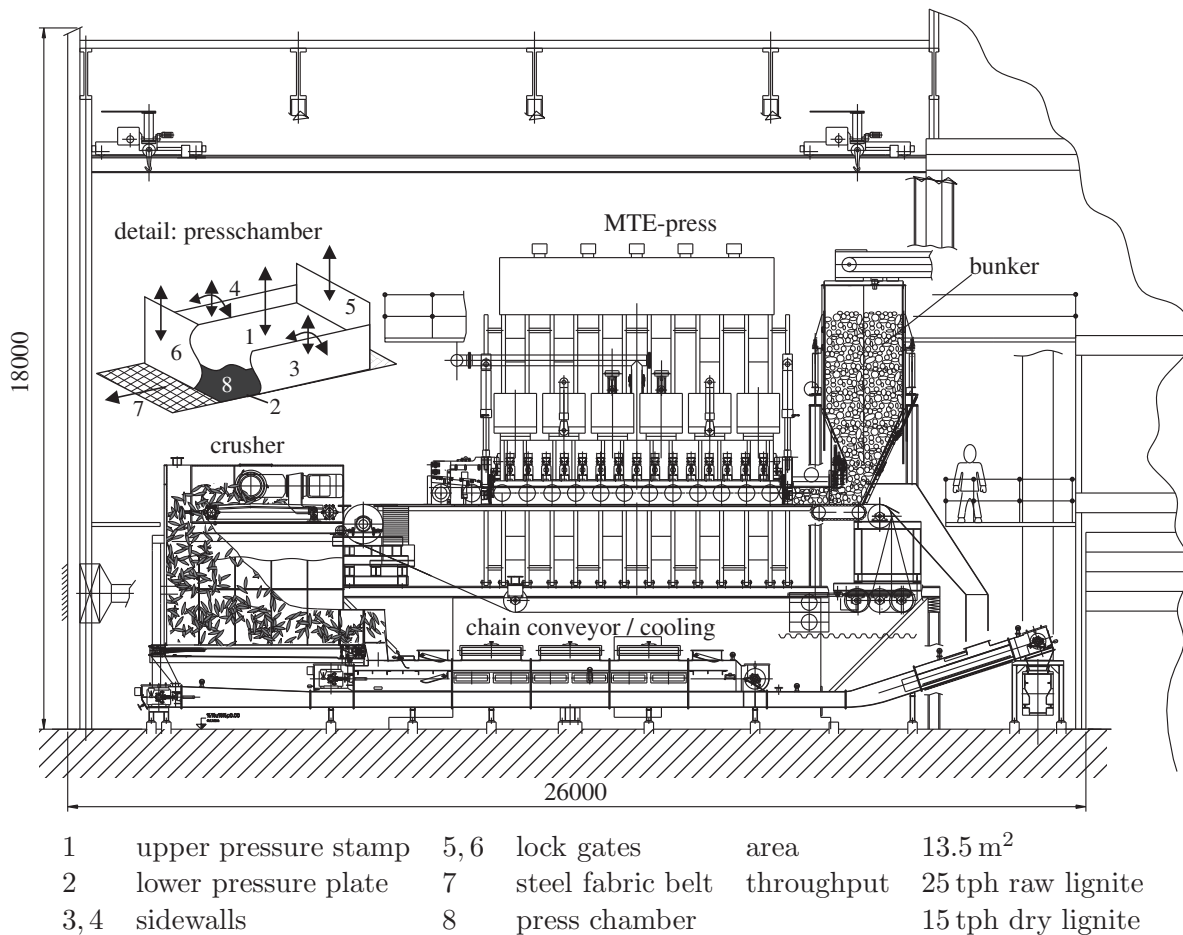
Figure 5.5: MTE demonstration plant Niederaußem

1	upper pressure stamp	5, 6	lock gates	area	$13.5\,\mathrm{m}^2$
2	lower pressure plate	7	steel fabric belt	throughput	25 tph raw lignite
3, 4	sidewalls	8	press chamber		15 tph dry lignite

In the course of a process cycle, the bunker is filled with coal via a conveyor belt. At the start of the process, the coal is transported by a continuous steel fabric belt at a speed of 0.5 m/s from bunker to press chamber. Lock gates I and II then are closed and the coal is compressed under the lock gates. During the process, the side walls and the various sealing systems are relocated in such a way that a press chamber is formed, that is sealed off to atmosphere. After completion of the MTE process, press stamp and lock gate II are lifted and the resulting flash vapour is discharged instantly through the chamber between lock gate II and lock gate III via the flash vapour valve. Finally, lock gates I, II and III are opened, the dried coal is removed from the system by conveyor belt, and a further batch of raw brown coal is fed into the system. The press chamber has a press surface of $1.3\,\mathrm{m}^2$ and the compression pressure is limited to 6.1 MPa. The plant can handle a coal fill height of 0.46 m. The press piston and the lower press plate have horizontal ducts and vertical drill-holes (nozzles) through which the heating medium can be fed, and the removed coal water can be discharged.

Operating experience gained in manually controlled sequences was turned into the development of a fully automatic control of the overall process. During the operation of the plant the new developed components and the availability of the technology were improved continually and in parallel the engineering for the demonstration plant started.

Figure 5.5 shows the quasi continuous 25 tph demonstration plant at the power plant Niederaußem. As in the final stage of the pilot plant the press chamber consists of six components movable with respect to each other. Those components are the upper press stamp (1), the lower press plate (2), two sidewalls (3, 4) and the lock gates (5, 6).

Starting the process the raw coal is transported from a continuously fed bunker into the press chamber (8) by a continuous steel fabric belt (7). When all the walls are moved to their position forming the press chamber, the process steps are carried out consecutively. After process completion the upper press stamp is lifted and flash evaporation takes place. In contrast to the pilot plant setup, the flash steam is removed from the press through the filter medium (stainless steel conveyor belt), the drill holes and ducts inside the press stamp and press plate to avoid the discharge of solids to the condenser. Finally the coal is removed from the system by the conveyor belt and transported to the crusher and cooled to 60°C with air in a chain conveyor. A detailed description of the process and plant engineering is given by BERGER [Ber02].

Cold process water emerged from the unit is led to a waste water treatment. This MTE demonstration unit with a raw coal throughput of 25 metric tons per hour is a direct scale-up of an pilot unit which was tested 1996 to 1998. The unit is part of the PTA plant for proof testing and demonstration of the brown coal dewatering with the MTE method including the conditioning of the coal water at the RWE Energie power plant in Niederaußem. The construction was completed in January 2001 and the commissioning was done at the end of 2001. At the beginning of 2002 RWE Energie has taken over the demonstration plant.

5.2 Dewatering of semi solids and suspensions

Since the initial filter cake formation is of great importance in particular during the treatment of suspensions, modifications are necessary in the procedure and plant design. The low permeability of the filter cake already requires a preheating of the suspension before beginning the process since only then the kinetic advantages can be fully utilised. The suspension can be heated either by steam injection (direct heat exchange) or by a combination of indirect heat exchange with hot filtrate and direct heating with condensing steam. Since semi solids or high compressible solids like younger lignites also cannot be heated directly by hot water and steam, a second process for the dewatering of such materials has been developed at the University of Dortmund [BCBS99, SB99], see Figure 5.6.

Though the dewatering device is similar to the plant for dewatering of bulk materials, the process takes into account the requirements specific to suspension treatment. Raw suspensions are fed to the mixing tank (1) and are preheated.
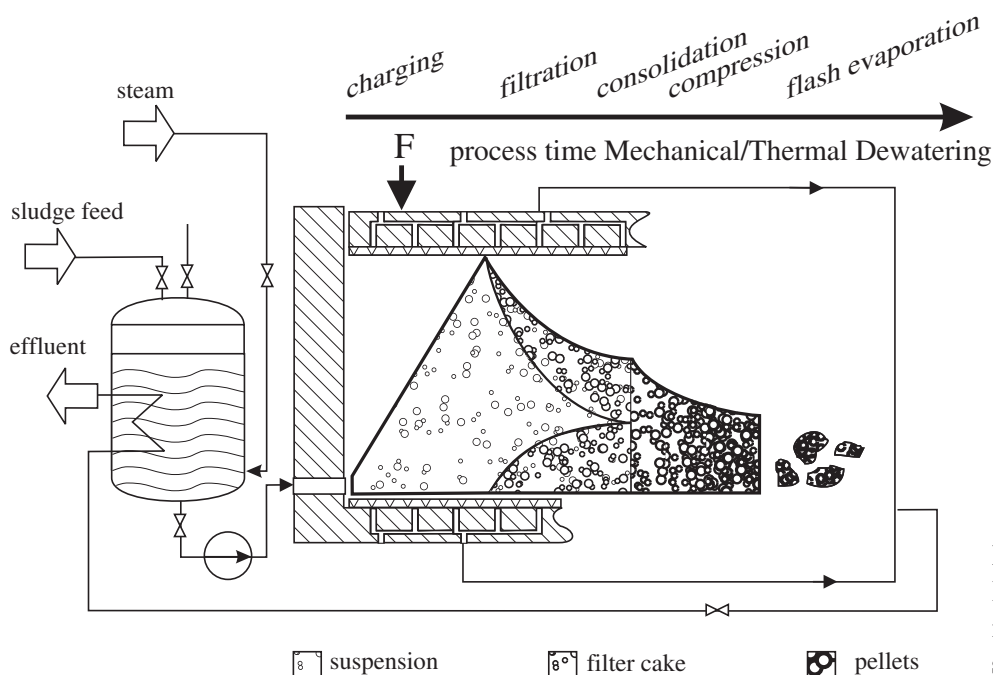
Figure 5.6: MTE process design for semi solids and suspensions
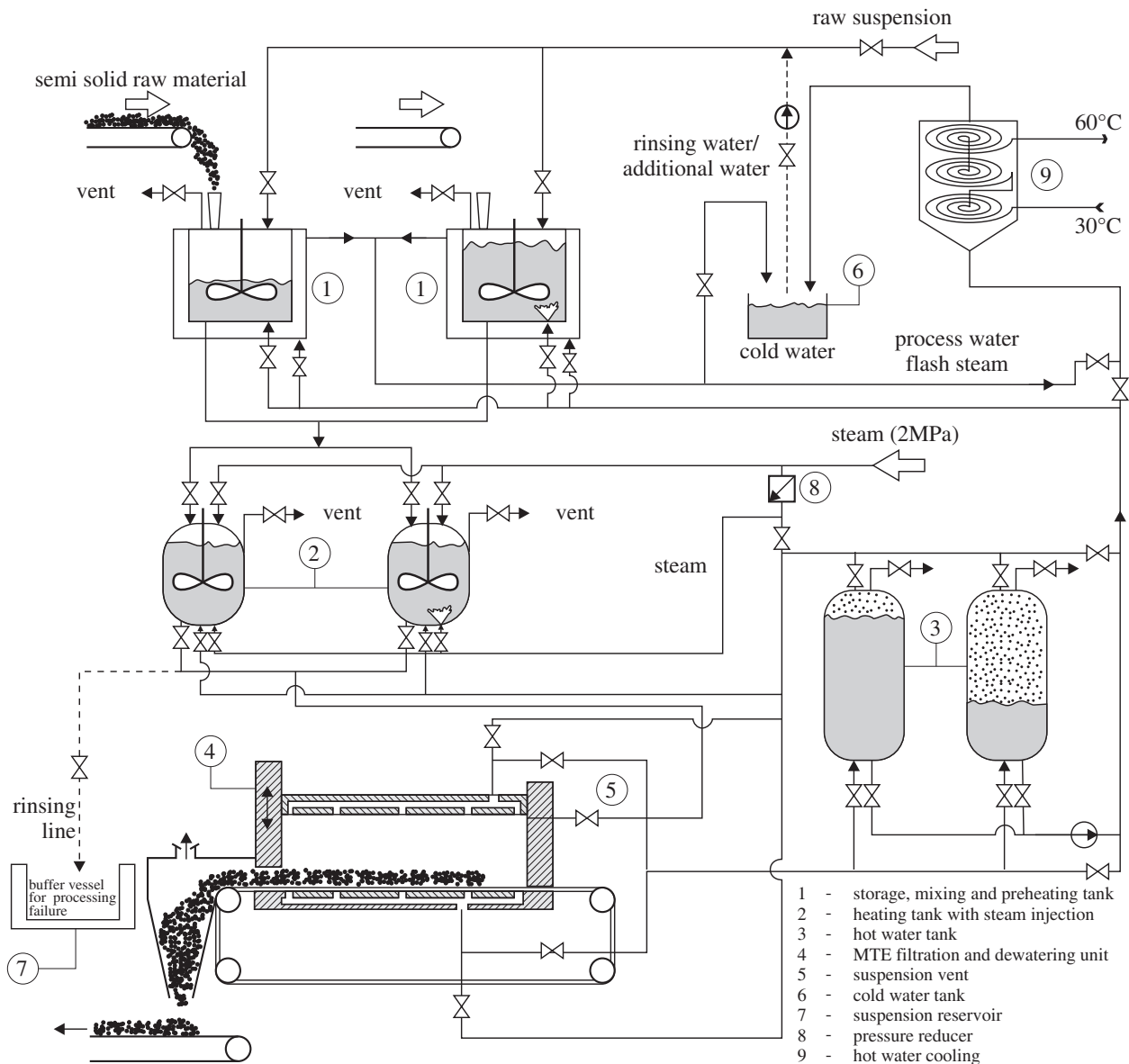
Figure 5.7: Process scheme for sludge dewatering

Semi solid materials have to be suspended and mixed with additional water from the hot water tank (3). The design allows the direct preheating of the raw suspension by a) flash steam from the MTE press and by b) flash steam from the hot water pressure release (3) and c) indirect preheating by the hot water from tank (3) just before it is further cooled down (9). All tanks are arranged in three levels as shown in the sketch, such that the feeding of the suspension to the heating tanks (2) and the MTE press (4) can be carried out by gravity. To ensure a quasi-continuous operation, the are two lines of vessels for preheating (1) and heating (2).

After preheating the suspensions are fed to the pressure tank (2) where the final direct heating with saturated steam is done. After this phase the suspension is fed through the suspension vent (5) to the MTE-press by steam pressure and gravity. Then the filtration starts and the hot water is collected in tank (3).

The dewatering is finalised by the consolidation of the filter cake and the subsequent flash evaporation. The flash steam is utilised for the preheating of the next batch of suspension in (1). The dry filter cake is removed from the MTE press by opening the lock gate and transporting via the conveyor belt which also acts as the filter medium.

(a)   (b)

$\varnothing\,270\,\text{mm}$ $200\,\text{mm}$
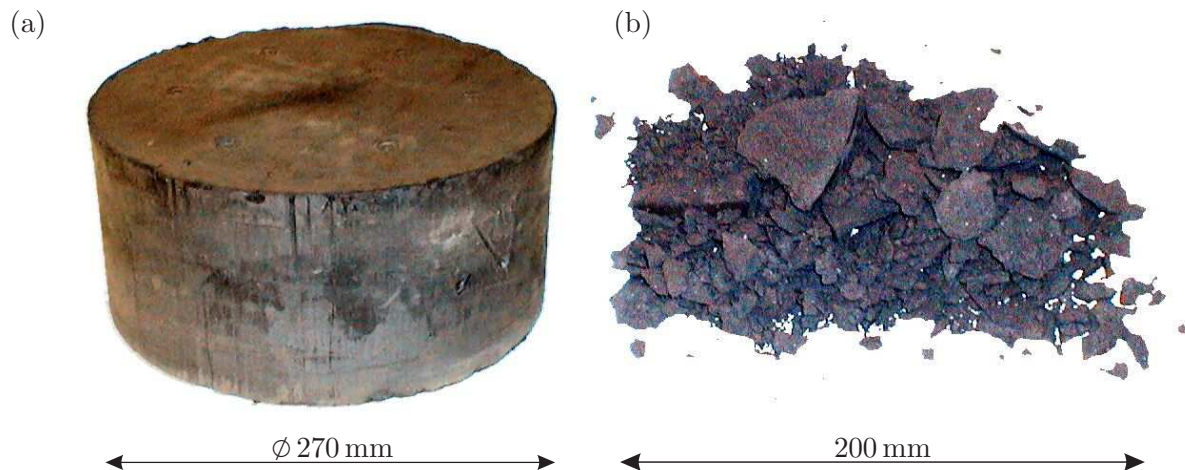
Figure 5.8: Products from the dewatering of ultrafine coal. a) Black coal 'briquette' after cooling, without flash evaporation. b) Coal after precrushing by flash evaporation.

This technology was developed in a cooperation of Dieffenbacher and the University of Dortmund [Bie97, Str97] and after testing in laboratory scale (Chapter 4.2) and at the process development unit (Figure 5.8) a feasibility study for the dewatering of ultrafine coal (waste product from black coal processing) showed, that the reduction of the plant size due to shorter filtration time results in lower cost compared to conventional technologies and provides the economical application of the MTE procedure also in this case. In Figure 5.9 the sketch of a 50 t/h dewatering unit for fine coal suspension is shown. The technology described is especially suited for the handling of large throughputs. For the dewatering of smaller mass flows a simplified apparatus, similar to the process development unit, can be used as shown in Figure 5.10 [MH03].
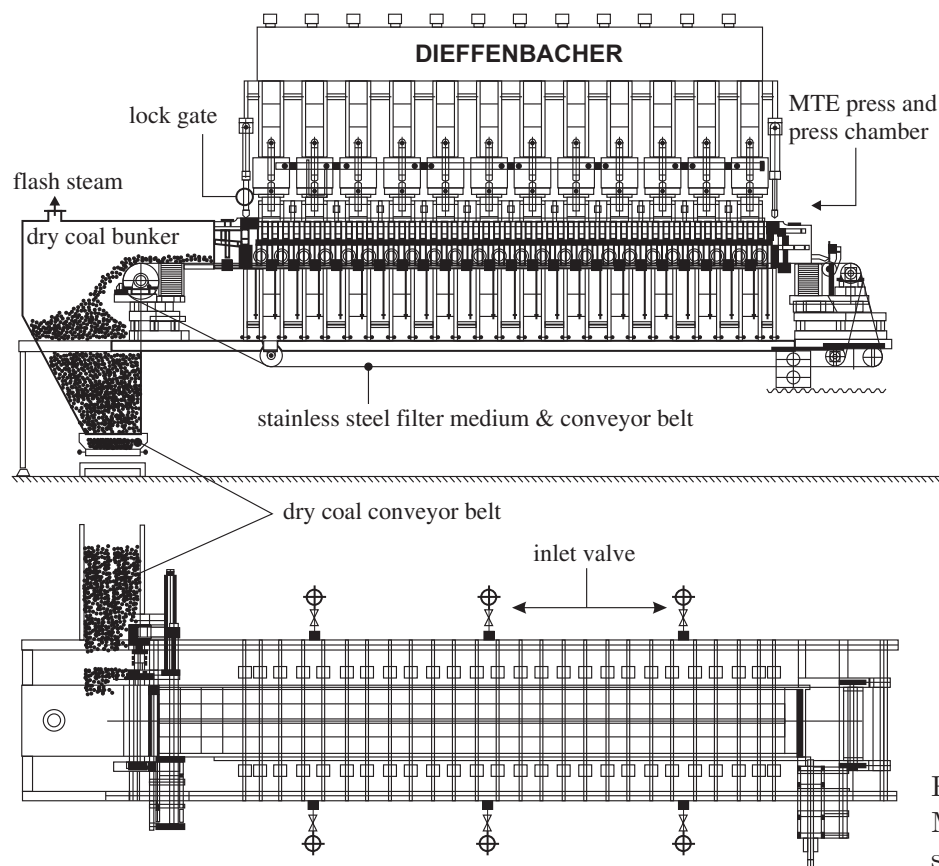
Figure 5.9:
MTE plant for fine coal
suspension dewatering
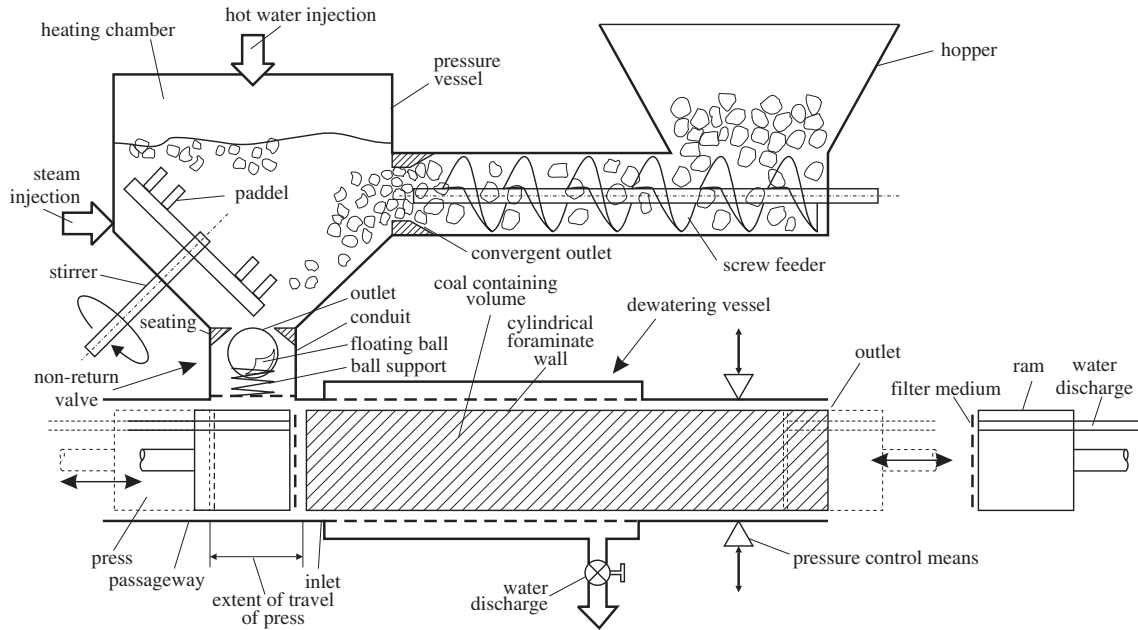
Figure 5.10: MTE dewatering unit for lignites and other semi solids [MH03], modified scheme.

Heating tank and dewatering unit are combined in this setup but also can be separated to enable an easier heat recovery [Str97]. The suspension is directly heated with hot water and/or steam and afterwards fed to the dewatering unit by the pressure arising from the heating with steam inside the heating vessel. The water can be removed either through the walls of the cylinder or through the filter medium covered pistons. The dry product is pushed out to the rhs of the dewatering unit. A similar unit has been tested for the dewatering of Australian lignite by the CRC for Clean Power from Lignite, Melbourne in pilot scale (1 t/h) and the construction of a 15 t/h demonstration plant is planned for late 2005.

5.3   Dimensioning

The length L of a number n of MTE dewatering plants for a throughput $\dot{m}$ can be calculated easily from the times t required for the individual process steps and a given width of the press w_{press} (up to 3.2 m in technical scale):

$$L = \frac{t_{\text{filling}} + t_{\text{preheating}} + t_{\text{heating}} + t_{\text{consolidation}} + t_{\text{flash evap.}} + t_{\text{add}}}{\dfrac{\ell\, w_{\text{press}}\, n}{\dot{m}} + \dfrac{1}{v_{\text{conveyor belt}}}}\ . \tag{5.1}$$

t_{filling} is the filling time for the feeding of suspensions to the MTE press (t_{filling}=0 for the dewatering of solids). $t_{\text{preheating}}$ and t_{heating} are the times for the heating of solids with hot water and steam. $t_{\text{preheating}}$ and t_{heating} can be neglected for the dewatering of suspensions, which were already heated outside the MTE press. For the dewatering of solids they have to be determined experimentally [Ber01] or estimated based on simplified models [Ber01, Ber02, BCS05]. For consolidation and flash evaporation the times $t_{\text{consolidation}}$ (depending on the final water content and loading ℓ) and $t_{\text{flash evap.}}$ (50 s) are included. t_{add} is an additional time with respect to the opening and closing of lock gates, the movement of the side walls and the precompression of the solid (70 s). $v_{\text{conveyor belt}}$ is the speed of the conveyor belt (0.5 m/s) feeding raw solids to the press and removing the dewatered material simultaneously. The transportation time $t_{\text{transportation}}$ is given by the ratio $L/v_{\text{conveyor belt}}$. From the ratio of loading ℓ and the summation of the times for the individual process steps the specific throughput can be calculated, which is about 2 t/(m^{2}h) for lignite dewatering and 3-4 t/(m^{2}h) for the filtration and consolidation of ultrafine coal suspension.

6 Combination of lignite drying and dewatering with power plant processes

In the last chapters the dewatering of different water containing materials was analysed concerning the amount of removed water, kinetics and physical/chemical changes in solid structure. In the following the different drying and dewatering processes known from literature (Chapter 2.2) are compared to each other and to the mechanical/thermal dewatering process concerning the efficiency increase and required changes in the power plant technology. The six processes which are analysed are the

- thermal dewatering (TD),
- mechanical/thermal dewatering (MTE),
- mechanical dewatering (MD),
- steam heated rotary tube dryer (SHRTD),
- steam fluidised bed dryer (SFBD) and the
- steam fluidised bed dryer with internal heat recovery (WTA).

Even if a large scale technical implementation for a pure mechanical dewatering does not exist, different concepts already exist for such technologies [MIB$^+$89, Süße99] and from the extrapolation of the dewatering results presented in Chapter 3 it seems to be possible to achieve sufficient high throughputs for a filter press working at 16 MPa and 100°C. Therefore this concept, which is similar to the MTE dewatering but works at atmospheric pressure (concerning the fluid phase), should be analysed, too.

6.1 Implementation

There are some previous studies on the efficiency increase of dry lignite power stations by some of the processes given above [WMJ83, FLW87, BKK92, EBWE96], but there is neither a detailed comparison of all processes under defined and comparable basic conditions with respect to both drying and power plant processes nor a comparison taking into account the changes in boiler and steam cycle design which actually differ in a wide range for the six processes. As a basis for all calculations a power plant similar to the new lignite fired power station of RWE Energie in Niederaußem with a steam cycle efficiency of 51 % is chosen, which is the state of the art for conventional power plants [HKKW96, HK99, Pfl99]. This power plant is connected to the coal preparation process via several heat flows as illustrated in Figure 6.1. As in all following energy balances Δq_{th} always denotes a specific heat flow [kJ per kg of raw coal] which can be transferred easily to an absolute heat flow $\dot{Q}_{\text{th}}$ by multiplication with the mass flow rate of raw coal. An asterisk (*) denotes heat flows to the coal preparation process (demand), all other values are recovery heat flows to the power station or losses. Generally there are two possibilities for the supply with process steam for the coal preparation which are

- the usage of bleed steam from the medium pressure section of the turbine ($\Delta q^*_{\text{th.MP}}$) [Str96c], which has the advantage of utilizing the positive effect of cogeneration on the total efficiency, since mainly 'waste heat' is used for the drying/dewatering [WKH91] and
- a flue gas heated auxiliary boiler for saturated steam ($\Delta q^*_{\text{th.fg}}$), placed at the cold end of the boiler which offers several advantages in the overall design of the power station especially for the MTE process [Str96b, SBB01].

In this concept waste heat from the coal preparation process can be recovered in the power station process by a) preheating of the combustion air $\Delta q_{\text{th.air}}$, b) in the preheating of the feed water
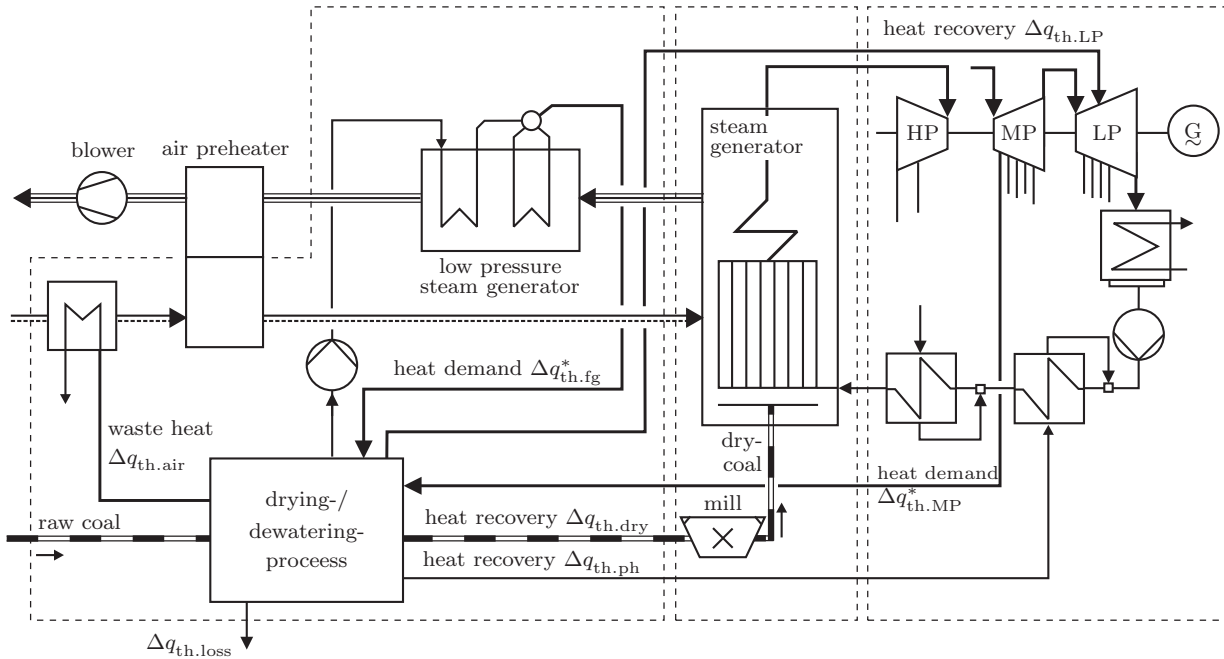
Figure 6.1: Heat flow chart of the dry lignite fired power station

$\Delta q_{\mathrm{th.ph}}$ or c) for power generation in a low pressure turbine. Since larger heat flows to the feed water preheaters would act similar to an additional regenerative feed water preheating this heat flow will be limited to the condensate of bleed steam and small amounts of exhaust steam. Larger steam flows from processes that use bleed steam (SFBD) can be further expanded in the low pressure turbine of the steam cycle ($\Delta q_{\mathrm{th.LP}}$) or an additional exhaust vapour turbine. Larger exhaust vapour flows, which are not pure enough for power generation, can also be used for the combustion air preheating (limited to a minimum temperature difference of 30°C). For safety reasons and to prevent spontaneous combustion of the coal in bunkers, the dried product has to be cooled down to 60°C after the preparation process. Nevertheless the remaining sensible heat (difference between ambient temperature and 60°C) can be recovered ($\Delta q_{\mathrm{th.dry}}$). Additional heat losses from radiation, which occur for all processes, are not considered since they can be minimised by insulation and naturally decrease with increasing plant size. Therefore measurements from pilot plants can not be used for an upscale of the technologies and the available numbers are also not consistent concerning the effort on heat loss minimisation.

6.2 Energy and mass balances

For the calculations two different low rank coals are considered, one from the Rhineland, Germany with 53.3 wt.% water, 8 wt.% ash (db.) and one from the Latrobe Valley, Australia with 62 wt.% water and 2 wt.% ash (db.). In this section the results for the heat flows in all processes are given for the German coal as direct results from the energy and mass balances. From the basic balances the heat demand, electricity demand for blowers, compressors and hydraulic pumps and the recovery heat flows can be determined. These numbers are used in the next section for the calculation of the total efficiencies and changes in power station dimensions and design. The additional electricity demand for crushing and grinding raw and dry coals is estimated based on previous works and also given in the next section.

6.2.1 Thermal dewatering (TD)

During thermal dewatering the water of the lignite is released in liquid form when the colloidal structure of the coal collapses during heating under pressure. High steam/water pressures have to be applied to prevent the evaporation, i.e. in all processes autoclaves or other pressurised reactors

are used. A generalised flow chart, shown in Figure 6.2, is used for the calculations due to the large variety of proposed and realised processes [Fle26, FMTS85, JMT85, FLWT87, HF90, ES70, DA92] utilizing steam or water as heating medium (thermal dewatering or hydrothermal dewatering/hot water drying), working continuous (Voest-Alpine) or discontinuous (FLEISSNER, VIAG). For each stream specific enthalpy q (basis 0°C), specific mass m, temperature T and pressure p are given as well as water content w (for coal), humidity φ (for air) and water saturation x (for wet steam).
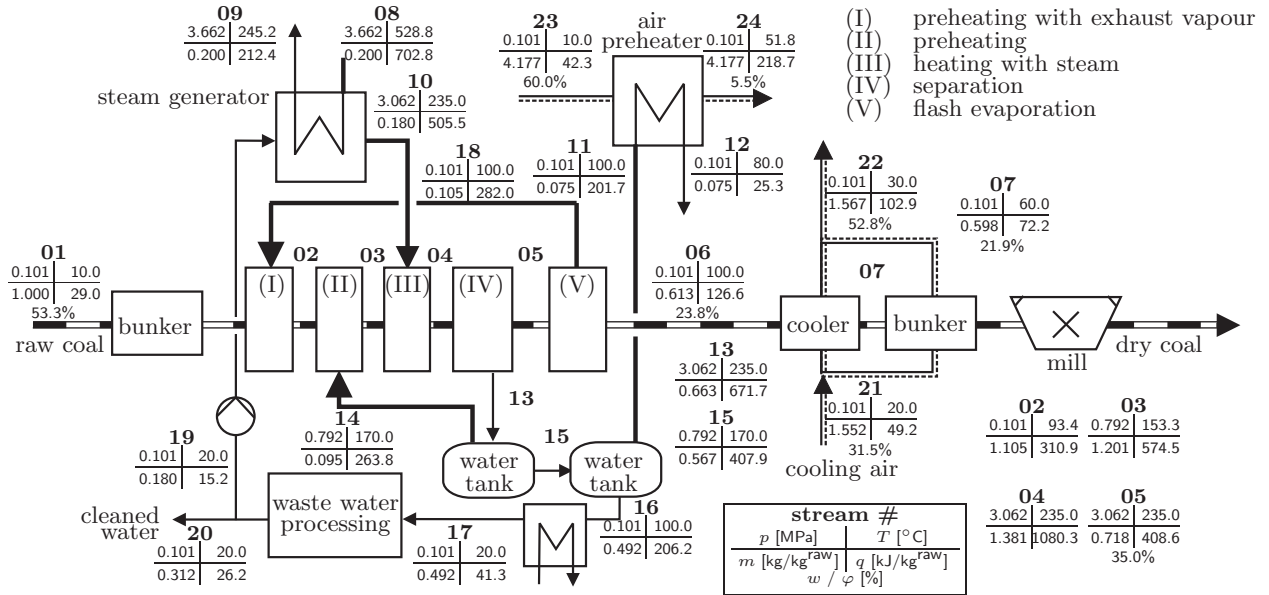
Figure 6.2: Thermal dewatering process

During the process the coarse grained ($d <50$ mm) raw lignite is preheated in the first two steps (I+II) with exhaust vapour (18) and (14) from the flash evaporation (V) of the coal and the depressurisation of the waste water. In the third step (III) the coal is heated to the process temperature of 235°C with saturated steam (10). During heating and keeping the temperature at this level the water released from the coal (35 wt.% water content after step IV) can be removed in liquid state (13) and afterwards depressurised to 0.79 MPa. The exhaust steam (14) from this depressurisation is used for the second preheating, the water phase (15) is further depressurised to ambient pressure while the additional exhaust vapour (11) is used for the preheating of the combustion air. The coal (6) after depressurisation (100°C) has a water content of below 24 wt.% which is further reduced slightly during cooling to 60°C with air (21). Air cooling can be applied in this process because the dry coal product contains only small amounts of fines and therefore does not tend to spontaneous combustion like the fine grained products of all drying processes (WTA, SFBD, SHRTD).

Due to the high organic load of the water (16), which originates from partial coal decomposition at temperatures above 210°C, a further heat recovery from this flow would require extensive construction work (due to the risk of fouling) on piping and heat exchange with the power plant and is therefore not considered in this case. Due to the direct contact of the heating medium steam with the coal also for the case of heating with bleed steam a secondary low pressure steam generator (ΔT=10 K) fed with cleaned waste water (19) is arranged in the flow chart to prevent the loss of high-purity boiler feed water.

All heat and mass flows in Figure 6.2 refer to 1 kg of raw coal. The temperature basis for the specific energies is 0°C. The chemical energy (heating value) is not regarded in the numbers for the heat flows (as in all following diagrams for the other processes) since the balance only should give the connective heat flows for the implementation of the process in a power station process.
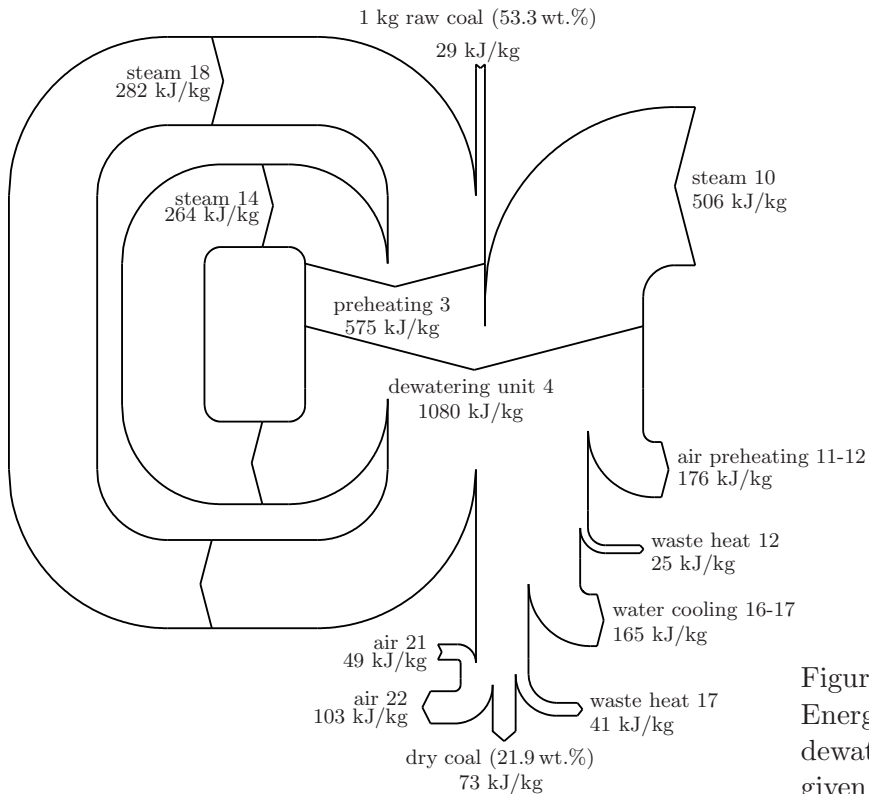
Figure 6.3:
Energy flow chart for the thermal dewatering. All enthalpy values are given in kJ per kg of raw coal.

Utilizing the waste heat from the exhaust vapour flows (11, 14, 18) for the preheating of air and raw coal provides a nearly complete recovery of waste heat within the process in this concept (Figure 6.3) and is an essential requirement for a high overall efficiency as the calculations in the next section will show.

6.2.2   Mechanical/thermal dewatering (MTE)

The process of mechanical/thermal dewatering [Str96a, BBS98] as described in the last chapter can be subdivided into the four phases

  I. preheating with hot water,
 II. heating with steam,
III. pressing phase and
 IV. flash evaporation.

The flow chart of the process is given in Figure 6.4. During the first phase the coal is heated directly in the pressure chamber of the MTE press by hot process water (13) which is led to the coal through a system of channels, nozzles and a stainless steel filter medium at the top pressure plate. The pressure chamber consists of an upper and lower pressure plate, movable sidewalls and two lock gates at the entrance and exit. The preheating water is cooled down to nearly ambient temperature due to the excellent heat transfer conditions and can be fed directly to a biological waste water processing unit after leaving the press (14) due to the additional filtering effect during the direct contact of water and coal. After the preheating saturated steam (10) is led into the coal (II). The steam condenses and a plug flow with a flat condensation front develops during heating the coal to the process conditions of 195°C at 1.4 MPa. In the third process phase the heat mobilised coal water (and little remaining condensate) is pressed out by lowering the upper pressure plate and increasing the pressure to about 6 MPa (III). The water (13) removed from the press during this phase is stored for the preheating of the next batch and the coal is de-pressurised by lifting the upper pressure plate (IV). Due to the release of pressure and the still high temperature of the coal

(I) preheating with water
(II) heating with steam
(III) pressing phase
(IV) flash evaporation

steam generator
air preheater
combustion air

09: 1.699 | 204.3 / 0.125 | 108.5
08: 1.699 | 411.9 / 0.125 | 408.3
17: 0.101 | 10.0 / 4.177 | 42.3 / 60.0%
18: 0.101 | 46.4 / 4.177 | 196.1 / 7.2%
20: 0.101 | 30.0 / 1.572 | 103.0 / 52.6%
11: 0.101 | 100.0 / 0.066 | 175.8
12: 0.101 | 80.0 / 0.066 | 22.0
10: 1.399 | 195.0 / 0.111 | 309.1
13
02 **03** **04**
05: 0.101 | 100.0 / 0.611 | 125.8 / 23.6%
06: 0.101 | 90.0 / 0.607 | 124.3 / 23.1%
07: 0.101 | 60.0 / 0.596 | 71.7 / 21.7%

mill

raw coal
bunker
(I) (II) (III) (IV)
MTE press
chrusher
cooler
bunker
dry coal

01: 0.101 | 10.0 / 1.000 | 29.0 / 53.3%
16: 0.101 | 20.0 / 0.111 | 9.3
13: water tank
13: 1.399 | 195.0 / 0.434 | 360.1
14: 0.101 | 20.0 / 0.434 | 36.5
15: 0.101 | 20.0 / 0.323 | 27.2
19: 0.101 | 20.0 / 1.557 | 49.3 / 31.5%
cooling air

waste water processing
cleaned water

02: 1.399 | 121.9 / 1.000 | 352.7
03: 1.399 | 195.0 / 1.111 | 661.7
04: 1.399 | 195.0 / 0.677 | 301.6 / 31.0%

stream #	
p [MPa]	T [°C]
m [kg/kg$^{\text{raw}}$]	q [kJ/kg$^{\text{raw}}$]
$w\,/\,\varphi$ [%]	

Figure 6.4: Mechanical/thermal dewatering process

a flash evaporation occurs. The exhaust vapour (11) is used for the preheating of the combustion air (17). After further crushing and cooling the dry coal water content is about 22 wt.%. As in the thermal dewatering process a secondary steam generator is used due to the direct contact of heating fluid and coal.

The results of the thermal analysis in Figures 6.4 and 6.5 demonstrate, that most of the heat from the hot water pressed out of the coal is recovered during the process itself due to the optimal heat transfer during preheating. An additional advantage compared to the thermal dewatering is the lower temperature level, which eases the technical implementation of dewatering and waste water processing. The specific mechanical work w_{mech} [kWs/kg of raw coal] necessary for the consolidation of the coal can be estimated from the solid compression pressure p (maximum: $p_{\text{s}}^{\infty} = 6\,\text{MPa}$), compression height x (which also can be written in terms of water content reduction $W_{\text{raw}} - W_{\text{mte}}$) and coal mass m. W_{raw} and W_{mte} are the water contents (dry basis) of the raw coal and the MTE coal after step (III).

$$w_{\text{mech}} = \frac{\int p\,A\,\mathrm{d}x}{m_{\text{raw}}} = \int \frac{p\,A}{m_{\text{raw}}}\frac{m_{\text{dry}}}{A\,\varrho_{\text{water}}}\mathrm{d}W \approx \frac{p_{\text{s}}^{\infty}}{\varrho_{\text{water}}}\frac{W_{\text{raw}} - W_{\text{mte}}}{W_{\text{raw}} + 1} \quad . \tag{6.1}$$

For the two coals under investigation this calculation gives a specific mechanical work of 2.3 (German) and 3.0 (Australian) kWs/kg of raw coal. Additionally the energy consumption of transport belt, lock gates and crusher has to be taken into account. Altogether the electric energy consumption does not exceed 10 kWs/kg of raw coal.

6.2.3 Mechanical dewatering (MD)

A pure mechanical dewatering at ambient temperature does not seem to be practicable at the current state of the art. Nevertheless former investigations show a potential for a moderate temperature (100°C) mechanical/thermal dewatering with a pressure of about 16 MPa [BB89, Ber03, Ber04] since even in that temperature range a remarkable increase in dewatering kinetics and decrease of water content down to 22 wt.% can be observed. The resulting heat and mass flows for this concept are given in Figures 6.7 and 6.6. The mechanical work for the compression can be calculated to 5.7 and 7.5 kWs/kg of raw coal for the two coal types. Including additional electrical devices a value of 20 kWs/kg is used for the calculations.
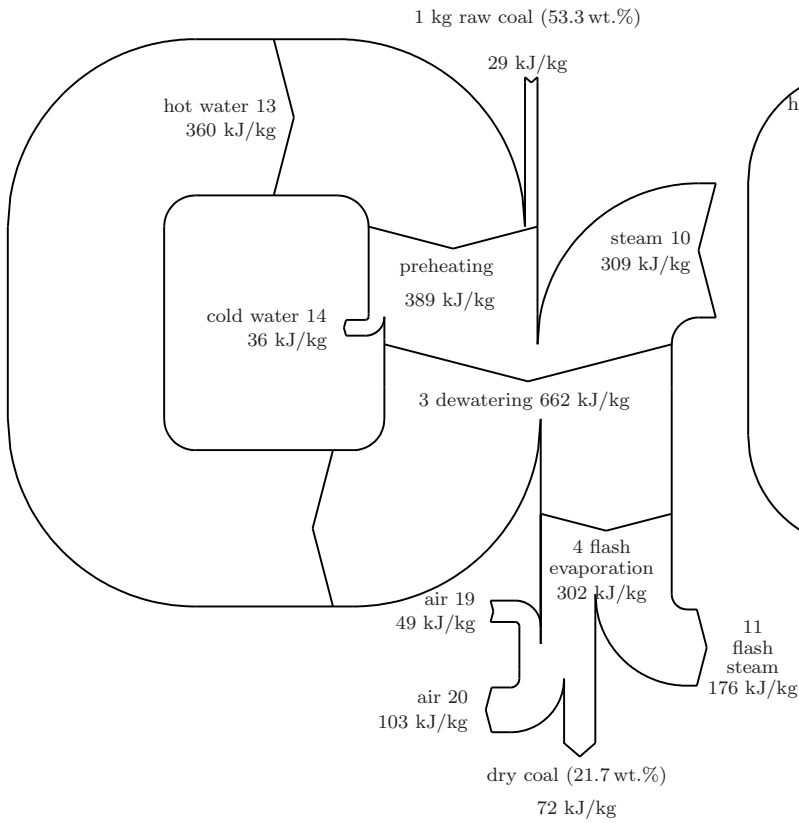
Figure 6.5:
Energy flow chart for the
mechanical/thermal dewatering
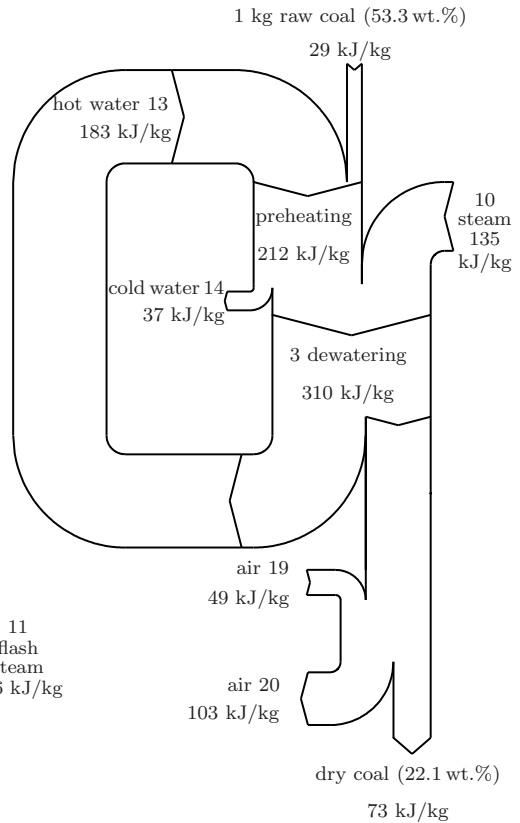
Figure 6.6:
Energy flow chart for the
mechanical dewatering
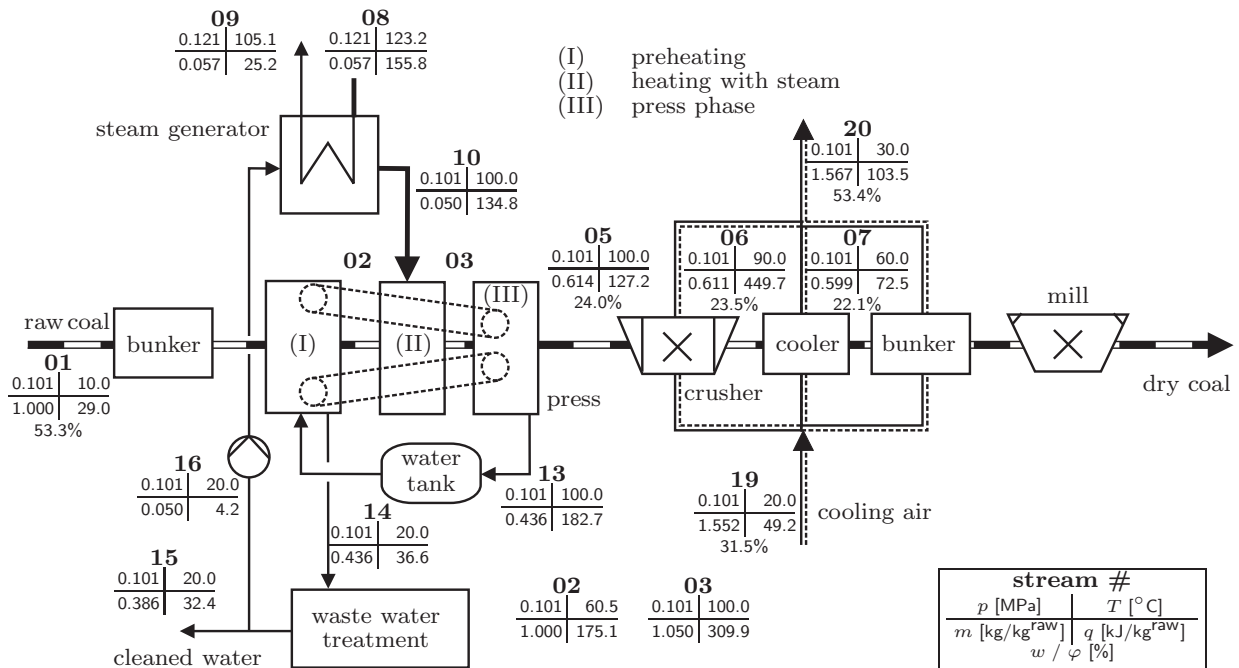
Figure 6.7: Mechanical dewatering process

Besides the MTE press technology [Str96a] also other presses [Süße99] can be used for a process like this, because there is no need for a closed press chamber due to the low pressure and temperature of the heating fluid.

6.2.4   Steam heated rotary tube dryer (SHRTD)

In a steam heated rotary tube dryer [KN78] the raw coal (1) is dried by indirect heating in tubes which are mounted in a rotating, inclined drum (Figure 6.8). Due to the rotation and the inclination of 6-10° of the drum the coal (d <10 mm) moves slowly through the tubes which are heated by condensing, saturated steam on the outside of the tubes. The evaporated coal water is carried by air (6) which flows in an co-current flow to the coal through the tubes. The steam (4) is injected in the drum at the upper axle shaft. The condensate (5) is removed through the lower one. As during the other drying processes, the water content of the dry coal (2) can be decreased to 12 wt.%.
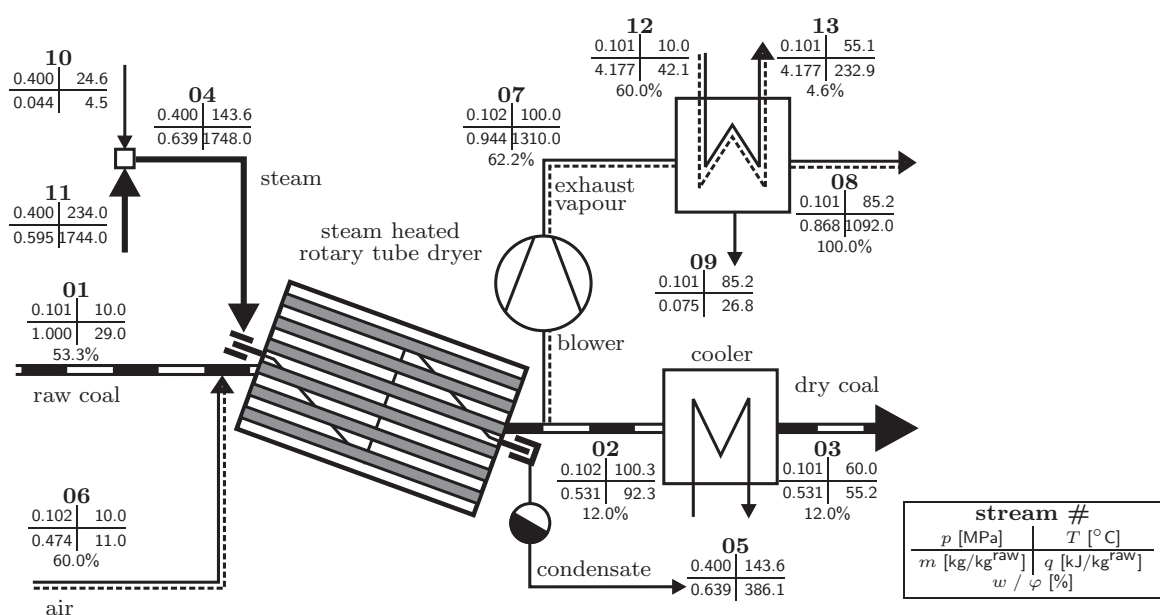
Figure 6.8: Steam heated rotary tube dryer

The biggest dryers of this type that are used for lignite drying in briquetting factories can evaporate about 25 tph of water with 1600 tubes of a length of 8 m in a drum with 5.6 m diameter and a total weight of 280 t. Apparatuses of this weight and increasing problems with bearings are the limit for a further increase of the throughput. Therefore this dryer is not really an option for a real power plant but represents the state of the art of lignite drying with experiences for nearly 100 years. Concerning the energy efficiency of dryers like this one, the largest problem is that the latent heat of the humid air can only be recovered in heat exchangers with continuously decreasing temperature on the cooling side due to the decreasing dew point of humid air. In this case the preheating of the combustion air (12-13) therefore is limited to 55°C providing a minimum temperature difference of 30°C. Two thirds of the energy fed to the dryer are contained in the exhaust vapour (8, see Figure 6.9) and released without further usage. The electrical self consumption of the dryer is assumed to 10 kWs/kg of raw coal.

6.2.5   Steam fluidised bed dryer (SFBD)

During steam fluidised bed drying [Pot81, WMJ83, WKH91] (Figure 6.10) the raw lignite (d <6mm) is fed to the top of the dryer (1), fluidised with slightly superheated recycled exhaust vapour (7) and additionally heated with saturated steam (4) condensing in heating tubes mounted inside the dryer.

1 kg raw coal (53.3 wt.%)

29 kJ/kg

air 6
11 kJ/kg

steam 4
1748 kJ/kg

dryer 1788 kJ/kg

condensate 5
386 kJ/kg

exhaust vapour 8
1092 kJ/kg

condensate 9
27 kJ/kg

air preheating 12-13
191 kJ/kg

cooling 2-3
37 kJ/kg

dry coal
55 kJ/kg (12.0 wt.%)
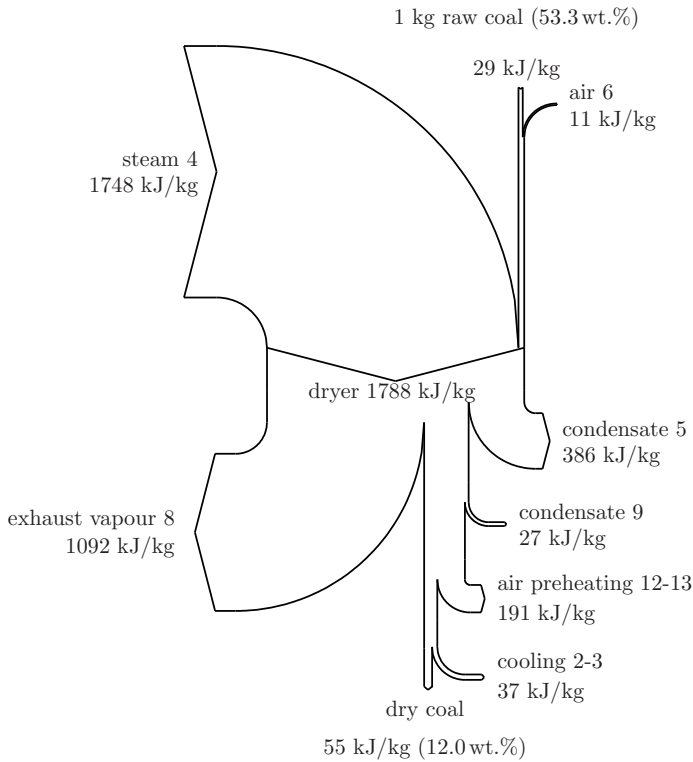
Figure 6.9:
Energy flow chart for the steam
heated rotary tube dryer

To provide sufficiently high heat transfer, the temperature of the heating steam ranges about 40°C
above the drying temperature. The sensible heat of the condensate (5) can be recovered in the
preheating of the main steam cycle. The larger part of the exhaust vapour (9), which is not used
for fluidisation can be used for the preheating of combustion air or – as shown in Figure 6.10 – for
electricity generation in the primary or a secondary steam cycle. Even if the vapour (8) leaving
the dryer is cleaned by an electrostatic precipitator, it is not pure enough to be used directly in a
turbine. Therefore a secondary steam generator has to be installed [EBWE96].
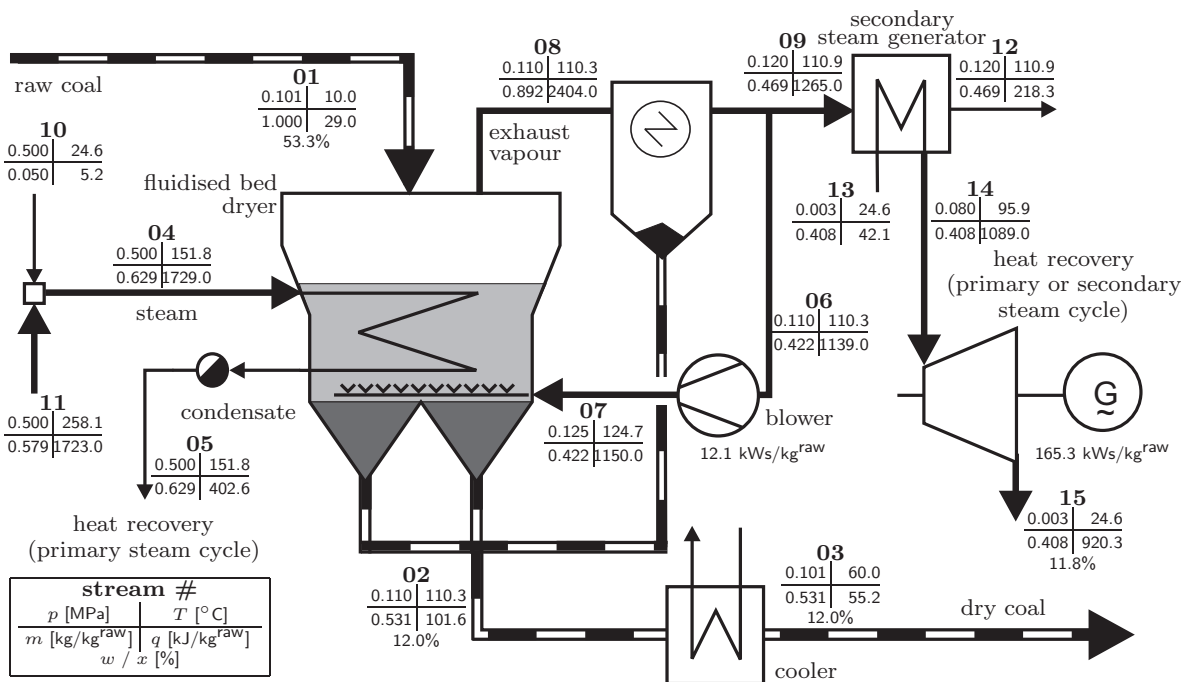
Figure 6.10: Steam fluidised bed drying
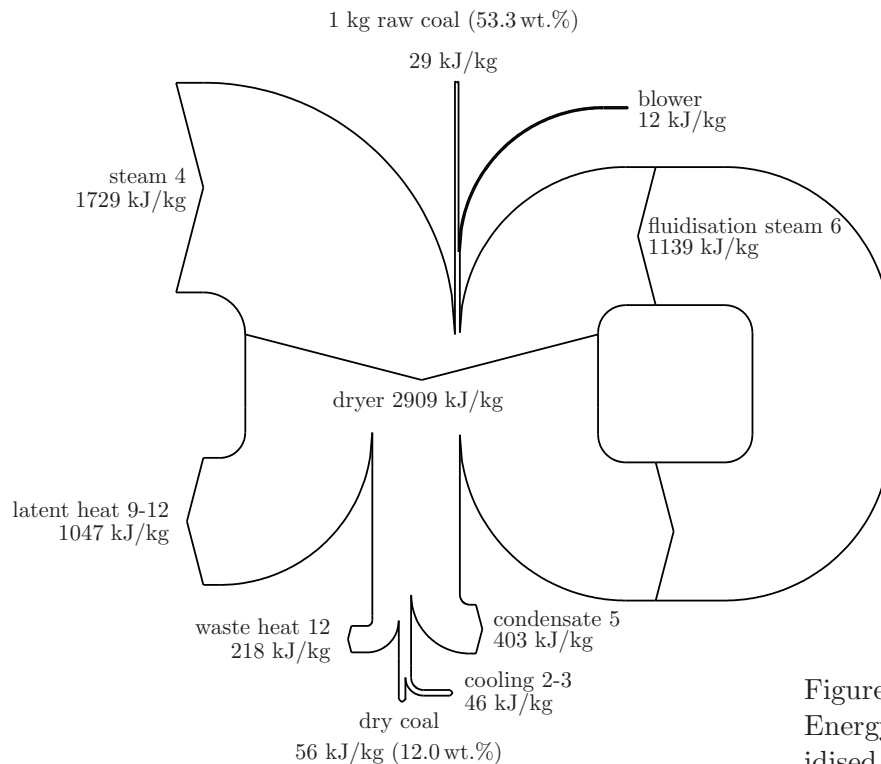
Figure 6.11:
Energy flow chart for the steam fluidised bed dryer dryer

The condensate (12) also has to be cleaned prior to further use, since it still contains coal particles and the pH value ranges in the acid region. From the energy balance in Figure 6.10 it is obvious, that the large energy content of the exhaust vapour (9) has to be recovered completely for providing high total efficiencies.

The coal leaves the dryer with a temperature of 110°C and a water content of about 12 wt.% and is cooled down to 60°C. The fraction of fluidisation vapour (6, 7) depends on the physical properties of the raw lignite (fineness, caking tendency). In the operation of the large scale demonstration plant at the Loy Yang power station, Australia, 0.73 t vapour per t of raw coal have to be recycled [ST96].

6.2.6   Steam fluidised bed drying with internal heat recovery (WTA)

In a steam fluidised bed dryer with internal heat recovery (WTA, '*Wirbelschicht-Trocknung mit interner Abwärmenutzung*', Figure 6.12) [Klu88, KKL94, KH96] the raw coal (1) is dried like in the SFBD process in a steam (8) fluidised bed. Unlike during the SFBD the heating steam (13) is recompressed exhaust steam (10).

By the three stage compression with water injection (12) the temperature and enthalpy is increased to a level that the latent heat can be used for the heating of the dryer. This way the process acts as a heat pump, recovering the latent heat on expense of the electricity required for the compressor. Additionally the sensible heat of the condensate (18) is recovered completely during (indirect) preheating of the raw coal. By this, all energy rich streams are recycled within the process, see Figure 6.13. The coal leaves the dryer with a temperature of 110°C and a water content of about 12 wt.% and is cooled down to 60°C to prevent self combustion. The energy of the (small) exhaust vapour flow (9) can be transferred to the preheating of the steam cycle.
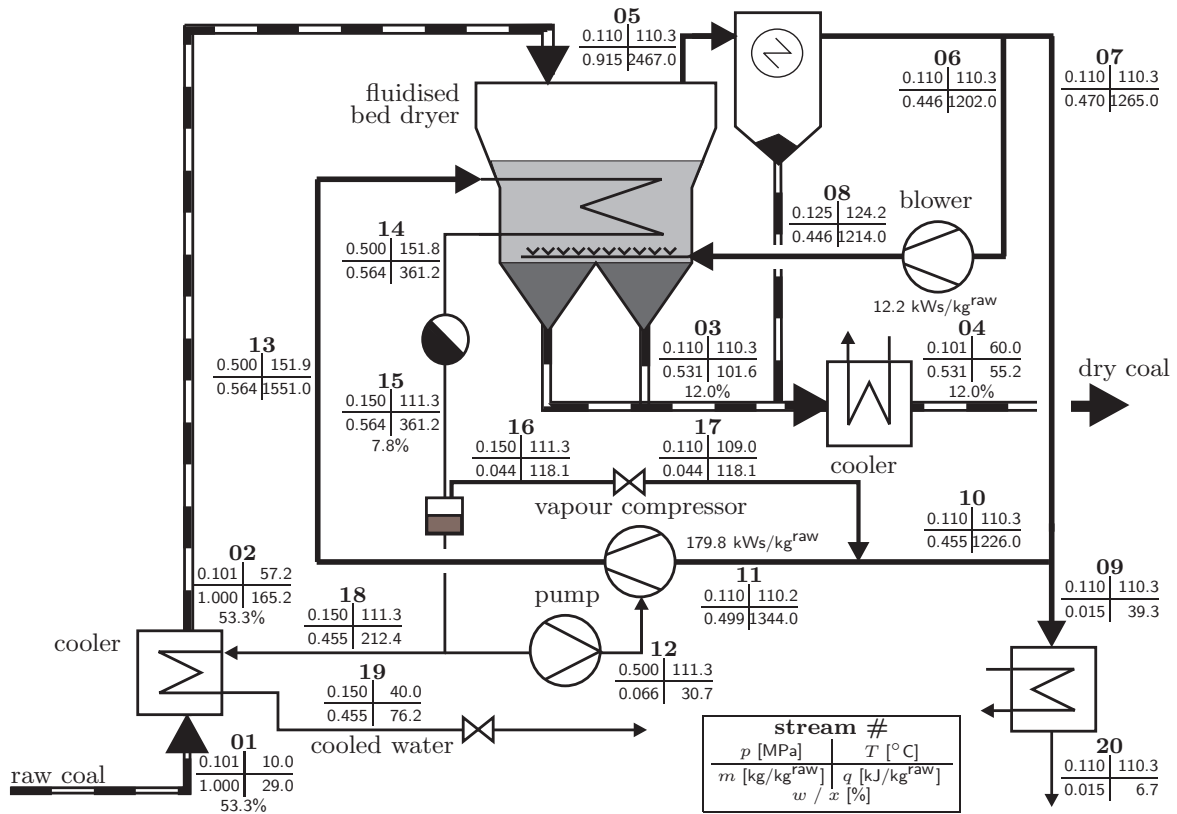
Figure 6.12: Steam fluidised bed drying with internal heat recovery
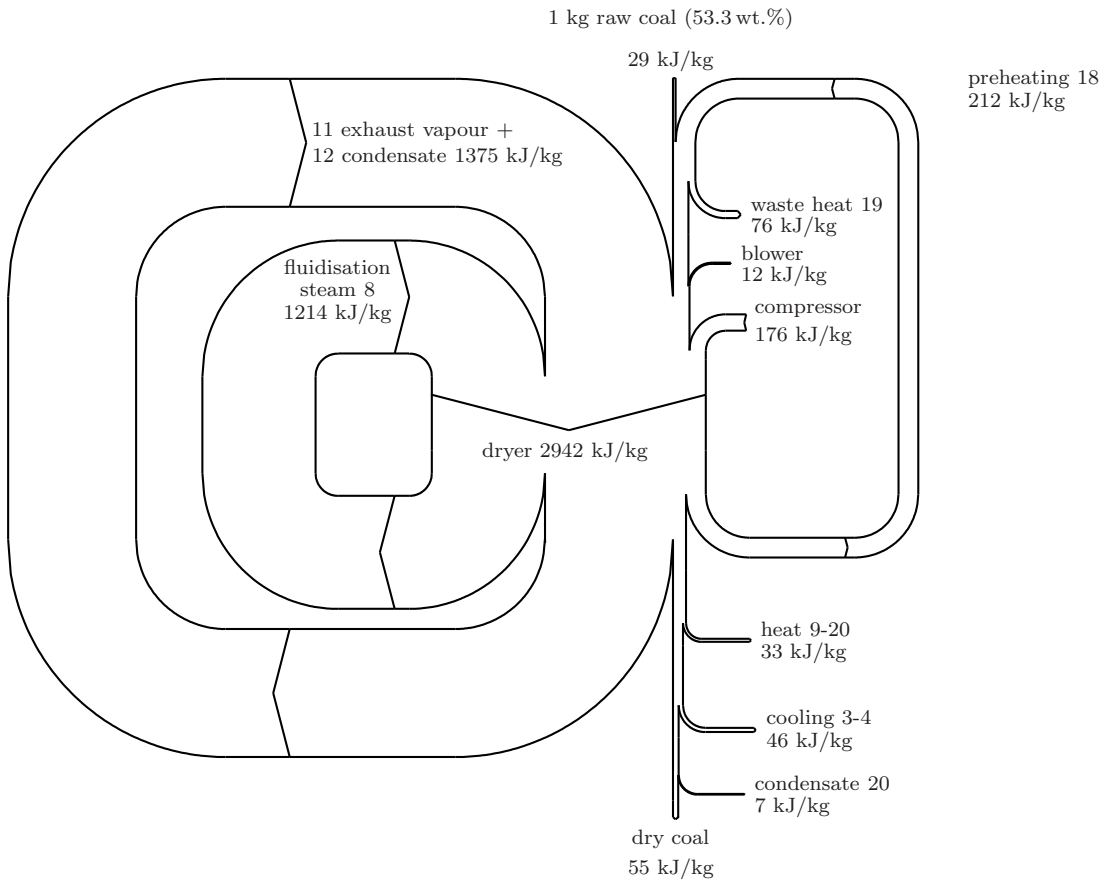
Figure 6.13: Energy flow chart for the steam fluidised bed dryer with internal heat recovery dryer

6.3 Energetic analysis

The total efficiency of the power station $\eta_{\text{net}}^{\text{dry}}$ (based on the lower heating value $H_{\text{low}}^{\text{raw}}$) can be written on the one hand as the product of an efficiency factor $f_{\text{net}}^{\text{dry}}$ and the raw coal fired efficiency $\eta_{\text{net}}^{\text{raw}}$. On the other hand it is the product of the thermal efficiency factors of drying process $f_{\text{th.dp}}$ and steam generator $f_{\text{th.sg}}$, of the electrical efficiency factors (self consumption) of drying process and power plant ($f_{\text{el.dp}}$, $f_{\text{el.pp}}$), of the steam cycle efficiency factor f_{sc} and of the steam cycle and steam generator efficiencies of the raw coal fired power station ($\eta_{\text{sc}}^{\text{raw}}$, $\eta_{\text{sg}}^{\text{raw}}$), see the illustration in Figure 6.14.
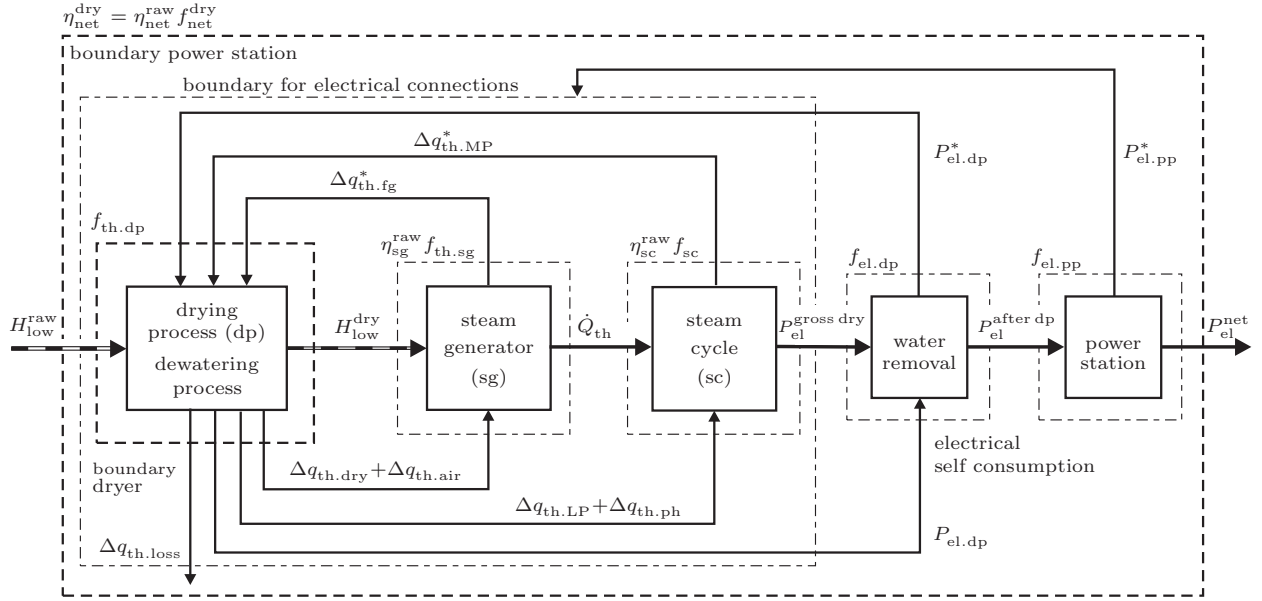
Figure 6.14: Illustration of the calculations

For the calculations the thermal heat flow $\dot{Q}_{\text{th}}$ which is transferred to the steam cycle is set to a constant value for all processes, see Table 6.1. The boiler efficiency $\eta_{\text{sg}}^{\text{dry}} = \eta_{\text{sg}}^{\text{raw}} f_{\text{th.sg}}$ (calculated according to [DIN94]) of a dry lignite fired power plant depends on the water content of the coal. It is increased by the efficiency factor $f_{\text{th.sg}}$ compared to the efficiency of a raw coal fired boiler due to the reduced heat losses by hot flue gas.

Additionally the heat flows between boiler, steam cycle and drying or dewatering process have to be regarded in the calculations. The thermal efficiency factor of the coal preparation process $f_{\text{th.dp}}$ includes additional heat flows to boiler (sensible heat of dry coal $\Delta q_{\text{th.dry}}$ and preheated combustion air $\Delta q_{\text{th.air}}$) and steam cycle (feed water preheating $\Delta q_{\text{th.ph}}$) as well as the heat demand of the process $\Delta q_{\text{th.fg}}^{*}/\eta_{\text{sg}}^{\text{dry}}$ (from a secondary steam generator). The additional increase in lower heating value by decreased water content can be calculated from the removed water Δm_{water} (kg water removed per kg of raw coal, calculated from the water contents w) and the heat of evaporation Δh_{evap}.

From these considerations the equations for the calculation of the raw coal mass flow to the power station $\dot{m}_{\text{raw}}$ and the thermal efficiency factor $f_{\text{th.dp}}$ result.

$$\dot{m}_{\text{raw}} = \frac{\dot{Q}_{\text{th.sg}}}{H_{\text{low}}^{\text{raw}} + \Delta q_{\text{th.sg}}} + \frac{\dot{m}_{\text{raw}}(\Delta q_{\text{th.fg}}^{*}/\eta_{\text{sg}}^{\text{dry}} - \Delta q_{\text{th.ph}})}{H_{\text{low}}^{\text{raw}} + \Delta q_{\text{th.sg}}} \, , \tag{6.2}$$

$$f_{\text{th.dp}} = \frac{H_{\text{low}}^{\text{raw}} + \Delta m_{\text{water}}\Delta h_{\text{evap}} - \Delta q_{\text{th.fg}}^{*}/\eta_{\text{sg}}^{\text{dry}} + \Delta q_{\text{th.ph}}}{H_{\text{low}}^{\text{raw}}} \, , \tag{6.3}$$

Table 6.1: Basic design data

Power station process			**Steam generator efficiency**		
steam pressure to MP turbine	5.55	MPa	53.3 wt.% German lignite	89.7	%
steam temperature to MP turbine	599	°C	22.0 wt.% German lignite	91.7	%
net heat to steam cycle $\dot{Q}_{th}$	1078	MW	12.0 wt.% German lignite	92.0	%
electrical power (basis) P_{el}^{gross}	550	MW	62.0 wt.% Australian lignite	88.7	%
flue gas temp. after air preheater	160	°C	22.0 wt.% Australian lignite	91.8	%
reference temperature	10	°C	12.0 wt.% Australian lignite	92.1	%
condensation temperature	24.6	°C			
isentropic efficiency MP turbine	93	%	**Properties of lignite**		
isentropic efficiency LP turbine	88	%	specific heat capacity (db.)	1.4	kJ/kg
efficiency of steam cycle	51	%	upper heating value (25°C) daf.	24.45	MJ/kg
isentropic efficiency compressor	85	%	ash content German lignite	8	%
efficiency generator / motor η_g	98	%	ash content Australian lignite	2	%
Combustion air (15% excess air)			**thermal losses (power station)**		
German lignite	4.158	kg/kg raw coal	radiation	0.375	%
Australian lignite	3.588	kg/kg raw coal	slag / ash	0.5	%
air humidity	0.006	kg/kg dry air			

Table 6.2: Concepts of processes, heating sources and exhaust vapour usage

#	process / concept	energy source	exhaust vapour usage
1	raw coal fired power station (reference)		
2	dry coal fired power station (max. efficiency without energy demand for drying)		
3a	SHRTD steam heated rotary tube dryer	bleed steam (MP-turbine)	-
3b	SHRTD	bleed steam (MP-turbine)	air preheating
3c	SHRTD	secondary steam generator (flue gas)	air preheating
4a	SFBD steam fluidised bed dryer	bleed steam (MP-turbine)	-
4b	SFBD	bleed steam (MP-turbine)	air preheating
4c	SFBD	bleed steam (MP-turbine)	steam cycle (LP turb.)
4d	SFBD	secondary steam generator (flue gas)	secondary turbine
5	WTA steam fluidised bed dryer with internal heat recovery		
6a	MTE mechanical/thermal dewatering	bleed steam (MP-turbine)	-
6b	MTE	bleed steam (MP-turbine)	air preheating
6c	MTE	secondary steam generator (flue gas)	air preheating
7a	MD mechanical dewatering at 100°C	bleed steam (MP-turbine)	
7b	MD	secondary steam generator (flue gas)	
8a	TD thermal dewatering	bleed steam (MP-turbine)	-
8b	TD	bleed steam (MP-turbine)	air preheating
8c	TD	secondary steam generator (flue gas)	air preheating

$$\dot{Q}_{th} = \dot{Q}_{th.sg}/\eta_{sg}^{dry} \, , \quad \Delta q_{th.sg} = \Delta q_{th.dry} + \Delta q_{th.air} \, , \quad \Delta m_{water} = \frac{w_{raw} - w_{dry}}{1 - w_{dry}}. \qquad (6.4)$$

If the drying or dewatering process is heated with bleed steam from the turbine, this stream is taken into account in the decrease $\Delta p_{el.MP}^*$ of electricity output from the turbine as the additional electricity production $\Delta p_{el.LP}$ in the low pressure turbine from the exhaust vapour heat recovery (only for the SFBD concept) for the calculation of the steam cycle efficiency factor.

$$f_{sc} = \frac{P_{el}^{gross\,raw} - \dot{m}_{raw}(\Delta p_{el.MP}^* - \Delta p_{el.LP})}{P_{el}^{gross\,raw}} = \frac{P_{el}^{gross\,dry}}{P_{el}^{gross\,raw}} \, . \qquad (6.5)$$

The electrical self consumption $P_{el.dp}^*$ of the drying process (preparation, crushing, grinding, power loss due to bleed steam $\Delta p_{el.MP}^* = \Delta q_{th.MP}^*/\eta_g$) as well as the additional electricity production in a separate turbine ($P_{el.dp} = \dot{m}_{raw}\Delta p_{el.LP}$, during SFBD) are taken into account in the electrical

efficiency factor $f_{\text{el.dp}}$ of the drying process.

$$f_{\text{el.dp}} = \frac{P_{\text{el}}^{\text{gross dry}} - P_{\text{el.dp}}^* + P_{\text{el.dp}}}{P_{\text{el}}^{\text{gross dry}}}. \tag{6.6}$$

The electrical self consumption for coal preparation and coal grinding or crushing is estimated to 26 kWs/kg of raw coal for all drying concepts. Similarly the electrical efficiency factor $f_{\text{el.pp}}$ with respect to the self consumption $P_{\text{el.pp}}^*$ of the power plant is calculated.

$$f_{\text{el.pp}} = \frac{P_{\text{el}}^{\text{gross dry}} - P_{\text{el.dp}}^* + P_{\text{el.dp}} - P_{\text{el.pp}}^*}{P_{\text{el}}^{\text{gross dry}} - P_{\text{el.dp}}^* + P_{\text{el.dp}}} = \frac{P_{\text{el}}^{\text{after dp}} - P_{\text{el.pp}}^*}{P_{\text{el}}^{\text{after dp}}} = \frac{P_{\text{el}}^{\text{net}}}{P_{\text{el}}^{\text{after dp}}}. \tag{6.7}$$

The self consumption (normally about 5 %) is decreased due to the reduced volumetric flow of air and flue gas and less effort for milling proportional to the reduction in coal mass flow. This can be estimated by

$$P_{\text{el.pp}}^* = 0.05 \, P_{\text{el}}^{\text{gross raw}} \left(1 - \left(f_{\text{th.dp}} - 1\right) 0.4\right). \tag{6.8}$$

For a comparison of investment costs the dimensions of the basic aggregates for the different concepts can be compared by scaling factors for the raw coal mass flow (concerning mills, boiler and flue gas cleaning) and the thermal heat flow to the steam cycle (concerning boiler, heating surfaces, turbine, condenser) at a constant net electrical capacity of the power station:

$$f_{\text{boiler}}^{\text{scaling}} = \left.\frac{\dot{m}_{\text{raw coal}}^{\text{dry coal fired}}}{\dot{m}_{\text{raw coal}}^{\text{raw coal fired}}}\right|_{P_{\text{el}}^{\text{net}} = \text{const.}} \quad \text{and} \quad f_{\text{steam cycle}}^{\text{scaling}} = \left.\frac{\dot{Q}_{\text{th}}^{\text{dry coal fired}}}{\dot{Q}_{\text{th}}^{\text{raw coal fired}}}\right|_{P_{\text{el}}^{\text{net}} = \text{const.}} . \tag{6.9}$$

The basis for these calculations are the results from the previous section and the design data in Table 6.1. Several different possibilities for the connection between coal drying and power plant were calculated according to Table 6.2.

6.4 Overall efficiency

In the following the results of the calculations shown in Figure 6.15 to Figure 6.18 are discussed. The complete results are given in Tables 6.3 and 6.4. As shown by the values of $f_{\text{net}}^{\text{dry}}$ and the total efficiencies[1] $\eta = \eta_{\text{net}}^{\text{dry}}$ in Figure 6.15 the highest efficiency increases can be reached by the process concepts optimised energetically and heated with bleed steam or electricity (8-12 %). In the former case the highest efficiencies are reached since the steam has released most of the mechanical work just before it is used for the dewatering or drying process like in cogeneration. In the latter case (WTA) the latent heat of the exhaust vapour is upgraded by the compression. Since the electricity used for the compression is already produced with a lower overall steam cycle efficiency, the efficiency factor for WTA is slightly lower.

Using steam from a secondary flue gas heated steam generator leads to lower efficiency increases especially for the processes with a large specific energy demand. In Figure 6.16 the specific thermal energy feed from outside is given for all processes. Electricity is weighted with $\eta_{\text{net}}^{\text{dry}}$. From the values it becomes clear that the high efficiencies for all dewatering processes (TD, MD, MTE) – even if heated with steam from a secondary steam generator – result from the low specific heat demand.

---

[1] Efficiencies are given based on the lower heating value. The efficiencies based on the higher heating value are listed in Tables 6.3 and 6.4. Efficiency factors $f_{\text{net}}^{\text{dry}}$ are valid for efficiencies based on the LHV as well as for those based on the HHV.
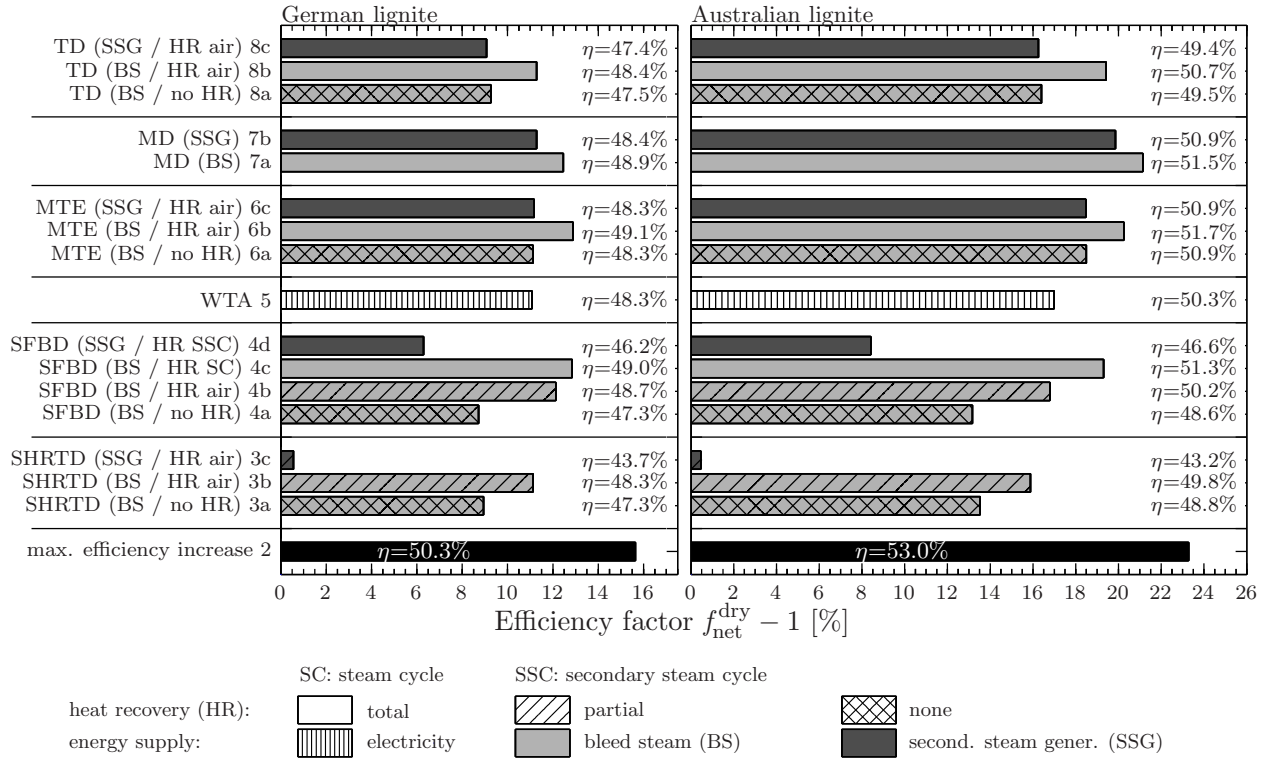
Figure 6.15:   Efficiency factor and overall efficiencies $\eta_{\mathrm{net}}^{\mathrm{dry}}$ (basis: $\eta_{\mathrm{net}}^{\mathrm{raw}}$=43.5 % for German coal and 43.0 % for Australian coal)

In the SHRTD and SFBD process more than 2.8 MJ/kg have to be supplied to the process, since not only the water is heated up and evaporated but also coal and air (SHRTD) have to be heated up. High efficiencies can only be reached if the exhaust vapour energy is completely recovered which is practically impossible for the air-vapour mixture leaving the SHRTD. Therefore at high water contents the full potential of efficiency increase can be realised only by dewatering processes with low specific energy demands.

For all concepts variations in the electrical self consumption of ± 10 kWs/kg or water contents of ± 1 wt.% lead to changes in the overall efficiency of about ∓ 0.1 percentage points. Therefore the uncertainty in some of the assumptions does not have a large effect on the results presented.
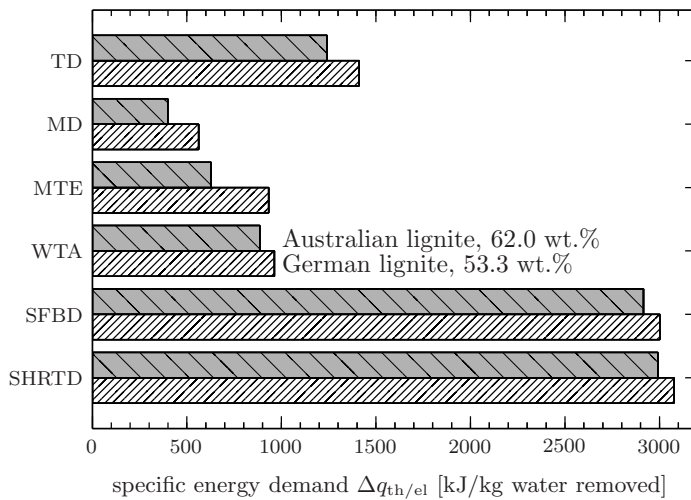
Figure 6.16:
Specific energy demand for water removal with the different drying technologies
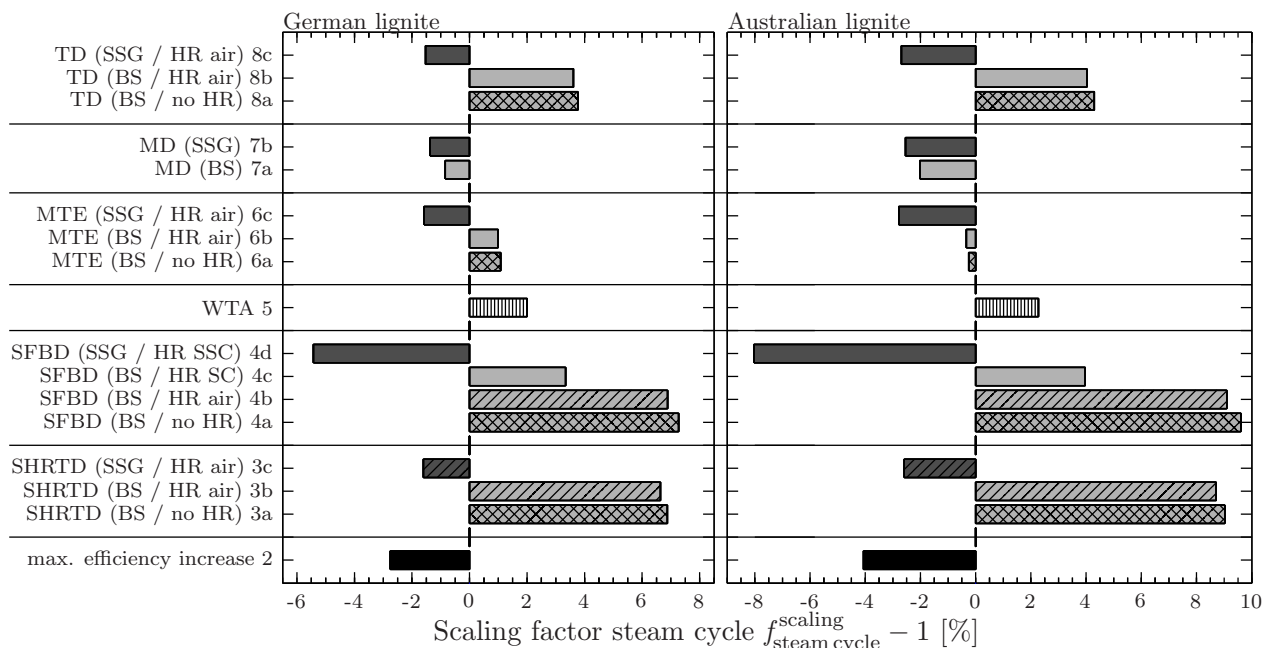
Figure 6.17: Scaling factor steam cycle
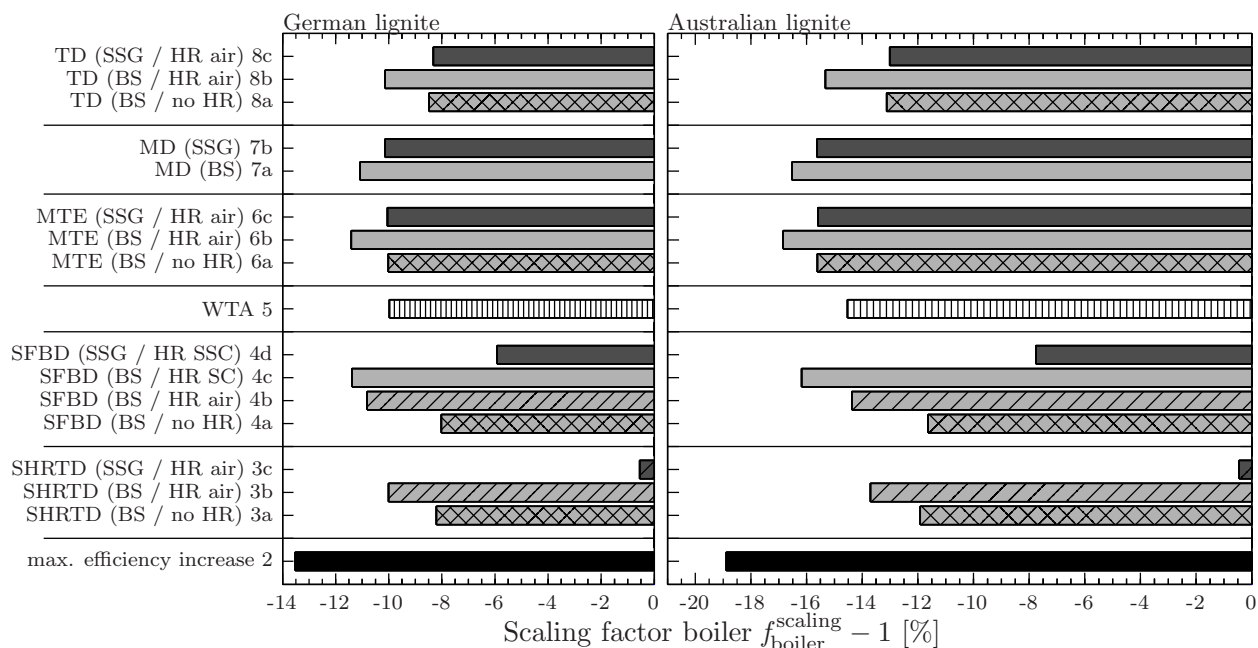
Figure 6.18: Scaling factor boiler

6.5 Power plant dimensions

In Figure 6.17 and Figure 6.18 the scaling factors $f_{\text{steam cycle}}^{\text{scaling}}$ and $f_{\text{boiler}}^{\text{scaling}}$ are given. For the processes using bleed steam or electricity and having high specific energy demands, the steam cycle throughput is increased by 4 to 10 % while it is about 2 % smaller for very efficient processes, which use steam produced in a secondary steam generator.

An exception is the SFBD with a secondary steam cycle (SSC). In this process the implementation of a secondary turbine for the recovery of the exhaust vapour energy leads to a larger decrease (up to 8 %) in the size of the main steam cycle. Nevertheless the decrease in the main boiler size for this concept is smaller than for most of the others, since the overall efficiency increase is smaller.

Table 6.3: Calculation results for German coal

process	concept	unit	raw 1	dry 2	SHRTD 3a	SHRTD 3b	SHRTD 3c	SFBD 4a	SFBD 4b	SFBD 4c	SFBD 4d	WTA 5	MTE 6a	MTE 6b	MTE 6c	MD 7a	MD 7b	TD 8a	TD 8b	TD 8c
water content	w	[wt.%]	53.3	12.0	12.0	12.0	12.0	12.0	12.0	12.0	12.0	12.0	22.0	22.0	22.0	22.0	22.0	22.0	22.0	22.0
water removed	Δm_water	[kg/kg$^\text{raw}$]		0.47	0.47	0.47	0.47	0.47	0.47	0.47	0.47	0.47	0.40	0.40	0.40	0.40	0.40	0.40	0.40	0.40
lower heating value	H_low^raw	[MJ/kg$^\text{dry}$]	9.20	19.50	19.50	19.50	19.50	19.50	19.50	19.50	19.50	19.50	17.01	17.01	17.01	17.01	17.01	17.01	17.01	17.01
lower heating value	H_low^raw	[MJ/kg$^\text{raw}$]	9.20	10.35	10.35	10.35	10.35	10.35	10.35	10.35	10.35	10.35	10.18	10.18	10.18	10.18	10.18	10.18	10.18	10.18
heat to steam cycle	$\dot{Q}_\text{th}$	[MW]	1078.4	1078.4	1078.4	1078.4	1078.4	1078.4	1078.4	1078.4	1078.4	1078.4	1078.4	1078.4	1078.4	1078.4	1078.4	1078.4	1078.4	1078.4
efficiency boiler	η_sg	[%]	89.7	92.0	92.0	92.0	92.0	92.0	92.0	92.0	92.0	92.0	91.7	91.7	91.7	91.7	91.7	91.7	91.7	91.7
efficiency factor boiler	$f_\text{th.sg}$	[−]	1.000	1.026	1.026	1.026	1.026	1.026	1.026	1.026	1.026	1.026	1.022	1.022	1.022	1.022	1.022	1.022	1.022	1.022
heat to boiler	$\dot{Q}_\text{th.sg}$	[MW]	1202.3	1172.2	1172.2	1172.2	1172.2	1172.2	1172.2	1172.2	1172.2	1172.2	1176.0	1176.0	1176.0	1176.0	1176.0	1176.0	1176.0	1176.0
heat to 2nd steam generator	$\dot{Q}^*_\text{th.fg}$	[MW]					190.6				182.6				38.2		16.6			63.6
heat to boiler (Σ)	$\dot{Q}_\text{th.sg}^\text{total}$	[MW]	1202.3	1172.2	1172.2	1172.2	1362.8	1172.2	1172.2	1172.2	1354.8	1172.2	1214.2	1176.0	1214.2	1176.0	1192.6	1176.0	1176.0	1239.7
thermal self consumption dryer																				
heat to dryer	$\Delta q^*_\text{th.fg}$	[kJ/kg$^\text{raw}$]					1362.0				1326.0				299.8	130.6				490.4
sensible heat coal	$\Delta q_\text{th.dry}$	[kJ/kg$^\text{raw}$]			46.0		46.0	46.0		46.0	46.0	46.0	59.7	59.7	59.7	60.4	60.4	60.1	60.1	60.1
heat to combustion air	$\Delta q_\text{th.air}$	[kJ/kg$^\text{raw}$]				190.8	190.8		297.3	297.3	297.3			153.8	153.8				176.5	176.5
heat to boiler (Σ)	$\Delta q_\text{th.sg}$	[kJ/kg$^\text{raw}$]			46.0	236.8	236.8	46.0	343.3	343.3	343.3	46.0	59.7	213.5	213.5	60.4	60.4	60.1	236.6	236.6
heat to preheater	$\Delta q_\text{th.ph}$	[kJ/kg$^\text{raw}$]			320.1	320.1		337.7	337.7	337.7		32.6	95.7	95.7		19.3		191.8	191.8	
heat to 2nd steam cycle	$\Delta q_\text{th.LP}$	[kJ/kg$^\text{raw}$]									1047.0									
mass flow raw coal	m_raw	[kg/s]	130.6	113.3	109.4	107.5	128.7	109.2	106.3	109.2	126.7	112.4	113.7	112.1	116.8	114.6	116.4	112.7	110.8	119.0
mass flow dry coal	m_dry	[kg/s]	130.6	60.1	58.1	57.0	68.3	58.0	56.4	58.0	67.2	59.7	68.1	67.1	69.9	68.6	69.7	67.5	66.4	71.2
efficiency factor dryer	$f_\text{th.dp}$	[−]	1.000	1.125	1.164	1.185	0.989	1.166	1.198	1.166	1.005	1.133	1.123	1.140	1.094	1.115	1.098	1.134	1.153	1.074
decrease in electricity output	$\Delta p^*_\text{el.MP}$	[kWs/kg$^\text{raw}$]			399.6	399.6		414.4	414.4	414.4			124.3	124.3		26.7		242.9	242.9	
increase in electricity output	$\Delta p^*_\text{el.LP}$	[kWs/kg$^\text{raw}$]								165.3	165.3									
decrease in electricity output	$P^*_\text{el.MP}$	[MW]			43.7	42.9		45.3	44.0	27.2	27.2		14.1	13.9		3.1		27.4	26.9	
electrical power output	$P_\text{el}^\text{gross dry}$	[MW]	550.0	550.0	506.3	507.1	550.0	504.7	506.0	522.8	550.0	550.0	535.9	536.1	550.0	546.9	550.0	522.6	523.1	550.0
efficiency steam cycle	$\eta_\text{el}^\text{dry}$	[%]	51.0	51.0	46.9	47.0	51.0	46.8	46.9	48.5	51.0	51.0	49.7	49.7	51.0	50.7	51.0	48.5	48.5	51.0
efficiency factor steam cycle	f_sc	[−]	1.000	1.000	0.920	0.922	1.000	0.918	0.920	0.951	1.000	1.000	0.974	0.975	1.000	0.994	1.000	0.950	0.951	1.000
electricity output 2nd steam cycle	$\Delta p_\text{el.dp}$	[kWs/kg$^\text{raw}$]									165.3									
electricity output 2nd steam cycle	$P_\text{el.dp}$	[MW]									20.9									
efficiency 2nd steam cycle	η	[%]									15.79									
electrical self consumption																				
raw coal treatment	$\Delta p_\text{el}^*/1$	[kWs/kg$^\text{raw}$]			10.0	10.0	10.0	10.0	10.0	10.0	10.0	10.0	6.0	6.0	6.0	6.0	6.0	6.0	6.0	6.0
dewatering/drying	$\Delta p_\text{el}^*/2$	[kWs/kg$^\text{raw}$]			10.0	10.0	10.0	12.1	12.1	12.1	12.1	192.1	10.0	10.0	10.0	20.0	20.0	10.0	10.0	10.0
dry coal treatment	$\Delta p_\text{el}^*/3$	[kWs/kg$^\text{raw}$]			16.0	16.0	16.0	16.0	16.0	16.0	16.0	16.0	20.0	20.0	20.0	20.0	20.0	20.0	20.0	20.0
dryer (Σ)	$\Delta p_\text{el.dp}^*$	[kWs/kg$^\text{raw}$]			36.0	36.0	36.0	38.1	38.1	38.1	38.1	218.1	36.0	36.0	36.0	46.0	46.0	36.0	36.0	36.0
dryer (Σ)		[MW]			3.9	3.9	4.6	4.2	4.0	4.2	4.8	24.5	4.1	4.0	4.2	5.3	5.4	4.1	4.0	4.3
electrical power output	$P_\text{el}^\text{after dp}$	[MW]	550.0	550.0	502.4	503.2	545.4	500.6	501.9	518.6	566.1	525.5	531.8	532.0	545.8	541.7	544.6	518.6	519.1	545.7
factor self consumption dryer	$f_\text{el.dp}$	[−]	1.000	1.000	0.992	0.992	0.992	0.992	0.992	0.992	1.029	0.955	0.992	0.993	0.992	0.990	0.990	0.992	0.992	0.992
power plant consumption	$\Delta p_\text{el.pp}^*$	[kWs/kg$^\text{raw}$]	210.5	230.7	234.9	236.9	214.5	235.1	238.2	235.1	216.6	231.6	229.8	231.6	226.6	228.9	226.3	231.0	233.0	224.3
power plant consumption	$P_\text{el.pp}^*$	[MW]	27.5	26.1	25.7	25.5	27.6	25.7	25.3	25.7	27.4	26.0	26.1	26.0	26.5	26.2	26.4	26.0	25.8	26.7
electrical power output	P_el^net	[MW]	522.5	523.9	476.7	477.7	517.7	474.9	476.6	493.0	538.7	499.5	505.6	506.1	519.3	515.4	518.2	492.5	493.3	519.0
factor self consumption power plant	$f_\text{el.pp}$	[−]	0.950	0.953	0.949	0.949	0.949	0.949	0.950	0.951	0.952	0.951	0.951	0.951	0.952	0.952	0.952	0.950	0.950	0.951
overall efficiency (LHV)	$\eta_\text{net}^\text{dry}$	[%]	43.46	50.26	47.34	48.30	43.70	47.25	48.73	49.04	46.19	48.28	48.30	49.06	48.32	48.87	48.36	47.49	48.36	47.40
overall efficiency (HHV)	$\eta_\text{net}^\text{dry}$	[%]	38.08	44.03	41.48	42.31	38.29	41.39	42.69	42.97	40.47	42.30	42.31	42.98	42.33	42.82	42.37	41.60	42.37	41.53
overall efficiency increase (LHV)	$\Delta\eta$	[Δ%]		6.80	3.88	4.84	0.24	3.79	5.27	5.59	2.73	4.82	4.84	5.60	4.86	5.41	4.90	4.03	4.90	3.94
overall efficiency increase	$f_\text{net.}-1^\text{dry}$	[%]		15.64	8.94	11.13	0.55	8.72	12.13	12.85	6.29	11.09	11.13	12.89	11.18	12.46	11.28	9.27	11.28	9.07
scaling factor steam cycle	$f^\text{scaling}_\text{steam cycle}-1$	[%]		−2.75	6.88	6.64	−1.61	7.27	6.89	3.34	−5.43	2.00	1.08	0.99	−1.58	−0.84	−1.37	3.77	3.61	−1.53
scaling factor boiler	$f^\text{scaling}_\text{boiler}-1$	[%]		−13.52	−8.21	−10.01	−0.55	−8.02	−10.82	−11.39	−5.92	−9.98	−10.02	−11.41	−10.05	−11.08	−10.14	−8.48	−10.14	−8.32

Table 6.4: Calculation results for Australian coal

process	concept	unit	raw	dry	SHRTD	SHRTD	SHRTD	SFBD	SFBD	SFBD	SFBD	WTA	MTE	MTE	MTE	MD	MD	TD	TD	TD
			1	2	3a	3b	3c	4a	4b	4c	4d	5	6a	6b	6c	7a	7b	8a	8b	8c
water content	w	[wt.%]	62.0	12.0	12.0	12.0	12.0	12.0	12.0	12.0	12.0	12.0	22.0	22.0	22.0	22.0	22.0	22.0	22.0	22.0
water removed	Δm_{water}	[kg/kg^{raw}]		0.57	0.57	0.57	0.57	0.57	0.57	0.57	0.57	0.57	0.51	0.51	0.51	0.51	0.51	0.51	0.51	0.51
lower heating value	H^{raw}_{low}	[MJ/kg^{raw}]	7.59	20.79	20.79	20.79	20.79	20.79	20.79	20.79	20.79	20.79	18.15	18.15	18.15	18.15	18.15	18.15	18.15	18.15
lower heating value	H^{dry}_{low}	[MJ/kg^{dry}]	7.59	8.98	8.98	8.98	8.98	8.98	8.98	8.98	8.98	8.98	8.84	8.84	8.84	8.84	8.84	8.84	8.84	8.84
heat to steam cycle	$\dot{Q}_{th}$	[MW]	1078.4	1078.4	1078.4	1078.4	1078.4	1078.4	1078.4	1078.4	1078.4	1078.4	1078.4	1078.4	1078.4	1078.4	1078.4	1078.4	1078.4	1078.4
efficiency boiler	η_{sg}	[%]	88.7	92.1	92.1	92.1	92.1	92.1	92.1	92.1	92.1	92.1	91.8	91.8	91.8	91.8	91.8	91.8	91.8	91.8
efficiency factor boiler	$f_{th.sg}$	[-]	1.000	1.038	1.038	1.038	1.038	1.038	1.038	1.038	1.038	1.038	1.035	1.035	1.035	1.035	1.035	1.035	1.035	1.035
heat to boiler	$\dot{Q}_{th.sg}$	[MW]	1215.8	1170.9	1170.9	1170.9	1170.9	1170.9	1170.9	1170.9	1170.9	1170.9	1174.8	1174.8	1174.8	1174.8	1174.8	1174.8	1174.8	1174.8
heat to 2nd steam generator	$\dot{Q}^*_{th.fg}$	[MW]					276.6				263.5				36.8		16.6			84.9
heat to boiler (Σ)	$\dot{Q}^{total}_{th.sg}$	[MW]	1215.8	1170.9	1170.9	1170.9	1447.5	1170.9	1170.9	1170.9	1434.5	1170.9	1174.8	1174.8	1211.6	1174.8	1191.4	1174.8	1174.8	1259.7
thermal self consumption dryer																				
heat to dryer	$\Delta q^*_{th.fg}$	[kJ/kg^{raw}]			474.1	474.1	1616.0	490.2	490.2	490.2	1569.0		104.3	104.3	251.7	23.3	114.1	279.2	279.2	563.6
sensible heat coal	$\Delta q_{th.dry}$	[kJ/kg^{raw}]			37.4	37.4	37.4	37.4	37.4	37.4	37.4	37.4	48.9	48.9	48.9	49.2	49.2	48.8	48.8	48.8
heat to combustion air	$\Delta q_{th.air}$	[kJ/kg^{raw}]			166.8	166.8	166.8	256.6	256.6	256.6	256.6		125.1	125.1	125.1			213.3	213.3	213.3
heat to boiler (Σ)	$\Delta q_{th.sg}$	[kJ/kg^{raw}]			204.3	204.3	204.3	294.0	294.0	294.0	294.0	37.4	174.0	174.0	174.0	49.2	49.2	262.1	262.1	262.1
heat to preheater	$\Delta q_{th.ph}$	[kJ/kg^{raw}]			379.8	379.8		399.5	399.5	399.5		67.2	80.3	80.3		16.9		220.4	220.4	
heat to 2nd steam cycle	$\Delta q_{th.LP}$	[kJ/kg^{raw}]									1267.0									
mass flow raw coal	m_{raw}	[kg/s]	160.2	130.4	124.6	122.4	157.6	124.4	121.1	124.4	154.7	128.9	130.9	129.1	134.4	131.8	134.0	128.9	126.0	138.3
mass flow dry coal	m_{dry}	[kg/s]	160.2	56.3	53.8	52.9	68.1	53.7	52.3	53.7	66.8	55.7	63.8	62.9	65.5	64.2	65.3	62.8	61.4	67.4
efficiency factor dryer	$f_{th.dp}$	[-]	1.000	1.183	1.238	1.260	0.979	1.240	1.274	1.240	0.997	1.196	1.182	1.198	1.152	1.174	1.155	1.200	1.228	1.119
decrease in electricity output	$\Delta p^*_{el.MP}$	[kWs/kg^{raw}]																		
increase in electricity output	$\Delta p^*_{el.LP}$	[kWs/kg^{raw}]																		
decrease in electricity output	$P^*_{el.MP}$	[MW]			59.1	58.0		61.0	59.3	36.1			13.7	13.5		3.1		36.0	35.2	
electrical power output	P^{gross}_{dry}	[MW]	550.0	550.0	490.9	492.0	550.0	489.0	490.7	513.9	550.0	550.0	536.3	536.5	550.0	546.9	550.0	514.0	514.8	550.0
efficiency steam cycle	η^{dry}_{el}	[%]	51.0	51.0	45.5	45.6	51.0	45.4	45.5	47.6	51.0	51.0	49.7	49.8	51.0	50.7	51.0	47.7	47.7	51.0
efficiency factor steam cycle	f_{sc}	[-]	1.000	1.000	0.893	0.894	1.000	0.889	0.892	0.934	1.000	1.000	0.975	0.976	1.000	0.994	1.000	0.935	0.936	1.000
electricity output 2nd steam cycle	$\Delta p^*_{el.dp}$	[kWs/kg^{raw}]									200.1									
electricity output 2nd steam cycle	$P_{el.dp}$	[MW]									31.0									
efficiency 2nd steam cycle	η	[%]									15.80									
electrical self consumption																				
raw coal treatment	$\Delta p^*_{el}/1$	[kWs/kg^{raw}]			10.0	10.0	10.0	10.0	10.0	10.0	10.0	10.0	6.0	6.0	6.0	6.0	6.0	6.0	6.0	6.0
dewatering/drying	$\Delta p^*_{el}/2$	[kWs/kg^{raw}]			10.0	10.0	10.0	14.6	14.6	14.6	14.6	227.1	10.0	10.0	10.0	20.0	20.0	10.0	10.0	10.0
dry coal treatment	$\Delta p^*_{el}/3$	[kWs/kg^{raw}]			16.0	16.0	16.0	16.0	16.0	16.0	16.0	16.0	20.0	20.0	20.0	20.0	20.0	20.0	20.0	20.0
dryer (Σ)	$\Delta p^*_{el.dp}$	[kWs/kg^{raw}]			36.0	36.0	36.0	40.6	40.6	40.6	40.6	253.1	36.0	36.0	36.0	46.0	46.0	36.0	36.0	36.0
dryer (Σ)	P^{net}_{el}	[MW]			4.5	4.4	5.7	5.0	4.9	5.0	6.3	32.6	4.7	4.6	4.8	6.1	6.2	4.6	4.5	5.0
electrical power output	$P^{after\,dp}_{el}$	[MW]	550.0	550.0	486.4	487.5	544.3	484.0	485.7	508.9	574.7	517.4	531.6	531.9	545.2	540.9	543.8	509.4	510.3	545.0
factor self consumption dryer	$f_{el.dp}$	[-]	1.000	1.000	0.991	0.991	0.990	0.990	0.990	0.990	1.045	0.941	0.991	0.991	0.991	0.989	0.989	0.991	0.991	0.991
power plant consumption	$\Delta p^*_{el.pp}$	[kWs/kg^{raw}]	171.7	195.5	199.7	201.3	176.0	199.9	202.3	199.9	178.0	196.6	194.8	196.1	192.3	194.1	192.5	196.2	198.4	189.4
power plant consumption	P^{net}_{el}	[MW]	27.5	25.5	24.9	24.6	27.7	24.9	24.5	24.9	27.5	25.3	25.5	25.3	25.8	25.6	25.8	25.3	25.0	26.2
electrical power output	P^{net}_{el}	[MW]	522.5	524.5	461.5	462.9	516.6	459.1	461.3	484.0	547.1	492.0	506.1	506.6	519.3	515.3	518.0	484.1	485.3	518.8
factor self consumption power plant	$f_{el.pp}$	[-]	0.950	0.954	0.949	0.950	0.949	0.949	0.950	0.951	0.952	0.951	0.952	0.952	0.953	0.953	0.953	0.950	0.951	0.952
overall efficiency (LHV)	η^{dry}_{net}	[%]	42.98	52.98	48.79	49.80	43.17	48.63	50.19	51.27	46.59	50.28	50.92	51.68	50.92	51.48	50.94	49.47	50.75	49.40
overall efficiency (HHV)	η^{dry}_{net}	[%]	35.83	44.17	40.68	41.52	35.99	40.55	41.84	42.75	38.84	41.92	42.46	43.09	42.45	42.92	42.47	41.24	42.31	41.19
overall efficiency increase (LHV)	$\Delta\eta$	[Δ%]		10.01	5.81	6.82	0.20	5.66	7.21	8.29	3.62	7.30	7.95	8.70	7.94	8.50	7.96	6.49	7.78	6.43
overall efficiency increase	$f^{dry}_{net}-1$	[%]		23.28	13.53	15.88	0.46	13.17	16.79	19.30	8.41	17.00	18.50	20.25	18.48	21.14	19.86	16.40	19.43	16.25
scaling factor steam cycle	$f^{scaling}_{steam\,cycle}-1$	[%]	-4.06		9.03	8.71	-2.59	9.60	9.10	3.97	-8.03	2.27	-0.25	-0.34	-2.79	-2.02	-2.55	4.29	4.03	-2.69
scaling factor boiler	$f^{scaling}_{boiler}-1$	[%]	-18.89		-11.91	-13.70	-0.45	-11.64	-14.38	-16.18	-7.76	-14.53	-15.61	-16.84	-15.60	-16.52	-15.63	-13.12	-15.32	-13.01

Accordingly the decrease in boiler size is high for the concepts with a high overall efficiency. Since both boiler and steam cycle contribute to a large proportion of the costs of the power station itself, the reduction in the size of these components can also compensate a bigger proportion of additional investment costs for the implementation of a drying or dewatering process [BSS04].

6.6   Concept for a dry lignite fired powerplant

From the dewatering and demineralisation results and the efficiency calculations it is obvious, that the implementation of a dewatering process like MTE into a power plant has many advantages, see Table 6.5. Reducing the water content prior to combustion leads to an increase of heating value and a decrease of CO_2 emissions resulting from a higher efficiency as described in the last section. Furthermore the water removal – which provides large mass flows of water for other applications – eases the process engineering for mills, burners and the boiler itself. The new technology resembles that of a black coal power plant and is much cheaper than conventional ones. Additional benefits result from the lowering of the fouling potential of the coal since alkali components are partially removed with the coal water. This way the furnace exit temperature can be increased slightly.

Table 6.5: Benefits of dry coal technology in lignite combustion

Reduction of the water content of raw lignite to about 20 to 25 wt.-% • Cleaned water available for other applications • Increase of the net heating value	⇒	Simplification of the firing system ('black coal system') • Hot gas coal drying no longer required • Beater wheel mills replaced by bowl mills
Partial removal of the alkali components of the coal with the water	⇒	Lowering of the fouling potential of the coal
Reduction of the mass-specific air and flue gas volume	⇒	• Significant reduction of the high pressure heating surfaces • Reduction of the stack loss • Increase of the boiler efficiency • Reduction of the power consumption of the plant (mills and fans)
⇓		⇓
Decrease of the CO_2 emissions to the same level as for black coal		Reduction of boiler cost

The most remarkable change is the reduction in the mass specific flue gas volume and flow rate (Figure 6.19) which leads to a smaller boiler size and a reduction in heat transfer surface. The self consumption of the boiler is also smaller due to the reduction of power consumption for fans and mills. Even though the boiler size can not be reduced in compliance with these values in consideration of the higher firing temperatures resulting from the increase in heating value, they give at least an idea of possible savings.

Concerning the physical properties of the coal further advantages for the power plant arise from the dewatering since the brown coal gets more similar to hard coal after the MTE treatment. This has remarkable consequences for the layout and operation of the firing systems and the boiler itself. Due to the reduced water content there is no necessity to use hot flue gas for coal drying, as it is needed for raw coal. For grinding the MTE coal bowl mills, as used for hard coal, can be utilised and burners and firing systems as for hard coal can be used.

In cooperation with Alstom Power Boiler, Stuttgart, and Dieffenbacher GmbH & Co. KG, Eppingen, a concept for the implementation of the MTE process in a power station process was developed. The scheme of the installation which takes into account all changes is shown in Figures 6.20 and 6.21. The power station has a capacity of 500 MW$_{el}$. Main components installed additionally for
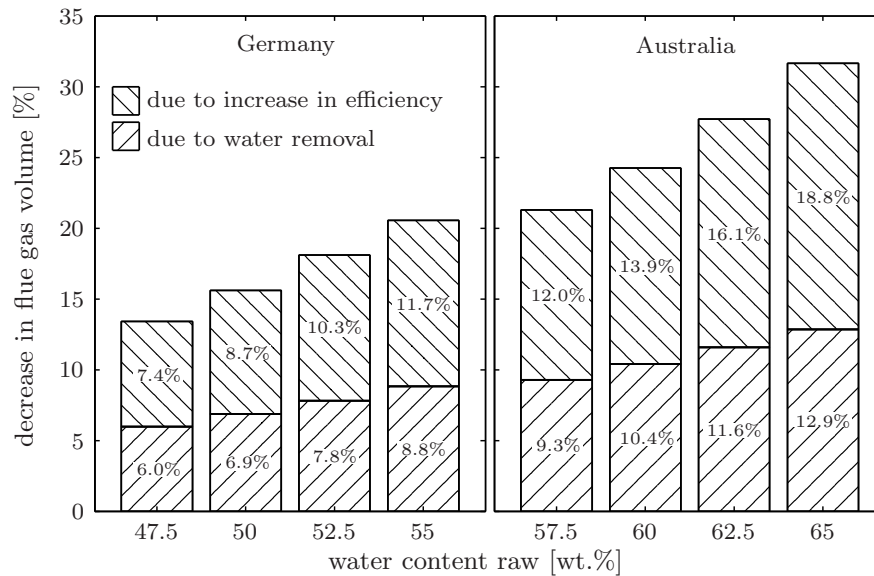
Figure 6.19:
Decrease in flue gas volume due to water removal and efficiency increase [BSS04]

the integration of the MTE-process are the machinery for the dewatering process (coal preparation and MTE press), the auxiliary steam generator for the MTE process steam and the additional air preheater for the utilisation of the flash steam (not shown).

The heating surfaces of the MTE steam generator are arranged between the economiser and the combustion air preheater of the boiler. Therefore there is no direct steam-sided connection between the power station process and the MTE steam generator. This is advantageous for the operation of the MTE plant and for the arrangement of the boiler heating surfaces. The separation of both steam cycles is also more economical since the requirements on the steam (and water) quality are
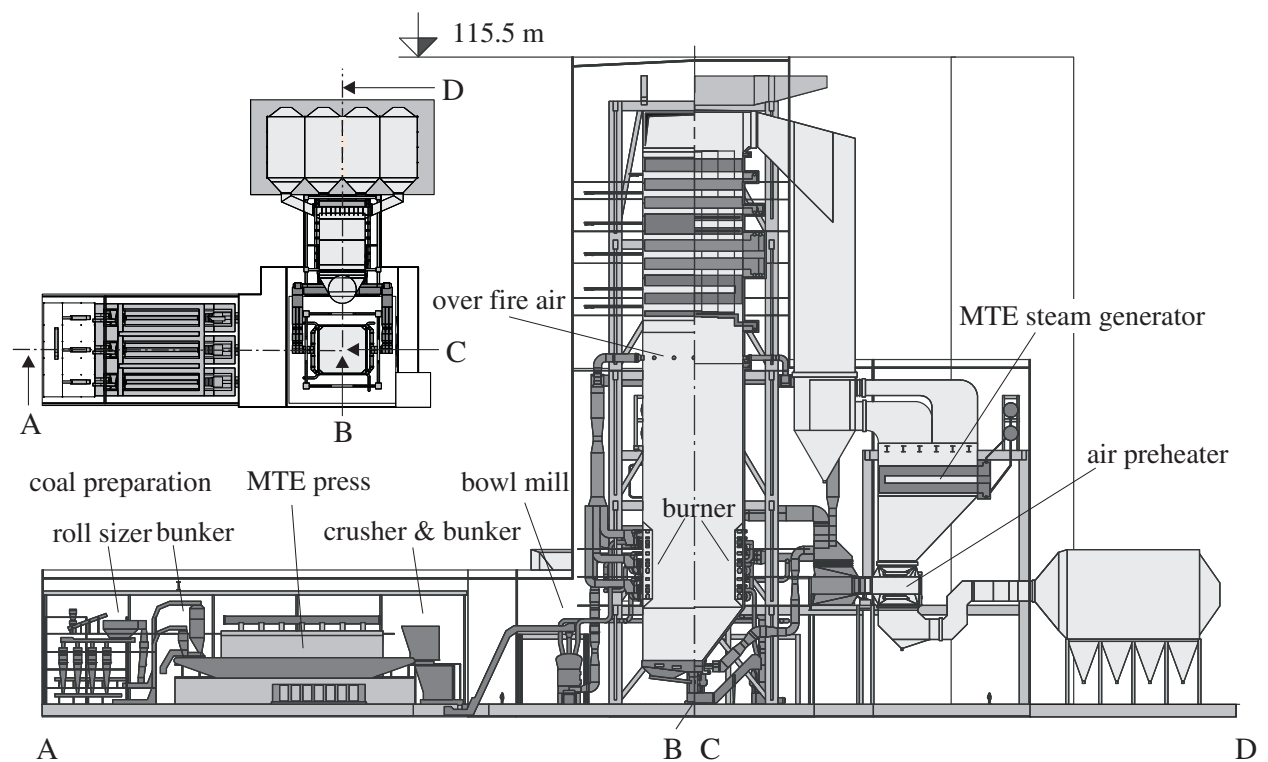
Figure 6.20: 500 MW$_{el}$ power station with MTE plant and dry lignite firing (Designed by Alstom Power Boiler) [BSS04]
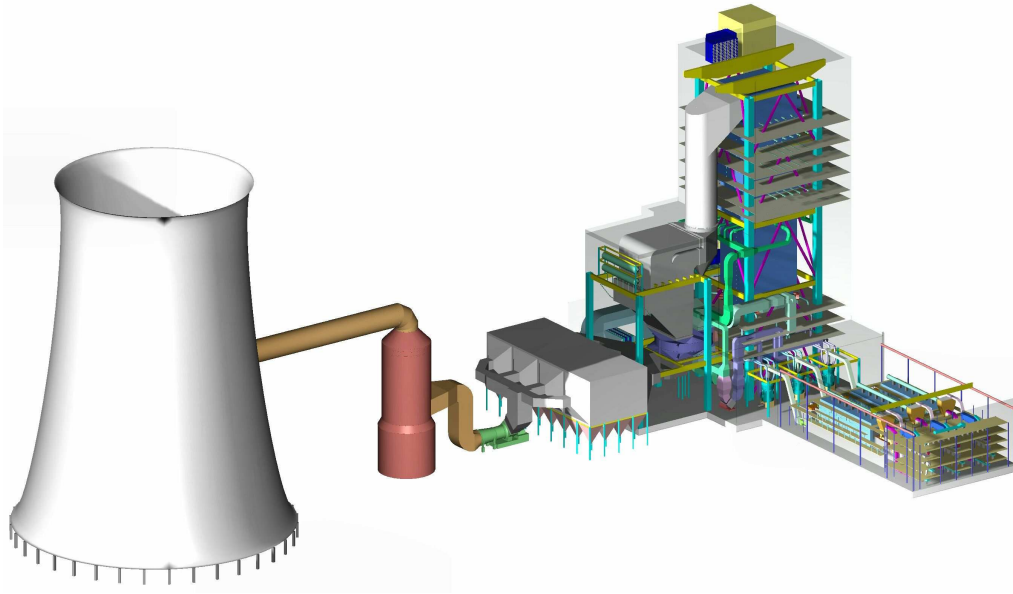
Figure 6.21: 500 MW$_{el}$ power station with MTE plant and dry lignite firing, 3D arrangement (Designed by Alstom Power Boiler)

much lower in the MTE process. The MTE steam generator is constructed as a buffer with pressure fluctuations between 3.7 and 4.3 MPa to equalise the energy demand of the three MTE process lines on the power station.

There are three MTE lines for the dewatering installed including a system of coal preparation utilities and bunkers. Since the permeability of the coal layer is of crucial importance for the uniformity of the heating with water and steam, roll sizers are installed for the separation of fine particles which later form the coal layer on the bottom of the transport belt. By this a so called gradient layer is formed which guarantees a homogeneous flow by increasing the fluid pressure loss during the progress of the heating front [Bie01, Cro03]. Each bunker contains the coal demand / output for 15 minutes and acts as interface between the batch dewatering process and the continuously working power station. Each MTE line provides the coal for one bowl mill which feeds one burner level. This is also the usual arrangement for hard coal fired power stations.

First calculations have proven, that the savings for reduced coal demand and self consumption and from the simplified firing system and boiler design compensate for the additional MTE cost. This way, the cost of an integrated MTE power station correspond approximately to the cost of a conventional, high efficiency power plant like the new BoA power station of RWE Energie in Niederaußem.

7 Summary

In the work at hand basic experimental results for the mechanical/thermal dewatering (MTE) during which lignites or other moisture containing materials are dewatered by the combined application of heat and mechanical forces have been presented. Models were developed for the description of the kinetics during the dewatering of different materials and physico-chemical properties of MTE products have been investigated. Efficiencies for power plant concepts with different drying and dewatering processes have been calculated and it has been proven, that the MTE process is a remarkable advance on the existing methods.

Dewatering kinetics Dewatering experiments for three different lignites from Germany, Greece and Australia have shown, that for all coals final water contents between 25 and 30 wt.% can be achieved at moderate pressures and temperatures. The dewatering kinetics depending on time, temperature and pressure can be described by a new model derived from soil-mechanical fundamentals, rheology and rate-process-theory (Chapter 3.2). Due to differences in lignite composition and behaviour during dewatering, the experimental determination of some model parameters is necessary for each coal.

Activation energies were determined from the dewatering experiments, which showed two consolidation phases, namely a primary and secondary consolidation ('creep') region. It can be deduced finally, that the drainage of water is the dominating process in these phases. While the water from larger capillaries and inter particle fractures is removed during primary consolidation, the water from small pores is expelled during the creep phase. The experiments also provide a clear distinction between the effect of the so-called 'thermal dewatering' due to heating of the lignite and the subsequent mechanical expression.

A rheological model was presented for the description of the dynamic behaviour of lignite during mechanical/thermal dewatering. The dewatering during the MTE-process is described depending on the technically relevant process parameters time, temperature, pressure, lignite permeability, creep velocity and the initial height of the coal filling in a press. Lignite permeability is expressed by the modified consolidation coefficient C_e, creep velocity by the coefficient of secondary consolidation C_α and the height of the coal filling is expressed as solid volume per unit sectional area ω_0.

The model was verified comparing the calculations with experimental data in a wide range of process parameters and it provides an excellent prediction of dewatering kinetics and water contents for the three lignites investigated. The same model was also applied successfully to the description of the dewatering of other carbonaceous materials. Due to the good agreement of experiments and model, the model and experimental procedure developed in this work are also applicable for the investigation of other coals and moist materials and for the technical process design. However, theoretical and experimental results also provide a deeper understanding of the consolidation process.

Additional experiments and calculations have been performed for a detailed analysis of the hydraulic pressure drop during the expression of water from lignite. It was found that the differences in geological history result in large variations of the lignite permeability and have remarkable influence on the duration of the primary consolidation. From the results it is also apparent, that at low temperatures the initial lignite height feasible in technical scale plants is limited by the increasing time for the completion of the primary consolidation. This limitation has to be considered especially for lignites with low preconsolidation pressures or during the mechanical/thermal dewatering of suspensions and sludges which form filter cakes with a low permeability. For such materials a different technology has been developed, which takes into account the specific requirements.

It was found from detailed analysis, that the best operating point for the MTE-process is near 200°C and 6 MPa. At higher temperatures the thermal decomposition increases, which would cause high additional cost in the plant engineering to prevent fouling of the filter medium and piping. Additionally the dry coal recovery from the process would decrease and increasing cost also would arise from higher pressures due to the required machinery.

Dry products In Chapter 3.3 it was investigated with mercury intrusion porosimetry (MIP) and other techniques as investigative tools, how MTE processing conditions, such as temperature and pressure, affect the *physical properties* pore size distribution and pore diameters, specific surface area, skeletal density, compressibility and shrinkage behaviour of the three low rank coals originating from Australia, Greece and Germany. Macro-, meso- and micropore volumes were determined from the MIP data and densities which were measured by helium pycnometry. Additionally, micropore volumes were calculated from the CO_2 adsorption experiments using the DUBININ-RADUSHKEVITCH equation.

It has been shown, that the mechanical/thermal dewatering produces coal products with a very low porosity, which undergo further *shrinkage* upon drying. The lowest total pore volumes measured are in the range of $0.1\,cm^3/g$, which appears to be a limiting pore volume for MTE products undergoing shrinkage during oven drying like also the dewatering is limited due to the resistance of the solid against compression.

All samples showed fairly constant mesopore volumes, as well as surface areas, at low MTE temperatures. However, values increased with increasing MTE temperature above 85°C, which is believed to be related to a hardening of the coal structure during thermal treatment, resulting in decreased shrinkage. The increase in mesopore volume for samples treated at higher temperatures also leads to higher compressibility values measured in the high pressure regime during MIP experiments. The reverse trend was seen with increasing MTE pressure, where the percentage shrinkage increased up to the limiting pore volume. This is believed to be caused by an increase in capillary forces, as the average pore diameter of the dried products was also found to decrease with increasing MTE pressure. Once the limiting pore volume had been reached, the percent shrinkage decreased again with increasing pressure and also temperature.

Due to the comprehensive analysis with different techniques, the results presented in this work provide a clear understanding, of how the MTE process affects coal (pore) structure and shrinkage on drying.

Upon *re-hydrating* the dry MTE products in a 100 % relative humidity environment, swelling was found to occur, where in some cases, the pore volume of the re-hydrated product exceeded the pore volume of the original wet MTE sample. Upon exposing the re-hydrated MTE products to ambient conditions (52 % relative humidity, determination of the 'equilibrium moisture content', EMC), a moisture loss was observed. However, at both relative humidities, the various processing conditions investigated had little effect on the moisture content. No relationship between the EMC and pore volume could be identified and for 100 % humidity only the MTE samples from tests with Greek lignite showed a slight decrease of moisture content with increasing severeness of MTE processing. The results therefore suggest, that the water uptake behaviour may be controlled by other factors, such as inorganic and mineral content, as well as the nature of surface functional groups. Comparing the three coals, an increase of the moisture contents at both humidities with increasing ash content of the coal was found.

The MTE process had little effect on the organic composition, although the volatile component of the Australian and Greek coals decreased while the fixed carbon content slightly increased with increasing temperature, suggesting the occurrence of thermal transformations.

The investigation of the *demineralisation* effect and the comparison of dewatering and leaching results showed, that the MTE process is also a powerful technique for the removal of alkali metals, as evidenced by significant reductions in the sodium and potassium content of the different fuels.

For the sodium concentration in lignites reductions of up to 70 % were obtained, depending on the process parameters temperature, dilution during leaching and on coal type. This reduces the problems of slagging and fouling in power plants.

During the combined leaching and dewatering of *wheat straw* (Chapter 4) up to 90 % of the water soluble potassium and also significant amounts of chloride were removed, thus proving, that the MTE process is also suitable for the biomass fuel upgrading to prevent corrosion and slagging.

The results were verified in experiments with other carbonaceous materials like peat and bark and also for different inorganic semi-solid materials and suspensions. In all cases a remarkable enhancement of the dewatering velocity and the total amount of water removable from these materials was found. From the results it is clear, that the MTE process allows an energy efficient dewatering and compaction, which is essential for both biomass fuel preparation and waste disposal. The apparent densities of the MTE products are comparable to those of commercial lignite briquettes or wood pellets.

Results from *thermal analysis* have shown, that the ignition behaviour of lignites is changed only slightly towards higher temperatures with increasing reduction of pore volume. Thus it can be stated, that no serious changes in combustibility have to expected when firing the MTE products in power plants. Concerning the risk of spontaneous combustion also only a slight enhancement is to be expected by the MTE processing. The change in 'ignition temperature', which was investigated qualitatively, depends on the decrease in pore volume, which is a function of coal type and processing conditions.

Process and plant technology Regarding the moderate temperatures and pressures which have to be applied, the equipment (Chapter 5) to carry out the process in technical scale is simplified in comparison to other methods and the cost of investment is reduced. This is the reason, why the development of process and plant engineering was supported by several German companies and could be done in the comparatively short time of 8 years (from laboratory scale to demonstration plant).

The process engineering, including heating with recycled hot water and steam, was developed and tested in technical scale at the University of Dortmund. After developing the plant technology, a pilot scale plant was constructed within the scope of the joint project promoted by the Federal Ministry of Education, Science, Research and Technology, involving the companies Dieffenbacher, RWE Energie and Rheinbraun, and the University of Dortmund. Testing was done on process-specific plant components designed to permit low-cost and reliable integration of the process into continuous power plant operations.

A further development step towards commercial implementation of the MTE process involved converting the discontinuous pilot press to quasi-continuous fully automatic operations with a throughput of approximately 1.6 metric tons dry brown coal per hour. Parallel to testing the MTE plant technology, Rheinbraun and RWE Energie investigated the feeding of the MTE press with coal in quasi-continuous operations, treatment of the raw brown coal and subsequent treatment of the dry brown coal produced. The various project phases provided evidence of the cost effectiveness and energy efficiency of dewatering brown coal using the MTE process.

After completion of this development RWE Energie ordered a MTE demonstration plant with an output of 15 tonnes of dry brown coal per hour, which was constructed at the Niederaußem power station and successfully went in operation at the end of 2001.

Technical scale implementation   In Chapter 6 the thermodynamic basics of different processes were analysed and described. It has been shown, that for lignite fired power plants overall efficiencies above 50 % (based on the lower heating value) are feasible based on available technologies, which provides a reduction in fuel and CO_2 emission of about 10-20 %, depending on the local quality of the raw coal. For the technical realisation of such projects the existing demonstration plants for the competing processes have to prove their operational availability. Steam fluidised bed drying with and without heat recovery (SFBD/WTA) and MTE process seem to have the greatest potential, since these technologies are farthest advanced in technological development and internal heat recovery. However, the processes show great differences in the requirements of power station design concerning the dimensions of important components like boiler and steam cycle since they differ in the heat and electricity demands and interconnection of heat flows between power station and coal preparation process.

Due to the specific process design presented in Chapter 6, the MTE process can be implemented in power station concepts energetically optimised without large energy flows being interconneted to the power station itself. Moreover the electrical self consumption is very low and from the demineralisation effect additional operational benefits arise. These features are advantageous concerning operational and economical reasons and unique characteristics of the MTE process compared to all other processes.

A   Nomenclature

Latin letters

Symbol	Quantity	Definition	Unit
a	coefficient of compressibility	$a = -\partial e / \partial p_\mathrm{s}$	$\mathrm{Pa^{-1}}$
A	cross-sectional area		$\mathrm{m^2}$
A	specific surface area		$\mathrm{m^2 kg^{-1}}$
$A^{(n)}$	compressibility constant		$\mathrm{Pa^{-1}}$
A_p	compressibility constant		$\mathrm{Pa^{-1}}$
B	constant		$\mathrm{Pa^{-1} s^{-1}}$
c_v	modified consolidation coefficient	$c_v = C_\mathrm{e} H^2 \omega_0^{-2}$	$\mathrm{m^2 s^{-1}}$
c	concentration		$\mathrm{kg\,kg^{-1}}$
C	constant		$-$
$C^{(n)}$	'dashpot constant', creep constant		$\mathrm{Pa^{-1} s^{-1}}$
C_α	creep coefficient	$C_\alpha = -\partial e / \partial \log(t)$	$-$
C_C	coefficient of consolidation	$C_\mathrm{C} = -\partial e / \partial \log(p_\mathrm{s})$	$-$
C_e	modified consolidation coefficient	$C_\mathrm{e} = K(\mu\,a\,(1+e))^{-1}$	$\mathrm{m^2 s^{-1}}$
d	(pore) diameter		m
D	(pellet) diameter		m
D	effective diffusion coefficient		$\mathrm{m^2 s^{-1}}$
e	void ratio	$e = W\,\varrho_\mathrm{s}\,\varrho_\ell^{-1} = \varepsilon(1-\varepsilon)^{-1}$	$-$
E	energy		$\mathrm{J\,mol^{-1}}$
F	force		N
f	function, (efficiency) factor		$-$
G	free enthalpy		$\mathrm{J\,mol^{-1}}$
h	PLANCK-constant		$\mathrm{J\,s}$
H	height		m
H_low	lower heating value		$\mathrm{J\,kg^{-1}}$
i	number of drainage surfaces (1,2)		$-$
i	index variable		$-$
k	BOLTZMANN-constant		$\mathrm{J\,K^{-1}}$
K	permeability		$\mathrm{m^2}$
ℓ	loading		$\mathrm{kg\,m^{-2}}$
L	lenght		m
m	mass		kg
n	index variable		$-$
N	AVOGADRO-constant		$\mathrm{mol^{-1}}$
p	pressure		Pa
p_s^∞	total consolidation pressure		Pa
p_0	preconsolidation pressure		Pa
p_C'	apparent preconsolidation pressure		Pa
p	specific work		$\mathrm{W\,s\,kg^{-1}}$
P	power output		W

Latin letters (continued)

Symbol	Quantity	Definition	Unit
q	specific heat		$\mathrm{J\,kg^{-1}}$
r	radius		m
R	mercury retention	$R = \frac{(V_{7\mu\mathrm{m}}^{\mathrm{extrusion}} - V_{7\mu\mathrm{m}}^{\mathrm{intrusion}})}{(V_{0.0036\mu\mathrm{m}}^{\mathrm{intrusion}} - V_{7\mu\mathrm{m}}^{\mathrm{intrusion}})}$	$-$
Q	heat		J
R	universal gas constant		$\mathrm{J\,mol^{-1}\,K^{-1}}$
t	time		s
T	temperature		K
u	velocity (pore velocity)		$\mathrm{m\,s^{-1}}$
u_D	DARCY-velocity	$u_\mathrm{D} = u\,\varepsilon$	$\mathrm{m\,s^{-1}}$
v	specific volume		$\mathrm{m^3 kg^{-1}}$
v	velocity of the conveyor belt		$\mathrm{m\,s^{-1}}$
V	volume		$\mathrm{m^3}$
w	water content (wet basis)	$w = m_\ell/(m_\ell + m_\mathrm{s})$	$-$
w	specific work		$\mathrm{W\,s\,kg^{-1}}$
w_press	width of the MTE press		m
W	water content (dry basis)	$W = m_\ell/m_\mathrm{s}$	$-$
W_0	limiting micro pore volume	$W_\mathrm{a} = W_0 \exp\left[-\left(\frac{R\,T}{\beta\,E_0}\right)^2 \left(\frac{p_0}{p}\right)^2\right]$	$\mathrm{m^3}$
x	length scale		m
x	steam saturation		$-$
$<x>$	time-, volumetric-mean value of x		$[x]$
$\bar{x}$	time-mean value x		$[x]$
$\dot{x}$	derivative of x with respect to time		$[x]\,\mathrm{s^{-1}}$

Greek letters

Symbol	Quantity	Definition	Unit
α	constant		$-$
β	affinity coefficient		$-$
Δ	difference		
ε	porosity	$\varepsilon = (V_\ell + V_\mathrm{i})/(V_\ell + V_\mathrm{i} + V_\mathrm{s})$	$-$
η	efficiency		$-$
κ	compressibility		$\mathrm{Pa^{-1}}$
λ	length		m
μ	dynamic viscosity		$\mathrm{Pa\,s}$
ν	kinematic viscosity		$\mathrm{m^2\,s^{-1}}$
φ	humidity		$-$
ϱ	density		$\mathrm{kg\,m^{-3}}$
σ	surface tension		$\mathrm{N\,m^{-1}}$
τ	shear stress		Pa
τ	time constant		s
Θ	normalised time, time factor	$\Theta = C_e\,i^2\,t\,\omega_0^{-2}$	$-$
Θ	contact angle		rad
ω_0	solid volume per unit sectional area	$\omega_0 = V_\mathrm{s}/A$	m

Subscripts and Superscripts

Symbol	Meaning
0	starting or reference value
a	adsorbed
C	consolidation
D	DARCY
diff	from difference
dp	drying process
dry	correlated to the dry coal
el	electrical
eop	end of primary
evap	evaporation
exp	experimental
f	filtration
fg	flue gas
fc	filter cake
g	geological (pressure)
g	generator
He	determined by helium pycnometry
i	inert gas, air
ℓ	liquid
K	potassium
LP	low pressure turbine
mech	mechanical
M	molar
MP	medium pressure turbine
Na	sodium
pc	precompression
ph	preheater
pp	power plant
raw	correlated to the raw coal
s	solid
sc	steam cycle
sg	steam generator
sp	suspension
th	thermal
v	vapour
w	water
∞	final value
*	reference value (dewatering)
*	demand (energy flows)

Abbreviations and Acronyms

AAS	atomic absorption spectrophotometry
BS	bleed steam
BoA	Braunkohlenkraftwerk mit optimierter Anlagentechnik
	(lignite fired power plant with optimised technology)
BOD_5	biological oxygen demand
COD	chemical oxygen demand
daf	dry and ash free basis
db	dry basis
DTA	differential thermal analysis
DWT	Dampf-Wirbelschicht Trocknung
EMC	equilibrium moisture content
HHV	higher heating value
HLA	Hambach low ash
HR	heat recovery
HTD	hydro-thermal dewatering
HWD	hot water drying
lhs	left hand side
LDI	logarithmic differential intrusion
LHV	lower heating value
LYLA	Loy Yang low ash
MD	mechanical dewatering
MIP	mercury intrusion porosimetry
MTE	Mechanisch/Thermische Entwässerung *(mechanical/thermal dewatering)*
	mechanical/thermal expression
PT	Ptolemais
rhs	right hand side
RPT	rate process theory
SC	steam cycle
SFBD	steam fluidised bed dryer
SHRTD	steam heated rotary tube dryer
SSC	secondary steam cycle
SSG	secondary steam generator
S.T.P.	standard temperature and pressure
tph	metric tons per hour
TD	thermal dewatering
TGA	thermogravimetric analysis
wb	wet basis
wt	weight
WTA	Wirbelschicht-Trocknung mit interner Abwärmenutzung
	(steam fluidised bed dryer with internal heat recovery)

Bibliography

[AA95]   D. J. Allardice and F. Anderson, B. Woskoboenko, *Developments and opportunities in the hydrothermal dewatering of low rank coals*, 5th Japan/Australian Joint Technical Meeting on Coal, Adelaide, 7 June 1995.

[AC04]   Y. Artanto and A. Chaffee, *Upgrading of low rank coals by mechanical thermal expression (MTE)*, 21st Annual Pittsburgh Coal Conference, Osaka, Japan, 2004.

[AE71a]   D. J. Allardice and D. G. Evans, *The brown-coal/water system: Part 1. The effect of temperature on the evolution of water from brown coal*, Fuel **50** (1971) 201–210.

[AE71b]   D. J. Allardice and D. G. Evans, *The brown-coal/water system: Part 2. Water sorption isotherms on bed moist Yallorn brown coal*, Fuel **50** (1971) 236–253.

[All91]   D. J. Allardice, *The water in brown coal*, Chapter 3, 103–150, In R. A. Durie [Dur91], 1991.

[Alv99]   Alvermann, G. and Luther, G. and Niemeyer, B. (Editor), *Kontaminierte Schlämme- Behandlung und Nutzungsmöglichkeiten feinkörniger Reststoffe*, GKSS Forschungszentrum, Geesthacht, 1999.

[AM73]   O. B. Andersland and J. P. Mathew, *Consolidation of high ash papermill sludges*, Journal of the Soil Mechanics and Foundations Division, ASCE **99** (1973) SM5, 365–374.

[Ana82]   A. G. Anagnostopoulos, *Compressibility behaviour of soft lignite*, Journal of the Geotechnical Engineering Division, ASCE **108** (1982) GT12, 1549–1566.

[ARA+04]   A. Arenillas, F. Rubiera, B. Arias, J. J. Pis, J. M. Faúndez, A. L. Gordon and X. A. García, *A TG/DTA study on the effect of coal blending on ignition behaviour*, Journal of Thermal Analysis and Calorimetry **76** (2004) 603–614.

[AS200]   *Methods for the analysis and testing of lower rank coal and its chars. Part 9. Determination of four acid-extractable inorganic ions in lower rank coal*, Australian Standard AS 2434.9, Standards Australia Committee MN/1, 2000.

[ASJ42a]   G. Agde, H. Schürenberg and R. Jodl, *Untersuchung über die Wasserbindungsverhältnisse, Bauform und Größe von Huminsäure-Kolloidteilchen*, Braunkohle **41** (1942) 545–547.

[ASJ42b]   G. Agde, H. Schürenberg and R. Jodl, *Untersuchungen über die Kolloidstruktur der erdigen Braunkohlen*, Braunkohle **41** (1942) 5/6, 5–48, 65–69.

[ASM95]   G. Amarasekera, M. J. Scarlett and D. E. Mainwaring, *Micropore size distributions and specific interactions in coals*, Fuel **74** (1995) 1, 115–118.

[AY01]   D. J. Allardice and B. C. Young, *Utilisation of low rank coals*, Proceedings of the 18th Annual Pittsburgh Coal Conference, Newcastle, Australia (December 2001).

[Bar68]   L. Barden, *Primary and secondary consolidation of clay and peat*, Géotechnique **18** (1968) 1, 1–24.

[BB84]   J. P. Banks and D. R. Burton, *Behaviour of brown coal in press dewatering*, Procceedings of Australian Coal Science Conference, Churchill, 1984, 199–206.

[BB89]   P. J. Banks and D. R. Burton, *Press dewatering of brown coal: Part 1: Exploratory studies*, Drying Technology **7** (1989) 3, 443–475.

[BBS98]   C. Bergins, S. Berger and K. Strauß, *Process technology for mechanical/thermal dewatering*, Aufbereitungs Technik – Mineral Processing **39** (1998) 2, 58–70.

[BBS+99]   S. Berger, C. Bergins, K. Strauß, F. B. Bielfeldt, R. O. Elsen and M. Erken, *Mechanical/Thermal Dewatering of brown coal*, VGB PowerTech **79** (1999) 2, 44–49.

[BCBS99]   C. Bergins, S. Crone, S. Berger and K. Strauß, *Mechanisch/Thermische Entwässerung von feuchten Schüttgütern und Schlämmen*, 147–161, In Alvermann, G. and Luther, G. and Niemeyer, B. [Alv99], 1999.

[BCOB00]   A. M. Bailey, A. D. Cohen, W. H. Orem and J. Blackson, *Mobilization of major inorganic ions during experimental diagenesis of characterized peats*, Chemical Geology **166** (2000) 287–300.

[BCS05]   C. Bergins, S. Crone and K. Strauß, *Multiphase flow in homogeneous porous media with phase change. Part II: Analytical solutions and experimental verification for constant pressure steam injection*, Transport in porous media **60** (2005) 3, 275–300.

[Ber01]   C. Bergins, *Mechanismen und Kinetik der Mechanisch/Thermischen Entwässerung von Braunkohle*, Dissertation, Universität Dortmund, Shaker, Aachen, 2001.

[Ber02]   S. Berger, *Entwicklung und technische Umsetzung der Mechanisch/Thermischen Entwässerung zum Einsatz als Vortrocknungsstufe in braunkohlegefeuerten Kraftwerken*, Dissertation, Universität Dortmund, Shaker, Aachen, 2002.

[Ber03]   C. Bergins, *Kinetics and mechanism during mechanical/thermal dewatering of lignite*, Fuel **82** (2003) 4, 355–364.

[Ber04]   C. Bergins, *Mechanical/thermal dewatering of lignite. Part 2: A rheological model for consolidation and creep process*, Fuel **83** (2004) 3, 267–276.

[BF46]   D. H. Bangham and R. E. Franklin, *Thermal expansion of coals and carbonised coals*, Transactions of the Faraday Society **42B** (1946) 289–295.

[BH55]   J. K. Brown and P. B. Hirsch, *Recent infra-red and X-ray studies of coal*, Nature **175** (1955) 229–233.

[Böh02]   M. Böhlmann, *Braunkohle - organisches Kolloid mit komplexem anorganischen Inventar*, Dissertation, Universität Dortmund, Shaker, Aachen, 2002.

[BHSC]   C. Bergins, J. Hulston, K. Strauss and A. L. Chaffee, *Mechanical/thermal dewatering of lignite. Part 3: Physical properties and pore structure of MTE product coals*, to be submitted to Fuel.

[Bie97]   F. B. Bielfeldt, *Anlage und Filterpresse zur Entfeuchtung von pastösen Feststoffen*, Patent DE 197 52 653 A1, 1997.

[Bie01]   F. B. Bielfeldt, *Verfahren und Anlage zur Reduzierung des in Faserzellen kapillar gebundenen Wassers*, Patent DE 100 16 944 A1, 2001.

[BJW00]   G. D. Bongers, W. R. Jackson and F. Woskoboenko, *Pressurised steam drying of Australian low-rank coals: Part 2. Shrinkage and physical properties of steam dried coals, preparation of dried coals with very high porosity*, Fuel Processing Technology **64** (2000) 1–3, 13–23.

[BKK92]   D. Böcker, K. J. Klöcker and H. J. Klutz, *Verfahren zur Trocknung und Mahlung von Braunkohle*, BWK **44** (1992) 7/8,.

[BP72]   P. L. Berry and T. J. Poskitt, *The consolidation of peat*, Géotechnique **22** (1972) 1, 27–52.

[BP97]   M. Blander and A. D. Pelton, *The inorganic chemistry of the combustion of wheat straw*, Biomass and Bioenergy **12** (1997) 4, 295–298.

[BS52]   N. Berkowitz and H. G. Schein, *Some aspects of the ultrafine structure of lignite*, Fuel **31** (1952) 19–32.

[BSS04]   C. Bergins, K. Strauß and J. Sigg, *Beneficial effects of the combination of mechanical/thermal dewatering and dry lignite fired power stations*, VGB Power Tech **84** (2004) 1/2, 60–65.

[Bui36]   A. S. K. Buisman, *Results of long duration settlement tests*, Proceedings of the first International Conference on Soil Mechanics and Foundation Engineering, 1, 1936, 103–106.

[Cas36]   A. Casagrande, *The determination of the pre-consolidation load and its practical significance*, Proceedings of the first International Conference on Soil Mechanics and Foundation Engineering, 3, 1936, 60–64.

[CB97]   A. D. Cohen and A. M. Baily, *Petrographic changes induced by artificial coalification of peat: comparison of two planar facies (Rhizophora and Cladium) from the Everglades-mangrove complex of Florida and a domed facies (Cyrilla) from the Okefenokee Swamp of Georgia*, International Journal of Coal Geology **34** (1997) 163–194.

[CB02]   S. Crone and C. Bergins, *Multiphase flow in homogeneous porous media with phase change. Part I: Numerical model*, Transport in porous media **49** (2002) 3, 291–312.

[CD81]   D. A. Cadenhead and J. F. Danielli (Editor), *Progress in surface and membrane science*, 14, Academic Press, New York, 1981.

[CFJ00]   A. L. Chaffee, G. Favas and W. R. Jackson, *Drying technologies for more efficient power generation from low rank coal: Comparison of products from various processes*, Proceedings of the 17th Annual Pittsburgh Coal Conference (2000).

[CH60]   L. Cartz and P. B. Hirsch, *A contribution to the structure of coals from x-ray diffraction studies*, Philosophical Transactions of the Royal Society of London **A252** (1960) 557–602.

[CMP96]   Y. Chen, S. Mori and W. P. Pan, *Studying the mechanisms of ignition of coal particles by tg-dta*, Thermochimica Acta **275** (1996) 149–158.

[Cro03]   S. Crone, *Nicht-isotherme mehrphasige Mehrkomponentenströmungen mit Phasenwechsel in porösen Medien*, Dissertation, Universität Dortmund, Shaker, Aachen, 2003.

[CS78a]   R. J. Carmier and S. R. Siemon, *Colloidal structure of Victorian brown coals. 1. Alkaline digestion of brown coals*, Fuel **57** (1978) 85–88.

[CS78b]   R. J. Carmier and S. R. Siemon, *Colloidal structure of Victorian brown coals. 2. Rod-shaped particles in brown coals*, Fuel **57** (1978) 693–696.

[DA92]   D. J. Dunne and J. B. Agnew, *Thermal upgrading of low-grade, low-rank South Australia coal*, Energy Sources **14** (1992) 169–181.

[Dar56]   H. P. G. Darcy, *Les fontaines publiques de la ville Dijon: exposition et application des principes a suivre et des formules a employer dans les questions de distribution d'eau; ouvrage terminé par un appendice relatif aux fournitures d'eau de plusieurs villes au filtrage des eaux et a la fabrication des tuyaux de fonte, de plomb, de tôle et de bitume*, Victor Dalmont, Paris, 1856.

[DC81]   B. V. Derjaguin and N. V. Churaev, *Structure of the boundary layers of liquids and its influence on the mass transfer in fine pores*, 69–130, In D. A. Cadenhead and J. F. Danielli [CD81], 1981.

[Dem03]   A. Demirbaş, *Demineralization of agriculture residues by water leaching*, Energy Sources **25** (2003) 679–687.

[DIN94]   *Abnahmeversuche an Dampferzeugern (VDI-Dampferzeugerregeln)*, DIN 1942, 1994.

[DIN01]   *Mikroporenanalyse mittels Gasadsorption, Teil3: Bestimmung des Mikroporenvolumens nach Dubinin und Radushkewich*, DIN 66135-3, Normenausschuß Bauwesen, Deutsches Institut für Normung, Juni 2001.

[DIN02]   *Prüfung fester Brennstoffe - Bestimmung des Wassergehaltes und der Analysenfeuchtigkeit*, DIN 51718, Normenausschuß Materialprüfung, Deutsches Institut für Normung, Juni 2002.

[Dub66]   M. M. Dubinin, *Porous structure and adsorption properties of active carbons*, 51–120, In P. L. Walker Jr. [Wal66], 2nd Ed., 1966.

[Dul54]   J. A. Dulhunty, *Geological factors in the metamorphic development of coal*, Fuel **33** (1954) 145–152.

[Dul60]   J. A. Dulhunty, *Experiments in physical metamorphism of brown coals*, Fuel **39** (1960) 115–162.

[Dur91]   R. A. Durie (Editor), *The science of Victorian brown coal: Structure, properties and consequences for utilization*, Butterworth-Heinemann Ltd, Oxford, 1991.

[EBWE96] R. O. Elsen, U. Blumenthal, W. Wick and J. Ewers, *Wirkungsgradverbesserung neuer Brankohlekraftwerke durch vorgeschaltete Trocknung*, VDI–Berichte **1280** (1996) 149–164.

[ES70]   D. G. Evans and S. R. Siemon, *Dewatering of brown coal before combustion*, Journal of the Institute of Fuel **43** (1970) 413–419.

[Eva73a] D. G. Evans, *The brown coal/water system: 4. Shrinkage on drying*, Fuel **52** (1973) 186–190.

[Eva73b] D. G. Evans, *Effects of colloidal structure on physical measurements on coals*, Fuel **52** (1973) 155–156.

[Eyr36]   H. Eyring, *Viscosity, plasticity and diffusion as examples of absolute reaction rates*, Journal of Chemical Physics **4** (1936) 283–291.

[Fav00]   G. Favas, *Hydrothermal dewatering - evaluation of a non-evaporative drying technology for the lignite power industry*, Ph.D thesis, Monash University, 2000.

[FCMJ04] Y. Fei, A. Chaffee, M. Marshall and W. R. Jackson, *Lignite water characterisation by phase transition – differential scanning calorimetry*, 21$^{\text{st}}$ Annual Pittsburgh Coal Conference, Osaka, Japan, 2004.

[FG92]   A. Filippidis and A. Georgakopoulos, *Mineralogical and chemical investigation of fly ash from the main and northern lignite fields in Ptolemais, Greece*, Fuel **71** (1992) 4, 373–376.

[FJ03]   G. Favas and W. R. Jackson, *Hydrothermal dewatering of lower rank coals. 2. Effects of coal characteristics for a range of Australian and international coals*, Fuel **82** (2003) 59–69.

[FJM03]   G. Favas, W. R. Jackson and M. Marshall, *Hydrothermal dewatering of lower rank coals. 3. High-concentration slurries from hydrothermally treated lower rank coals*, Fuel **82** (2003) 1, 71–79.

[Fle26]   H. Fleissner, *Die Trocknung stückiger Braunkohle*, Berg– und Hüttenmännisches Jahrbuch **74** (1926) 3, 104–109.

[FLW87]   J. Fohl, W. Lugscheider and F. Wallner, *Entfernung von Wasser aus der Braunkohle: Teil 1: Grundlagen der Trocknungsverfahren*, Braunkohle **39** (1987) 3, 45–57.

[FLWT87] J. Fohl, W. Lugscheider, F. Wallner and G. Tessmer, *Entfernung von Wasser aus der Braunkohle: Teil 2: Thermische Entwässerungsverfahren*, Braunkohle **39** (1987) 4, 78–87.

[FM88]   W. Friesen and R. Mikula, *Mercury porosimetry of coals: Pore volume distribution and compressibility*, Fuel **67** (1988) 1516–1520.

[FMTS85] J. Fohl, F. Mayer, G. Tessmer and D. Seidl, *Verfahren zur kontinuierlichen Trocknung von wasserreicher Feinbraunkohle auf der Basis der Sattdampfbehandlung*, TIZ–Fachberichte **109** (1985) 493.

[Fra49]   R. E. Franklin, *A study on the fine structure of carbonaceous solids by measurements of true and apparent densities: Part I. Coals*, Trans Faraday Soc **45** (1949) 274–286.

[FT67]   S. Fujii and H. Tsuboi, *Helium densities and related properties of Japanese coal*, Fuel **46** (1967) 361–366.

[GA71]   D. C. Green and M. I. E. Aust, *Aspects of consolidation of Morwell brown coal*, Proceedings of the 1st ANZ Conference on Geomechanics, Melbourne, August 1971, 119–126.

[GLE41]   S. Glasstone, K. J. Laidler and H. Eyring, *The theory of rate processes*, McGraw-Hill, New York, 1941.

[GM79]   J. Godwin and S. E. Manahan, *Interchange of metals and organic matter between water and subbituminous coal or lignite under simulated coal slurry pipeline conditions*, Environmental Science & Technology **13** (1979) 9, 1100–1104.

[GNWJ72] H. Gan, S. P. Nandi and P. L. Walker Jr, *Nature of the porosity in American coals*, Fuel **51** (1972) 272–277.

[GTU99]   J. Guo, C. Tiu and P. H. T. Uhlherr, *Modelling of mechanical-thermal expression of brown coal*, 9th Japan/Australia Joint Technical Meeting on Coal, Melbourne, June 1999.

[GTU03]   J. Guo, C. Tiu and P. H. T. Uhlherr, *Modelling of hydrothermal-mechanical expression of brown coal*, The Canadian Journal of Chemical Engineering **81** (2003) 94–102.

[Guo00]   J. Guo, *Hydrothermal-mechanical dewatering of brown coal*, Ph.D thesis, Department of Chemical Engineering, Monash University, Melbourne, 2000.

[Guy02]   P. J. Guy, *The solvent-induced swelling behaviour of victorian brown coals*, Master of applied science, Swinburne University of Technology, 2002.

[HB97]   W. Hlubek and D. Böcker, *Entwicklungslinien der Braunkohle-Kraftwerkstechnik*, Energiewirtschaftliche Tagesfragen **47** (1997) 9, 512–519.

[HBCS]   J. Hulston, C. Bergins, A. L. Chaffee and K. Strauß, *Mechanical/thermal dewatering of lignite. Part 4: Physico-chemical properties of MTE product coals*, to be submitted to Fuel.

[HBCS04] J. Hulston, C. Bergins, A. L. Chaffee and K. Strauß, *Comparison of physico-chemical properties for various lignites treated by mechanical thermal expression*, Proceedings of the 21st Pittsburgh Coal Conference (2004).

[HBCS05] J. Hulston, C. Bergins, A. L. Chaffee and K. Strauß, *Comparison of physico-chemical properties of various lignites treated by mechanical thermal expression*, Coal Preparation, accepted (2005).

[HF90]   P. Herber and J. Fohl, *Neue Kohletrocknungsanlage, System Fleißner der REIK Kolubara*, Braunkohle **42** (1990) 5, 16–21.

[HFC]   J. Hulston, G. Favas and A. L. Chaffee, *Physico-chemical properties of Loy Yang lignite dewatered by mechanical thermal expression*, submitted to Fuel.

[Hir54]   P. B. Hirsch, *X-ray scattering from coals*, Proceedings of the Royal Society of London / A, A226, 1954, 143–196.

[HK99]   R. J. Heitmüller and A. Kather, *Wärme- und feuerungstechnisches Konzept des Dampferzeugers für den BoA-Block Niederaußem K*, VGB KraftwerktsTechnik **79** (1999) 2, 75–82.

[HKKW96] R. Heitmüller, D. Kallmeyer, K. Kückelhaus and W. Wick, *Neue Braunkohleblöcke mit hohem Wirkungsgrad bei RWE Energie AG*, VDI–Berichte **1280** (1996) 77–90.

[HM87]   K. J. Hüttinger and A. W. Michenfelder, *Ein Molekülmodell rheinischer Braunkohle*, Erdöl und Kohle, Erdgas, Petrochemie, Brennstoff–Chemie **40** (1987) 4, 166–171.

[Hua96]   W. L. Huang, *Experimental study of vitrinte maturation: effect of temperature, time, pressure, water, and hydrogen index*, Organic Geochemistry **24** (1996) 2, 233–241.

[JBW96]   B. M. Jenkins, R. R. Bakker and J. B. Wei, *On the properties of washed straw*, Biomass and Bioenergy **10** (1996) 4, 177–200.

[JMT85]   A. Janusch, F. W. Mayer and G. Tessmer, *Trocknungsanlage für wasserreiche Braunkohlen*, Patent EP 0 155 927 A2, 1985.

[JSDJ01]   P. A. Jensen, B. Sander and K. Dam-Johansen, *Removal of K and Cl by leaching of straw char*, Biomass and Bioenergy **20** (2001) 447–457.

[KH96]   H. J. Klutz and M. Holzenkamp, *Verfahren und Anlagen zur Braunkohletrocknung*, VDI–Berichte **1280** (1996) 91–105.

[KJSDJ98]   N. O. Knudson, P. A. Jensen, B. Sander and K. Dam-Johansen, *Possibilities and evaluation of straw pretreatment*, Biomass for Energy and Industry, Proc. of the 10th European Conference and Technology Exhibition, 8.-10. June 1998, Würzburg, 1998, 224–228.

[KKL94]   H. J. Klutz, K. J. Klöcker and J. Lambertz, *Die Rheinbraun-WTA-Trocknungstechnik - Entwicklung und erste Betriebsergebnisse der WTA-Demonstrationsanlage*, Braunkohle (1994) 6, 4–11.

[KKP04]   J. Kučerík, J. Kovář and M. Pekař, *Thermoanalytical investigation of lignite humic acids fractions*, Journal of Thermal Analysis and Calorimetry **76** (2004) 55–65.

[Klo94]   J. Kloubek, *Investigation of porous structures using mercury reintrusion and retention*, Journal of Colloid and Interface Science **163** (1994) 10–18.

[Klu88]   H. J. Klutz, *Verfahren und Anlage zum Trocknen von Rohbraunkohle in einem Wirbelbett-Trockner*, Patent EP 0 273 406 A2, 1988.

[KN78]   H. Krug and W. Naundorf, *Zum Phänomen der Entstehung fester Braunkohlenbriketts, Teil 1: Theoretische Betrachtungen*, Neue Bergbautechnik **8** (1978) 11, 647–653.

[KPK94]   M. Kavvadas, B. Papadopoulos and N. Kalteziotis, *Geotechnical properties of the Ptolemais lignite*, Geotechnical and Geological Engineering **12** (1994) 87–112.

[KS66]   J. Kravtchenko and P. M. Sirieys (Editor), *Rheology and soil mechanics: International union of theoretical and applied mechanics: Symposium Grenoble 1964*, Springer Verlag, 1966.

[Ler96]   S. Leroueil, *Compressibility of clays: Fundamental and practical aspects*, Journal of Geotechnical Engineering, ASCE **122** (1996) 7, 534–543.

[LG52]   A. Lissner and W. Göbel, *Bestimmung des Alkaligehaltes in Salzkohlen*, Schriftenreihe des Verlags Technik Berlin, 4, 82–89, 1952.

[LHOB03]   H. J. v. d. Linden, S. Herber, W. Olthuis and P. Bergveld, *Stimulus-sensitive hydrogels and their applications in chemical (micro)analysis*, The Analyst **128** (2003) 325–331.

[Low61]   P. F. Low, *Physical chemistry of clay-water interaction*, Advances in Agronomy **13** (1961) 296–327.

[LW79a]   T. W. Lambe and R. V. Whitman, *Soil mechanics, SI version*, John Wiley & Sons Inc., New York, 1979.

[LW79b]   L. J. Lynch and D. S. Webster, *An n.m.r. study of the water associated with brown coal*, Fuel **58** (1979) 429–432.

[LW82]   L. J. Lynch and D. S. Webster, *Effect of thermal treatment on the interaction of brown coal and water: a nuclear magnetic resonance study*, Fuel **61** (1982) 271–275.

[Mah84]   O. P. Mahajan, *Physical characterization of coal*, Powder Technology **40** (1984) 1–15.

[Mah91]   O. P. Mahajan, *CO_2 surface area of coals: The 25-year paradox*, Carbon **29** (1991) 6, 735–742.

[McK83]   D. W. McKee, *Mechanisms of the alkali metal catalysed gasification of carbon*, Fuel **62** (1983) 2, 170–175.

[MCS68]   J. K. Mitchell, R. G. Campanella and A. Singh, *Soil creep as a rate process*, Journal of the Soil Mechanics and Foundations Division, ASCE **94** (1968) SM1, 231–253.

[ME72]   J. B. Murray and D. G. Evans, *The brown-coal/water system: Part 3. Thermal dewatering of brown coal*, Fuel **51** (1972) 290–296.

[Mes73]   G. Mesri, *Coefficient of secondary compression*, Journal of the Soil Mechanics and Foundations Division, ASCE **99** (1973) SM1, 123–137.

[MH03]   M. McIntosh and D. Huynh, *Coal dewatering system and method*, Patent WO 03/018716 A1, 6.3. 2003.

[MIB+89]   T. Murase, M. Iwata, P. J. Banks, N. Hayashi and M. Shirato, *Press dewatering of brown coal: Part 2: Batch and continuous-screw operations*, Drying Technology **7** (1989) 4, 697–721.

[MMA+02]   K. Miura, K. Mae, R. Ashida, T. Tamura and T. Ihara, *Dewatering of coal through solvent extraction*, Fuel **81** (2002) 1417–1422.

[MS65]   H. Marsh and T. Siemieniewska, *The surface areas of coal as evaluated from the adsorption isotherms of carbon dioxide using the Dubinin-Polanyi equation*, Fuel **44** (1965) 355–367.

[MSAC97]   G. Mesri, T. D. Stark, M. A. Ajlouni and C. S. Chen, *Secondary compression of peat with or without surcharging*, Journal of Geotechnical and Geoenvironmental Engineering, ASCE **123** (1997) 5, 411–421.

[NFK84]   S. H. Ng, D. P. C. Fung and S. D. Kim, *Some physical properties of Canadian coals and their effects on coal reactivity*, Fuel **63** (1984) 1564–1569.

[NJ56]   K. Neumann and H. Jacob, *Drucksetzungsversuche mit Weichbraunkohlen*, Zeitschrift für angewandte Geologie (1956) 7, 307–322.

[NKH+97]   K. Norinaga, H. Kumagai, J. I. Hayashi, T. Chiba and M. Sasaki, *Type of water associated with coal*, Reprints of papers presented at the American Chemical Society / Division of Fuel Chemistry, 42, 1997, 238–243.

[NLN+98]   C. Nielsen, M. G. Larsen, V. Nielsen, U. Zielke, J. K. Kristensen and B. Holm-Christensen, *Straw for Energy Production, Technology - Environment - Economy*, Trøjborg Bogtryk, ISBN 87-90074-20-3, 1998.

[NMW80]   J. R. Nelson, O. P. Mahajan and P. L. Walker, *Measurement of swelling of coal in organic liquids: a new approach*, Fuel **59** (1980) 831–837.

[NNBM04]   H. Nakagawa, A. Namba, M. Böhlmann and K. Miura, *Hydrothermal dewatering of brown coal and catalytic hydrothermal gasification of the organic compounds dissolving in the water using a novel Ni/carbon catalyst*, Fuel **83** (2004) 719–725.

[NNK77]   R. C. Neavel, N. C. Nashas and K. K. Koh, *Removal od sodium from Illinois coal by water extraction*, Transactions of the Society of Mining Engineers of AIME **262** (1977) 263–267.

[OM92]   O. I. Ogunsola and R. J. Mikula, *Effect of thermal upgrading on spontaneous combustion characteristics of western Canadian low rank coals*, Fuel **71** (1992) 3–8.

[ONG+97]   J. I. Ozaki, Y. Nishiyama, P. J. Guy, G. J. Perry and D. J. Allardice, *Role of carboxyl groups in the disintegration of brown coal briquettes by water sorption*, Fuel Processing Technology **50** (1997) 57–68.

[ONLC96]   W. H. Orem, S. G. Neuzil, H. E. Lerch and C. B. Cecil, *Experimental early-stage coalification of a peat sample and a peatified wood sample from indonesia*, Org. Geochem. **24** (1996) 2, 111–125.

[Pan88]   W. P. Pan, *Effect of calcium chloride and calcium acetate on the reactivity of a lignite coal at low heating rate*, Thermochimica Acta **125** (1988) 285–294.

[Pfl99]   M. Pflugbeil, *BoA-Niederaußem - der 950-MW-Braunkohlekraftwerksblock mit optimierter Anlagentechnik*, VDI–Berichte **1456** (1999) 133–142.

[Pot81]   O. E. Potter, *Drying solid materials*, Patent US 4 295 281, 1981.

[PTF93]   W. P. Pan, J. Timmons and A. A. F., *Applications of thermal analysis in the physical chemistry laboratory*, Transactions of the Kentucky Academy of Science **54** (1993) 1/2, 7–12.

[Qi04]   Y. Qi, *Characterisation of organic and inorganic components in process water from a novel lignite dewatering process*, Ph.d thesis, Monash University, 2004.

[QL01]   Y. Qi and C. A. L., *Effects of processing conditions on the nature of product water from a novel coal drying process*, 6th World Congress on Chemical Engineering, Melbourne, Australia, 2001.

[QR87]   K. B. Quast and D. J. Readett, *The surface chemistry of low rank coals*, Advances in Colloid and Interface Science **27** (1987) 169–187.

[Rea89]   Q. K. B. Readett D. J., *Benefication of Bowmans lignite: Water leaching of soluble salts*, Proceedings of CHEMECA 87 'Technology for our Third Century', Broadbeach, 13 d, 23rd-25th August 1989, 459–463.

[Ros29]   P. Rosin, *Die Fleißner-Trocknung lignitischer Braunkohlen*, Braunkohle **28** (1929) 648–658.

[Ros63]   K. J. Rosengren, *Consolidation of some Victorian brown coals*, Proceedings of the Australasian Institute of Mining and Metallurgy **208** (1963) 157–193.

[RQ88]   D. Readett and K. Quast, *Mechanical dewatering of South Australian brown coals: Applications in inorganics characterisation*, Procceedings of the Australian Coal Science Conference 3, Adelaide, Nr. A2, 1988, 3.1–3.8.

[RQFK87]   D. J. Readett, K. B. Quast, H. S. F. and I. B. Ketterige, *Mechanical benefictaion of Bowmans brown coal*, Proceedings of CHEMECA 87, Melbourne, 1987, 89–147.

[RQMK84]   D. J. Readett, K. B. Quast, D. E. Mulcahy and I. B. Ketteridge, *Modelling the leaching of NaCl from Bowmans lignite*, Symposium on 'Extractive Metallurgy', The Aus.I.M.M. Melbourne Branch, November 1984, 103–109.

[RRP93]   T. C. Roth, J. T. Riley and W. P. Pan, *The effect of limestone on the combustion of fuel blends*, Journal of Thermal Analysis **40** (1993) 249–255.

[SAE74]   P. D. Swann, D. J. Allardice and D. G. Evans, *Low temperature oxidation of brown coal. 1. Changes in internal surface due to oxidation*, Fuel **53** (1974) 85–87.

[SB99]   K. Strauß and C. Bergins, *Aufbereitung von Reststoffen und Biomasse mit dem MTE-Verfahren zur energetisch effizienten Verwertung in Energieanlagen*, VDI–Berichte **1495** (1999) 581–592.

[SBB⁺96]   K. Strauß, S. Berger, C. Bergins, F. B. Bielfeldt, M. Erken and M. Hoffmann, *Mechanisch/Thermische Entwässerung als Vortrocknungsstufe für braunkohlegefeuerte Kraftwerke*, VDI–Berichte **1280** (1996) 165–173.

[SBB97]   K. Strauß, S. Berger and C. Bergins, *Mechanisch/Thermische Entwässerung von Rohbraunkohle*, Abschlußbericht Forschungsprojekt BEO 0327031, Laufzeit: 01.10.1995-31.09.1996, Universitätsbibliothek und TIB Hannover, 1997.

[SBB99]   K. Strauß, S. Berger and C. Bergins, *Mechanisch/Thermische Entwässerung von Rohbraunkohle*, Abschlußbericht Forschungsprojekt BEO 0327031a, Laufzeit: 01.08.1997-31.12.1998, Universitätsbibliothek und TIB Hannover, 1999.

[SBB01]   K. Strauß, C. Bergins and M. Böhlmann, *Beneficial effects of the integration of a MTE plant into a brown coal fired power station*, Proceedings of the VGB/EPRI conference 'Lignites and Low Rank Coals: Operational and Environmental Issues in a Competitive Climate', 2001, 213–223.

[Sch74]   A. E. Scheidegger, *The physics of flow through porous media*, 3. Ed., University of Toronto Press, Toronto, 1974.

[Sch00]   G. E. Schaumann, *Water uptake and swelling behaviour of soil organic matter (SOM)*, Mitteilungen der Deutschen Bodenkundlichen Gesellschaft **92** (2000) 25–28.

[SDK54]   J. Schuyer, H. Dijkstra and D. W. van Krevelen, *Chemical structure and properties of coal VII - Elastic constants*, Fuel **33** (1954) 409–418.

[SDY95]   E. M. Suuberg, S. C. Deevi and Y. Yun, *Elastic behaviour of coals studied by mercury porosimetry*, Fuel **74** (1995) 10, 1522–1530.

[SE67]   R. Stewart and D. G. Evans, *The bonding of water to brown coal*, Fuel **46** (1967) 263–274.

[SHH⁺94]   D. Shao, E. J. Hutchinson, J. Heidbrink, W. P. Pan and C. L. Chou, *Behavior of sulfur during coal pyrolysis*, Journal of Analytical and Applied Pyrolysis **30** (1994) 91–100.

[SHL⁺00]   B. Sander, N. Henriksen, O. H. Larsen, A. Skriver, C. Ramsgaard-Nielsen, K. Jensen, J. N. Stærkind, H. Livbjerg, M. Thellefsen, K. Dam-Johansen, F. Frandsen, R. van der Lans and J. Hansen, *Emissions, corrosion and alkali chemistry in straw fired combined heat and power plants*, Proceedings of the 1st World Conference on Biomass for Energy and Industry, 5-9 June 2000, Sevilla, 2000.

[SLC66]   R. L. Schiffman, C. C. Ladd and A. T. F. Chen, *The secondary consolidation of clay*, Chapter 3.2, 273–304, In J. Kravtchenko and P. M. Sirieys [KS66], 1966.

[SMI86]   M. Shirato, T. Murase and M. Iwata, *Deliquoring by expression - theory and practice*, 181–287, In R. J. Wakeman [Wak86], 1986.

[SMIN86]   M. Shirato, T. Murase, M. Iwata and S. Nakatsuka, *The Terzaghi-Voigt combined model for constant-pressure consolidation of filter cakes and homogeneous semi-solid materials*, Chemical Engineering Science **41** (1986) 12, 3213–3218.

[Smo93]   D. Smoot, *Fundamentals of coal combustion for clean and efficient use*, Coal Science and Technology, 20, Elsevier, Amsterdam, 1993.

[Spi81]   Z. Spitzer, *Mercury porosimetry and its application to the analysis of coal pore structure*, Powder Technology **29** (1981) 1, 177–186.

[SS99]   T. Saus and H. W. Schiffer, *Braunkohle in Europa*, Rheinbraun Aktiengesellschaft, Köln, 1999.

[ST96]   J. Schmalfeld and C. Twigger, *Erfahrungen mit dem Betrieb der Dampf-Wirbelschicht-Trockungsanlage Loy Yang, Australien*, VDI–Berichte **1280** (1996) 107–117.

[Str94]   K. Strauß, *Verfahren und Vorrichtung zur Reduzierung des Wassergehaltes von kohlenstoffhaltigen Feststoffmaterialien*, Patent DE 44 34 447 A1, 1994.

[Str96a]   K. Strauß, *Method and device for reducing the water content of water-containing brown coal*, Patent EP 0 784 660 B1; WO 96/10064, 1996.

[Str96b]   K. Strauß, *Verfahren zur Erzeugung von Heißdampf zum Betreiben eines Dampfkraftwerkes - Process for generating superheated steam for operating a steam power plant*, Patentschrift DE 196 06 153 A1; PCT/EP97/00740; WO 97/31222, 1996 1996.

[Str96c]   K. Strauss, *Verfahren zur Reduzierung des Wassergehaltes von wasserhaltiger Braunkohle*, Patent DE 196 27 626 A1, 1996.

[Str97]   K. Strauss, *Verfahren zur kombinierten Mechanisch-/Thermischen Entfeuchtung von pastösen Feststoffen, Schlämmen und Suspensionen*, Patent DE 197 52 017 A1, 1997.

[Süße99]   W. Süße, *Verfahren zum Trocknen gemahlener Roh-Braunkohle und Einrichtung zur Durchführung des Verfahrens*, Patent DE 197 35 233 A1, 1999.

[Ter25]   K. Terzaghi, *Erdbaumechanik auf bodenphysikalischer Grundlage*, Deutike, Wien, 1925.

[THT+72]   Y. Toda, M. Hatami, S. Toyada, Y. Yoshida and H. Honda, *Fine structure of carbonized coals*, Carbon **8** (1972) 565–571.

[TK94]   I. Towhata and P. Kuntiwattanakul, *Behavior of clays undergoing elevated temperature*, 13. International Conference on Soil Mechanics and Foundation Engineering, New Delhi, January 1994, 85–88.

[TKI97]   S. Q. Turn, C. M. Kinoshita and D. M. Ishimura, *Removal of inorganic constituents of boimass feedstocks by mechanical dewatering and leaching*, Biomass and Bioenergy **12** (1997) 4, 241–252.

[Toda72]   Y. Toda, *Densities of coals measured with various liquids*, Fuel **51** (1972) 3, 108–112.

[TP61]   K. Terzaghi and R. B. Peck, *Die Bodenmechanik in der Baupraxis*, Springer-Verlag, Berlin, 1961.

[TSL03]   D. N. Thompson, P. G. Shaw and J. A. Lacey, *Post-harvest processing methods for reduction of silica and alkali metals in wheat straw*, Applied Biochemistry and Biotechnology **105–108** (2003) 205–218.

[TT72]   Y. Toda and S. Toyoda, *Application of mercury porosimetry to coal*, Fuel **51** (1972) 3, 199–201.

[TT02]   M. Teichmüller and R. Teichmüller, *The chemical and structural metamorphosis of coals*, International Journal of Earth Science **91** (2002) 75–99.

[TTJ+04]   A. Thygesen, M. H. Thomsen, H. Jørgensen, B. H. Christensen and A. B. Thomsen, *Hydrothermal treatment of wheat straw on pilot plant scale*, Proceedings of the 2nd World Conference and Technology Exhibition on Biomass for Energy, Industry and Climate Protection, Rome, Italy, 2004.

[Val00]   T. Valmari, *Potassium behaviour during combustion of wood in circulating fluidised bed power plants*, Technical Research Center of Finland (VTT), ISBN 951-38-5569-4, Vuorimiehentie, 2000.

[Vel95]   B. Velde, *Composition and mineralogy of clay minerals*, Origin and mineralogy of clays (B. Velde, Editor), Springer-Verlag, New York, 1995, 8–42.

[Wah62]   H. Wahls, *Analysis of primary and secondary consolidation*, Journal of the Soil Mechanics and Foundations Division, ASCE **88** (1962) SM6, 207–231.

[Wak86]   R. J. Wakeman (Editor), *Progress in filtration and separation*, 4, Elsevier, Amsterdam, 1986.

[Wal66]   P. L. Walker Jr. (Editor), *Chemistry and physics of carbon*, 2nd Ed., Marcel Dekker, New York, 1966.

[WBS04]   T. Wild, C. Bergins and K. Strauß, *Demineralisierung von Braunkohle in Kombination mit der mechanisch/thermischen Entwässerung*, Chemie Ingenieur Technik **76** (2004) 11, 1715–1720.

[WCD$^+$00] W. Wagner, J. R. Cooper, A. Dittmann, J. Kijima, H. J. Kretschmar, A. Kruse, R. Mareš, K. Oguchi, H. Sato, I. Stöcker, O. Šifner, Y. Takaishi, Y. Tanishita, J. Trübenbach and T. Willkommen, *The IAPWS Industrial Formulation 1997 for the thermodynamic properties of water and steam*, Transactions of the ASME **122** (2000) 150–182.

[WF90]   T. Wahl and B. Franke, *Zum Wärmeverbrauch bei der Braunkohletrocknung*, Braunkohle **42** (1990) 30–34.

[Wild]   T. Wild, *Demineralisierung und Mechanisch/Thermische Entwässerung von Braunkohle und Biobrennstoffen*, Dissertation, Universität Dortmund, to be submitted.

[Wir52]   G. Wirth, *Zur Trocknung der Braunkohle (Die Trocknung von Rohbraunkohle nach dem Viag- und Fleißner-Verfahren)*, Allgemeine Wärmetechnik **3** (1952) 8/9, 191–201.

[WKH91]   H. J. Weiss, H. J. Klutz and C. J. Hamilton, *Trocknung von Braunkohle in der Dampf-Wirbelschicht*, VGB–Kraftwerkstechnik **71** (1991) 7, 664–668.

[WMJ83]   B. Wolf, B. Müller and T. Jannasch, *Thermodynamische Analyse der Verfahren zur Braunkohletrocknung*, Energieanwendung **32** (1983) 5, 181–187.

[WO97]   P. Webb and C. Orr (Editor), *Analytical methods in fine particle technology*, Micromeritics Instrument Corporation, Norcross, USA, 1997.

[WQCS02]   T. Wild, Y. Qi, A. Chaffee and K. Strauß, *Analysis of organic and inorganic contents in product water from a novel low-rank coal dewatering process*, Proceedings of the 19th Annual International Pittsburgh Coal Conference (2002) 23–26.

[XLXZ99]   L. Xu, C. Liu, X. Xian and D. Zhang, *Compressibility of coal matter and coal pore*, Colloids and Surfaces A: Physicochemical and Engineering Aspects **157** (1999) 219—222.

[YC90]   R. S. Yost and D. E. Creasy, *Shrinkage, swelling and true density of Mowell brown coal*, Fuel **69** (1990) 648–650.

[ZK54]   P. Zwittering and D. W. van Krevelen, *Chemical structure and properties of coal IV-Pore structure*, Fuel **33** (1954) 3, 331–337.

[ZL95]   C. Zimmer and R. Leithner, *Wirkungsgradverbesserung eines konventionellen Kraftwerkes durch Braunkohletrocknung mit Abgas*, BWK **47** (1995) 3, 78–81.